

Diplomarbeit

Sommerfeld Effect in Models with Vector
Dark Matter



Julius-Maximilians-Universität

Würzburg

vorgelegt von

Enrico Herrmann,

geboren am 10. Februar 1986 in Schlema,

am **26. Juni 2012**

Betreuer: Prof. Dr. R. Rückl und Dr. T. Flacke

Contents

1. Zusammenfassung	1
2. Abstract	3
3. Introduction - Motivation	5
3.1. Dark Matter and the "WIMP Miracle"	5
3.2. Indirect Dark Matter Detection and a First Glance at the Sommerfeld Effect	7
3.2.1. General Features of the Sommerfeld Effect	7
3.3. Vector Dark Matter in Standard Model Extensions	10
3.4. Construction of a Vector Dark Matter Toy Model - Dimensional (De)construction	11
4. $SU(2) \times SU(2) \times U(1) \times U(1)$ - Model	14
4.1. Notation and Moose Diagram	15
4.2. Lagrangian	16
4.2.1. The Gauge Sector	16
4.2.2. The Higgs Sector	17
4.2.3. Counting the Degrees of Freedom	21
4.3. $SU(2)_I \times SU(2)_{II} \rightarrow SU(2)_{\text{diag}}$ Breaking	22
4.3.1. H_{W^5} Potential to Break the $SU(2)_I \times SU(2)_{II}$ Gauge Group	22
4.3.2. VEV Structure and Tadpole Equations for the $SU(2)_I \times SU(2)_{II} \rightarrow$ $SU(2)_{\text{diag}}$ Breaking	23
4.3.3. The Scalar Mass Spectrum for the $SU(2)_I \times SU(2)_{II} \rightarrow SU(2)_{\text{diag}}$ Breaking	24
4.3.4. The Gauge Boson Mass Spectrum for the $SU(2)_I \times SU(2)_{II} \rightarrow$ $SU(2)_{\text{diag}}$ Breaking	25
4.4. $SU(2)_{\text{diag}} \times U(1)_{\text{diag}}$ Breaking	27

4.5.	Complete Higgs Mass Spectrum	28
4.5.1.	Tadpole Equations and Potential Minimum	28
4.5.2.	Neutral Higgs Sector	29
4.5.3.	Charged Higgs Sector	31
4.5.4.	Higgs Boson Summary	31
4.6.	Complete Gauge Boson Mass Spectrum	34
4.6.1.	The Neutral Gauge Bosons	35
4.6.2.	Mass mixing in the Neutral Sector and Weinberg Angles	36
4.6.3.	The Charged Gauge Bosons	38
4.6.4.	Gauge Boson Summary	39
4.7.	Gauge Fixing and Interactions	42
5.	Sommerfeld Effect	44
5.1.	General Features of the Bethe-Salpeter Ansatz	45
5.2.	The Ladder Approximation - Discussion of Positronium Bound States à la Landau Lifshitz	48
5.3.	Derivation of the Sommerfeld Enhancement à la Iengo	52
5.4.	Iengo's Solution of the Schrödinger Equation	59
5.5.	Sommerfeld Effect for Vector Dark Matter in $SU(2) \times SU(2) \times U(1) \times U(1)$ - Model	66
5.5.1.	Leading Order $Z^{(1)}Z^{(1)} \rightarrow Z^{(1)}Z^{(1)}$ Bethe-Salpeter Kernel	67
5.5.2.	Off-diagonal $Z^{(1)}Z^{(1)} \rightarrow W^{(1)}W^{(1)}$ Bethe-Salpeter Kernel	73
5.5.3.	Off-diagonal $Z^{(1)}Z^{(1)} \rightarrow W^{(1)}W^{(1)}$ u-channel Diagram	75
5.5.4.	Off-diagonal $Z^{(1)}Z^{(1)} \rightarrow W^{(1)}W^{(1)}$ contact Diagram	76
5.5.5.	Reversed off-diagonal Diagrams: $W^{(1)}W^{(1)} \rightarrow Z^{(1)}Z^{(1)}$	77
5.5.6.	Diagonal $W^{(1)}W^{(1)} \rightarrow W^{(1)}W^{(1)}$ Scattering Diagrams	77
5.5.7.	$W^{(1)}W^{(1)} \rightarrow W^{(1)}W^{(1)}$ Photon exchange Diagram	78
5.5.8.	$W^{(1)}W^{(1)} \rightarrow W^{(1)}W^{(1)}$ contact Diagram	79
5.6.	Neglected Terms in the Ladder Approximation	80
5.7.	Definition of the Bethe-Salpeter Wavefunction	82
5.8.	Summary of Integral Kernels	84

5.9. Spin Decomposition of Tensor Fields	85
5.9.1. Tensor Decomposition of the Bethe-Salpeter Amplitude	87
5.10. Solution of the Coupled Schrödinger Equations	93
6. Summary and Outlook	111
A. Parameters and Relations in the Standard Model	114
B. Gauge Fixing	115
B.0.1. Mixing Terms between Gauge Fields and Goldstone Bosons	116
B.0.2. Construction of Gauge Functions	118
B.0.3. Gauge Fixing Lagrangian $\mathcal{L}_{\text{gauge-fixing}}$	119
B.0.4. Discussion	124
B.1. Approximations to the Basistransformation between Gauge- and Mass Eigenstates	127
B.1.1. Approximation of the $\text{GB}_{Z(1)}$ Eigenvector	128
B.1.2. Approximation of the $\text{GB}_{\gamma(1)}$ Eigenvector	130
B.2. Faddeev-Popov-Ghosts	132
C. Feynman Rules for the $SU(2) \times SU(2) \times U(1) \times U(1)$ Gauge Theory	135
C.1. Field Content and Propagators	135
C.2. Vertex Rules	137
C.2.1. Notation	137
C.2.2. Triple Vector Boson Vertices	139
C.2.3. Quartic Vector Boson Vertices	139
C.2.4. Vector-Vector-Scalar-Vertices	140
C.2.5. Scalar-Scalar-Gauge-Vertices	142
C.2.6. Scalar-Scalar-Gauge-Gauge-Vertices	143
C.2.7. Triple Scalar Vertices	146
C.2.8. Quartic Scalar Vertices	147
C.2.9. Ghost - Anti-Ghost - Gauge Vertices	148
C.2.10. Ghost - Anti-Ghost - Scalar Vertices	149
D. Gauge Transformations	150

E. Numerical Shooting Routine	152
. Bibliography	157
. List of Figures	167
. Acknowledgment	169
. Selbständigkeitserklärung	170

1. Zusammenfassung

Die genaue Natur Dunkler Materie [1, 2] ist weiterhin unbekannt und einer der Gründe, die Suche nach Erweiterungen des Standard Modells der Teilchenphysik¹ an Hochenergiebeschleunigern [3] und in Experimenten zur direkten und indirekten Dunkle Materie Detektion [1, 4, 5] voranzutreiben. Eine Reihe von Anomalien bei der Beobachtung der kosmischen Hintergrundstrahlung [7, 8, 9, 10] hat einige Teilchenphysiker dazu veranlasst, die experimentellen Daten mittels Dunkler Materie Annihilation zu erklären [11, 12, 13, 14, 15, 16, 17]. Um diese Interpretation aufrecht zu erhalten, stellt es sich heraus, dass man einen Effekt benötigt, der die heutige Dunkle Materie Annihilationsrate im Vergleich zur Annihilationsrate zur Zeit der thermischen Entkopplung um einige Größenordnungen [11, 18] verstärkt. Wie sich zeigt, kann dies durch den Sommerfeld-Effekt geleistet werden.

Inhalt dieser Arbeit ist die Untersuchung des Sommerfeld-Effekts [19] für Vektor Dunkle Materie. Vektor Dunkle Materie ist in einer Reihe von Standard Modell Erweiterungen, z.B. Universellen Extra Dimensionen (UED) [20] oder Little Higgs Modellen [21] anzutreffen, wobei der Sommerfeld-Effekt für diese Teilchenklasse nach unserem Wissen noch nicht genauer untersucht wurde. Explizit handelt es sich beim Sommerfeld-Effekt um einen nicht-perturbativen Effekt, der mit dem Zusammenbrechen der Störungsreihe, durch Anwesenheit einer attraktiven Wechselwirkung, im nichtrelativistischen Limes einhergeht. Im Falle von Dunkle Materie Paar-Vernichtung kann die Sommerfeld-Verstärkung zum einen die richtige Dunkle Materie Dichte erklären und gleichzeitig bei der Interpretation der oben angesprochenen Anomalien in der kosmischen Hintergrundstrahlung aus Sicht der Teilchenphysik helfen. Wir gehen auf diese Punkte in den Abschnitten 3.1, 3.2 und besonders in Kapitel 5 näher ein.

Da die Untersuchung des Sommerfeld-Effekts für eine der bereits erwähnten Erweiterungen des Standard Modells den Rahmen dieser Arbeit sprengen würde, konstruieren wir zunächst ein "minimales" Spielzeugmodell, welches stabile Eichbosonen als Dunkle Materie Kandidaten enthält und dennoch die für den Sommerfeld-Effekt wichtigsten Eigenschaften der komplexeren Theorien wiedergibt. Insbesondere ist unser Modell durch sogenannte "dekonstruierte" Theorien inspiriert [22], welche einen nützlichen Bausatz zur

¹Eine Einführung in das Standard Modell der Teilchenphysik (SM) findet man z.B. in [6].

Modellkonstruktion liefern. Die detaillierte Vorstellung des Modells und die Berechnung des Massenspektrums erfolgt in Kapitel 4. Daran anknüpfend erhalten wir aus der kompletten eichfixierten Lagrangedichte (4.1) die Feynman-Regeln in der Masse-Eigenbasis, welche in Anhang C aufgelistet sind.

Als weiterer wichtiger Programmpunkt unserer Arbeit steht nach der Modellkonstruktion eine detaillierte Analyse des Sommerfeld-Effekts für Vektor Dunkle Materie auf dem Plan. Hierbei diskutieren wir zunächst allgemeine Eigenschaften des Sommerfeld-Effekts in Abschnitt 3.2.1 und erläutern den Bethe-Salpeter Formalismus als feldtheoretisches Werkzeug zur Behandlung nichtperturbativer Effekte in Kapitel 5.1. Anschließend wenden wir uns in Absatz 5.3 überblicksartig dem Sommerfeld-Effekt für fermionische Dunkle Materie zu, um die technischen Details des Formalismus an einem aus der Literatur bekannten Beispiel [23] zu reproduzieren. Wie sich in 5.3 und 5.4 herausstellt, entspricht die nichtperturbative Behandlung der Wechselwirkung zwischen den Dunkle Materie Teilchen der Lösung eines quantenmechanischen Streuproblems, welches in einer 2-Teilchen-Schrödingergleichung beschrieben wird. In der nichtrelativistischen instantanen Näherung wird die Wechselwirkung zwischen den Dunkle Materie Zuständen durch ein effektives Potential beschrieben, welches wir für unser Vektor Dunkle Materie Modell explizit in den Abschnitten 5.5 und 5.7 herleiten. Darauf aufbauend konzentrieren wir uns auf die Lösung des Streuproblems in Kapitel 5.10. Als Hauptergebnis dieser Arbeit finden wir, dass für gewisse Parameterpunkte eine Verstärkung des Dunkle Materie Annihilations-Wirkungsquerschnittes um mehrere Größenordnungen erzielt werden kann. Dies wird besonders in Abbildung 5.15 deutlich.

2. Abstract

The mysterious nature of dark matter [1, 2] is one of many compelling reasons to look for extensions of the Standard Model of particle physics¹ in high energy colliders [3] as well as direct and indirect dark matter detection experiments [1, 4, 5]. In recent years, certain astrophysical cosmic ray observations [7, 8, 9, 10] have triggered a wide interest in the particle physics community to interpret a number of anomalies in the experimental data in terms of dark matter signals [11, 12, 13, 14, 15, 16, 17]. For this interpretation to hold, it turns out that one has to devise a mechanism - the Sommerfeld effect - to enhance the present day dark matter annihilation cross section by several orders of magnitude (see e.g. [11, 18]) in comparison to the cross section at the time of thermal decoupling. The main goal of this thesis is the study of the Sommerfeld effect [19] for vector dark matter, which, to our knowledge, has not been addressed in the literature so far.

Our work is split in three major sections:

First, we give a short review of the standard thermal evolution of dark matter and elaborate on the necessity for enhanced dark matter annihilation cross sections for the interpretation of the cosmic ray anomalies described in sections 3.1 and 3.2. As introduction, we summarize some general properties of the Sommerfeld effect in section 3.2.1. In section 3.3, we motivate our interest in vector dark matter and subsequently introduce a method called "deconstruction" [22] as model building guide (section 3.4).

The topic of the second major part of this work (chapter 4) is the detailed introduction of our "deconstructed", renormalizable, gauge invariant vector dark matter toy model. We derive the complete scalar and gauge boson mass spectrum in sections 4.5 and 4.6 as the result of gauge symmetry breaking and show that we are able to describe stable vector dark matter. A detailed discussion of technical details including gauge fixing, Goldstone bosons and Faddeev-Popov-ghosts can be found in Appendix B. Subsequently, an exhaustive list of Feynman rules of our model is given in Appendix C.

¹for an introduction to the Standard Model (SM), c.f. [6]

The third part (chapter 5) of this thesis is concerned with the Sommerfeld effect itself. We describe the Bethe-Salpeter ansatz as a field-theoretic tool to deal with the nonperturbative Sommerfeld enhancement in section 5.1. In paragraph 5.3, we employ this machinery and present Iengo's work [23] on the Sommerfeld effect for fermionic dark matter candidates in order to understand the formalism along a known example. To leading order, it turns out that one has to sum up ladder-type Feynman diagrams in the non-relativistic regime which corresponds to the solution of a quantum mechanical scattering problem. In this picture, the nonperturbative nature of the interaction is encoded in an effective potential. Within the remaining sections of chapter 5, we present our results on the Sommerfeld enhancement to vector dark matter for the "deconstructed" model. The line of reasoning, however, follows analogously for generic models, once one fixes the particle spectrum and the interactions. Section 5.5 is devoted to the derivation of the relevant interaction kernels, which are subsequently used in the effective description of the annihilating dark matter pair. Analogously to the fermionic case, we are able to introduce a Bethe-Salpeter wavefunction in section 5.7 as scattering solution to the coupled system of Schrödinger equations. In section 5.10, we discuss the connection of the scattering solution with the Sommerfeld enhancement factor and give numerical results for the vector dark matter case. The important conclusion from this section is, that significant enhancement factors arise for special regions of the model parameter space. The essence of our calculation is summarized in figure 5.15.

We complete our work with a final summary of results in chapter 6 and also give a brief outlook on potential improvements.

3. Introduction - Motivation

3.1. Dark Matter and the "WIMP Miracle"

Measurements of rotation curves of galaxies [2, 24, 25], gravitational lensing effects of background radiation on galaxies [26, 27] and the observation of the microwave background with the WMAP satellite [28] convincingly support the idea of non-baryonic dark matter that accounts for 23% of the energy content of the Universe [29]. Yet, the detailed nature of dark matter has not been revealed by either direct or indirect searches¹ so far.

Despite its immense success in explaining a variety of experimental results, the Standard Model of particle physics² falls short in accounting for the existence of the above mentioned dark matter candidate. In addition to some other open questions³, this motivated the exploration of a wide range of beyond Standard Model (BSM) theories. Among these, supersymmetry⁴ and extra dimensions [20] are probably the most compelling classes of new physics models at the TeV scale and naturally contain weakly interacting massive particles (WIMP) as paradigm dark matter candidates [1]. In the following, we do not want to elaborate on dark matter phenomenology in great detail, as there is excellent literature available (see e.g. [1, 4]), but only briefly review the thermal "WIMP-miracle", common to many BSM models along the lines of Ref. [4].

In the simplest picture, the time evolution of the number density n_χ of a non-degenerate dark matter species χ is given by the Boltzmann equation

$$\frac{dn_\chi}{dt} + 3Hn_\chi = -\langle\sigma_a v\rangle [n_\chi^2 - (n_\chi^{eq})^2], \quad (3.1)$$

where $H = (8\pi\rho/3M_{Pl})^{1/2}$ denotes the Hubble parameter, $\langle\sigma_a v\rangle$ the thermally averaged cross section times relative velocity of the $\chi\bar{\chi}$ -pair and n_χ^{eq} the equilibrium number density of the χ particles:

$$n_\chi = \frac{g}{(2\pi)^3} \int f(\vec{p}) d^3p. \quad (3.2)$$

¹for review of direct and indirect dark matter detection, c.f. e.g. [1, 4, 5]

²see e.g. [6] for an introduction

³for a review cf. e.g. [3]

⁴for review, c.f. e.g. [30]

g accounts for internal degrees of freedom of the particle species and $f(\vec{p})$ is the Fermi-Dirac or Bose-Einstein distribution, depending on the spin of χ . In the extremely hot and dense early Universe, the temperature⁵ T is much larger than m_χ so that n_χ scales as $n_\chi \propto T^3$. In this era, the Universe was radiation dominated and the Hubble parameter is proportional to T^2 ($\rho \sim T^4$). Therefore, H decreases slower with temperature than n_χ . Due to the temperature scaling, the Hubble term in eq. (3.1) is negligible at early times and the number density essentially follows its thermal equilibrium value.

As the Universe expands and cools, the temperature eventually falls below the mass m_χ of the dark matter particle and n_χ drops exponentially

$$n_\chi \propto g \left(\frac{m_\chi T}{2\pi} \right)^{\frac{3}{2}} \exp(-m_\chi/T) \quad (3.3)$$

in the $T \ll m_\chi$ limit. Eventually, the annihilation rate $\Gamma = \langle \sigma_a v \rangle n_\chi$ falls below the Hubble expansion rate H and the annihilations of χ cease to be efficient. At this point, the χ particles fall out of equilibrium - the thermal "freeze-out" occurs and one is left with the cosmological relic abundance. Since the freeze-out condition, $\Gamma \approx H$, depends on the thermally averaged annihilation cross section $\langle \sigma_a v \rangle$, it is clear, that the resulting relic density Ω_χ also depends on this parameter. The higher the interaction cross section, the longer the dark matter species stays in equilibrium with the thermal bath. This gives the Universe more time to cool before the decoupling occurs. According to the exponential depletion of the equilibrium dark matter number density with falling temperature eq. (3.3), one naturally expects a lower relic density for higher annihilation cross sections and approximately finds [4]:

$$\Omega_\chi h^2 = \frac{m_\chi n_\chi}{\rho_c} \approx \frac{3 \times 10^{-27} \text{ cm}^3 \text{ s}^{-1}}{\langle \sigma_a v \rangle}, \quad (3.4)$$

where h is the Hubble constant in units of $100 \text{ km s}^{-1} \text{ Mpc}^{-1}$ and $\rho_c \approx 10^{-5} h^2 \text{ GeV cm}^{-3}$ today's critical density. For WIMPs, the annihilation cross section can be estimated as $\langle \sigma_a v \rangle \sim \left(\frac{\alpha}{10^{-2}} \right)^2 \left(\frac{m_\chi}{1 \text{ TeV}} \right)^{-2} \times 10^{-27} \text{ cm}^3 \text{ s}^{-1}$. Now the "miracle" is, that plugging $\langle \sigma_a v \rangle$ back into the relic density estimate eq. (3.4) together with a weak scale coupling $\alpha_2 = \mathcal{O}(0.03)$ and a TeV mass, encountered in common BSM scenarios, yields a relic density, which is of the same order of magnitude as the observed value $\Omega_\chi h^2 = 0.1109 \pm 0.0056$ [29].

If the dark sector contains more than one particle species with mass close to m_{DM} , coannihilation and threshold resonances⁶ can occur and the crude estimate that leads to (3.4) can be altered considerably. In such cases, the system has to be described by a coupled set of Boltzmann equations in order to trace the thermal evolution of the Universe.

⁵we adopt natural units with $\hbar = c = k_B = 1$

⁶cf. e.g. [31, 32, 33, 11, 34] for specific examples

3.2. Indirect Dark Matter Detection and a First Glance at the Sommerfeld Effect

Besides yielding the correct relic abundance, WIMPs are appealing from another perspective as well. Since they commonly have some kind of non-gravitational couplings to Standard Model particles, the possibility of direct and indirect detection opens up and relates these observables directly to the relic abundance [11]. Unfortunately, the low cross sections required for the WIMP miracle seem to make indirect detection a difficult task. Yet, recent experiments including PAMELA [7], ATIC [8], HESS [9] and Fermi LAT [10] found indications for an excess of electrons, positrons and photons in the 10 GeV - (at least) 100 GeV range of the cosmic radiation. Apart from astrophysical explanations (see e.g. [35, 36, 37]), it has also been suggested, that these results might be understood in terms of annihilating dark matter [11]. In order for this interpretation to hold, one has to address the question how to obtain present day annihilation cross sections that are at least of $\mathcal{O}(10^2)$ larger than the ones favored by the WIMP miracle at the time of decoupling. Following a number of authors [14, 18, 23, 38, 39], we will show that the so-called "Sommerfeld effect" is able to alleviate this tension and can reconcile the WIMP miracle with potential indirect dark matter signals.

3.2.1. General Features of the Sommerfeld Effect

In 1931, Arnold Sommerfeld calculated the distortion of the scattering wavefunction in the presence of a Coulomb potential [19] leading to a velocity dependent $\frac{1}{v}$ enhancement of the electron-nucleon scattering cross section. In principle, one can think about this phenomenon as the quantum mechanical counterpart to the classical enhanced cross section in the presence of an attractive force.⁷ In the language of quantum field theory⁸, however, the notion of an instantaneously acting force has to be abolished and replaced by the exchange of field quanta as mediators of the interaction. One can understand the typical interaction range in terms of the mass of the mediator m_ϕ itself: $r_{int} \propto \frac{1}{m_\phi}$ (interaction potential corresponds to the Fourier transformed propagator).

In order to calculate annihilation cross sections for relativistic scattering processes in particle physics, one commonly employs perturbative methods for weakly coupled theories. In the low energy limit, however, this procedure breaks down in the presence of

⁷In Ref. [11], Arkani-Hamed et al. give a nice example of this analogy as found in celestial mechanics.

⁸for an introduction to quantum field theory (QFT), c.f. e.g. [40, 41]

long range interactions [34]. Physically, this breakdown is attributed to the formation of a loosely bound state [39]. In order to obtain the correct annihilation cross section, one has to resort to nonperturbative methods and sum up an infinite number of field theory diagrams [18]. It turns out that this procedure is equivalent to introducing a non-relativistic Schrödinger wavefunction for the DM pair that contains the information about the short distance annihilation properties in the presence of a long-range interaction [23, 18, 38]. In the quantum mechanical framework, the long-distance behavior is encoded in a potential that distorts the initial state two-particle wavefunctions away from plane waves, thereby invalidating the usual Born expansion [34]. This breakdown directly reflects the presence of nonperturbative effects.

With respect to the non-relativistic reduction, starting from a field theoretic point of view, we are going to follow the work of Iengo [23] and make use of the Bethe-Salpeter ansatz, which we review in chapter 5.1. The conversion of the nonperturbative summation of field theory diagrams into a Schrödinger problem simplifies the calculation considerably. Upon deriving the Schrödinger equation from first principles, the problem of finding the correct wavefunction is a matter of standard potential scattering theory known from non-relativistic quantum mechanics⁹. Note, in case of inelastic scattering, the potential is matrix valued in the space of two particle states and off-diagonal interactions introduce mixings amongst them [11, 39]. These points will be highlighted in greater detail, once we work out the detailed examples in sections 5.3 and 5.5.

Before we explain the technicalities of the derivation, it is instructive to compare¹⁰ the length or equivalently the energy scales involved in the scattering problem. This outline is useful for the treatment of our vector dark matter toy model, in particular when we discuss the mass spectrum (sections 4.5 and 4.6) and interactions (see Sec. 4.7). In the following, we focus on the specific application of the Sommerfeld effect we have in mind, i.e. dark matter annihilation. Above, the notion of forming a loosely bound state due to the mutual interaction between the incoming particles has been evoked. In the instantaneous limit,¹¹ the presence of a massive force carrier leads to a Yukawa potential [39]:

$$V(r) = \alpha \frac{e^{-m_\phi r}}{r},$$

where the coupling strength α is determined by the type of incoming particles and their interactions. The appearance of this potential sets the scale for the binding energy. Similar

⁹for an introduction to scattering theory in non-relativistic QM, see e.g. [42, 43, 44]

¹¹This discussion follows the comments of Hryczuk et al. [39].

¹¹The instantaneous limit is discussed in section 5.3 in greater detail.

to the Bohr energy in the hydrogen atom, we find the scale of the binding energy for incoming dark matter particles with mass m_χ that interact via light mediators with mass $m_\phi \rightarrow 0$ to be of $\mathcal{O}(m_\chi \alpha^2)$. For finite exchange boson masses, the energy can only be reduced, due to the Yukawa cutoff [34]. In order to form a bound state, the characteristic Bohr energy $m_\chi \alpha^2$ has to be larger than the kinetic energy of the incoming particles $\mathcal{E} \approx m_\chi v_{sp}^2$ which yields the first characteristic requirement for a sizable Sommerfeld effect¹²:

$$\begin{aligned} m_\chi \alpha^2 &\gtrsim m_\chi v_{sp}^2 \\ \Rightarrow \alpha &\gtrsim v_{sp}. \end{aligned} \tag{3.5}$$

The velocity dependence of the cross section is the intriguing feature of the Sommerfeld effect. In case of dark matter annihilation, this particular property provides the foundation of the difference between the annihilation cross section at the present time ($v \sim 10^{-3}$) compared to the time of thermal decoupling in the early universe ($v \sim 0.3$) [11], rendering the effect attractive for indirect dark matter detection. For a typical WIMP, the interaction strength is of the order of the weak coupling $\alpha_2 = \frac{g_2^2}{4\pi} \approx 0.03$, one order of magnitude smaller than the typical velocity at the decoupling time. The occurrence of nearly mass degenerate states might however modify this argument. As Hisano et al. [18] pointed out, if the mass splitting is sufficiently small and the additional states can be produced on-shell with almost zero velocity, a threshold resonance might occur which could modify the relic density, see also [39].

The discussion above suggests, that one has to consider the mass splitting δm in the dark sector for systems involving multiple (near mass degenerate) states. If the mass splitting δm is significantly larger than the kinetic energy of the incoming dark matter pair, the heavier states can not be produced on-shell and do not experience any enhancement. This effective cutoff is the main reason, why we only take into account a very special subset of particles and interactions for the Sommerfeld effect. All states that are considerably heavier than the dark matter candidate (mass splitting $\delta m \gg \mathcal{E}$) effectively decouple from the enhanced annihilation process and need not to be considered in this analysis. The naive estimate $2\delta m < \mathcal{E}$ for the participation of a particle species in the Sommerfeld effect, however, has to be modified in the presence of the interaction potential V . At short distances, where the interaction strength is relevant, one has to include the Bohr energy. Consistent with Hryczuk et al. [39], one finds:

$$2\delta m \lesssim \mathcal{E} + m_\chi \alpha^2. \tag{3.6}$$

¹² v_{sp} denotes the single particle velocity of the dark matter candidate.

Besides the strength of the interaction potential, which is determined by α , we have to consider another property related to the exchange of the mediator ϕ . As we have mentioned in the beginning of this section, the nonperturbative nature of the Sommerfeld effect can be encoded in the deformation of the two-particle wavefunction. In order for the interaction to distort the free scattering state significantly, the range of the Yukawa interaction $(m_\phi)^{-1}$ has to be at least comparable to the Bohr radius of the bound state $(\alpha m_\chi)^{-1}$, which leads to the condition:

$$\frac{1}{m_\phi} \gtrsim \frac{1}{\alpha m_\chi} \quad (3.7)$$

This condition suggests additional simplifications for any particular particle physics setup. The requirement of light mediators with masses $m_\phi \lesssim \alpha m_\chi$ limits the number of fields and vertices that are relevant for the Sommerfeld effect even further. In our specific model describing vector dark matter, it turns out that we only have to consider Standard Model modes as mediators in generic regions of parameter space. We are able to reject an extensive number of field theory diagrams that have to be considered for the Sommerfeld effect, based on these simple order of magnitude estimates.

3.3. Vector Dark Matter in Standard Model Extensions

To our knowledge, the Sommerfeld enhancement has only been discussed for scalar and fermionic dark matter so far. However, a number of Standard Model extensions lead to vector dark matter candidates. Amongst such theories, there are "Little Higgs models" that contain new gauge bosons, fermions, and scalars at the TeV scale (for review, cf. e.g. [45]). A discrete symmetry, called "T-parity" [21] ensures the stability of the lightest parity-odd particle. As has been shown in the work of Cheng et al. [21], one of the heavy new neutral vector bosons is a viable dark matter candidate.

Another promising idea to describe physics beyond the Standard Model involves the introduction of extra spatial dimensions. In this thesis, we present a minimal vector dark matter model, that is inspired by such theories, which is why we review them in a little more detail. Yet, we would like to emphasize that the scope of our model is not limited to this scenario. In Universal Extra Dimensions (UED) [20], one introduces an additional spatial dimension that is compactified to a circle of radius R , where opposite points are identified.¹³ Mathematically, this geometry of the extra dimension corresponds to a S^1/\mathbb{Z}_2 -orbifold. In UED, it is assumed that all Standard Model fields can propagate in this higher

¹³For detailed discussions on the concepts of UED and the special choice of the geometry of the extra dimension, we refer to e.g. [20, 46].

dimensional space. The compactification of the extra dimension leads to the discretization of the momentum in this direction, which is reflected in the appearance of a tower of excitations on top of every Standard Model field in an effective four-dimensional description. Each level of this tower is characterized by a quantum number n , the Kaluza-Klein (KK) number, where Standard Model fields are identified with $n = 0$ and consecutive KK-levels are separated in mass by $\sim 1/R$. Due to the additional \mathcal{Z}_2 symmetry, there are two fixed points in the extra dimension. Operators at these points break Lorentz invariance and momentum conservation in the fifth dimension explicitly, so that n is not a good quantum number. However, the fixed points leave a discrete \mathcal{Z}_2 reflection symmetry intact, which is called KK-parity. In UED, this discrete \mathcal{Z}_2 symmetry guarantees the stability of the lightest Kaluza-Klein particle (LKP) and is also responsible for the fact, that KK-(1)-modes can only be produced in pairs. In Ref. [47], it has been shown, that the first KK-excitation of the $U(1)_Y$ gauge boson, denoted by $B^{(1)}$, is the generic dark matter candidate. However, additional operators, that have not been considered in [47] can modify this statement and the first excitation of the W^3 -gauge boson could become the LKP [48].

3.4. Construction of a Vector Dark Matter Toy Model - Dimensional (De)construction

The Sommerfeld calculation for a complete UED model is beyond the scope of this thesis due to a number of complications arising in extra dimensional theories.

First, couplings with negative mass dimension render the UED-Lagrangian intrinsically nonrenormalizable [47]. UED should therefore be considered as an effective field theory (EFT), valid up to some cut-off scale Λ [47, 49]. In such a framework non-trivial computational techniques are necessary for higher order field theory calculations. On top of the technical difficulties associated with the calculation process, we would like to mention, that even though an EFT treatment is known for minimal UED [47], it remains elusive for extended models so far.

Second, in UED models, mixing among different KK-modes [48] as well as KK-number violating vertices [47] occur, which complicate matters even further. These features, however, play a subdominant role for the Sommerfeld calculation, since the mixing is suppressed by at least $\mathcal{O}\left(\frac{m_{W^{(0)}}^2}{(1/R)^2}\right)$ [48]¹⁴, so that the correction to the $Z^{(1)}W^{(1)}W^{(0)}$ -vertex for example is negligible for a typical compactification scale $\mathcal{O}(1/R) \approx \text{TeV}$.

¹⁴ $m_{W^{(0)}} = 80.398 \pm 0.025 \text{ GeV}$ [50] denotes the Standard Model W-boson mass.

The KK-number violating couplings of a full UED model, exemplarily depicted in fig.3.1, do not significantly contribute to a sizable Sommerfeld enhancement either, for the large mass splitting between different KK-levels of $\mathcal{O}(1/R) \approx \text{TeV}$ (see discussion in Sec. 3.2.1).

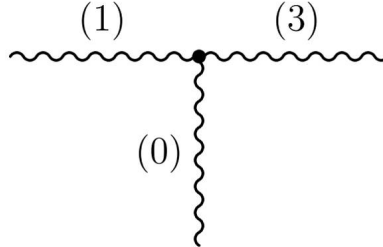


Figure 3.1.: Exemplary KK-number-violating vertex. We depict a generic interaction between a KK-0-, a KK-1- and a KK-3-mode.

In order to avoid the above mentioned complications altogether, we restrict ourselves to constructing a 4D renormalizable toy model that contains a vector dark matter candidate on top of the scalar and gauge sector of the Standard Model. In section 3.2.1 we have demonstrated, that only a specific subset of the particle spectrum contributes to sizable enhancement factors. In particular, only light states (in our minimal case, these are the SM-gauge bosons) acting as long range force carriers have to be considered in addition to the (potentially mass degenerate) heavy dark matter component of the model. For the heavy neutral $SU(2)$ -gauge boson, dubbed $Z^{(1)}$, one naturally expects a near mass degeneracy with the charged $W_{(1)}^{\pm}$ -bosons from the same gauge multiplet, which is only lifted by electroweak symmetry breaking. Therefore we include these states in the dark matter sector of our toy model. In comparison to the $SU(2)$ -gauge-boson triplet, a priori, there is no symmetry reason why the gauge bosons should be degenerate with the fermionic sector and one generically expects a larger splitting between heavy fermions and gauge bosons. As we have outlined in section 3.2.1, the near mass degeneracy with the dark matter candidate is critical for the contribution of the particle species to the Sommerfeld effect. On account of the larger fermion mass split-off, we are going to neglect the fermions in the construction of our toy model as a first approximation.

In conclusion: besides 4D renormalizability, our model has to reproduce the electroweak sector of the Standard Model as phenomenological starting point. In the dark sector, we consider a set of particles that contains a neutral gauge boson with mass $m_{DM} \sim 1 \text{ TeV}$ and additional states that are split-off by $\frac{\delta m}{m_{DM}} \lesssim \mathcal{O}(10^{-2})$ at most.

For the construction of a toy model emulating many phenomenological properties of extra-dimensional theories, we have a particularly compelling toolbox at hand. In their influential paper on *(De)Constructing Dimensions*, Arkani-Hamed, Cohen and Georgi [22] have shown how to "build" extra dimensions from renormalizable, asymptotically free, 4D gauge theories. Physically, these field theories may be imagined as latticized picture of the additional spacial directions [51, 52, 53, 54, 55]. The 4D gauge theories that generate the extra dimension dynamically are easily depicted in so called "moose" or "quiver" diagrams that also help keeping track of the field content of those theories.

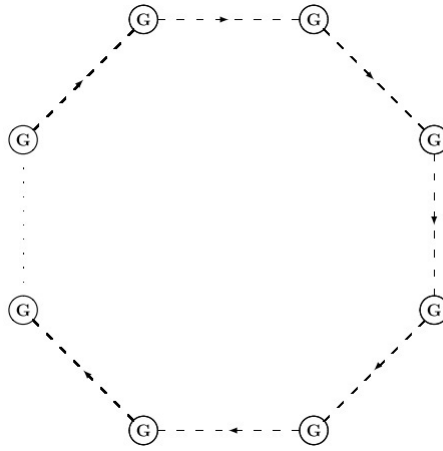


Figure 3.2.: *Cartoon of a moose diagram with $N + 1$ gauge groups G . The dashed lines between adjacent nodes represent non-linear sigma fields that correspond to link variables of lattice gauge theory. Graphic taken from [22].*

In the context of moose diagrams, one can follow the interpretation of Ref. [51] and regard fig. 3.2 as an image of the latticized extra dimension. This point of view primarily focuses on a manifestly gauge-invariant effective description of higher KK-modes. Normally, the truncation of the KK-tower after a finite number of modes corresponds to a hard momentum cutoff in the fifth dimension which spoils the higher dimensional gauge invariance. The effective 4D gauge theory description of the KK-tower on the other hand remains gauge invariant [53] by construction, which is the appealing feature of this approach.

In comparison to the periodic geometry insinuated in figure 3.2, it turns out that the linear moose diagram ("aliphatic" model [51]) corresponds to the S_1/\mathbb{Z}_2 -orbifold construction in UED and contains no unwanted zero-modes [51]. One is left with a direct product of $N + 1$ gauge groups G that are sequentially connected by N link fields transforming under the bifundamental representation of adjacent groups. In Ref. [51], Cheng et al. give a comprehensive treatment of the latticized Standard Model and many ideas for our simple dark matter toy model are guided by this source.

4. SU(2) × SU(2) × U(1) × U(1) - Model

Inspired by (de)constructed theories [22], we have built a "minimal" four dimensional gauge theory that contains a stable heavy vector boson ($Z^{(1)}$) and is able to mimic the Standard Model electroweak gauge sector.¹ By varying the parameters of the scalar potential, we are able to switch between $U(1)_Y$ - and $SU(2)_L$ -like dark matter. The stability of our dark matter candidate is guaranteed by a KK-parity-like discrete \mathcal{Z}_2 symmetry, implemented by choosing equal vacuum expectation values, gauge couplings and hypercharges for both "lattice-sites". We introduce a number of fundamental scalars that give mass to the gauge bosons and reproduce the electroweak sector of the Standard Model. In comparison to other authors² working on latticized extra dimensions, we make use of fundamental "link fields" instead of a nonlinear realization of the electroweak symmetry breaking in order to evade renormalization issues connected to non-linear sigma models [40] and keep our theory as simple as possible.

For the Sommerfeld phenomenology of the $Z^{(1)}$, we are interested in a scenario, where the dark matter particle is nearly mass degenerate with the second lightest states of the dark sector - the charged $SU(2)$ gauge bosons $W_{(1)}^\pm$ (see discussion in Sec. 3.2.1). In order to obtain a sizable Sommerfeld enhancement, couplings of order $\mathcal{O}(\alpha \approx v)$ between the DM particles and the light force carriers are required (also see Sec. 3.2.1, v denotes the present day DM velocity). In our model, this is implemented by electroweak couplings between the heavy vector particles and their light Standard Model counterparts. In the context of the Minimal Supersymmetric Standard Model³ scenario, the connection between the enhancement factor, the coupling strength and the mass spectrum has been discussed in the cardinal paper on the Sommerfeld effect by [18].

¹For a certain parameter range (see Sec. 4.5.4), we are able to identify the field content of our 4D gauge theory with the lowest scalar and gauge boson excitations of a UED model. Using only two lattice sites in the 4D gauge theory language corresponds to a truncation of the KK-tower after the 1st KK-excitation in the effective description of the extradimensional model.

²e.g. [51, 52, 53, 54, 55]

³for review c.f. e.g. [30]

4.1. Notation and Moose Diagram

A "moose" representation of our theory, including important parameters and the field content, is shown in fig. 4.1. The notation is chosen in the style of a UED⁴ theory, the scope of our model, however, is of more general nature. For the discussion of the spontaneous symmetry breaking pattern, the derivation of the mass spectrum and the interaction vertices, we follow the latticized extra dimensions literature closely [51, 52, 53, 54, 55], especially in Sec. 4.2.2 where we treat the scalar sector.

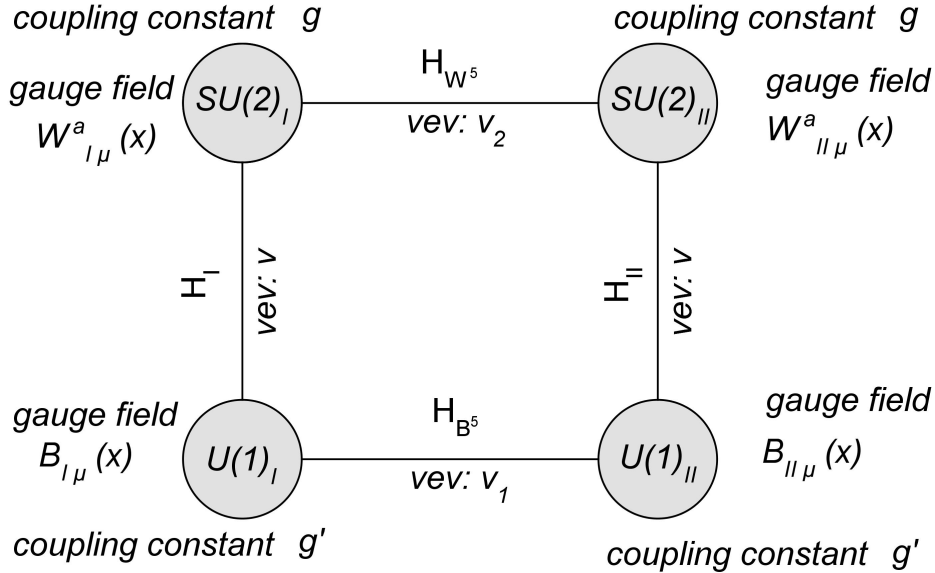


Figure 4.1.: Moose diagram with description of Higgs fields, vacuum expectation values and gauge couplings. Discrete Kaluza-Klein-like parity is implemented by a reflection symmetry between the left and right lattice sites. The special parameter choice (equal gauge couplings, hypercharges, VEVs v for H_I and H_{II}) also reflects this symmetry.

In the following sections we fix our notation and elaborate on the model-parameterization in greater detail. We are going to introduce the specific terms of the Lagrangian explicitly, derive the mass spectrum of the theory and finally summarize the Feynman rules in App.C.

⁴In particular, our theory can be seen as a simplified and truncated version of latticized extra dimensions [51] in a certain region of parameter space. The connection to the UED notation is refined in a comment on the scalar sector of UED in Sec. 4.2.2

4.2. Lagrangian

Our minimal "deconstructed" dark matter model is characterized by the gauge-fixed Lagrangian:

$$\mathcal{L} = \mathcal{L}_{gauge} + \mathcal{L}_{Higgs} + (\mathcal{L}_{gauge-fixing} + \mathcal{L}_{Ghost}) \quad (4.1)$$

We are going to give explicit expressions for all contributions in the following sections. For conciseness, we defer the detailed discussion of the gauge-fixing and ghost sector to appendix A, since these matters are not the prime objective of this work.

4.2.1. The Gauge Sector

The gauge sector of the $SU(2)_I \times SU(2)_{II} \times U(1)_I \times U(1)_{II}$ -theory follows from a straight forward generalization of the Standard Model case (for the SM gauge sector, see e.g.[40]).

$$\mathcal{L}_{gauge} = -\frac{1}{4}G_{I,\mu\nu}^a G_I^{a,\mu\nu} - \frac{1}{4}G_{II,\mu\nu}^a G_{II}^{a,\mu\nu} - \frac{1}{4}F_{I,\mu\nu} F_I^{\mu\nu} - \frac{1}{4}F_{II,\mu\nu} F_{II}^{\mu\nu}, \quad (4.2)$$

where $a = 1, 2, 3$ denotes $SU(2)$ gauge indices and μ, ν represent Lorentz indices. In the following, we are going to write out the expressions for the field strength tensors explicitly.

Field Strength Tensors

The field strength tensors for $SU(2)_I$ and $SU(2)_{II}$ are given by

$$G_{I/II,\mu\nu}^a = \partial_\mu W_{I/II,\nu}^a(x) - \partial_\nu W_{I/II,\mu}^a(x) + g\epsilon^{abc}W_{I/II,\mu}^b(x)W_{I/II,\nu}^c(x), \quad (4.3)$$

where we chose the couplings g of both $SU(2)$ equal in order to preserve the \mathcal{Z}_2 reflection symmetry under $I \leftrightarrow II$ exchange in the Lagrangian. In case of the abelian $U(1)$ gauge groups the field strength tensors simplify and no gauge boson self-couplings occur, since the structure constants are identically zero:

$$F_{I/II,\mu\nu} = \partial_\mu F_{I/II,\nu}(x) - \partial_\nu F_{I/II,\mu}(x). \quad (4.4)$$

4.2.2. The Higgs Sector

Before we introduce the scalar sector of our "deconstructed" dark matter toy model, we take a short detour to discuss the KK-excitations of the Higgs field in UED, for it will clarify our notation. In this exposition, we closely follow [47]. The KK-modes of the W and Z bosons acquire their masses via the higher dimensional Higgs mechanism. The corresponding Goldstone bosons are linear combinations of the 5th component of the gauge fields (denoted by A_5) and the Higgs KK-modes. The orthogonal combinations represent physical scalar particles in the spectrum. For $1/R \gg m_{W,Z}^0$, it can be shown that the longitudinal components of the KK gauge bosons are dominated by the respective A_5 's, and the physical scalars are approximated by the KK-excitations of the $SU(2)$ Higgs-doublet [56, 57]. In total, there are four physical scalars at each non-zero KK-level⁵, $H_{(n)}^\pm$, $H_{(n)}^0$, $a_{(n)}^0$.

Let us now return to the scalar sector of our "deconstructed" model. The Higgs-Lagrangian is given by:

$$\mathcal{L}_{Higgs} = \text{tr} [|D_\mu H_{W^5}|^2] + |D_\mu H_{B^5}|^2 + |D_\mu H_I|^2 + |D_\mu H_{II}|^2 + V_{Higgs} \quad (4.5)$$

In the following, we are going to give a detailed account of the covariant derivatives $D_\mu H_i$ and the Higgs potential V_{Higgs} .

The Covariant Derivatives

The covariant derivatives couple the scalar content of our theory to the gauge fields and eventually lead to gauge boson masses after spontaneous symmetry breaking.

1. H_{W^5} transforms under $SU(2)_I \times SU(2)_{II}$ as $(\bar{\mathbf{2}}, \mathbf{2})$. Due to an isomorphism between $\mathbb{C}^2 \otimes \mathbb{C}^2 \cong \mathcal{M}_2(\mathbb{C})$, H_{W^5} might be represented as a 2×2 matrix carrying two gauge indices, one for the $SU(2)_I$ (in the following denoted by $b, c \in \{1, 2\}$) and the other for the $SU(2)_{II}$ group (denoted by $i, j \in \{1, 2\}$).

$$(H_{W^5})_{ci} = \begin{pmatrix} \phi_{11} & \phi_{12} \\ \phi_{21} & \phi_{22} \end{pmatrix}_{ci} \quad (4.6)$$

Each of the ϕ 's represents one complex or equivalently two real degrees of freedom adding up to eight real degrees of freedom within the H_{W^5} field. The covariant derivative acts on the H_{W^5} field in the bi-fundamental representation as:

$$(D_\mu H_{W^5})_{ci} = (\partial_\mu H_{W^5})_{ci} + ig\vec{W}_{I,\mu} \delta_{cb} (H_{W^5})_{bj} \frac{\vec{\tau}_{ji}}{2} - ig\vec{W}_{II,\mu} \frac{\vec{\tau}_{cb}}{2} (H_{W^5})_{bj} \delta_{ji} \quad (4.7)$$

⁵Notice that $H_{(0)}^\pm$ and $a_{(0)}^0$ are just the usual Goldstone bosons in the SM. The 5-components of the gauge fields vanish for the 0-modes owed to the boundary conditions in the extra dimension [56, 57]. This comment should also elucidate our notation in the moose diagram 4.1. H_{W^5} mimics the 5th component of the $SU(2)$ gauge fields, denoted by W and H_{B^5} the $U(1)$ counterpart.

Since $D_\mu H_{W^5}$ carries gauge indices that are uncontracted in a conventional kinetic term, one has to introduce an extra trace in order to obtain a gauge invariant singlet required for the Lagrangian.

2. H_{B^5} transforms under $U(1)_I \times U(1)_{II}$ as $(-Y^{H_{B^5}}, +Y^{H_{B^5}})$.

With this transformation property the covariant derivative acting on H_{B^5} is:

$$D_\mu H_{B^5} = [\partial_\mu + ig' Y^{H_{B^5}} B_{I,\mu} - ig' Y^{H_{B^5}} B_{II,\mu}] H_{B^5} \quad (4.8)$$

3. H_I transforms under $SU(2)_I \times U(1)_I$ as $(\mathbf{2}, +Y_I^{H_I})$.

Again, this transformation property implies a covariant derivative acting on H_I of the form:

$$D_\mu H_I = \left[\partial_\mu - ig \frac{\vec{\tau}}{2} \vec{W}_{I,\mu} - ig' Y_I^{H_I} B_{I,\mu} \right] H_I \quad (4.9)$$

4. Finally, H_{II} transforms under $SU(2)_{II} \times U(1)_{II}$ as $(\mathbf{2}, +Y_{II}^{H_{II}})$. Subsequently, the covariant derivative acts on H_{II} as:

$$D_\mu H_{II} = \left[\partial_\mu - ig \frac{\vec{\tau}}{2} \vec{W}_{II,\mu} - ig' Y_{II}^{H_{II}} B_{II,\mu} \right] H_{II} \quad (4.10)$$

In the definition of the covariant derivatives, we fixed the gauge couplings g and g' to be equal for both the $SU(2)$ and $U(1)$ groups, respectively. This has already been specified in the moose diagram fig. 4.1 and implements the discrete \mathcal{Z}_2 reflection symmetry of our theory under $I \leftrightarrow II$ exchange responsible for the stability of the DM-candidate.

Parameterization of the Higgs Fields

The scalar sector of our theory mediates the symmetry breaking according to the moose diagram in section 4.1. Contrary to other work on latticized extra dimensions (cf. e.g. [51, 54]) we implement the breaking via fundamental Higgs fields with properties discussed below.

1. H_{W^5} transforms under the bi-fundamental representation as $H_{W^5} \mapsto G_{SU(2)_{II}} H_{W^5} G_{SU(2)_I}^\dagger$, where the G_j 's are elements of the respective $SU(2)$ group. As noted before, H_{W^5} can be represented as a complex 2×2 matrix. It is instructive to expand the complex 2×2 H_{W^5} field in terms of the τ matrices $\tau^0, \tau^+, \tau^-, \tau^3$, which form a basis of $\mathcal{M}_2(\mathbb{C})$.

$$H_{W^5} = \sum_{\alpha=0,\pm,3} \phi_\alpha(x) \tau^\alpha \quad (4.11)$$

We use the Pauli matrices in the form:

$$\tau^1 = \begin{pmatrix} 0 & 1 \\ 1 & 0 \end{pmatrix} \quad \tau^2 = \begin{pmatrix} 0 & -i \\ i & 0 \end{pmatrix} \quad \tau^3 = \begin{pmatrix} 1 & 0 \\ 0 & -1 \end{pmatrix} \quad (4.12)$$

In (4.11), we defined the 2×2 identity matrix τ^0 and introduced the $SU(2)$ raising and lowering operators $\tau^\pm = \frac{1}{2}(\tau^1 \pm i\tau^2)$. As will be shown, this parameterization indicates the charge assignment of the unbroken $U(1)_{em}$ for each H_{W^5} component. The charge assignment for the expansion coefficients ϕ_α is clarified by investigating an infinitesimal gauge transformation around the 3 axis of $SU(2)_{diag}$. H_{W^5} is not charged under any $U(1)$, which is why $(Q = T_3 + \frac{Y}{2})$ [40] reduces to $Q = T_3 \propto \tau^3$ in the absence of hypercharge Y and we are left with:

$$\delta H_{W^5} \propto [\tau^3, H_{W^5}] \propto q$$

$$[\tau^3, \tau^+] \propto +\tau^+ \quad [\tau^3, \tau^-] \propto -\tau^- \quad (4.13)$$

$$[\tau^3, \tau^0] = 0 \quad [\tau^3, \tau^3] = 0. \quad (4.14)$$

Therefore, we write⁶

$$H_{W^5} = \begin{pmatrix} \frac{1}{\sqrt{2}}(v_3 + \psi_{w^5,1}[x] - i\chi_{w^5,1}^{(3)}[x]) & v_4 + i\chi_{w^5,1}^{(+)}[x] \\ v_5 + i\chi_{w^5,2}^{(-)}[x] & \frac{1}{\sqrt{2}}(v_6 + \psi_{w^5,2}[x] - i\chi_{w^5,2}^{(3)}[x]) \end{pmatrix}, \quad (4.15)$$

with general VEV's in all components of the field. The VEV's are determined by the potential minimum which is encoded in the tadpole equations.

2. H_{B^5} is a complex scalar singlet charged under $U(1)_I \times U(1)_{II}$

$$H_{B^5} = \frac{1}{\sqrt{2}} \begin{pmatrix} v_1 + h_{B^5}^{(1)}[x] + ih_{B^5}^{(2)}[x] \end{pmatrix} \quad (4.16)$$

3. H_I is a complex scalar doublet charged under $SU(2)_I \times U(1)_I$ according to $(T_I^3, Y_I^{H_I})$, where T_I^3 is fixed by the representation of H_I and $Y_I^{H_I}$ will be set to the common hypercharge Y in later calculations. It is convenient to chose a parameterization in terms of charged, scalar and pseudoscalar degrees of freedom:

$$H_I = \begin{pmatrix} i\chi_I^{(+)}[x] \\ \frac{1}{\sqrt{2}}(v + \psi_I[x] - i\chi_I^{(3)}[x]) \end{pmatrix} \quad (4.17)$$

4. H_{II} is a complex scalar doublet charged under $SU(2)_{II} \times U(1)_{II}$.

We parameterize H_{II} as:

$$H_{II} = \begin{pmatrix} i\chi_{II}^{(+)}[x] \\ \frac{1}{\sqrt{2}}(v + \psi_{II}[x] - i\chi_{II}^{(3)}[x]) \end{pmatrix} \quad (4.18)$$

⁶According to [51], it is possible to choose potential parameters such that H_{W^5} acquires a vacuum expectation value v_2 proportional to the identity matrix.

The Higgs Potential

In this thesis, we consider the following scalar potential⁷ for our multi-Higgs system:

$$\mathbf{V}_{\text{Higgs}} = \mathbf{V}[H_{W^5}] + \mathbf{V}[H_I] + \mathbf{V}[H_{II}] + \mathbf{V}[H_{B^5}] + \mathbf{V}_{WW}$$

$$\begin{aligned} V[H_{W^5}] = & -M^2 \text{tr}[H_{W^5}^\dagger H_{W^5}] + \lambda_1 \text{tr}[(H_{W^5}^\dagger H_{W^5})^2] \\ & + \lambda_2 (\text{tr}[H_{W^5}^\dagger H_{W^5}])^2 + M' (e^{i\theta} \det(H_{W^5}) + h.c.) \end{aligned}$$

$$V[H_I] = -\mu^2 |H_I|^2 + \lambda |H_I|^4 \quad (4.19)$$

$$V[H_{II}] = -\mu^2 |H_{II}|^2 + \lambda |H_{II}|^4$$

$$V[H_{B^5}] = -\mu_B^2 |H_{B^5}|^2 + \lambda_B |H_{B^5}|^4$$

$$V_{WW} = M_0^2 \left(\left| \frac{H_{W^5}^\dagger H_{II}}{v_2} - \frac{H_I H_{B^5}}{v_1} \right|^2 + \left| \frac{H_{W^5} H_I}{v_2} - \frac{H_{II} H_{B^5}^\dagger}{v_1} \right|^2 \right)$$

Our scalar potential is inspired by the one introduced for the latticized extradimensional Standard Model [51]. It respects gauge invariance and fulfills the common renormalizability condition, i.e. no coupling constants with negative mass dimension [41].

The scalar potential (4.19) allows a vacuum structure, so that all Higgs fields acquire VEVs according to the moose diagram in fig. 4.1. Due to the coupling of the gauge to the scalar sector via the covariant derivatives (see paragraph 4.2.2), the vacuum structure leads to a gauge boson mass spectrum which reflects the symmetry breaking pattern $SU(2)_I \times SU(2)_{II} \times U(1)_I \times U(1)_{II} \rightarrow SU(2)_{diag} \times U(1)_{diag} \rightarrow U(1)_{em}$. Owing to (4.19), we obtain a gauge sector which contains one massless particle - the SM photon - in addition to seven massive modes. These are the $W_{(0)}^\pm$ and $Z^{(0)}$ -bosons from the SM as well as their heavy KK-counterparts (see discussion in the introductory chapter 3.4). To guarantee the stability of our dark matter candidate, we implement an additional \mathcal{Z}_2 symmetry that limits the number of allowed interactions. This is achieved via a discrete reflection symmetry of the moose diagram in fig. 4.1 under $I \leftrightarrow II$ exchange, which the scalar potential has to respect as well.

⁷We follow the convention of [51]. Note, that M' has mass dimension 2, due to the particular representation of H_{W^5} .

Eq. (4.19) is not the most general multi-Higgs model one can envision. We have for instance neglected terms of the form $|H_I|^2 |H_{II}|^2$ and similar quartic interactions. Fortunately, we can show in a simple order of magnitude estimate, that the scalar degrees of freedom are irrelevant for the Sommerfeld enhancement to vector dark matter in the majority of the parameter space (see discussion in Sec. 3.2.1), which is the primary concern of this thesis. The above statement holds as long as we do not consider special parameter regions where fine-tuning could lead to near mass degeneracies of the heavy scalars with the dark matter candidate or regions where $m_{scalar} \approx 2m_{DM}$. In the following we are going to disregard these possibilities. In some sense, the most important task of our scalar sector becomes the implementation of the correct vacuum structure in order to give the desired gauge boson mass spectrum. The desired mass hierarchy is implemented by the vacuum expectation values of the scalar fields which in turn are determined by the scalar potential and its parameters.

4.2.3. Counting the Degrees of Freedom

Before symmetry breaking⁸, the gauge bosons are massless in order for the Lagrangian to respect gauge invariance. Analog to the SM-photon, each massless vector particle accounts for two real degrees of freedom. Our theory contains eight gauge bosons, three from the respective SU(2) and one from each U(1) group. In the course of spontaneous symmetry breaking, gauge bosons that are associated with broken group generators, acquire mass via the Higgs mechanism. In this process, the Goldstone bosons from the scalar sector get "eaten" to become the longitudinal component of the gauge field. For the scalar sector, the number of degrees of freedom for each field is determined by its representation under the gauge groups. For completeness, we list the degrees of freedom:

before symmetry breaking:		after symmetry breaking	
$SU(2)_I$ gauge bosons (massless)	3x2 dof	7 massive vector bosons	7x3 dof
$SU(2)_{II}$ gauge bosons (massless)	3x2 dof	1 massless vector boson	1x2 dof
$U(1)_I$ gauge boson (massless)	1x2 dof	total	23 dof
$U(1)_{II}$ gauge boson (massless)	1x2 dof		
H_{W^5} bifundamental representation	8 dof		
H_{B^5} complex scalar singlet	2 dof		
H_I complex scalar doublet	4 dof		
H_{II} complex scalar doublet	4 dof		
total	34 dof	\Rightarrow 11 dof for scalar fields	

⁸For details concerning spontaneous symmetry breaking and the Higgs mechanism, c.f. e.g. [40, 41, 58]

4.3. SU(2)_I × SU(2)_{II} → SU(2)_{diag} Breaking

The analysis in this section is meant to be a pedagogical preparation for the symmetry breaking of the complete gauge model. Furthermore, it constitutes a reasonable consistency check, whether the H_{W^5} potential (4.20) is able to induce the desired breaking pattern $SU(2)_I \times SU(2)_{II} \rightarrow SU(2)_{diag}$. This breaking scheme is equivalent to a Higgs sector containing three Goldstone bosons that get "eaten" to become the longitudinal components of the vector bosons of the broken $SU(2)$ gauge group. The following calculation only takes into account the H_{W^5} potential and does not consider mixing terms with the other Higgs fields which will be discussed in Sec. 4.5. The notation and the potential is adopted from [51].

4.3.1. H_{W^5} Potential to Break the SU(2)_I × SU(2)_{II} Gauge Group

We consider a Higgs potential that allows a common VEV on the diagonal entries of the H_{W^5} field in order to break $SU(2)_I \times SU(2)_{II} \rightarrow SU(2)_{diag}$ which we will identify with the Standard Model $SU(2)_L$ later. Gauge covariance and renormalizability limited the number of operators that had to be considered. Following [51, 53, 54] the potential at hand is:

$$V[H_{W^5}] = -M^2 \text{tr}[H_{W^5}^\dagger H_{W^5}] + \lambda_1 \text{tr}[(H_{W^5}^\dagger H_{W^5})^2] + \lambda_2 (\text{tr}[H_{W^5}^\dagger H_{W^5}])^2 + M' (e^{i\theta} \det[H_{W^5}] + h.c.) \quad (4.20)$$

where we have used the notation of $\text{tr}[\dots]$ and $\det[\dots]$ to construct gauge singlets of H_{W^5} :

- $(H_{W^5}^\dagger H_{W^5})_{il} = (H_{W^5}^*)_{i\alpha} (H_{W^5})_{\alpha l} \Rightarrow \text{tr}[H_{W^5}^\dagger H_{W^5}] = (H_{W^5}^*)_{i\alpha} (H_{W^5})_{\alpha i}$
- $\det[H_{W^5}] = \epsilon^{i\alpha} (H_{W^5})_{1i} (H_{W^5})_{2\alpha}$, with the Levi-Civita symbol $\epsilon^{i\alpha}$

4.3.2. VEV Structure and Tadpole Equations for the $SU(2)_I \times SU(2)_{II} \rightarrow SU(2)_{\text{diag}}$ Breaking

Generally, the vacuum expectation values in spontaneously broken gauge theories have to be determined via minimizing the scalar potential with respect to the dynamical field variables; $\frac{\partial V(\phi_i)}{\partial \phi_j} \stackrel{!}{=} 0$. In order to obtain the so-called "tadpole equations", we expand (4.20) using the parameterization of H_{W^5} given in (4.15). Our tree-level analysis works as follows:

1. Write the H_{W^5} field with generic real VEVs in all four components of the matrix.
2. Expand the Higgs potential in terms of the dynamical degrees of freedom which gives rise to a large number of terms.
3. Identify all expressions linear in dynamical degrees of freedom (those are the tadpole terms that one obtains from the requirement that the field configuration leads to a minimum in the potential $\frac{\partial V}{\partial (h_{W^5}^{(i)})} \stackrel{!}{=} 0$) and demand their coefficients to be zero. This leads to a coupled system of equations, the tadpole-equations, connecting the vacuum expectation values to the parameters of the scalar sector.
4. Solve the tadpole equations for the VEVs and keep in mind that each extreme field configuration gives rise to a distinct solution of the tadpole equations. In particular, extreme field configurations also include local maxima or saddle points. To find a local minimum one has to assess (at least) the second derivative of the potential $(M^2)_{ij} = \frac{\partial^2 V}{\partial (h_{W^5}^{(i)}) \partial (h_{W^5}^{(j)})}$ and check the positive definiteness of the mass matrix (corresponds to Hessian matrix).

Following the outlines of [51], we can always arrange the parameters in the potential (4.20), such that the vacuum expectation value of H_{W^5} is proportional to the identity matrix with diagonal entries denoted by v_2 . Doing so, the VEVs in eq. (4.15) reduce to $v_3 = v_6 \equiv v_2$ and $v_4 = v_5 \equiv 0$ and we obtain two equivalent sets of solutions⁹ to the tadpole equations:

$$\begin{aligned} v_2^2 &= \frac{M^2 - M'}{\lambda_1 + 2\lambda_2} & v_2^2 &= \frac{M^2 + M'}{\lambda_1 + 2\lambda_2} \\ \theta &= 0 & \theta &= \pm\pi \end{aligned} \quad (4.21)$$

Besides the values for v_2 given above, there is one additional solution $v_2 = 0$ that would lead to a local maximum of the potential and is not considered any further.

⁹In order to obtain these solutions we had to solve for the relative phase θ as well, that way restricting the range of the θ parameter in our setting.

4.3.3. The Scalar Mass Spectrum for the SU(2)_I × SU(2)_{II} → SU(2)_{diag} Breaking

Determining the scalar mass spectrum for a given scalar potential is a straight forward but somewhat tedious assignment. Therefore, we developed a *Mathematica* routine to extract all expressions from the potential (4.20) that are bilinear in dynamical degrees of freedom. We are going to give the main results for a parameterization of H_{W^5} in terms of charged, scalar and pseudoscalar modes, since this parameterization facilitates the physical interpretation of different field components. In the following we are going to decompose the scalar mass matrix into a charged and neutral block:

1. The charged scalar mass matrix is defined via:

$$\left(\chi_{w^5,1}^{(+)} \chi_{w^5,2}^{(+)} \right) \left(\widehat{M}_{H_{W^5}}^{\text{ch}} \right)^2 \left(\chi_{w^5,1}^{(-)} \chi_{w^5,2}^{(-)} \right)^T, \quad (4.22)$$

where χ^\pm have been defined in eq. (4.15). After collecting the relevant expressions from the potential, we find:

$$\left(\widehat{M}_{H_{W^5}}^{\text{ch}} \right)^2 = \begin{pmatrix} -M^2 + 2v_2^2(\lambda_1 + \lambda_2) & e^{i\theta} M' - v_2^2 \lambda_1 \\ e^{-i\theta} M' - v_2^2 \lambda_1 & -M^2 + 2v_2^2(\lambda_1 + \lambda_2) \end{pmatrix}$$

To obtain the mass eigenstates at the potential minimum, we apply the tadpole condition (4.21) $v_2^2 = \frac{M^2 + M'}{\lambda_1 + 2\lambda_2}$ and $\theta = \pi$ to obtain the following spectrum:

$$\left(0, \frac{2M^2 \lambda_1 + 4M'(\lambda_1 + \lambda_2)}{\lambda_1 + 2\lambda_2} \right) \quad (4.23)$$

The massless mode belongs to the symmetric eigenvector¹⁰ $(1, 1)^T$, whereas the massive mode is related to the antisymmetric eigenvector $(-1, 1)^T$.

2. The neutral Higgs mass matrix is defined by¹¹:

$$\frac{1}{2} \left(\psi_{W^5,1} \psi_{W^5,2} \chi_{W^5,1}^{(3)} \chi_{W^5,2}^{(3)} \right) \left(\widehat{M}_{H_{W^5}}^{\text{n}} \right)^2 \left(\psi_{W^5,1} \psi_{W^5,2} \chi_{W^5,1}^{(3)} \chi_{W^5,2}^{(3)} \right)^T.$$

The expansion of (4.20) yields:

$$\left(\widehat{M}_{H_{W^5}}^{\text{n}} \right)^2 = \begin{pmatrix} -M^2 + v_2^2(3\lambda_1 + 4\lambda_2) & 2v_2^2 \lambda_2 + M' \cos(\theta) & 0 & M' \sin(\theta) \\ 2v_2^2 \lambda_2 + M' \cos(\theta) & -M^2 + v_2^2(3\lambda_1 + 4\lambda_2) & M' \sin(\theta) & 0 \\ 0 & M' \sin(\theta) & -M^2 + v_2^2(\lambda_1 + 2\lambda_2) & -M' \cos(\theta) \\ M' \sin(\theta) & 0 & -M' \cos(\theta) & -M^2 + v_2^2(\lambda_1 + 2\lambda_2) \end{pmatrix}. \quad (4.24)$$

Applying the tadpole conditions $v_2^2 = \frac{M^2 + M'}{\lambda_1 + 2\lambda_2}$ and $\theta = \pi$ in the neutral sector leads to the following eigenvalues of $\left(\widehat{M}_{H_{W^5}}^{\text{n}} \right)^2$:

$$\left(0, 2M', 2(M^2 + M'), \frac{2M^2 \lambda_1 + 4M'(\lambda_1 + \lambda_2)}{\lambda_1 + 2\lambda_2} \right), \quad (4.25)$$

¹⁰Normalization of all eigenvectors is implied, such that the kinetic terms are canonically normalized.

¹¹The factor $\frac{1}{2}$ for the definition of neutral masses as $\frac{m^2}{2}$ in the Lagrangian is factored out.

which belong to the eigenvectors $(0, 0, -1, 1)^T$, $(0, 0, 1, 1)^T$, $(1, 1, 0, 0)^T$ and $(-1, 1, 0, 0)^T$ respectively. Note, for $\theta = 0, \pm\pi$ there is no scalar-pseudoscalar mixing and different parity states remain decoupled.

The analytic results for the scalar mass spectrum obtained from the $SU(2)_I \times SU(2)_{II} \rightarrow SU(2)_{\text{diag}}$ breaking look very promising¹². In total we obtain three massless modes - two in the charged and one in the neutral Higgs sector. These correspond to two charged Goldstone bosons required to give mass to the charged gauge bosons of the broken $SU(2)$. Analogously, the neutral Goldstone boson plays the role of the longitudinal component of the neutral massive gauge boson. In a more general treatment with an R_ξ gauge fixing prescription applied, we expect the three massless Goldstone modes to acquire gauge parameter dependent masses. We deal with the gauge fixing Lagrangian and its influence on the Goldstone boson masses in Appendix B and direct our attention to the gauge boson sector.

4.3.4. The Gauge Boson Mass Spectrum for the $SU(2)_I \times SU(2)_{II} \rightarrow SU(2)_{\text{diag}}$ Breaking

In models with spontaneous symmetry breaking via the Higgs mechanism [59], the gauge bosons acquire their mass when the scalar fields develop a vacuum expectation value. In this case, the kinetic term for the scalar field, $\text{tr} [D_\mu H_{W^5}]^2$, contains mass terms $W^\alpha M_{\alpha\beta}^2 W^\beta$, $\alpha, \beta \in \{1, 2, 3\}$ for the gauge bosons W^α . In eq. (4.7) it is advantageous to rotate the gauge field basis:

$$W_{j,\mu}^\pm = \frac{1}{\sqrt{2}} (W_{j,\mu}^1 \mp iW_{j,\mu}^2) \quad \tau^\pm = \frac{1}{2} (\tau^1 \pm i\tau^2), \quad (4.26)$$

using $SU(2)$ -raising and -lowering operators:

$$\tau^+ = \begin{pmatrix} 0 & 1 \\ 0 & 0 \end{pmatrix} \quad \tau^- = \begin{pmatrix} 0 & 0 \\ 1 & 0 \end{pmatrix}. \quad (4.27)$$

This substitution yields:

$$\left(\vec{\tau} \cdot \vec{W}_{j,\mu} \right) = \sqrt{2} (\tau^+ W_{j,\mu}^+ + \tau^- W_{j,\mu}^-) + \tau^3 W_{j,\mu}^3, \quad (4.28)$$

where $j = I, II$ label the different gauge groups and the Lorentz indices $\mu \in \{0, \dots, 3\}$. With this transformation, we are able to extract the quadratic terms for the charged as well as the neutral gauge bosons and combine them in the respective mass matrices.

¹² Note that there is one scalar with mass squared directly proportional to M' . If one were to drop the $\det(H_W)$ term from the potential one loses that particular massive Higgs mode. This field corresponds to a *pseudo-Nambu-Goldstone boson* that would have occurred due to a spontaneous breaking of a global $U(1)$. Introducing the M' term in the potential breaks the global $U(1)$ explicitly and no additional Goldstone boson appears.

1. The charged gauge boson mass matrix

$$\left(\widehat{M}_{SU(2)}^{ch}\right)^2 = \begin{pmatrix} W_I^+ W_I^- & W_I^+ W_{II}^- \\ W_I^- W_{II}^+ & W_{II}^+ W_{II}^- \end{pmatrix} = \frac{1}{2} \begin{pmatrix} g^2 v_2^2 & -g^2 v_2^2 \\ -g^2 v_2^2 & g^2 v_2^2 \end{pmatrix} \quad (4.29)$$

Diagonalization of $\left(\widehat{M}_{SU(2)}^{ch}\right)^2$ yields the following eigensystem:

- a) one massless
- b) one massive mode with $m^2 = g^2 v_2^2$ belongs to the eigenvector $(-1, 1)^T$

2. The neutral gauge boson mass matrix

$$\left(\widehat{M}_{SU(2)}^n\right)^2 = \begin{pmatrix} W_I^3 W_I^3 & \frac{1}{2} W_I^3 W_{II}^3 \\ \frac{1}{2} W_I^3 W_{II}^3 & W_{II}^3 W_{II}^3 \end{pmatrix} = \frac{1}{2} \begin{pmatrix} g^2 v_2^2 & -g^2 v_2^2 \\ -g^2 v_2^2 & g^2 v_2^2 \end{pmatrix} \quad (4.30)$$

where the factor $\frac{1}{2}$ for the definition of neutral fields has already been pulled out.

Diagonalization of $\left(\widehat{M}_{SU(2)}^n\right)^2$ yields the following eigensystem:

- a) one massless mode with $m^2 = 0$ belongs to the eigenvector $(1, 1)^T$
- b) one massive mode with $m^2 = g^2 v_2^2$ belongs to the eigenvector $(-1, 1)^T$

In total we are left with three massive vector bosons from the broken SU(2). They are degenerate in mass which indicates that they belong to a triplet. On top of the massive modes, we find an unbroken SU(2) with massless gauge bosons. Thus, the spontaneous symmetry breaking via the diagonal H_{W^5} VEV is a viable starting point to proceed with the complete analysis of the full $SU(2)_I \times SU(2)_{II} \times U(1)_I \times U(1)_{II}$ model later.

A similar and straight forward analysis yields the breaking pattern of the respective U(1) groups according to $U(1)_I \times U(1)_{II} \rightarrow U(1)_{diag}$, which we do not outline explicitly. We find a mass spectrum with:

1. one massless mode belonging to the symmetric eigenvector $(1, 1)^T$
2. one massive mode¹³ with $m^2 = 2g'^2 v_1^2 Y^2$ for the antisymmetric eigenvector $(-1, 1)^T$

Note that the massive gauge bosons correspond to \mathcal{Z}_2 -odd modes, whereas the massless gauge bosons are \mathcal{Z}_2 -even under $I \leftrightarrow II$ exchange. We call these states KK-(1)- and KK-(0)-modes respectively.

¹³In comparison to the SU(2) gauge boson mass square $m^2 = g^2 v_2^2$, there is an additional factor of $\frac{1}{2}$ for the U(1) gauge boson mass square $m^2 = \frac{1}{2} g'^2 v_1^2$ ($Y = \frac{1}{2}$). This difference originates from the trace over the free SU(2) gauge indices and is ultimately a matter of defining v_2 .

4.4. $SU(2)_{\text{diag}} \times U(1)_{\text{diag}}$ Breaking

The diagonal groups get broken by the H_I and H_{II} fields, which are contained in two separate parts of the full Higgs potential (4.19):

1. In $V[H_I] = -\mu^2 |H_I|^2 + \lambda |H_I|^4$ and $V[H_{II}] = -\mu^2 |H_{II}|^2 + \lambda |H_{II}|^4$
2. In the interaction part $V_{WW} = M_0^2 \left(\left| \frac{H_{W^5}^\dagger H_{II}}{v_2} - \frac{H_I H_{B^5}}{v_1} \right|^2 + \left| \frac{H_{W^5} H_I}{v_2} - \frac{H_{II} H_{B^5}^\dagger}{v_1} \right|^2 \right)$ with H_{W^5} and H_{B^5} set to their respective VEVs $\frac{v_2}{\sqrt{2}}$ and $\frac{v_1}{\sqrt{2}}$. This leads to mass terms for H_I and H_{II} of the following form:

$$V_{WW} \mapsto M_0^2 \left(\left| \frac{H_{II}}{\sqrt{2}} - \frac{H_I}{\sqrt{2}} \right|^2 + \left| \frac{H_I}{\sqrt{2}} - \frac{H_{II}}{\sqrt{2}} \right|^2 \right) = M_0^2 |H_{II} - H_I|^2 \quad (4.31)$$

Combining the appropriate quadratic expressions in the mass matrix yields:

$$M_{H_i}^2 = \begin{pmatrix} H_I H_I & \frac{1}{2} H_I H_{II} \\ \frac{1}{2} H_{II} H_I & H_{II} H_{II} \end{pmatrix} = \begin{pmatrix} M_0^2 - \mu^2 & -M_0^2 \\ -M_0^2 & M_0^2 - \mu^2 \end{pmatrix} \quad (4.32)$$

The eigensystem of (4.32) contains one mode with $m^2 = -\mu^2$ associated to the symmetric eigenvector $(1, 1)^T$. For a suitably chosen potential parameter $M_0^2 > 2\mu^2$, the second eigenvalue $m^2 = 2M_0^2 - \mu^2$ is positive for the antisymmetric $(-1, 1)^T$ eigenmode.

We construct a unitary transformation to switch from the gauge eigenstates H_I and H_{II} to the mass eigenstates \tilde{H}_0 and \tilde{H}_1 :

$$\begin{pmatrix} H_I \\ H_{II} \end{pmatrix} = \begin{pmatrix} \frac{1}{\sqrt{2}} & -\frac{1}{\sqrt{2}} \\ \frac{1}{\sqrt{2}} & \frac{1}{\sqrt{2}} \end{pmatrix} \begin{pmatrix} \tilde{H}_0 \\ \tilde{H}_1 \end{pmatrix}. \quad (4.33)$$

In the new basis, only \tilde{H}_0 has a negative mass squared and consequently acquires a VEV v_0 , whereas the VEV of the \tilde{H}_1 remains zero. The fact that only one mass eigenstate acquires a vacuum expectation value leads to the desired property that both H_I and H_{II} have the common VEV¹⁴ $v = \frac{1}{\sqrt{2}} v_0$ in the gauge eigenbasis. In the following, we choose to work with the \tilde{H}_0 , \tilde{H}_1 fields and parameterize the Higgs doublets as:

$$\tilde{H}_0 = \begin{pmatrix} i\chi_0^{(+)}[x] \\ \frac{1}{\sqrt{2}}(v_0 + \psi_0[x] + i\chi_0^{(3)}[x]) \end{pmatrix} \quad \tilde{H}_1 = \begin{pmatrix} i\chi_1^{(+)}[x] \\ \frac{1}{\sqrt{2}}(\psi_1[x] + i\chi_1^{(3)}[x]) \end{pmatrix}$$

¹⁴this VEV assignment is a result of the additional factor $\frac{1}{\sqrt{2}}$ in the rotation matrix

4.5. Complete Higgs Mass Spectrum

Having completed the discussion of preliminary breaking schemes, we are in the position to calculate the Higgs mass spectrum of the entire $SU(2)_I \times SU(2)_{II} \times U(1)_I \times U(1)_{II}$ system. We use the Higgs potential given in eq. (4.19) and write all fields in terms of charged, scalar and pseudoscalar degrees of freedom. The procedure to determine the tadpole equations is completely analogous to the one described for the $SU(2)_I \times SU(2)_{II}$ breaking (see Sec. 4.3) and shall not be repeated here in detail. The expansion of the complete scalar potential yields a plethora of terms, fortunately, an automated procedure allows us to extract the relevant expressions in *Mathematica*.

4.5.1. Tadpole Equations and Potential Minimum

For the tadpole equations, we collect all terms linear in scalar dynamical degrees of freedom from (4.19) and demand their coefficients to be identically zero (extremum condition) at tree level¹⁵. This leads to a coupled system of equations that can be solved analytically. To find the vacuum structure of the complete theory we solve for the VEVs in terms of the remaining potential parameters and obtain the following results¹⁶:

$$\begin{aligned}
 v_0 &= \frac{\sqrt{2}\mu}{\sqrt{\lambda}} \Rightarrow v = \frac{1}{\sqrt{2}}v_0 = \frac{\mu}{\sqrt{\lambda}} \\
 v_1 &= \frac{\mu_B}{\sqrt{\lambda_B}} \\
 v_2 &= \frac{\sqrt{M^2 + M'}}{\sqrt{\lambda_1 + 2\lambda_2}} \\
 \theta &= \pi.
 \end{aligned} \tag{4.34}$$

In (4.34), v denotes the VEV for the H_I and H_{II} fields, v_1 belongs to H_{B^5} and v_2 is the VEV in the diagonal entries of H_{W^5} .

¹⁵N.B. that we expand our scalar fields around the vacuum expectation values.

¹⁶Note, there are other classes of solutions to the tadpole equations of our scalar potential (4.19) that do not give VEVs to all Higgs fields and consequently lead to a different mass spectrum in the Higgs as well as in the gauge boson sector. Many of these extremes belong to local maxima or saddle points of the potential. In those cases the scalar mass matrix has negative eigenvalues or contains additional zero mass modes. Note that we did not check all solutions explicitly.

4.5.2. Neutral Higgs Sector

Extracting all bilinear terms of the neutral sector within (4.19) requires some effort but can be automated in a computer algebra system. In total there are 10 neutral scalar degrees of freedom that have to be combined in a 10×10 mass matrix. In the $(\chi_0^{(3)}, \psi_0, \psi_1, \psi_{W^5,1}, \psi_{W^5,2}, h_{B^5}^{(1)}, h_{B^5}^{(2)}, \chi_1^{(3)}, \chi_{W^5,2}^{(3)}, \chi_{W^5,1}^{(3)})^T$ field basis we find a matrix, that is block diagonal¹⁷:

$$(M_H^n)^2 = \begin{pmatrix} (M_{diag}^n)^2 & \mathbf{0} & \mathbf{0} \\ \mathbf{0} & (M_{scalar}^n)^2 & \mathbf{0} \\ \mathbf{0} & \mathbf{0} & (M_{ps}^n)^2 \end{pmatrix}, \quad (4.35)$$

The neutral 10×10 mass matrix decomposes into the following three blocks.

1. The diagonal block in the field basis $(\chi_0^{(3)} \psi_0 \psi_1) (M_{diag}^n)^2 (\chi_0^{(3)} \psi_0 \psi_1)^T$

$$(M_{diag}^n)^2 = \begin{pmatrix} 0 & 0 & 0 \\ 0 & v_0^2 \lambda & 0 \\ 0 & 0 & 2M_0^2 + v_0^2 \lambda \end{pmatrix} \quad (4.36)$$

2. The scalar block in the field basis $(\psi_{W^5,1} \psi_{W^5,2} h_{B^5}^{(1)}) (M_{scalar}^n)^2 (\psi_{W^5,1} \psi_{W^5,2} h_{B^5}^{(1)})^T$

$$(M_{scalar}^n)^2 = \begin{pmatrix} M' + 2v_2^2(\lambda_1 + \lambda_2) & -M' + 2v_2^2\lambda_2 & 0 \\ -M' + 2v_2^2\lambda_2 & M' + \frac{M_0^2 v_0^2 + 4v_2^4(\lambda_1 + \lambda_2)}{2v_2^2} & -\frac{M_0^2 v_0^2}{2v_1 v_2} \\ 0 & -\frac{M_0^2 v_0^2}{2v_1 v_2} & \frac{M_0^2 v_0^2}{2v_1^2} + 2v_1^2 \lambda_B \end{pmatrix} \quad (4.37)$$

3. The pseudo-scalar block in the field basis $(h_{B^5}^{(2)} \chi_1^{(3)} \chi_{W^5,2}^{(3)} \chi_{W^5,1}^{(3)}) (M_{ps}^n)^2 (h_{B^5}^{(2)} \chi_1^{(3)} \chi_{W^5,2}^{(3)} \chi_{W^5,1}^{(3)})^T$

$$(M_{ps}^n)^2 = \begin{pmatrix} \frac{M_0^2 v_0^2}{2v_1^2} & \frac{M_0^2 v_0}{v_1} & -\frac{M_0^2 v_0^2}{2v_1 v_2} & 0 \\ \frac{M_0^2 v_0}{v_1} & 2M_0^2 & -\frac{M_0^2 v_0}{v_2} & 0 \\ -\frac{M_0^2 v_0^2}{2v_1 v_2} & -\frac{M_0^2 v_0}{v_2} & M' + \frac{M_0^2 v_0^2}{2v_2^2} & M' \\ 0 & 0 & M' & M' \end{pmatrix} \quad (4.38)$$

The first block (4.36) is already diagonal and we are able to read off the eigenvalues straight away. The first massless Goldstone mode is found in this sector.

¹⁷ In (4.36), (4.37) and (4.38) the tadpole relations have already been applied. However, instead of plugging in the minimization condition for the VEVs we have solved for the mass parameters of the potential $\left\{ \mu \rightarrow \frac{v_0 \sqrt{\lambda}}{\sqrt{2}}, \mu_B \rightarrow v_1 \sqrt{\lambda_B}, M \rightarrow \sqrt{-M' + v_2^2 \lambda_1 + 2v_2^2 \lambda_2}, \theta \rightarrow -\pi \right\}$, which makes the mass matrices look somewhat more compact.

The block diagonal form of (4.35) implies that scalar and pseudoscalar modes do not mix in our tree-level calculation.

Remarks on the Diagonalization of $(M_{scalar}^n)^2$ and $(M_{ps}^n)^2$

The structure of $(M_{scalar}^n)^2$ (4.37) makes it particularly hard to diagonalize, even though it is "merely" a real 3×3 matrix. The analytic results of the diagonalization look very complicated and we are not able to give a compact form for the eigenvalues and their respective eigenvectors.

However, looking at the structure of (4.37) and using physical input for the parameter values, we realize that the off-diagonal terms which mix $\psi_{W^{5,2}}$ and $h_{B^5}^{(1)}$ are proportional to $\frac{v_0^2}{v_1 v_2}$. In our model, the VEVs v_0 and $v_{1,2}$ are of $\mathcal{O}(250 \text{ GeV})$ and $\mathcal{O}(\text{TeV})$ respectively, thus these mixing elements are suppressed by the mass hierarchy between the Standard Model particles and the 1st heavy excitations. As a first approximation to the exact eigenvalues, we therefore diagonalize $(M_{scalar}^n)^2$, neglecting terms of $\mathcal{O}\left(\frac{v_0^2}{v_1 v_2}\right)$, i.e. we ignore further mixing via a Standard Model like Higgs field. In comparison to the gauge sector where the additional mass splitting is of utmost importance for the Sommerfeld effect, this does not play an important role in the Higgs sector. In this approximation we find the eigenspectrum:

$$(M_{scalar}^n)^2 \approx \{2(M' + v_2^2 \lambda_1), 2(v_2^2 \lambda_1 + 2v_2^2 \lambda_2), 2v_1^2 \lambda_B\} \quad (4.39)$$

with the corresponding eigenvectors:

$$\{(-1, 1, 0)^T, (1, 1, 0)^T, (0, 0, 1)^T\} \quad (4.40)$$

The pseudoscalar mass matrix (4.38) can also be diagonalized analytically, yielding another two massless Goldstone bosons. The exact results are rather lengthy, which is why we only give the approximate values here. Neglecting terms of order $\mathcal{O}\left(\frac{v_0}{v_2}\right)$, we obtain the approximate eigenvalues:

$$(M_{ps}^n)^2 \approx \{0, 0, 2M_0^2, 2M'\} \quad (4.41)$$

with the corresponding eigenvectors:

$$\{(0, 0, -1, 1)^T, (1, 0, 0, 0)^T, (0, 1, 0, 0)^T, (0, 0, 1, 1)^T\} \quad (4.42)$$

4.5.3. Charged Higgs Sector

Having treated the complete neutral Higgs sector, we extract the mass matrix for the charged degrees of freedom in terms of $(\chi_0^{(+)} \chi_1^{(+)} \chi_{W^5,1}^{(+)} \chi_{W^5,2}^{(+)}) (M_H^{ch})^2 (\chi_0^{(-)} \chi_1^{(-)} \chi_{W^5,1}^{(-)} \chi_{W^5,2}^{(-)})^T$ from (4.19). After applying the tadpole conditions, we are left with a 4×4 matrix of the following form:

$$(M_H^{ch})^2 = \begin{pmatrix} 0 & 0 & 0 & 0 \\ 0 & 2M_0^2 & -\frac{M_0^2 v_0}{2v_2} & -\frac{M_0^2 v_0}{2v_2} \\ 0 & -\frac{M_0^2 v_0}{2v_2} & M' + \frac{M_0^2 v_0^2}{4v_2^2} + v_2^2 \lambda_1 & -M' - v_2^2 \lambda_1 \\ 0 & -\frac{M_0^2 v_0}{2v_2} & -M' - v_2^2 \lambda_1 & M' + \frac{M_0^2 v_0^2}{4v_2^2} + v_2^2 \lambda_1 \end{pmatrix} \quad (4.43)$$

$(M_H^{ch})^2$ can be diagonalized analytically, yielding the eigenspectrum:

$$\left\{ 0, 0, \frac{1}{4} M_0^2 \left(8 + \frac{v_0^2}{v_2^2} \right), 2M' + \frac{M_0^2 v_0^2}{4v_2^2} + 2v_2^2 \lambda_1 \right\} \quad (4.44)$$

In total there are 7 massless Goldstone bosons in addition to 11 massive Higgs modes, which is exactly the mass spectrum we expect for a theory containing 1 massless and 7 massive gauge bosons (see Sec. 4.2.3).

4.5.4. Higgs Boson Summary

In this section, we work towards one particular application of our model. In order to obtain a sizable Sommerfeld enhancement¹⁸ to vector dark matter, we opt for a mass spectrum where the neutral vector dark matter candidate is nearly mass degenerate with the accompanying heavy states from the same gauge multiplet. This direction in mind, we try to find regions in the model parameter space, such that the $Z^{(1)}$ gauge boson remains the lightest non-SM particle and is nearly degenerate with the $W_{(1)}^\pm$ gauge bosons.

The hypercharge Y , as well as the gauge couplings for the $SU(2)$ s and $U(1)$ s are going to be determined in Sec. 4.6.4 by comparing the low mass modes of our gauge sector to their Standard Model counterparts. We pre-empt the results¹⁹ $Y = \frac{1}{2}$, $g = 0.652 \cdot \sqrt{2}$ and $g' = 0.357 \cdot \sqrt{2}$ and also fix $v_0 = 246$ GeV as well as $\lambda = 0.26$, so that the SM-Higgs in (4.36) obtains a mass $m_{H^{(0)}} = v_0 \sqrt{\lambda} \approx 125$ GeV, consistent with recent evidence from ATLAS [60] and CMS [61]. Applying the restrictions above, we are left with seven additional parameters of our model, namely $\{M_0, M', \lambda_1, \lambda_2, \lambda_B, v_1, v_2\}$.

¹⁸see Sec. 3.2.1 for detailed discussion

¹⁹In latticized extradimensional theories [51] it is common to define the 4D gauge couplings g_1 and g_2 as $g_2 = \frac{g}{\sqrt{N+1}}$ and $g_1 = \frac{g'}{\sqrt{N+1}}$, where $N+1$ is the number of lattice sites and g, g' denotes the "5D" coupling constants. The suppression of the coupling constant by $\propto \frac{1}{\sqrt{N}}$ corresponds to the classical volume suppression in the $4+1$ dimensional theory [51].

Demanding that the neutral SU(2) gauge boson has to be the lightest stable non-Standard Model state in the spectrum²⁰, these parameters can be constrained. Neglecting the SM VEV v_0 in comparison to the new physics scale associated with v_1, v_2 , we use the preliminary results of the gauge boson spectrum (Sec. 4.3.4) and compare it to the approximate mass eigenvalues of the scalar particles (Sec. 4.5.2). Demanding SU(2)-like vector DM ($g^2 v_2^2 < \frac{1}{2} g'^2 v_1^2$), we find:

$$2v_1^2 \lambda_B > g^2 v_2^2 \qquad 2M_0^2 > g^2 v_2^2 \qquad (4.45)$$

$$2v_2^2(\lambda_1 + 2\lambda_2) > g^2 v_2^2 \qquad 2M' > g^2 v_2^2 \qquad (4.46)$$

In the following, we are going to briefly discuss the features of the scalar mass spectrum.

1st Parameter Point for the Higgs Spectrum

As starting point, we choose parameters that appear as natural as possible, i.e. ϕ^4 couplings λ_i are of $\mathcal{O}(\lesssim 1)$ and mass parameters of the new physics scale M', v_1 and v_2 are set to a TeV-scale value. In the scalar potential (4.19), we realize that M_0^2/v_2^2 is the coefficient of a ϕ^4 -interaction and therefore should be $\mathcal{O}(\lesssim 1)$ in the perturbative regime. Together with condition (4.45), we first restrict M_0 to $\frac{1}{2}g^2 v_2^2 < M_0^2 < v_2^2$ and use:

$$\begin{aligned} Y &= \frac{1}{2}; & v_0 &= 246 \text{ GeV}; & \lambda_2 &= 0.48; \\ v_1 &= 4000 \text{ GeV}; & v_2 &= 1100 \text{ GeV}; & \lambda_B &= 0.22; \\ g &= 0.652 \cdot \sqrt{2}; & g' &= 0.357 \cdot \sqrt{2}; & M' &= (10^3)^2 \text{ GeV}^2; \\ \lambda &= 0.26; & \lambda_1 &= 0.29; & M_0 &= 900 \text{ GeV}; \end{aligned} \qquad (4.47)$$

We employ the exact diagonalization of (4.36),(4.37),(4.38) and (4.43) to find numerical values for the scalar spectrum at this parameter point:

1. The neutral sector

- a) $(M_{diag}^n) : \{1279 \text{ GeV}, 125 \text{ GeV}, 0 \text{ GeV}\}$
- b) $(M_{scalar}^n) : \{2654 \text{ GeV}, 1742 \text{ GeV}, 1647 \text{ GeV}\}$
- c) $(M_{ps}^n) : \{1432 \text{ GeV}, 1262 \text{ GeV}, 0 \text{ GeV}, 0 \text{ GeV}\}$

2. The charged sector

- a) $(M_H^{ch}) : \{1647 \text{ GeV}, 1277 \text{ GeV}, 0 \text{ GeV}, 0 \text{ GeV}\}$

²⁰This is taken as input for our particular application. In general, we can obtain other DM-candidates such as the $U(1)_Y$ gauge boson or a heavy scalar field as well.

We anticipate the results for the neutral gauge bosons (4.53) in order to show, that the $Z^{(1)}$ is in fact the dark matter candidate for this parameter point:

$$\begin{aligned} m_{Z^{(1)}} &= 1017.433 \text{ GeV} \\ m_{W_{\pm}^{(1)}} &= 1017.439 \text{ GeV} \\ m_{\gamma^{(1)}} &= 1428.679 \text{ GeV}. \end{aligned}$$

Concerning the Sommerfeld phenomenology of the $Z^{(1)}$ this parameter point is very interesting, since all non-Standard Model scalar modes are split-off by $\gtrsim 200$ GeV in comparison to the $Z^{(1)}$, thereby decoupling from the effect (see Sec. 3.2.1). At the same time, all coupling constants remain within the perturbative regime. We would like to mention that the point we have chosen here, is by no means special and similar spectra are obtained with other parameter choices²¹. The massless modes in the spectrum correspond to the Goldstone bosons of the spontaneous symmetry breaking pattern $SU(2)_I \times SU(2)_{II} \times U(1)_I \times U(1)_{II} \rightarrow U(1)_{em}$. In this particular breaking scheme, there are seven broken generators, which is why we expect an equal number massless modes according to the Goldstone theorem [40].

For parameter point (4.47), we count 10 scalar modes at the TeV scale. If we compare this to a common UED spectrum (see remarks in the first paragraph of 4.2.2 or [47]), we find a mismatch of modes. This is owed to our specific description of the breaking of the extended $SU(2)_I \times SU(2)_{II} \times U(1)_I \times U(1)_{II}$ gauge group via fundamental scalars²². We can, however, show that our model is able to mimic UED in a strongly coupled region of parameter space.

2nd Parameter Point for the Scalar Spectrum - UED Spectrum

We vary the remaining free parameters to fit a UED-like scalar spectrum [47] containing one Standard Model like Higgs with a mass of $\mathcal{O}(100 \text{ GeV})$ and four additional Higgs modes around the TeV scale. In this section, we are able to find parameters in the scalar potential (4.19) so that all but $H_{(0)}^0$ and the KK-(1)-scalar fields become very massive and effectively decouple from the theory. Doing so, the additional modes become dispensable and do not contribute to low energy phenomena we are mainly interested in. However, for this to happen, we have to resort to a strongly coupled theory, which coincides with the remarks of e.g. [55]. This observation indicates, that the nonrenormalizable nature of

²¹This is true, if we keep our restrictions (4.45) in mind.

²²Cheng et al. [51] avoid some of the modes by resorting to a nonlinear σ -model to break the gauge groups and comment, that they can make all but the four scalar KK-(1)-modes very heavy by tuning the parameters in their scalar potential. For the second parameter point we follow the same spirit.

the extradimensional theory [47, 49] eventually reenters the picture if one tries to match the "deconstructed" with the continuous 5D results²³. One exemplary parameter point, that is consistent with the low energy scalar- and gauge- spectrum of an extradimensional theory is:

$$\begin{aligned}
Y &= \frac{1}{2}; & v_0 &= 246 \text{ GeV}; & \lambda_2 &= 9 \times 10^8; \\
v_1 &= 4000 \text{ GeV}; & v_2 &= 1100 \text{ GeV}; & \lambda_B &= 0.7 \times 10^8; \\
g &= 0.652 \cdot \sqrt{2}; & g' &= 0.357 \cdot \sqrt{2}; & M' &= (5.4 \times 10^5)^2 \text{ GeV}^2; \\
\lambda &= 0.26 & \lambda_1 &= 10^8; & M_0 &= 900 \text{ GeV};
\end{aligned} \tag{4.48}$$

As for the first parameter (4.47) point in paragraph 4.5.4, we use the exact diagonalization of (4.36),(4.37),(4.38) and (4.43) to find numerical expressions for the scalar spectrum²⁴:

1. The neutral sector

- a) (M_{diag}^n) : {1279 GeV, 125 GeV, 0 GeV}
- b) (M_{scalar}^n) : { 6.8×10^7 GeV, 4.7×10^7 GeV, 1.6×10^7 GeV}
- c) (M_{ps}^n) : { 7.7×10^5 GeV, 1277 GeV, 0 GeV, 0 GeV}

2. The charged sector

- a) (M_H^{ch}) : { 1.6×10^7 GeV, 1277 GeV, 0 GeV, 0 GeV}

Looking at the mass spectrum and the approximate eigenvectors (4.40) and (4.42) for the diagonalization of (4.35) we identify $\chi_1^{(3)} \leftrightarrow a_{(1)}^0$, $\psi_1 \leftrightarrow H_{(1)}^0$ and $\psi_0 \leftrightarrow H_{(0)}^0$. For the UED fields $a_{(1)}^0$ and $H_{(1)}^0$ we follow the notation introduced in Sec. 4.2.2.

4.6. Complete Gauge Boson Mass Spectrum

Having investigated the vacuum structure and mass spectrum of the scalar sector, we proceed with the calculation of the gauge boson masses. Most of the methods may be transferred from the preliminary calculations of $SU(2)_I \times SU(2)_{II}$ breaking. The vector boson masses originate from the kinetic terms of the various scalar fields (4.2) after symmetry breaking. Note, that we prefer to work with the unmodified gauge coupling constants g and g' for the moment, consequently there is no additional normalization factor $\frac{1}{\sqrt{2}}$ incorporated yet (see footnote in Sec. 4.5.4).

²³In contrast to [22], we pursue a more modest agenda and do not opt for an UV-completion of extra dimensional models.

²⁴The gauge boson masses are unaffected and remain in the 1 TeV region, since we leave the VEVs v_i untouched.

4.6.1. The Neutral Gauge Bosons

In the neutral sector we express the gauge boson mass matrix as follows:

$(B_I W_I^{(3)} B_{II} W_{II}^{(3)}) \left(\widehat{M}_{gauge}^n \right)^2 (B_I W_I^{(3)} B_{II} W_{II}^{(3)})^T$ and subsequently find²⁵:

$$\left(\widehat{M}_{gauge}^n \right)^2 = \begin{pmatrix} \frac{1}{2}g'^2 (v^2 + 2v_1^2) Y^2 & -\frac{1}{4}gg'v^2Y & -g'^2v_1^2Y^2 & 0 \\ -\frac{1}{4}gg'v^2Y & \frac{1}{8}g^2 (v^2 + 4v_2^2) & 0 & -\frac{1}{2}g^2v_2^2 \\ -g'^2v_1^2Y^2 & 0 & \frac{1}{2}g'^2 (v^2 + 2v_1^2) Y^2 & -\frac{1}{4}gg'v^2Y \\ 0 & -\frac{1}{2}g^2v_2^2 & -\frac{1}{4}gg'v^2Y & \frac{1}{8}g^2 (v^2 + 4v_2^2) \end{pmatrix}. \quad (4.49)$$

If we rotate the gauge fields to a \mathcal{Z}_2 -even and -odd basis²⁶:

$$B_{e/o}(x) \equiv B_{even/odd}(x) = \frac{1}{\sqrt{2}} (B_I(x) \pm B_{II}(x)) \quad (4.50)$$

$$W_{e/o}^{(3)}(x) \equiv W_{even/odd}^{(3)}(x) = \frac{1}{\sqrt{2}} \left(W_I^{(3)}(x) \pm W_{II}^{(3)}(x) \right), \quad (4.51)$$

the mass matrix becomes block diagonal and the \mathcal{Z}_2 -even and -odd modes decouple:

$$\begin{pmatrix} \frac{1}{2}g'^2v_0^2Y^2 & -\frac{1}{4}gg'v_0^2Y & 0 & 0 \\ -\frac{1}{4}gg'v_0^2Y & \frac{1}{8}g^2v_0^2 & 0 & 0 \\ 0 & 0 & \frac{1}{2}g'^2 (v_0^2 + 4v_1^2) Y^2 & -\frac{1}{4}gg'v_0^2Y \\ 0 & 0 & -\frac{1}{4}gg'v_0^2Y & \frac{1}{8}g^2 (v_0^2 + 8v_2^2) \end{pmatrix} \quad (4.52)$$

A subsequent diagonalization yields the eigenvalues²⁷:

$$m_{\gamma^{(0)}}^2 = 0 \quad m_{Z^{(0)}}^2 = \frac{1}{8} v_0^2 (g^2 + 4g'^2Y^2) \quad (4.53)$$

$$m_{\gamma^{(1)}, Z^{(1)}}^2 = \frac{1}{16} \left(g^2 (v_0^2 + 8v_2^2) + 4g'^2 (v_0^2 + 4v_1^2) Y^2 \right. \\ \left. \pm \sqrt{g^4 (v_0^2 + 8v_2^2)^2 + 8g^2g'^2 (v_0^4 - 4v_0^2v_1^2 - 8 (v_0^2 + 4v_1^2) v_2^2) Y^2 + 16g'^4 (v_0^2 + 4v_1^2)^2 Y^4} \right)$$

Upon redefining the gauge couplings g and g' to their 4D values (see footnote in section 4.5.4), we are compatible with the Standard Model gauge boson masses (see e.g.[58]).

In the limit $\frac{v_0^2}{v_1v_2} \ll 1$, the eigenvalues of the heavy gauge bosons simplify considerably. Setting the hypercharge $Y = \frac{1}{2}$, we obtain:

$$m_{\gamma^{(1)}, Z^{(1)}}^2 \approx \frac{1}{4} \left(g'^2v_1^2 + 2g^2v_2^2 \pm \sqrt{(g'^2v_1^2 - 2g^2v_2^2)^2} \right).$$

²⁵the factor $\frac{1}{2}$ in the definition of the neutral vector field masses has been accounted for

²⁶"Even" and "odd" can be understood in terms of the "KK-parity", i.e. the discrete \mathcal{Z}_2 reflection symmetry under $I \leftrightarrow II$ exchange of our model, which leads to the stability of the dark matter candidate.

²⁷the attribution of the mass eigenvalues to $Z^{(1)}$ and $\gamma^{(1)}$ is explained in Section 4.6.4

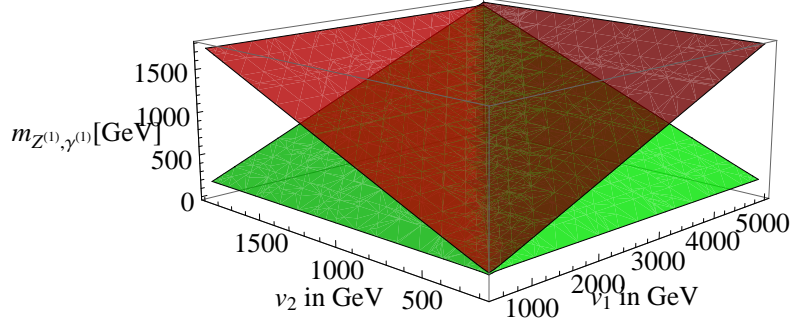


Figure 4.2.: v_1, v_2 dependence of $m_{Z^{(1)}}$ and $m_{\gamma^{(1)}}$; $Y = \frac{1}{2}$, $v_0 = 246$ GeV
The dark matter candidate is mostly SU(2) like in the parameter region
 $v_2 < a \cdot v_1$, $a \approx 0.385$. green: $m_{Z^{(1)}}$, red: $m_{\gamma^{(1)}}$

4.6.2. Mass mixing in the Neutral Sector and Weinberg Angles

The neutral gauge boson mass matrix (4.52) is diagonalized by the basis transformation:

$$\begin{pmatrix} \gamma^{(0)} \\ Z^{(0)} \\ \gamma^{(1)} \\ Z^{(1)} \end{pmatrix} = \begin{pmatrix} \gamma^{(0)} \\ Z^{(0)} \\ \text{neutral}_4 \\ \text{neutral}_3 \end{pmatrix} = \begin{pmatrix} \cos \theta_W^{(0)} & \sin \theta_W^{(0)} & 0 & 0 \\ -\sin \theta_W^{(0)} & \cos \theta_W^{(0)} & 0 & 0 \\ 0 & 0 & \cos \theta_W^{(1)} & \sin \theta_W^{(1)} \\ 0 & 0 & -\sin \theta_W^{(1)} & \cos \theta_W^{(1)} \end{pmatrix} \begin{pmatrix} B_e \\ W_e^{(3)} \\ B_o \\ W_o^{(3)} \end{pmatrix} \quad (4.54)$$

In the Standard Model sector, we immediately obtain the known tree level relations by demanding a massless photon²⁸.

$$\begin{aligned} m_{\gamma^{(0)}}^2 \stackrel{!}{=} 0 &= \frac{1}{8} v_0^2 \left(-2g'Y \cos \theta_W^{(0)} + g \sin \theta_W^{(0)} \right)^2 \\ &\Rightarrow \tan \theta_W^{(0)} = \frac{2g'Y}{g} \end{aligned} \quad (4.55)$$

The Weinberg angle in the dark sector is somewhat more involved and the relationship between $\theta_W^{(1)}$ and g, g', v_0, v_1, v_2 and Y was found by transforming (4.52) with the basis transformation (4.54) and requiring the off-diagonal mass matrix elements in the dark sector to be zero.

$$\tan \left[2 \theta_W^{(1)} \right] = \frac{4gg'v_0^2 Y}{g^2(v_0^2 + 8v_2^2) - 4g'^2 Y^2 (v_0^2 + 4v_1^2)}$$

We obtain the analytic solution for $\theta_W^{(1)}$, which we express in terms of the gauge boson masses:

$$\theta_W^{(1)} = \arccos \left[\sqrt{\frac{m_{\gamma^{(1)}}^2 - m_{W_{(1)}^\pm}^2}{m_{\gamma^{(1)}}^2 - m_{Z^{(1)}}^2}} \right]. \quad (4.56)$$

²⁸Weinberg angles are not affected by the redefinition of the gauge couplings, as they only depend on the ratios of the coupling constants and therefore the factor $\frac{1}{\sqrt{N+1}}$ drops out.

In the parameterization of $\theta_W^{(1)}$ we realize the analogy to the Standard Model eq. (A.3), where $m_{\gamma(0)}^2 = 0$. In case of near mass degeneracy between $W_{(1)}^\pm$ and $Z^{(1)}$, the mixing angle is small and hence $\cos \theta_W^{(1)}$ large. We visualize the v_1 and v_2 dependence of the dark Weinberg angle in a contour plot in order to show the parameter region in which the dark matter candidate is mostly $SU(2)$ -like.

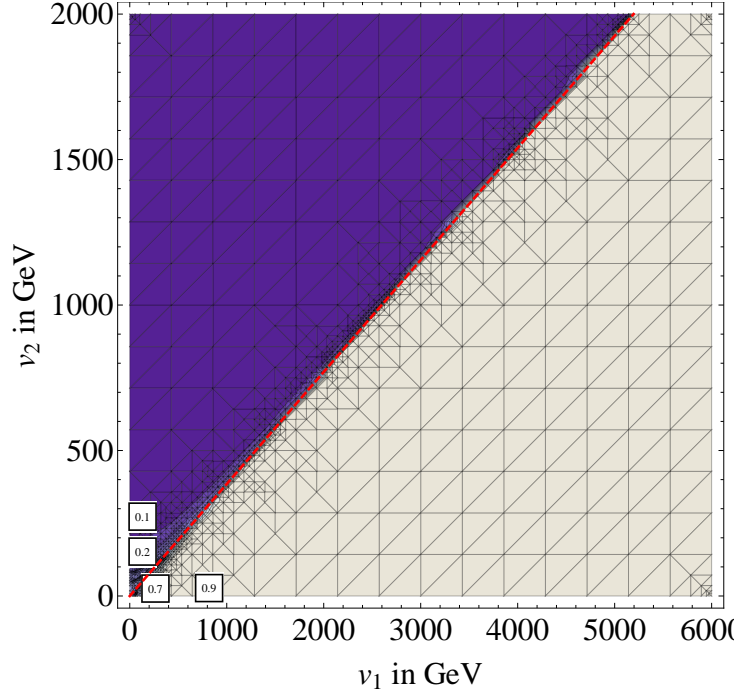


Figure 4.3.: v_1 and v_2 dependence of $\cos \theta_W^{(1)}$ for $Y = \frac{1}{2}$, $v_0 = 246$ GeV
The dark matter candidate is mostly $SU(2)$ like in the parameter region
 $v_2 < a \cdot v_1$, $a \approx 0.385$ to the right of the red dashed line

Looking at the v_1, v_2 dependence of the neutral KK-(1) gauge boson masses in fig. 4.2 combined with the v_1 and v_2 dependence of $\cos \theta_W^{(1)}$ depicted in fig. 4.3, we realize that our dark matter candidate is mostly $SU(2)$ like in the $v_2 < a \cdot v_1$, $a \approx 0.385$ region of parameter space.

The seemingly strange $a \approx 0.385$ parameter for the ratio $\frac{v_2}{v_1}$ is easily understood, once we realize that, neglecting terms of order v_0/v_1 for the gauge boson masses, the $U(1)$ gauge boson has to be as heavy as the $SU(2)$ gauge boson at the ideal mixing point. This relation implies:

$$\frac{v_2}{v_1} = \frac{g_1}{\sqrt{2}g_2} = \frac{g'}{\sqrt{2}g} = 0.387, \quad (4.57)$$

which readily explains the slope in the $v_1 - v_2$ plane.

4.6.3. The Charged Gauge Bosons

An analog treatment of the charged sector yields the mass matrix:

$$\left(\widehat{M}_{gauge}^{ch}\right)^2 = \begin{pmatrix} \frac{g^2 v_0^2}{8} + \frac{g^2 v_2^2}{2} & -\frac{1}{2} g^2 v_2^2 \\ -\frac{1}{2} g^2 v_2^2 & \frac{g^2 v_0^2}{8} + \frac{g^2 v_2^2}{2} \end{pmatrix} \quad (4.58)$$

with eigenvalues:

$$\left\{ m_{W_{(0)}}^2, m_{W_{(1)}}^2 \right\} = \left\{ \frac{g^2 v_0^2}{8}, \frac{1}{8} g^2 (v_0^2 + 8v_2^2) \right\} \quad (4.59)$$

and eigenvectors:

$$\begin{aligned} EV_{W_{(0)}}^\pm &= (1, 1)^T \\ EV_{W_{(1)}}^\pm &= (-1, 1)^T \end{aligned}$$

As for the neutral gauge fields, once we employ the redefinition of the gauge couplings $g_2 = \frac{g}{\sqrt{2}}$ and $g_1 = \frac{g'}{\sqrt{2}}$ we are consistent with the charged Standard Model gauge boson masses (see e.g. [58]).

Comparing the neutral and charged gauge boson masses, we realize that the mass splitting in the SU(2) multiplet of the dark sector is naturally small. For our analysis, we parameterize the dark sector of (4.52) as:

$$\begin{pmatrix} M_1^2 & -\Delta^2 \\ -\Delta^2 & M_2^2 \end{pmatrix}, \quad (4.60)$$

where $M_1^2 = \frac{1}{2} g'^2 (v_0^2 + 4v_1^2) Y^2$ and $M_2^2 = \frac{1}{8} g^2 (v_0^2 + 8v_2^2)$ are the mass scales of the heavy U(1) and SU(2) gauge bosons respectively. $\Delta^2 = \frac{1}{4} g g' v_0^2 Y$ is of the order of the electroweak gauge boson mass $\Delta \approx 60$ GeV. Diagonalizing (4.60) in the limit $\Delta^2 \ll |M_1^2 - M_2^2|$, we obtain the approximate eigenvalues of (4.60):

$$\lambda_2^2 = M_2^2 - \frac{\Delta^4}{M_1^2 - M_2^2} + O[\Delta]^5 \quad \lambda_1^2 = M_1^2 + \frac{\Delta^4}{M_1^2 - M_2^2} + O[\Delta]^5$$

The mass square splitting $|\Delta m^2| = |m_{W_{(1)}}^2 - m_{Z_{(1)}}^2| = |M_2^2 - \lambda_2^2|$ in the SU(2) gauge sector is $|\Delta m^2| \approx \left| \frac{\Delta^4}{M_1^2 - M_2^2} \right|$. With $M_1 \approx 1.5$ TeV and $M_2 \approx 1$ TeV (see parameter point in section 4.5.4), we obtain a natural mass splitting $|\delta m| = |m_{W_{(1)}} - m_{Z_{(1)}}| \approx \left| \frac{\Delta m^2}{2M_2} \right| \approx \mathcal{O}(10^{-2})$ GeV. Note that Δm^2 and δm are related via:

$$|\Delta m^2| = |M_2^2 - \lambda_2^2| = |(M_2 - \lambda_2)(M_2 + \lambda_2)| \approx |(\delta m)(2M_2)|$$

4.6.4. Gauge Boson Summary

We obtained analytical results for the masses of all eight gauge bosons. Seven out of the eight obtained a mass via the Higgs mechanism while the latter one corresponds to the gauge boson of an unbroken $U(1)$.

After symmetry breaking, our model contains four gauge bosons with masses independent of v_1 and v_2 . However, their masses are related to the VEV of \tilde{H}_0 which is responsible for the breaking of the $SU(2)_{diag} \times U(1)_{diag} \rightarrow U(1)$. We attribute this pattern to the breaking of the Standard Model gauge group $SU(2)_L \times U(1)_Y \rightarrow U(1)_{em}$ and consequently, identify the four gauge bosons with $W_{(0)}^\pm$, $Z_{(0)}$ -bosons and the photon of the Standard Model. Due to this identification, we are able to fix a subset of our model parameters, these are (v_0, g_1, g_2) . Numerical values are given in Appendix. A.

For the following gauge boson mass spectra plots, we set v_1 to $\mathcal{O}(\text{TeV})$ compliant with a typical scale for new physics beyond the Standard Model [3]. In particular, we tune the VEVs v_1 and v_2 in such a way that the dark matter candidate lies in the mass range of 500 GeV to several TeV. Note that a level crossing occurs in the region where $\cos\theta_W^{(1)}$ changes from ≈ 0 to ≈ 1 . This crossover scales directly with the parameter v_1 and shifts upwards (downwards) if one increases (decreases) the value of v_1 (see fig. 4.3).

As mentioned before, the Weinberg angle of the dark sector depends on the VEVs v_1 and v_2 . Subsequently, the ratio of the B-like and W-like fractions in $neutral_3$ and $neutral_4$ change with v_2 . By looking at the v_2 dependence (for fixed $v_1 = 4000$ GeV) of the gauge boson masses in figure (4.4) it is applicable that a mostly $SU(2)$ like neutral dark matter candidate is obtained in the regime below the crossing point at $v_2 \approx 1550$ GeV. In this particular region of parameter space we identify $neutral_3$ with $Z^{(1)}$ and $neutral_4$ with $\gamma^{(1)}$.

We would like to direct the attention to the $\delta m - v_2$ graph (fig. 4.6). In the analysis of the Sommerfeld enhancement, it turns out that the mass splitting between the DM-candidate and the partner states of the multiplet is of vital importance and determines the magnitude of resonant enhancement factors. In the SUSY inspired literature on the Sommerfeld effect [18, 62] a mass splitting of the order $\mathcal{O}(10^{-1})$ GeV is commonly used. In our case however, we find a tree-level mass splitting of order $\mathcal{O}(10^{-2})$ GeV in most of the parameter space, where the $SU(2)$ -like gauge boson is the DM-candidate.

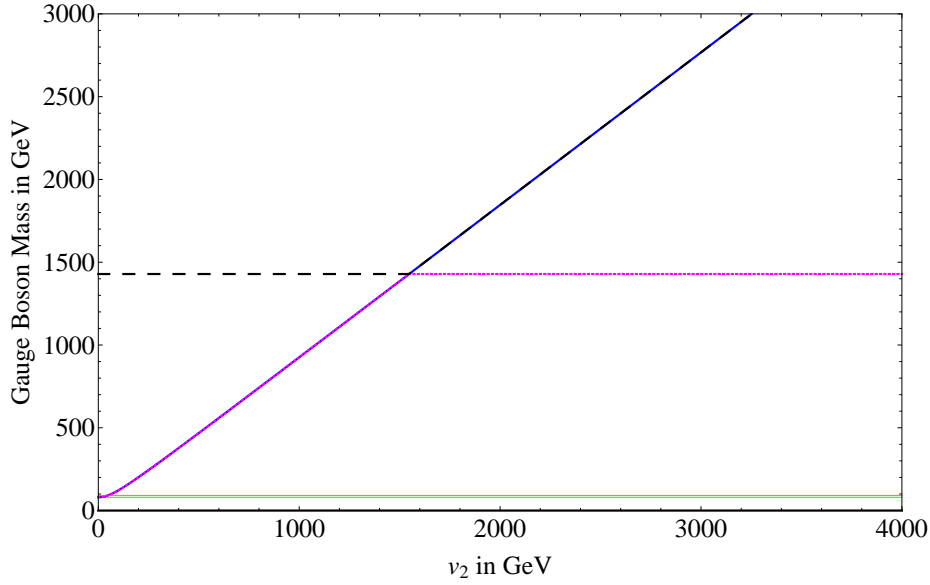


Figure 4.4.: VEV dependence of the gauge boson mass spectrum

$$v_1 = 4000 \text{ GeV}, Y = \frac{1}{2}.$$

Above the crossing point $v_2 \approx 1550 \text{ GeV}$ the DM-candidate becomes U(1)-like.

green: $W_{(0)}^\pm$ blue: $W_{(1)}^\pm$ orange: $Z^{(0)}$ dotted: $Z^{(1)}$ dashed: $\gamma^{(1)}$

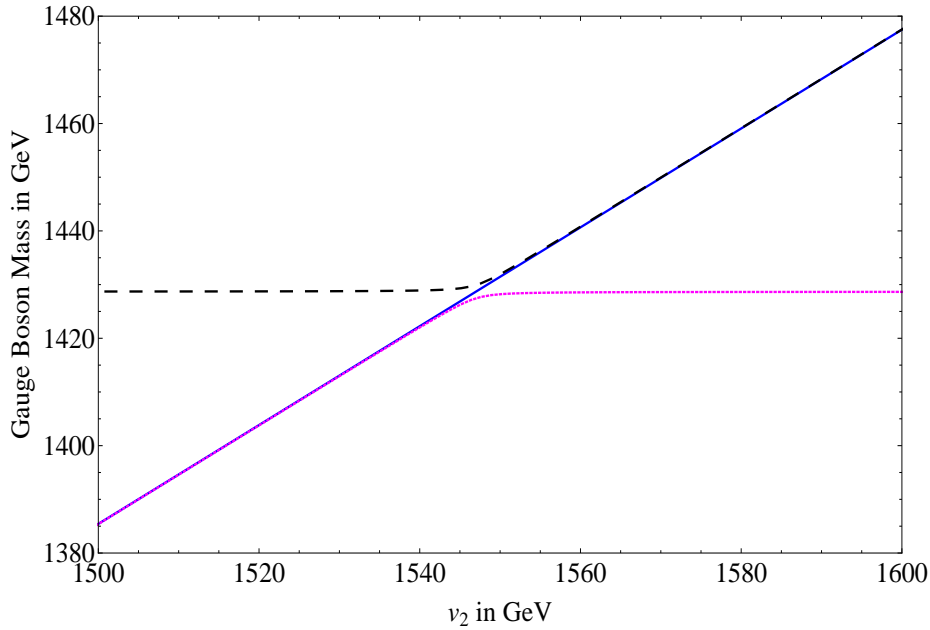


Figure 4.5.: Gauge boson mass spectrum - closeup of the level crossing. In regions where the gauge boson mass changes with v_2 the corresponding particle has mostly SU(2)-like character. Parameter choice: $v_1 = 4000 \text{ GeV}$, $Y = \frac{1}{2}$

blue: $W^{\pm(1)}$ dotted: $Z^{(1)}$ dashed: $\gamma^{(1)}$

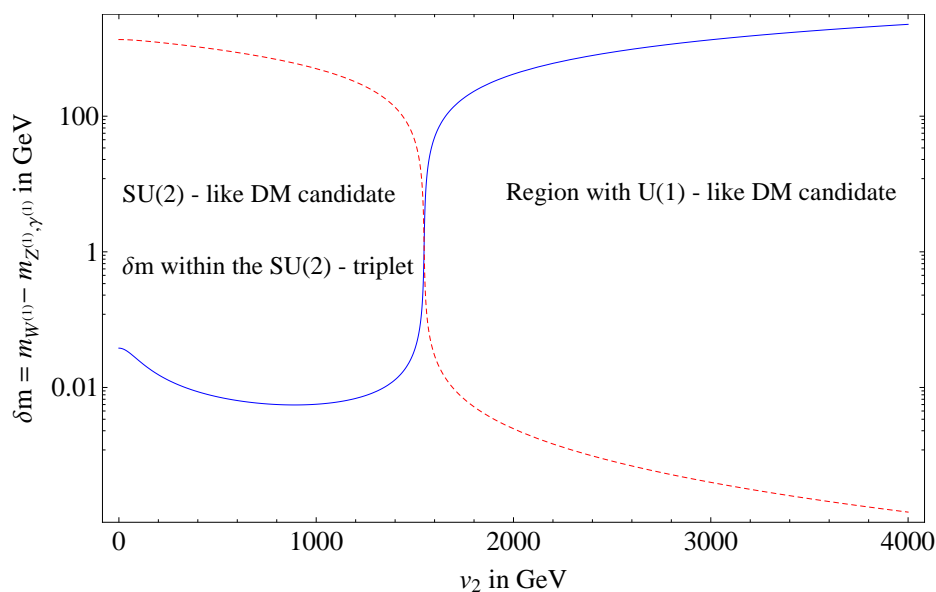


Figure 4.6.: *Generic mass splitting in the heavy gauge boson sector* $\delta m = m_{W^{(1)}} - m_{Z^{(1)}, \gamma^{(1)}}$
 $v_1 = 4000 \text{ GeV}$, $Y = \frac{1}{2}$
blue: $\delta m = m_{W_{(1)}^\pm} - m_{Z^{(1)}}$ *dashed:* $\delta m = m_{W_{(1)}^\pm} - m_{\gamma^{(1)}}$

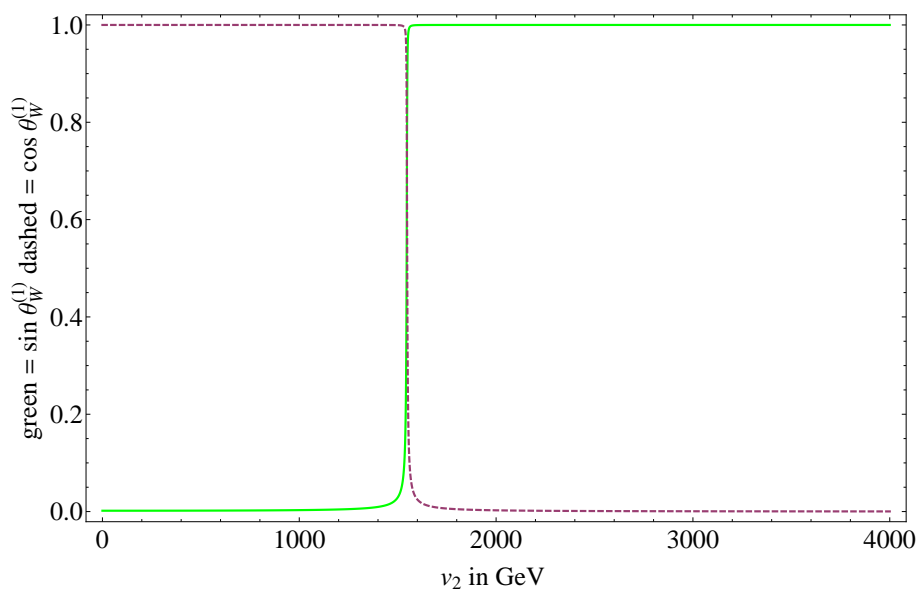


Figure 4.7.: *Weinberg mixing angle of the dark sector;* $v_1 = 4000 \text{ GeV}$, $Y = \frac{1}{2}$
green: $\sin(\theta_W^{(1)})$ *dashed:* $\cos(\theta_W^{(1)})$

4.7. Gauge Fixing and Interactions

In order to quantize a gauge theory consistently, one has to devise a mechanism to cancel or constrain redundant degrees of freedom [40, 41, 58]. In the construction of quantum electrodynamics (QED) for example, one also faces this problem. The vector field A_μ , representing the photon, principally contains four degrees of freedom, whereas the physical polarizations of the photon are the two helicity states, only. The procedure that allows constraining the artificial degrees of freedom consistently, is called gauge-fixing²⁹.

In this work, we have adapted the gauge fixing prescription of [58] to write down the gauge fixing Lagrangian (B.1) and derive the ghost interactions in Sec. B.2 for our $SU(2) \times SU(2) \times U(1) \times U(1)$ theory. The gauge fixing Lagrangian (B.1) fulfills three roles. First, it allows us to write down the generalized propagators for the gauge fields. Second, it cancels mixing terms between Goldstone bosons and gauge fields arising from the kinetic part of the scalar Lagrangian (4.5) and third, it gives rise to gauge parameter dependent masses of the Goldstone bosons. For the Sommerfeld calculation within our minimal vector dark matter model in Sec. 5.5, we employ the unitary gauge for all massive gauge bosons, where only the physical degrees of freedom are retained from the start. Therefore, we defer a detailed discussion of technical details of the gauge fixing procedure, including Goldstone bosons and Faddeev-Popov ghosts, to Appendix B.

We cover the complete gauge fixed scalar sector in B.0.3 as well as the rotation from the gauge to the mass eigenbasis in paragraph B.1.2. Upon this calculation, we are in the position to derive the interaction vertices in the physical field basis. In order to do this, we use the (approximate) eigenvectors obtained from diagonalizing the mass matrices and construct unitary transformations to relate gauge and mass eigenstates. With these transformations, we obtain the Lagrangian (4.1) in the physical field basis and are able to read off the Feynman rules, which are documented in Appendix C.

Here we summarize a list of Feynman rules, that are relevant for the calculation of the Sommerfeld effect in unitary gauge. We use the conventions of Ref.[58] for the propagators:

$$\begin{array}{l}
 \mu \bullet \text{---} \overset{V}{\text{wavy}} \text{---} \bullet \nu \\
 \bullet \text{---} \overset{\phi}{\text{dashed}} \text{---} \bullet
 \end{array}
 \quad
 \begin{array}{l}
 \frac{-i}{k^2 - m_V^2 + i\epsilon} [g_{\mu\nu} - (1 - \xi) \frac{k_\mu k_\nu}{k^2 - \xi m_V^2}] \\
 \text{Scalars:} \quad \frac{i}{k^2 - m_\phi^2 + i\epsilon}
 \end{array}$$

²⁹For an introduction to gauge fixing, c.f. e.g. [40, 41, 58]

The relevant vertex rules are:

$$i g_{V_1 V_2 V_3} \left[g_{\mu_1 \mu_2} (p_2 - p_1)_{\mu_3} + g_{\mu_1 \mu_3} (p_1 - p_3)_{\mu_2} + g_{\mu_2 \mu_3} (p_3 - p_2)_{\mu_1} \right]$$

with the couplings:

$$g_{A^{(0)} W_{(1)}^+ W_{(1)}^-} = g_2 \sin \theta_W^{(0)} = e \quad (4.61)$$

$$g_{Z^{(1)} W_{(0,1)}^+ W_{(1,0)}^-} = g_2 \cos \theta_W^{(1)} \theta_W^{(1)} \approx g_2 \quad (4.62)$$

$$g_{Z^{(0)} W_{(1)}^+ W_{(1)}^-} = g_2 \cos \theta_W^{(0)} \quad (4.63)$$

$$i g_{V_1 V_2 V_3 V_4} \left[2g_{\mu_1 \mu_2} g_{\mu_3 \mu_4} - g_{\mu_1 \mu_3} g_{\mu_2 \mu_4} - g_{\mu_1 \mu_4} g_{\mu_2 \mu_3} \right]$$

with the couplings:

$$g_{W_{(1)}^+ W_{(1)}^+ W_{(1)}^- W_{(1)}^-} = g_2^2 \quad (4.64)$$

$$g_{Z^{(1)} Z^{(1)} W_{(1)}^+ W_{(1)}^-} = -g_2^2 \cos \theta_W^{(1)} \approx -g_2^2 \quad (4.65)$$

$$i \overbrace{\left(\frac{1}{2} g_2^2 v_0 \cos^2 \theta_W^{(1)} + g_1 g_2 v_0 \sin \theta_W^{(1)} \cos \theta_W^{(1)} + \frac{1}{2} g_1^2 v_0 \sin^2 \theta_W^{(1)} \right)}^{\approx g_2 m_W^{(0)}} g_{\mu_1 \mu_2}$$

5. Sommerfeld Effect

Cosmic ray experiments including PAMELA [7], ATIC [8], HESS [9] and Fermi LAT [10] have reported an excess of electrons, positrons and photons in the 10 GeV - (at least) 100 GeV region, which might be interpreted as annihilating dark matter [11, 13, 14, 63]¹. In order to explain the cosmic ray "anomalies" from a particle physics perspective, the Sommerfeld effect has been invoked by a number of authors (see e.g. [14, 18, 34, 46, 65]). For reconciling the cosmic ray anomalies with the WIMP miracle, one has to devise a mechanism that provides current day annihilation cross sections more than $\mathcal{O}(100)$ larger [66] than the ones during freeze-out ($\langle\sigma v\rangle \sim 3 \times 10^{-26} \text{cm}^3 \text{s}^{-1}$, for details see Sec. 3.1). In the context of a supersymmetric dark matter scenario, Hisano et al. [18] have proposed a velocity dependent cross section, generated by the so-called "Sommerfeld effect" that fulfills exactly this requirement. Additionally, boost factors of $\mathcal{O}(> 10^4)$ can arise in the presence of long range interactions due to near threshold bound states [12] of dark matter pairs.

In this chapter we are concerned with the main aspect of this thesis: the derivation of the Sommerfeld factor in a model with spin-1 vector dark matter, which has not been addressed in the literature so far. We have already discussed the general aspects of the Sommerfeld effect in paragraph 3.2.1 and now focus on the machinery, necessary to deal with bound states in the language of field theory (Sec. 5.1). In this description, we encounter the "ladder" approximation scheme and show that box diagrams are enhanced in the kinematic region near the pole of a bound state (Sec. 5.2). Before we finally turn our attention to vector dark matter (Sec. 5.5), we are going to review an existing article on the Sommerfeld effect for supersymmetric fermionic dark matter (Sec. 5.3) in order to identify possible issues of the calculational framework on a known example.

¹Note that astrophysical explanations have been suggested in the literature as well, c.f. e.g. [35, 36, 37, 64]

5.1. General Features of the Bethe-Salpeter Ansatz

The Bethe-Salpeter (BS) equation principally allows for a rigorous treatment of relativistic bound states in the language of quantum field theory and was proposed in its general form in 1951 [67]. In our case, this framework is particularly useful, since it naturally accommodates the nonperturbative resummation of field theory diagrams. For a comprehensive introduction to the BS-ansatz, we refer to the excellent review articles (e.g. [68, 69]) and quantum field theory textbooks [70, 71]. We do not want to repeat the entire derivation which is nicely documented in the articles referenced above, but only state important intermediate results for scalar particles that can be transferred to vector bosons in a straight forward manner. We review the result given by Nakanishi [68] for the diagonal interaction of scalar particles $a + b \rightarrow a + b$. A graphical representation of the Bethe-Salpeter equation in momentum space (5.1) is given in figure 5.1. $G(p, q, P)$ denotes the full scattering Greens function and $I(p, p'; P)$ the sum of all 2-particle irreducible (2PI) diagrams (external propagators not included). The notion "reducible diagram" is characterized by the fact, that the diagram can be separated into two unconnected parts by "horizontally" cutting two particle lines. Correspondingly, a diagram is called 2PI, if such a decomposition is not possible [71]. The 2PI kernel I still contains an infinite number of Feynman diagrams, yet, the particular form suggested in fig.5.1 has the decisive advantage that it already contains an infinite number of interactions, even if $I(p, p'; P)$ is calculated only to lowest order in perturbation theory [71]. This feature is relevant for the description of bound states, where, in principle, the constituent particles interact an arbitrary number of times [67].

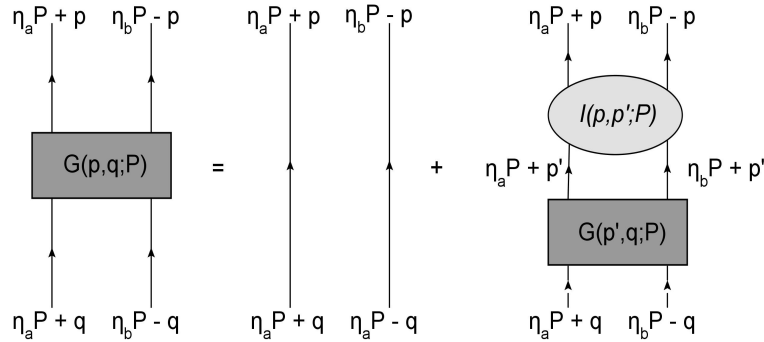


Figure 5.1.: Graphical representation of elastic $2 \rightarrow 2$ scattering event for scalar particles. P denotes the momentum of the center of mass, p , p' and q denote relative momenta. I represents all 2-particle irreducible (2PI) graphs in the $a + b \rightarrow a + b$ scattering process (external lines not considered). $G(p, q, P)$ denotes the full scattering Greens function.

The iteration in fig. 5.1 insinuates that all irreducible Feynman graphs are connected in such a way, that one obtains a complete set of all possible diagrams. This statement holds, since every reducible diagram can be expressed as a sum of irreducible ones [71].

The graphical representation of the Bethe-Salpeter equation (fig. 5.1) can subsequently be transcribed into an analytic expression:

$$[\Delta'_{F,a}(\eta_a P + p)\Delta'_{F,b}(\eta_b P - p)]^{-1} G(p, q; P) = \delta^{(4)}(p - q) + \int d^4 p' I(p, p'; P) G(p', q; P). \quad (5.1)$$

$\Delta'_{F,i}$ denotes the full scalar propagator for particle i , to be approximated by a free propagator ($\Delta_{F,i}$) in the so called "ladder" approximation later on. The η 's are in principle arbitrary real quantities with the property $\eta_a + \eta_b = 1$. It is instructive to choose them in analogy to center of mass variables in the non-relativistic case, i.e. $\eta_{a/b} = \frac{m_{a/b}}{m_a + m_b}$. To avoid any confusion, let us stress beforehand that we are going to follow Iengo and use a somewhat different definition of P . By introducing the Bethe-Salpeter wavefunction for a bound state

$$\phi_{B,r}(x_a, x_b; P_B) = \langle 0 | T [\phi_a(x_a) \phi_b(x_b)] | B, r \rangle \quad (5.2)$$

$$\bar{\phi}_{B,r}(x_a, x_b; P_B) = \langle B, r | T [\phi_a^\dagger(x_a) \phi_b^\dagger(x_b)] | 0 \rangle, \quad (5.3)$$

it is possible to recast eq. (5.1) into a more common form. $|B, r\rangle$ represents a state with 4-momentum P_B , T denotes the time ordering operator and the index r accounts for possible bound state degeneracies. Translation invariance allows one to define the reduced amplitude $\phi_{B,r}(x; P_B)$, with $X = \eta_a x_a + \eta_b x_b$ and $x = x_a - x_b$:

$$\begin{aligned} \phi_{B,r}(x_a, x_b; P_B) &= (2\pi)^{-3/2} e^{-iP_B X} \phi_{B,r}(x; P_B) \\ \bar{\phi}_{B,r}(x_a, x_b; P_B) &= (2\pi)^{-3/2} e^{+iP_B X} \bar{\phi}_{B,r}(x; P_B). \end{aligned} \quad (5.4)$$

The transformation procedure works as follows: one inserts a complete set of states $|B, r\rangle$ into the scattering Greens function $\mathcal{G}(x_a, x_b; y_a, y_b)$:

$$\mathcal{G}(x_a, x_b; y_a, y_b) = \langle 0 | T [\phi_a(x_a) \phi_b(x_b) \phi^\dagger(y_a) \phi^\dagger(y_b)] | 0 \rangle \quad (5.5)$$

to find the contribution from the intermediate states $|B, r\rangle^2$:

$$\begin{aligned} &\sum_{r=1}^n \int d^4 P \phi_{B,r}(x_a, x_b; P) \bar{\phi}_{B,r}(y_a, y_b; P) \theta(P_0) \delta(P^2 - P_B^2) \theta(X_0 - Y_0) \\ &\stackrel{(5.4)}{=} \sum_{r=1}^n \int \frac{d^3 P}{2\omega_B (2\pi)^3} \phi_{B,r}(x; P_B) \bar{\phi}_{B,r}(y; P_B) \\ &\quad \times e^{-i\omega_B(X_0 - Y_0) + i\vec{P}(\vec{X} - \vec{Y})} \theta(X_0 - Y_0) \end{aligned} \quad (5.6)$$

$$\omega_B = \sqrt{\vec{P}^2 + P_B^2}$$

²In principle we should choose $\theta(\min[(x_a)_0, (x_b)_0] - \max[(y_a)_0, (y_b)_0]) = \theta(X_0 - Y_0 - \frac{1}{2}|x_0| - \frac{1}{2}|y_0|)$ in stead of $\theta(X_0 - Y_0)$, because each of the constituent particles in the initial state should be chronologically earlier than any of the final state particles. This change, however leaves the residue at $P_0 = \omega_B$ unaltered and only adds a phase to the integrand.

Representing the Heaviside step function θ in terms of a contour integral

$$\theta(z) = \frac{i}{(2\pi)} \int dk \frac{e^{-ikz}}{k + i\epsilon}, \quad (5.7)$$

eq. (5.6) can be written as:

$$i \sum_{r=1}^n \int \frac{d^4 P}{(2\pi)^4} \phi_{B,r}(x; P_B) \bar{\phi}_{B,r}(y; P_B) \frac{e^{-iP(X-Y)}}{2\omega_B(P_0 - \omega_B + i\epsilon)}. \quad (5.8)$$

Adding the contributions from the anti-particle states of $|B, r\rangle$, i.e. contributions with denominator $\frac{1}{2\omega_B(P_0 + \omega_B - i\epsilon)}$, the Fourier transform of the scattering Greens function takes the form:

$$G(p, q; P) = \frac{i \sum_{r=1}^n \phi_{B,r}(p; P_B) \bar{\phi}_{B,r}(q; P_B)}{P^2 - P_B^2 + i\epsilon} + \text{regular terms} \quad (5.9)$$

At the pole of the bound state, the Bethe-Salpeter equation (5.1) reduces to its homogeneous manifestation:

$$[\Delta'_{F,a}(\eta_a P_B + p) \Delta'_{F,b}(\eta_b P_B - p)]^{-1} \phi_{B,r}(p; P_B) = \int d^4 p' I(p, p'; P_B) \phi_{B,r}(p'; P_B) \quad (5.10)$$

For a more thorough treatment of the derivation of the Bethe-Salpeter equation and comments on the normalization of the BS-amplitude, we refer directly to [68]. Transferring the results from the scalar case given above to the situation of vector particle scattering is straight forward. One has to replace the scalar propagators in eq. (5.10) by vector boson ones and $\phi_{B,r}$ now represents a bound state of two vector bosons carrying the appropriate Lorentz structure. Off-diagonal interactions are incorporated by replacing the delta-function in eq. (5.1) by the appropriate four-point function.

We would like to mention that some authors (e.g. [72]) prefer to start their work with vertex functions Γ instead of the Bethe-Salpeter amplitude ϕ . The two quantities, however, are closely related:

$$\phi(p; P) = [\Delta'_{F,a}(\eta_a P + p) \Delta'_{F,b}(\eta_b P - p)] \Gamma(p; P). \quad (5.11)$$

Practically, it is impossible to solve the Bethe-Salpeter equation without any approximation [70] and one has to devise some truncation scheme to simplify this integral equation. Probably the most common truncation procedure used throughout the literature is the so called "ladder" approximation. In this method, one neglects all but the lowest order diagrams in the interaction kernel I and replaces the full propagators Δ' by the free ones Δ [68]. In the next section we would like to illustrate the reasoning behind the special choice of "ladder"-type diagrams for the description of bound states. For this purpose, we investigate positronium as the paradigm system in QED.

5.2. The Ladder Approximation - Discussion of Positronium Bound States à la Landau Lifshitz

Reviewing the chapter on positronium in Landau/Lifshitz [72], we are going to highlight the reason for summing up ladder-type diagrams in the nonrelativistic field theory description of bound states³. In comparison to the tree level diagrams in QED, all one loop amplitudes come with an additional factor of α , the electromagnetic coupling constant. As we will show in an order of magnitude estimate, the anomalously large contribution of box diagrams is the result of a small denominator in the low energy limit. Consequently, the size of the one-loop amplitude is comparable to the tree level case and the perturbative treatment breaks down. Comparing the normal box diagram fig. 5.2(a) with its crossed version fig. 5.2(b), we come to realize, that the normal box diagrams are dominant close to the bound state pole. Understanding this feature in the one-loop amplitudes explicitly, we conjecture that the suppression of diagrams with crossed internal exchange particle lines also holds for higher order ladder diagrams.

For positronium, the electron and positron momenta p_{\mp} are expressed in the center of mass system (CMS):

$$\vec{p}_- = -\vec{p}_+ = \vec{p} \qquad \vec{p}'_- = -\vec{p}'_+ = \vec{p}' \quad (5.12)$$

External lines are NOT assumed to be on shell, i.e. $p^2 \neq m^2 \rightarrow \epsilon_+ \neq \epsilon_-$, but $\vec{p}_- = -\vec{p}_+$

$$\begin{aligned} p_- &= (\epsilon_-, \vec{p}) & p_+ &= (\epsilon_+, -\vec{p}) \\ p'_- &= (\epsilon'_-, \vec{p}') & p'_+ &= (\epsilon'_+, -\vec{p}') \end{aligned} \quad (5.13)$$

$$\epsilon_- + \epsilon_+ = \epsilon'_- + \epsilon'_+$$

In analogy to the hydrogen problem, the binding energy of a composite state is:

$$E_B \approx m\alpha^2 \ll m, \quad (5.14)$$

where m denotes the mass of the external particles (which will correspond to the mass of the dark matter candidates later on) and $\alpha = \frac{e^2}{4\pi}$ is the finestructure constant. In the neighborhood of the bound-state pole of the scattering amplitude it is necessary that:

$$\begin{aligned} |\vec{p}| &\sim |\vec{p}'| \sim m\alpha \ll m \\ |\epsilon_- - m| &\sim |\epsilon_+ - m| \sim \frac{\vec{p}^2}{m} \sim m\alpha^2, \end{aligned} \quad (5.15)$$

³In the nonrelativistic instantaneous limit, the dominant term of the potential comes from the lowest order 2PI diagram, i.e. the one vector boson exchange [23]. The reason why this is in fact the case becomes clear once we investigate the analytical structure of box diagrams in the instantaneous approximation. As we will see in this section, the anomalous enhancement of boxes is a direct result of the interplay between the poles of the **two** heavy particle propagators in the kinematic bound state region. Therefore, we neglect triangle diagrams in our non-abelian gauge theory to leading order.

which reflects the fact that the kinetic energy of the external states should be of the same order of magnitude as the potential binding energy in order to form a loosely bound state. We continue the discussion of the one-loop box diagrams, depicted here:

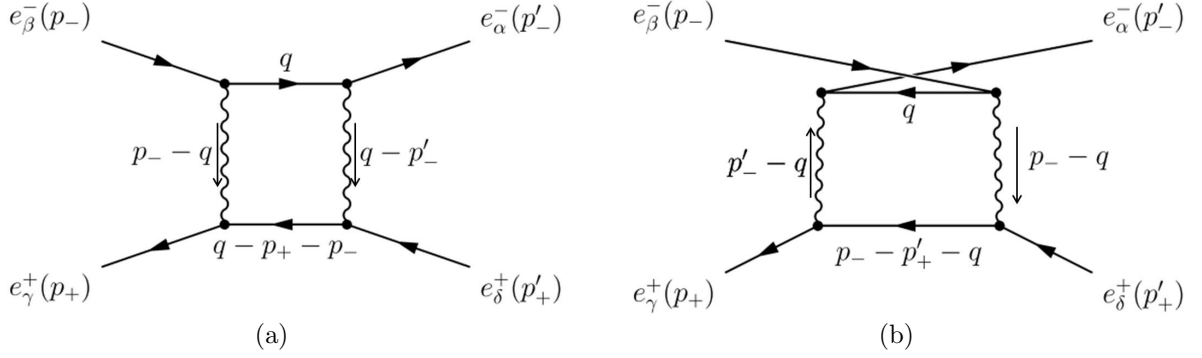


Figure 5.2.: Box diagrams relevant for the description of positronium in QED.

(a) Box diagram (b) crossed photon lines

External momenta are taken to be ingoing for initial states and outgoing for final state particles. $\alpha, \beta, \gamma, \delta$ denote Dirac indices.

For the vertex function⁴ Γ of diagram 5.2(a), one finds:

$$\begin{aligned} \Gamma_{\alpha\beta\gamma\delta} &= -i \int \frac{d^4q}{(2\pi)^4} (ie\gamma^\nu iS_F(q)ie\gamma^\mu)_{\alpha\beta} D_{\nu\rho}(q - p'_-) (ie\gamma^\sigma iS_F(q - p_+ - p_-)ie\gamma^\rho)_{\gamma\delta} D_{\mu\sigma}(p_- - q) \\ &= +ie^4 \int \frac{d^4q}{(2\pi)^4} (\gamma^\nu S_F(q)\gamma^\mu)_{\alpha\beta} D_{\nu\rho}(q - p'_-) (\gamma^\sigma S_F(q - p_+ - p_-)\gamma^\rho)_{\gamma\delta} D_{\mu\sigma}(p_- - q). \end{aligned} \quad (5.16)$$

$D_{\nu\rho}$ and $D_{\mu\sigma}$ denote photon propagators in the Feynman gauge, with the convention $D_{\mu\nu}^{\xi=1}(k) = \frac{-ig_{\mu\nu}}{k^2 + i\epsilon}$. $S_F^{\alpha\beta}(q) = \frac{(\not{q} + m)^{\alpha\beta}}{q^2 - m^2 + i\epsilon}$ are fermionic propagators for the electron and positron. The important $q^\mu = (q_0, \vec{q})$ loop-momentum range is close to the poles of both fermionic propagators S_F simultaneously, as such poles potentially cancel the usual one-loop suppression (by a factor $\sim e^2$) compared to the tree level diagram. In the relevant parameter region $|\vec{q}|$ and $|q_0 - m|$ are small. For the fermion propagator we write:

$$S_F(q) = \frac{\gamma^0 q_0 - \vec{\gamma}\vec{q} + m}{(q_0 + m)(q_0 - m) - \vec{q}^2 + i\epsilon}. \quad (5.17)$$

To leading order, we set all values $q_0 = m$, unless we find expressions of the form $q_0 - m$ where subleading corrections are relevant.

$$= \frac{\gamma^0 q_0 - \vec{\gamma}\vec{q} + m}{(q_0 + m) \left[(q_0 - m) - \underbrace{\frac{\vec{q}^2}{q_0 + m}}_{\approx 2m} + i\tilde{\epsilon} \right]} \quad (5.18)$$

⁴The scattering amplitude A involves the four-point vertex function $\Gamma_{\alpha\beta\gamma\delta}$ and the polarization spinors u, \bar{u}, v, \bar{v} of the external states. It is convenient to ignore the polarizations and work with the vertex part Γ itself [72].

Due to (5.15), we also neglect the spatial component of q in the numerator:

$$\approx \frac{\gamma^0 m + m}{(2m) \left[(q_0 - m) - \frac{\vec{q}^2}{2m} + i\tilde{\epsilon} \right]} = \frac{1}{2} (\gamma^0 + 1) \frac{1}{(q_0 - m) - \frac{\vec{q}^2}{2m} + i\tilde{\epsilon}} \quad (5.19)$$

The second fermionic propagator in the box diagram 5.2(a) is a little more involved:

$$S_F(q - p_- - p_+) = \frac{\gamma^0 \overbrace{(q_0 - \epsilon_- - \epsilon_+)}^{\approx -m} - \vec{\gamma} \overbrace{(\vec{q} - \vec{p}_- - \vec{p}_+)}^{=\vec{0} \text{ in the CMS}} + m}{(q_0 - \epsilon_- - \epsilon_+ + m) \underbrace{(q_0 - \epsilon_- - \epsilon_+ - m)}_{\approx -2m} - (\vec{q} - \vec{p}_- - \vec{p}_+)^2 + i\epsilon} \quad (5.20)$$

In the center of mass system and the kinematic region close to the bound state pole ($|\vec{q}| \ll m$), the propagator reduces to:

$$\begin{aligned} S_F(q - p_- - p_+) &\approx \frac{\gamma^0(-m) + m}{(-2m) \left((q_0 - \epsilon_- - \epsilon_+ + m) - \frac{\vec{q}^2}{-2m} + \frac{i\epsilon}{-2m} \right)} \\ &= \frac{1}{2} (\gamma^0 - 1) \left[\frac{1}{q_0 - \epsilon_- - \epsilon_+ + m + \frac{\vec{q}^2}{2m} - i\tilde{\epsilon}} \right] \end{aligned} \quad (5.21)$$

The poles of the two fermion propagators are at $q_0 = m + \frac{\vec{q}^2}{2m} - i\tilde{\epsilon}$ and $q_0 = \epsilon_- + \epsilon_+ - m - \frac{\vec{q}^2}{2m} + i\tilde{\epsilon}$ respectively. From the Feynman pole prescription, one immediately realizes, that they are on opposite sides of the real axis in the complex q_0 plane.

Contracting the $ie\gamma$ -vertices with the photon propagators⁵ $D^{\nu\rho}$ and $D^{\mu\sigma}$ in (5.16), leads to structures of the form $\gamma_{(1)}^\nu D_{\nu\rho}(q - p'_-) \gamma_{(2)}^\rho \sim \frac{\gamma_{(1)\nu} \gamma_{(2)}^\nu}{(q - p'_-)^2}$ and $\gamma_{(3)}^\mu D_{\mu\sigma}(p_- - q) \gamma_{(4)}^\sigma \sim \frac{\gamma_{(3)\mu} \gamma_{(4)}^\mu}{(p_- - q)^2}$. Here we use the notation (1), (2), (3) and (4) to label the Dirac structure of different γ -matrices. Note that γ^ν and γ^ρ originate from different spinor chains. The same is true for γ^μ and γ^σ . One can split this interaction into an instantaneous and retarded part [70]:

$$\frac{\gamma_{(i)\mu} \gamma_{(j)}^\mu}{k^2} = \underbrace{-\frac{\gamma_{(i)}^0 \gamma_{(j)}^0}{\vec{k}^2}}_{\text{instantaneous interaction}} + \underbrace{\left[\frac{\gamma_{(i)}^0 \gamma_{(j)}^0 (k^0)^2}{(k^2)(\vec{k}^2)} - \frac{\vec{\gamma}_{(i)} \vec{\gamma}_{(j)}}{k^2} \right]}_{\text{noninstantaneous corrections}}, \quad (5.22)$$

$\{i, j\} \in \{\{1, 2\}, \{3, 4\}\}$, $k \in \{(q - p'_-), (p_- - q)\}$. The second part of (5.22) contains both retardation and magnetic interactions [70] and will be treated as perturbation. To zeroth-order in the classical limit, one only keeps the instantaneous contribution of (5.22).

⁵The photon propagators are taken in the t'Hooft-Feynman gauge $\xi = 1$.

In this approximation, we are able to evaluate eq. (5.16). In the numerator, one has to carefully contract the correct Dirac structure. We calculate the q_0 integral by closing the contour in either half of the complex q_0 plane and use residue calculus to obtain:

$$\Gamma_{\alpha\beta\gamma\delta} \sim \alpha^2 \int \frac{\frac{1}{2}(\gamma^0 + 1)_{\alpha\beta} \frac{1}{2}(\gamma^0 - 1)_{\gamma\delta} \overbrace{d^3q}^{\sim(m\alpha)^3}}{(\underbrace{\vec{q} - \vec{p}'_-}_{\sim(m\alpha)^2})^2 (\underbrace{\vec{p}'_- - \vec{q}}_{\sim(m\alpha)^2})^2 \underbrace{(2m - \epsilon_- - \epsilon_+ + \frac{\vec{q}^2}{m})}_{\sim \epsilon_{\pm} - m \sim m\alpha^2}}. \quad (5.23)$$

In an order of magnitude estimate, dropping the Dirac structure in the numerator, one ends up with a contribution from 5.2(a) [72]:

$$\Gamma \sim \alpha^2 \frac{(m\alpha)^3}{(m\alpha)^4 m\alpha^2} = \frac{1}{m^2 \alpha}, \quad (5.24)$$

which is comparable to the tree-level value. In a similar way, one can evaluate the crossed diagram in fig. 5.2(b). For the fermion propagator that carries momentum q , no work has to be done and we can readily transfer the result from eq. (5.17). Due to the crossing of the photon lines, the momentum flow will be different which leads to the fact, that fig. 5.2(b) does not significantly contribute to the scattering amplitude in the vicinity of the bound state pole. For the second fermion propagator in diagram 5.2(b), one finds:

$$S_F(p_- - p'_+ - q) = \frac{\gamma^0 \overbrace{(\epsilon_- - \epsilon'_+ - q_0)}^{-m} + \vec{\gamma}(\vec{p}'_- - \vec{p}'_+ - \vec{q}) + m}{(\underbrace{\epsilon_- - \epsilon'_+ - q_0 - m}_{-2m})(\epsilon_- - \epsilon'_+ - q_0 + m) - (\vec{p}'_- - \vec{p}'_+ - \vec{q})^2 + i\epsilon} \quad (5.25)$$

Ignoring the spatial components in the numerator, we are left with:

$$S_F(p_- - p'_+ - q) \sim \frac{1}{2}(\gamma^0 - 1) \left[\frac{-1}{q_0 - \epsilon_- + \epsilon'_+ - m - \frac{(\vec{p}'_- - \vec{p}'_+ - \vec{q})^2}{2m} + i\tilde{\epsilon}} \right] \quad (5.26)$$

In this approximation, the poles of the two fermion propagators are on the same side of the real axis in the complex q_0 plane and we can close the contour in the region without poles. According to the residue theorem, the integration gives zero which indicates, that diagram 5.2(b) only gives subdominant contributions to the scattering amplitude. Physically, we can understand this in terms of the picture pointed out by Bethe and Salpeter [67], relying on a perturbative approach. In the ladder approximation one can always find a Lorentz system where only one virtual field quantum is excited at a time. According to the argument, as long as g is sufficiently small, the probability of "finding two field quanta simultaneously" is sufficiently suppressed. Including such diagrams would give rise to

higher order corrections which are necessary if one is interested in the hyperfine splitting of the bound state energy levels (see Itzykson/Zuber [70] for a more detailed treatment). Now that we have introduced the concept of bound states in the language of the Bethe-Salpeter equation in chapter 5.1 and motivated the "ladder" approximation by considering analytical features of one-loop amplitudes for positronium, we turn our attention to an existing application of this computational machinery.

5.3. Derivation of the Sommerfeld Enhancement à la Iengo

In his 2009 paper, *Sommerfeld enhancement: general results from field theory diagrams* [23], Iengo closely follows the treatment of bound states in Itzykson/Zuber [70] to derive the Sommerfeld enhancement factor by summing up ladder diagrams. He obtains the Bethe-Salpeter kernel which leads to an effective Schrödinger equation in the non-relativistic limit. We present Iengo's derivation [23] for fermionic dark matter⁶ to understand the important points of the calculation in detail and carry over as many steps as possible to the case of vector dark matter. $A(p, p', P_0)$ denotes the full amplitude, including nonperturbative effects, for the annihilation process of two dark matter particles into Standard Model states:

$$\chi(p_1) + \chi(p_2) \longrightarrow \underbrace{a_1(p'_1) + a_2(p'_2)}_{\text{SM states}} \quad (5.27)$$

The kinematics is described by a set of center of mass (CMS)-like momenta⁷:

$$P = \frac{p_1 + p_2}{2} = \frac{p'_1 + p'_2}{2} \quad p = \frac{p_1 - p_2}{2} = \frac{p'_1 - p'_2}{2}. \quad (5.28)$$

In this frame of reference, one finds:

$$P_0 = \sqrt{\vec{p}^2 + m_\chi^2}, \quad \vec{P} = \vec{0} \quad (5.29)$$

$$p_0 = \sqrt{m_1^2 + \vec{p}_1^2} - \sqrt{m_2^2 + \vec{p}_2^2} \stackrel{m_1 \equiv m_2}{=} 0. \quad (5.30)$$

As we have outlined in section 3.2.1, in order for the Sommerfeld enhancement to be significant, one has to consider a setup where the mass of the force carrier m_ϕ is much smaller than the dark matter mass m_χ (see also [11]).

⁶Aspects of the Sommerfeld effect for fermionic dark matter have also been discussed by other authors, see e.g. [18, 38, 46, 14].

⁷Iengo's momentum convention is somewhat unorthodox, usually one finds the definition $P = p_1 + p_2$, i.e. a difference by a factor $\frac{1}{2}$

For fermionic external states it is advantageous to label the γ -matrices from different vertices by an additional index for book keeping purposes. In this setup, a boson⁸ exchange between the fermions generically leads to an integral kernel of the form [70]:

$$\frac{\gamma_{(1)\mu}\gamma_{(2)}^\mu}{k^2 - m_\phi^2} = \underbrace{-\frac{\gamma_{(1)}^0\gamma_{(2)}^0}{\vec{k}^2 + m_\phi^2}}_{\text{instantaneous interaction}} + \underbrace{\left[\frac{\gamma_{(1)}^0\gamma_{(2)}^0(k^0)^2}{(k^2 - m_\phi^2)(\vec{k}^2 + m_\phi^2)} - \frac{\vec{\gamma}_{(1)}\vec{\gamma}_{(2)}}{k^2 - m_\phi^2} \right]}_{\text{noninstantaneous corrections}} \quad (5.31)$$

One conveniently writes (5.31), so that the non-relativistic instantaneous approximation is evident. In this context, instantaneousness denotes the absence of relative energy coordinates k_0 , which corresponds to the absence of a relative time variable after Fourier transformation.

Following the analytical structure of the Bethe-Salpeter ansatz (Sec. 5.1) to accommodate the resummation of field theory diagrams, the full amplitude A satisfies the recursion relation [23] (Dirac indices are not shown explicitly):

$$A(p, p', P_0) = A_0(p, p', P_0) - ig^2 \int \frac{d^3q dq_0}{(2\pi)^4} \frac{\gamma_{(1)}^0\gamma_{(2)}^0}{(\vec{p} - \vec{q})^2 + m_\phi^2} S_2(q, P) A(q, p', P_0) \quad (5.32)$$

$$\text{with:} \quad S_2(q, P) = \frac{(\not{P} + \not{q} + m_\chi)_1}{(P + q)^2 - m_\chi^2 + i\epsilon} \cdot \frac{(\not{P} - \not{q} + m_\chi)_2}{(P - q)^2 - m_\chi^2 + i\epsilon},$$

written in the instantaneous limit of the "ladder" approximation scheme for the ϕ exchange. At this point, we would like to mention some of the problems related to the instantaneous Bethe-Salpeter ansatz, which are rarely discussed in the articles on the Sommerfeld effect that take this approach. The question of how to derive the proper non-relativistic limit of the Bethe-Salpeter equation has been the subject of extensive discussion especially in the late sixties (see the excellent review of Nakanishi [68] and references therein). Retarded interactions, connected to a relative time variable, inherent to a full relativistic treatment of the physical situation are normally considered as an approximation similar to higher order corrections of the interaction kernel [70]. In the late seventies and early eighties, effective models for quark bound states have also led to an era of increased interest in the problem of deriving a non-relativistic potential from field theory [73, 74] and some improvements have been suggested, such as the introduction of a noninstantaneous gauge [73]. Despite the deficiencies mentioned above, the non-relativistic instantaneous ladder approximation of the Bethe-Salpeter equation leads to a Lippmann-Schwinger-type equation with a nonrelativistic interaction potential which presents a reasonable result in the weak coupling limit [74]. As a first approximation we will therefore continue our analysis with three-dimensional propagators as in eq. (5.31)

⁸The gauge boson propagator is taken to be in the t'Hooft-Feynman gauge $\xi = 1$.

for the exchange particles following other publications on the Sommerfeld phenomenology of dark matter annihilations [23, 38, 75].

Similar to the pictorial representation of the 4-point scattering Greens function in section 5.1, we represent the recursion step for the dark matter annihilation amplitude $A(q, p', P_0)$ diagrammatically⁹:

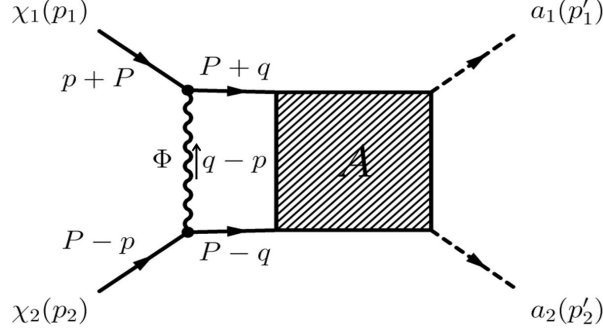


Figure 5.3.: Graphical representation of $2 \rightarrow 2$ scattering iteration for lowest order interaction kernel in the ladder approximation. Momentum flow follows the propagator arrows.

The external momenta are taken off-shell in the course of the computation and are put to their on-shell values at the very end. We evaluate the loop integration in (5.32) by closing the contour in the complex q_0 -plane and disregard possible singularities of the amplitude $A(q, p', P_0)$ itself, which would give rise to subleading contributions in the non-relativistic limit [23]. In (5.32), $A_0(p, p', P_0)$ represents the bare annihilation amplitude, neglecting the multiple interactions between the incoming dark matter states. In case of WIMP annihilation, $A_0(p, p', P_0)$ is in principle accessible via perturbation theory.

It turns out to be convenient, to represent the fermionic propagators as [70]:

$$S_F(p) = \frac{\not{p} + m}{p^2 - m^2 + i\epsilon} = \left[\frac{\Lambda^+(\vec{p})}{p_0 - \omega + i\epsilon} + \frac{\Lambda^-(\vec{p})}{p_0 + \omega - i\epsilon} \right] \gamma^0 \quad (5.33)$$

and introduce the notation¹⁰:

$$\begin{aligned} H(\vec{p}) &= \vec{\alpha} \cdot \vec{p} + \gamma^0 \cdot m \\ \Lambda^\pm(\vec{p}) &= \frac{\omega \pm H(\vec{p})}{2\omega} \\ \text{with: } H(\vec{p})\Lambda^\pm(\vec{p}) &= \pm \omega \Lambda^\pm(\vec{p}) \\ \omega &= \sqrt{\vec{p}^2 + m^2}, \quad \vec{\alpha} = \gamma^0 \cdot \vec{\gamma} \end{aligned} \quad (5.34)$$

⁹In comparison to Sec. 5.1, we have rotated the diagrams 90° .

¹⁰ $H(\vec{p})$ depends only on the 3-momentum \vec{p} . In the CMS reference frame, the $\vec{P} = \vec{0}$ dependence in $S_2(q, P)$ of eq. (5.32) drops out in the numerator, which will be different for vector particles in a general gauge.

The energy projectors Λ^\pm effectively act as the amplitude of the associated pole in the complex q_0 plane. Plugging the right hand side of eq. (5.33) into the Bethe-Salpeter amplitude (5.32), one obtains:

$$A(p, p', P_0) = A_0(p, p', P_0)$$

$$-ig^2 \int \frac{d^3q}{(2\pi)^3} \frac{\gamma_{(1)}^0 \gamma_{(2)}^0}{(\vec{p} - \vec{q})^2 + m_\phi^2} \int \frac{dq_0}{2\pi} \left[\overbrace{\frac{\Lambda_1^+(\vec{q})}{q_0 + P_0 - \omega + i\epsilon}}^{\text{pole 1}} + \frac{\Lambda_1^-(\vec{q})}{q_0 + P_0 + \omega - i\epsilon} \right] \gamma_{(1)}^0 \cdot \left[\frac{-\Lambda_2^+(-\vec{q})}{q_0 - P_0 + \omega - i\epsilon} + \underbrace{\frac{-\Lambda_2^-(-\vec{q})}{q_0 - P_0 - \omega + i\epsilon}}_{\text{pole 2}} \right] \gamma_{(2)}^0 \cdot A(q, p', P_0) \quad (5.35)$$

The fermion propagators have poles at:

$$\begin{aligned} q_0 &= \omega - P_0 - i\epsilon & q_0 &= -(\omega - P_0) + i\epsilon \\ q_0 &= -(\omega + P_0) + i\epsilon & q_0 &= (P_0 + \omega) - i\epsilon \end{aligned}$$

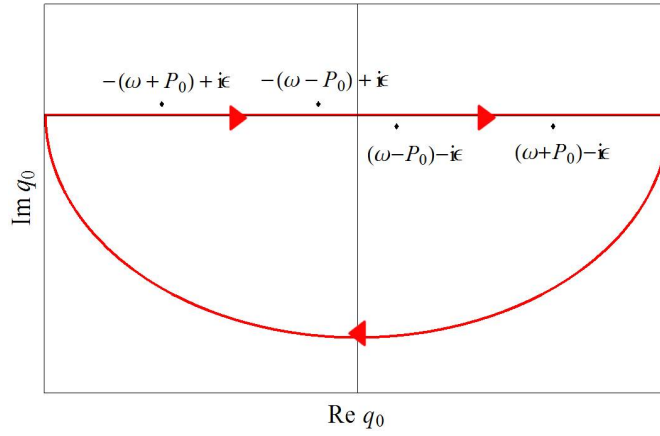


Figure 5.4.: Poles in the q_0 plane for fermionic dark matter candidates in the Bethe-Salpeter equation for the scattering amplitude

The contour is arbitrarily closed in the lower half of the complex q_0 plane.

In order to evaluate the contour integral in (5.35), one uses ordinary residue calculus and ignores possible poles of the amplitude $A(q, p', P_0)$ (to be justified below).

- pole 1 @ $q_0 = \omega - P_0$ (ignoring contributions from $A(q, p', P_0)$):

$$\begin{aligned}
& g^2 \int \frac{dq_0}{2\pi i} \left[\frac{\Lambda_1^+(\vec{q})}{q_0 + P_0 - \omega + i\epsilon} \right] \gamma_{(1)}^0 \left[\frac{-\Lambda_2^+(-\vec{q})}{q_0 - P_0 + \omega - i\epsilon} + \frac{-\Lambda_2^-(-\vec{q})}{q_0 - P_0 - \omega + i\epsilon} \right] \gamma_{(2)}^0 \\
&= \underbrace{\frac{+g^2(-2\pi i)}{2\pi i}}_{\text{integration around pole}} \Lambda_1^+(\vec{q}) \gamma_{(1)}^0 \left[\underbrace{\frac{-\Lambda_2^+(-\vec{q})}{(\omega - P_0) - P_0 + \omega}}_{=q_0} + \underbrace{\frac{-\Lambda_2^-(-\vec{q})}{(\omega - P_0) - P_0 - \omega}}_{=q_0} \right] \gamma_{(2)}^0 \\
&= -g^2 \Lambda_1^+(\vec{q}) \left[\frac{\Lambda_2^-(-\vec{q})}{2P_0} - \frac{\Lambda_2^+(-\vec{q})}{2(\omega - P_0)} \right] \gamma_{(1)}^0 \gamma_{(2)}^0 \tag{5.36}
\end{aligned}$$

- pole 2 @ $q_0 = \omega + P_0$

$$\begin{aligned}
& g^2 \int \frac{dq_0}{2\pi i} \left[\frac{\Lambda_1^+(\vec{q})}{q_0 + P_0 - \omega + i\epsilon} + \frac{\Lambda_1^-(\vec{q})}{q_0 + P_0 + \omega - i\epsilon} \right] \gamma_{(1)}^0 \left[\frac{-\Lambda_2^-(-\vec{q})}{q_0 - P_0 + \omega - i\epsilon} \right] \gamma_{(2)}^0 \\
&= \frac{+g^2(-2\pi i)}{2\pi i} \left[\frac{\Lambda_1^+(\vec{q})}{(P_0 + \omega) + P_0 - \omega} + \frac{\Lambda_1^-(\vec{q})}{(P_0 + \omega) + P_0 + \omega} \right] [-\Lambda_2^-(-\vec{q})] \gamma_{(1)}^0 \gamma_{(2)}^0 \\
&= -g^2 \left[\frac{\Lambda_1^+(\vec{q})}{(2P_0)} + \frac{\Lambda_1^-(\vec{q})}{2(P_0 + \omega)} \right] [-\Lambda_2^-(-\vec{q})] \gamma_{(1)}^0 \gamma_{(2)}^0 \tag{5.37}
\end{aligned}$$

Note that $(\omega - P_0) = \sqrt{\vec{q}^2 + m_\chi^2} - \sqrt{\vec{p}^2 + m_\chi^2}$ is a small quantity in the limit $m_\chi \gg |\vec{q}|, |\vec{p}|$ ($m_\chi \rightarrow \infty$ is the static limit). Only the pole at $q_0 = \omega - P_0$ leads to a small denominator and therefore an anomalously large contribution to the amplitude. To leading order, we drop all but these terms in the instantaneous approximation and the non-relativistic limit. Conceptually, the procedure introduced by Iengo is equivalent to the Landau/Lifshitz method [72], where one analyzes the pole structure of the one-loop diagrams to find enhanced contributions.

The approximation of ignoring possible poles of the amplitude $A(q, p', P_0)$ in the q_0 -integration of eq. (5.35) is justified, considering the **first** iteration of said equation (see also [76]). For the bare amplitude $A_0(q, p', P_0)$, we use the tree-level graph with a massive particle exchange (Φ with mass \hat{m} of the order of the dark matter candidate or above¹¹). We follow the outlines in Appendix A of Iengo's work [23], treat the final state Standard Model particles as massless and use the notation $p'_0 = \omega(\vec{p})$, $\vec{p}' = \omega(\vec{p})\vec{n}$, $\omega(\vec{p}) = \sqrt{\vec{p}^2 + m_\chi^2}$. The singularities of this amplitude stem from the denominator of the massive propagator.

$$(q - p')^2 - \hat{m}^2 + i\epsilon = [q_0 - (u(q, p) + \omega(p)) + i\epsilon][q_0 + (u(q, p) - \omega(p)) - i\epsilon] \tag{5.38}$$

where $u(p, q) = \sqrt{\omega(\vec{p})^2 + \hat{\omega}(\vec{q})^2 - 2\vec{q} \cdot \vec{n} \omega(\vec{p})}$ and $\hat{\omega}(\vec{q}) = \sqrt{\vec{q}^2 + \hat{m}^2}$

Plugging these expressions back into the first iteration of eq. (5.35) leads to a contour

¹¹This is due to the discrete \mathcal{Z}_2 -symmetry that guarantees the stability of the dark matter candidate. This symmetry implies that all vertices contain only even number of heavy parity-odd states.

integral of the form:

$$\int dq_0 N(q_0, \vec{q}, \vec{p}) \times \frac{1}{[q_0 - (\omega(q) - (\omega(p) + i\epsilon))] [q_0 + (\omega(q) + (\omega(p) - i\epsilon))]} \frac{1}{[q_0 - (\omega(q) + (\omega(p) + i\epsilon))] [q_0 + (\omega(q) - (\omega(p) - i\epsilon))]} \frac{1}{[q_0 - (u(q, p) + \omega(p)) + i\epsilon] [q_0 + (u(q, p) - \omega(p)) - i\epsilon]} \quad (5.39)$$

The numerator $N(q_0, \vec{q}, \vec{p})$ does not play a crucial role in the integration since all singularities were already factored out. Closing the contour in the lower complex q_0 plane we have to consider three poles.

1. $q_0 = \omega(q) - \omega(p)$
2. $q_0 = \omega(q) + \omega(p)$
3. $q_0 = \sqrt{w(p)^2 + \widehat{w}(p)^2 - 2\vec{q} \cdot \vec{n} \cdot \omega(p)} + \omega(p)$

Similar to the calculations carried out in eq. (5.36) and eq. (5.37) one realizes that the first pole leads to a small denominator $\omega(q) - \omega(p)$ in the limit of large mass m_χ which is unrelated to the poles of A itself. Consequently, we ignore the poles of the amplitude $A(q, p', P_0)$ as a first approximation. This prescription even remains valid for higher order iterations within the instantaneous treatment, since the propagator that forms the ladder-steps is independent of q_0 in this limit (see eq. (5.31)), therefore not contributing any poles to the integrand.

Keeping only the leading contribution of (5.36), one obtains the approximate Bethe-Salpeter equation for the scattering amplitude from (5.35).

$$A(p, p', P_0) = A_0(p, p', P_0) + \frac{g^2}{(2\pi)^3} \int d^3q \frac{1}{(\vec{p} - \vec{q})^2 + m_\phi^2} \frac{\Lambda_1^+(\vec{q})\Lambda_2^+(-\vec{q})}{2(\omega - P_0)} A(\vec{q}, p', P_0) \quad (5.40)$$

The γ^0 's of the fermionic propagators have been canceled by the ones contained in the ϕ -boson exchange kernel.

In eq. (5.40), the leading term (in the $m \rightarrow \infty$ limit) for $\Lambda_1^+\Lambda_2^+$ is given by:

$$\Lambda_1^+(\vec{q})\Lambda_2^+(-\vec{q}) = \left[\frac{\omega + \vec{\alpha} \cdot \vec{q} + \gamma^0 m_\chi}{2\omega} \right]_1 \left[\frac{\omega - \vec{\alpha} \cdot \vec{q} + \gamma^0 m_\chi}{2\omega} \right]_2$$

$$\underset{\omega \approx m}{\overset{|\vec{q}| \ll m}{\approx}} \frac{1}{2}(1 + \gamma^0)_1 \frac{1}{2}(1 + \gamma^0)_2$$

In this approximation, one can use the projector properties of $\Lambda^\pm = \frac{1}{2}(1 \pm \gamma^0)$, i.e. the relation $\Lambda^\pm \Lambda^\pm = \Lambda^\pm$, to project (5.40) onto the A^{++} -subspace¹²[70]. It is important to

¹²In this subspace, the Dirac-structure of the numerator factors out. We use the notation $A^{++} \equiv \Lambda^+ \Lambda^+ A$, we are going to drop the $^{++}$ indices for the rest of the discussion. Note that Iengo claims that $\gamma^0 \sim 1$ in the nonrelativistic limit, so that $\Lambda^+ \Lambda^+ \sim 1$.

note that this approximation neglects \vec{q} dependent terms in the numerator even though q acts as the integration variable. We assert this approximation is justified, considering the relevant q region. The major contribution to the scattering amplitude is fixed by the bound-state pole condition which subsequently fixes q to be small. Therefore the integral is effectively evaluated at this particular pole only and the suppression of the numerator with $\frac{\mathcal{O}(\vec{q}^2)}{m_\chi^2}$ allows us to drop these terms as a first approximation. We will employ this kinematical fact excessively to simplify the Sommerfeld calculations for vector DM (see section 5.5). To continue with Iengo's analysis, we expand the small denominator in terms of three-momenta to leading order:

$$\begin{aligned} \frac{1}{2(\omega - P_0)} &= \frac{1}{2[\sqrt{\vec{q}^2 + m_\chi^2} - \sqrt{\vec{p}^2 + m_\chi^2}]} \\ &\approx \frac{1}{2m_\chi \left[1 + \frac{1}{2} \frac{\vec{q}^2}{m_\chi^2} - \left(1 + \frac{1}{2} \frac{\vec{p}^2}{m_\chi^2}\right)\right]} \\ &= \frac{1}{\frac{\vec{q}^2}{m_\chi} - \frac{\vec{p}^2}{m_\chi}} \equiv \frac{1}{\frac{\vec{q}^2}{2m_r} - \mathcal{E}}, \end{aligned}$$

introduce the reduced mass $m_r = \frac{m_\chi}{2}$ and the total non-relativistic energy \mathcal{E} .

$$\mathcal{E} \equiv \frac{2(P_0^2 - m_\chi^2)}{2m_\chi} \approx \frac{\vec{p}^2}{2m_r}$$

In the Bethe-Salpeter approach, it is conventional to introduce the Bethe-Salpeter wavefunction of the bound state [67], which can be thought of as a generalized form factor. To leading order in the nonrelativistic limit ($p_0 = 0$, $q_0 \approx \omega - P_0 \approx 0$), one defines¹³:

$$A(\vec{q}, p', P_0) = \left(\frac{\vec{q}^2}{2m_r} - \mathcal{E}\right) \tilde{\Psi}_\mathcal{E}(\vec{q}, p') \quad (5.41)$$

and eq. (5.40) becomes:

$$\begin{aligned} \left(\frac{\vec{p}^2}{2m_r} - \mathcal{E}\right) \tilde{\Psi}_\mathcal{E}(\vec{p}, p') &= A_0(\vec{p}, p', P_0) + \int d^3q V(\vec{p}, \vec{q}) \tilde{\Psi}_\mathcal{E}(\vec{q}, p') \\ V(\vec{p}, \vec{q}) &= \frac{g^2}{(2\pi)^3} \frac{1}{(\vec{p} - \vec{q})^2 + m_\phi^2} \end{aligned} \quad (5.42)$$

Eq. (5.42) has the form of an effective Schrödinger equation for the bound state amplitude and the interaction potential can be read off in momentum space¹⁴.

¹³Note that p is independent of p_0 in the frame of reference we work in (see eq. (5.30)), so that

$A(p, p', P_0) \rightarrow A(\vec{p}, p', P_0)$.

¹⁴Note that eq. 5.42 deviates from a common Schrödinger equation by the presence of the source term

$A_0(\vec{p}, p', P_0)$ which encodes the short range interaction in the final annihilation step.

5.4. Iengo's Solution of the Schrödinger Equation

Iengo continues to derive an analytic expression of the solution to the Schrödinger equation. It is advantageous Fourier transform of the expressions in (5.42):

$$\frac{1}{\vec{k}^2 + \mu^2} = \frac{1}{4\pi} \int d^3r \frac{e^{-i\vec{k}\cdot\vec{r} - \mu r}}{r} \quad (5.43)$$

$$\alpha = \frac{g^2}{4\pi} \quad (5.44)$$

$$\Psi_{\mathcal{E}}(\vec{r}) = \int d^3p e^{+i\vec{p}\cdot\vec{r}} \tilde{\Psi}_{\mathcal{E}}(\vec{p}, p') \quad (5.45)$$

$$U_0(\vec{r}) = \int d^3p e^{+i\vec{p}\cdot\vec{r}} A_0(\vec{p}, p', P_0), \quad (5.46)$$

to obtain an inhomogeneous equation in configuration space:

$$\left(-\frac{1}{2m_r} \partial^2 - \frac{\alpha e^{-m_\phi r}}{r} - \mathcal{E} \right) \Psi_{\mathcal{E}}(\vec{r}) = U_0(\vec{r}). \quad (5.47)$$

One can prove, that eq. (5.47) is formally solved by¹⁵:

$$\Psi_{\mathcal{E}}(\vec{r}) = \int d^3r' \int \frac{d^3k}{(2\pi)^3} \frac{\phi_{\vec{k}}(\vec{r}) \phi_{\vec{k}}^*(\vec{r}')}{\frac{\vec{k}^2}{2m_r} - \mathcal{E} - i\epsilon} U_0(\vec{r}'), \quad (5.48)$$

where Iengo chooses a Feynman contour prescription of $-i\epsilon$ with the remark that the sign is not important. $\phi_{\vec{k}}(\vec{r})$ form a complete set of solutions to the homogeneous equation:

$$\left(-\frac{1}{2m_r} \partial^2 - \frac{\alpha e^{-m_\phi r}}{r} - \frac{\vec{k}^2}{2m_r} \right) \phi_{\vec{k}}(\vec{r}) = 0, \quad (5.49)$$

obeying the completeness relation:

$$\int \frac{d^3k}{(2\pi)^3} \phi_{\vec{k}}(\vec{r}) \phi_{\vec{k}}^*(\vec{r}') = \delta^{(3)}(\vec{r} - \vec{r}') \quad (5.50)$$

To realize that eq. (5.48) indeed fulfills the Schrödinger equation (5.47), one can simply plug in the formal solution into (5.47) and use:

$$\left(-\frac{1}{2m_r} \partial^2 - \frac{\alpha e^{-m_\phi r}}{r} - \mathcal{E} \right) \phi_{\vec{k}}(\vec{r}) = \left(\frac{k^2}{2m_r} - \mathcal{E} \right) \phi_{\vec{k}}(\vec{r}). \quad (5.51)$$

¹⁵Note that $G(\vec{r}, \vec{r}') = \int \frac{d^3k}{(2\pi)^3} \frac{\phi_{\vec{k}}(\vec{r}) \phi_{\vec{k}}^*(\vec{r}')}{\frac{\vec{k}^2}{2m_r} - \mathcal{E} - i\epsilon}$ is the Greens function to the differential operator on the left hand side of eq. (5.47). One can think of $G(\vec{r}, \vec{r}')$ as nonrelativistic Greens function for the bound state in the Lehmann representation.

This cancels the denominator and one is left with:

$$\int \frac{d^3k}{(2\pi)^3} \phi_{\vec{k}}(\vec{r}) \int d^3r' \phi_{\vec{k}}^*(\vec{r}') U_0(\vec{r}') = U_0(\vec{r}), \quad (5.52)$$

where one has to take into account the completeness relation (5.50) in the last step to prove the validity of (5.48). As has been demonstrated by Iengo [23], one can relate the complete annihilation amplitude A to the bare annihilation amplitude A_0 via the solution of the nonrelativistic Schrödinger equation ϕ . For details, we refer to [23] directly:

$$A(\vec{p}, p', P_0) = \int d^3r \phi_{\vec{p}}^*(\vec{r}) \int \frac{d^3q}{(2\pi)^3} e^{i\vec{q}\cdot\vec{r}} A_0(\vec{q}, p', P_0). \quad (5.53)$$

In case of s-wave annihilation, $A_0(\vec{q}, p', P_0)$ is an angular-independent constant $A_0(\vec{q}, p', P_0) \rightarrow a_0$, which leads to $\int \frac{d^3q}{(2\pi)^3} e^{i\vec{q}\cdot\vec{r}} A_0(\vec{q}, p', P_0) \rightarrow a_0 \delta(\vec{r})$. Using this asymptotic behavior in eq. (5.53) yields:

$$A(\vec{p}, p', P_0) = a_0 \phi_{\vec{p}}^*(0). \quad (5.54)$$

Relation between Amplitudes, the Schrödinger Equation and Enhancement Factors

We present a detailed study of the relation between the Sommerfeld enhancement factor and the solution of the homogeneous Schrödinger equation for a diagonal interaction with one annihilation channel (discussed e.g. in [23, 11, 65]), since we try to profit from the insights gained in solving this simpler problem first and transfer many points to our coupled system of equations for off-diagonal interactions later. Iengo [23] is rather explicit in his calculation of the enhancement factor and considers Coulomb- and Yukawa potentials separately for arbitrary partial wave l . The enhancement factor S factorizes from the annihilation cross section:

$$\sigma = S \times \sigma_0, \quad (5.55)$$

where the cross section σ is directly related to the amplitudes A by:

$$\sigma \propto |A(\vec{p}, p')|^2 \quad (5.56)$$

$$\sigma_0 \propto |A_0(\vec{p}, p')|^2. \quad (5.57)$$

From eq. (5.53) we immediately realize, that the solution of the homogeneous Schrödinger equation $\phi_{\vec{p}}(\vec{r})$ is intimately related to the Sommerfeld enhancement factor S . Following Arkani-Hamed et al. [11], we enforce appropriate boundary conditions for the scattering problem (5.49):

$$\phi_{\vec{p}}(\vec{r}) \rightarrow e^{ipz} + f(\theta) \frac{e^{ipr}}{r}, \text{ as } r \rightarrow \infty, \quad (5.58)$$

where the scattering amplitude $f(\theta)$ vanishes in the free case $\phi_{\vec{p}}^{(0)}$. In this language, the enhancement factor is defined as¹⁶:

$$S_p = \frac{|\phi_{\vec{p}}(0)|^2}{|\phi_{\vec{p}}^{(0)}(0)|^2} = |\phi_{\vec{p}}(0)|^2 \quad (5.59)$$

The particular form of the Sommerfeld factor is motivated by a simple physical argument [65]. The s-wave annihilation reaction is assumed to be mediated by a delta function interaction, which is why one expects an annihilation rate proportional to $|\phi_{\vec{p}}(0)|^2$. (5.59) also implies that the influence of non-perturbative effects in the dark matter annihilation is effectively encoded in a modified two-particle wavefunction.

Scattering theory in non-relativistic Quantum Mechanics is treated in a number of textbooks (see e.g. [42, 43, 44]) and we only repeat results that are important for further discussions of the Sommerfeld effect. As it turns out, we are primarily concerned with rotationally invariant potentials, which renders the scattering problem cylindrically symmetric around the axis defined by the scattering geometry (here we take incoming particles along the z-axis). In light of this symmetry, it is appropriate to expand the $\phi_{\vec{p}}(\vec{r})$ in terms of Legendre polynomials $P_l(\hat{p} \cdot \hat{r})$ and radial wavefunctions $R_{p,l}(r)$:

$$\phi_{\vec{p}}(\vec{r}) = \sum_l A_{p,l} P_l(\hat{p} \cdot \hat{r}) R_{p,l}(r) \quad (5.60)$$

We have introduced the notation $\hat{p} = \frac{\vec{p}}{p}$ and $p = |\vec{p}|$ for the momentum vector. An analogous notation is adopted for the position vector \vec{r} . The modulus of the expansion coefficients $A_{p,l}$ can be determined from the normalization condition imposed on the wavefunction:

$$\int d^3r \phi_{\vec{p}}^*(\vec{r}) \phi_{\vec{q}}(\vec{r}) \stackrel{!}{=} \delta(\vec{p} - \vec{q}) \quad (5.61)$$

We find, consistent with Arkani-Hamed, $A_{p,l} = \frac{1}{p} i^l (2l+1) e^{i\delta_l}$, where the phase factor $i^l e^{i\delta_l}$ has been chosen so that $R_{p,l}$ behaves asymptotically as:

$$R_{p,l}(r) \rightarrow \frac{1}{r} \sin(pr - \frac{1}{2}l\pi + \delta_l), \text{ for } r \rightarrow \infty. \quad (5.62)$$

δ_l is commonly referred to as scattering phase. In order to obtain a physically sensible result, we have to require a regular behavior for $R_{p,l}(r)$ as $r \rightarrow 0$. If the potential does not diverge faster than r^{-1} at the origin, which is the case for a Yukawa as well as a Coulomb potential, $R_{p,l}(r)$ scales as $\sim r^l$ as $r \rightarrow 0$. From (5.59) we know, that the Sommerfeld enhancement is related to the wavefunction at the origin. With the asymptotic behavior $R_{p,l} \sim r^l$, all but the $l = 0$ terms vanish, thus we write with the help of (5.60):

$$S_p = \left| \frac{R_{p,l=0}(0)}{p} \right|^2. \quad (5.63)$$

¹⁶In eq. (5.59), $\phi_{\vec{p}}^{(0)} = e^{ipz}$ denotes the free two-particle wavefunction.

Upon introducing the reduced radial wavefunction $\chi_{p,l}(r) = rR_{p,l=0}(r)$, the Schrödinger equation (5.49) turns into a one-dimensional problem. The boundary condition (BC) at the origin, $R_{p,l}(r \rightarrow 0) = \text{regular}$, induces the corresponding BC for $\chi_{p,l}(0)$, i.e. $\chi_{p,l}(0) = 0$. Principally, for s-wave annihilation, we should solve the boundary value problem:

$$\frac{1}{m_\chi} \frac{d^2 \chi_{p,0}(r)}{dr^2} + \left(\frac{\alpha}{r} e^{-m_\phi r} + \mathcal{E} \right) \chi_{p,0}(r) = 0 \quad (5.64)$$

$$\chi_{p,0}(0) = 0 \quad (5.65)$$

$$\chi_{p,0}(r) \xrightarrow{r \rightarrow \infty} \sin(kr + \delta), \quad (5.66)$$

in order to obtain the enhancement factor S_p . However, due to the linearity of (5.64), we can replace the boundary condition at infinity by a value for $\frac{d\tilde{\chi}_{p,0}(r)}{dr}$ at the origin [65]. If we set $p \frac{d\tilde{\chi}_{p,0}(r)}{dr} = 1$ ¹⁷ and solve the initial value problem for $\tilde{\chi}$ instead, the two solutions are related by $\chi = \tilde{\chi} C^{-1}$. This procedure was also adapted by Iengo [23]; for a Yukawa potential and arbitrary partial wave l , he finds the enhancement factor:

$$S_l = \left| \frac{(2l+1)!}{C} \right|^2. \quad (5.67)$$

C is defined as the amplitude of the reduced radial wavefunction $\tilde{\chi}_l(x)$, $x \equiv p \cdot r$ in the limit of large x for the initial value problem. We introduce the dimensionless reduced radial Schrödinger equation¹⁸ favorable for numerical calculations

$$\tilde{\chi}_l''(x) + \left(1 + \frac{2a}{x} e^{-bx} - \frac{l(l+1)}{x^2} \right) \tilde{\chi}_l(x) = 0. \quad (5.68)$$

As advertised above, the initial condition $\tilde{\chi}_l(x)_{x \rightarrow 0} \rightarrow x^{l+1}$ leads to an asymptotic behavior at infinity:

$$\tilde{\chi}_l(x)_{x \rightarrow \infty} \rightarrow C \sin\left(x - \frac{l\pi}{2} + \delta_l\right). \quad (5.69)$$

$a = \frac{\alpha}{v}$, $b = \frac{m_\phi}{m_r v}$ denote dimensionless parameters, $v = \frac{p}{m_r}$ is the relative velocity of the dark matter particles and m_r denotes the reduced mass of the dark matter pair. Relating $\tilde{\chi}_l(x)$ to the radial wavefunction $R_{p,l}(r)$

$$R_{p,l}(r) = \frac{1}{C} p \frac{\tilde{\chi}_l(x)}{x}, \quad (5.70)$$

we realize the compatibility of (5.63) and (5.67) for s-wave ($l = 0$) annihilations. In order to obtain the amplitude C - defined in eq. (5.69) - Iengo describes a numerical procedure to extract this value. One uses for example the *NDSolve* command in *Mathematica* and

¹⁷Defining the initial condition with the additional factor p , simplifies the the solution of the dimensionless equation 5.68.

¹⁸We will explicitly demonstrate the reduction of the Schrödinger equation for our model in section 5.10.

solves the initial value problem (5.68) with $\tilde{\chi}_l(x)_{x \rightarrow 0} \rightarrow x^{l+1}$. The s-wave case ($l = 0$) does not cause numerical troubles, but we have had difficulties finding stable numerical results for higher partial waves, due to the $\propto \frac{1}{x^2}$ divergence at the origin. Owing to the special asymptotic behavior of the scattering solution, we are able to extract C^2 from the constant value of $\tilde{\chi}_l(x)^2 + \tilde{\chi}_l(x - \frac{\pi}{2})^2$ for large values of x :

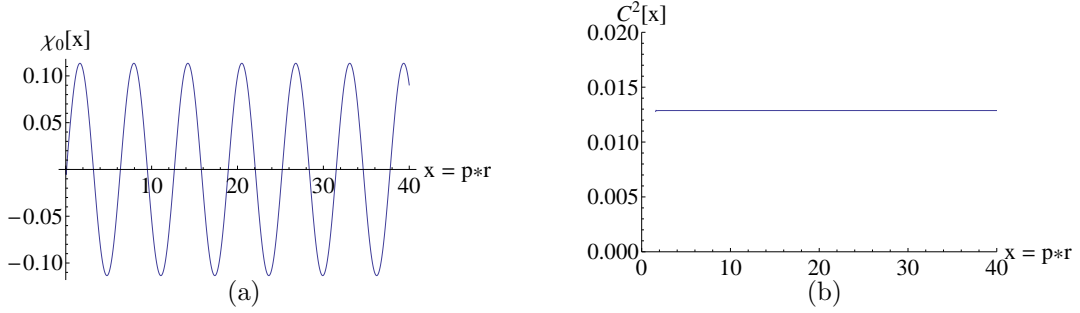


Figure 5.5.: Numerical solution to eq. (5.68) for $l = 0$ with initial conditions $\tilde{\chi}_0(0) = 0$ and $\tilde{\chi}'_0(0) = 1$. Input parameters were chosen $\alpha = 10^{-2}$, $m_\phi = 1\text{GeV}$, $m_\chi = 1\text{TeV}$, $v = 8.2 \times 10^{-5}$.

- a) Reduced wavefunction $\tilde{\chi}_0(x)$ vs. the dimensionless $x = p \cdot r$ variable.
b) $\tilde{\chi}_0(x)^2 + \tilde{\chi}_0(x - \frac{\pi}{2})^2$ vs. the dimensionless $x = p \cdot r$ variable. For large x , the reduced wavefunction takes its asymptotic form (5.69) and we effectively plot C^2 .

Since we are able to reproduce the numerical procedure described by Iengo [23] to extract the Sommerfeld enhancement for a specific parameter point, we are going to investigate the dependence of the enhancement factor S on the relative particle velocity v as well as the dark matter mass $m_{DM} \equiv m_\chi$ for this simple model with diagonal interactions. We take this as starting point for the validation of our own numerical setup to determine the Sommerfeld enhancement to vector dark matter in Sec. 5.10. For completeness, we reproduce some of the plots from the literature to have them at our disposal in this thesis. Specifically, we check our calculation against the parameter choice of Arkani-Hamed et al. [11] and the one of Lattanzi and Silk [16]. These two benchmark scenarios are also discussed in [17]. We follow the data presentation of the latter article and fig. 5.6 can directly be compared to fig. 2 in [17]. We find excellent agreement, qualitatively and quantitatively for both parameter points.

For the results presented here are reproduced from the literature, we direct the attention to [11, 23, 38, 16] for a detailed analysis of the Sommerfeld effect in this model. A particularly concise discussion is found in [16], which we follow to sketch the physics behind eq. (5.64) and fig. 5.6.

Starting from eq. (5.64), the Schrödinger equation reduces to the well known hydrogen problem in the limit $m_\phi \rightarrow 0$. In this case, analytical solutions for $\chi(r)$ are obtained in terms of hypergeometric functions¹⁹ and the Sommerfeld enhancement is given by:

$$S = \frac{\pi\alpha}{v} (1 - e^{-\pi\alpha/v})^{-1} \xrightarrow{v \rightarrow 0} \frac{\pi\alpha}{v}. \quad (5.71)$$

with the famous $1/v$ behavior at low velocities. At very small velocities $v^2 \ll \frac{\alpha m_\phi}{m_\chi}$, however, the Yukawa part of the potential becomes relevant and we have to expand (5.64) in this regime in terms of small $m_\phi r \ll 1$ to first order:

$$\chi''(r) + \frac{\alpha m_\chi}{r} \chi(r) = \alpha m_\phi m_\chi \chi(r). \quad (5.72)$$

The positiveness of the r.h.s. of (5.72) indicates the existence of bound states analog to hydrogen, when:

$$m_\chi = 4m_\phi \frac{n^2}{\alpha}, \quad n \in \mathbb{N} \quad (5.73)$$

Comparing eq. (5.73) to the numerical results in fig. 5.6(a),(b), it is applicable that the naive estimate of the peak position via the hydrogen analogy deviates by a factor of 2 from the numerical results, the n^2 peak spacing however is approximately reproduced in fig. 5.6(b).

¹⁹c.f. e.g. [44] for the solution of the hydrogen problem

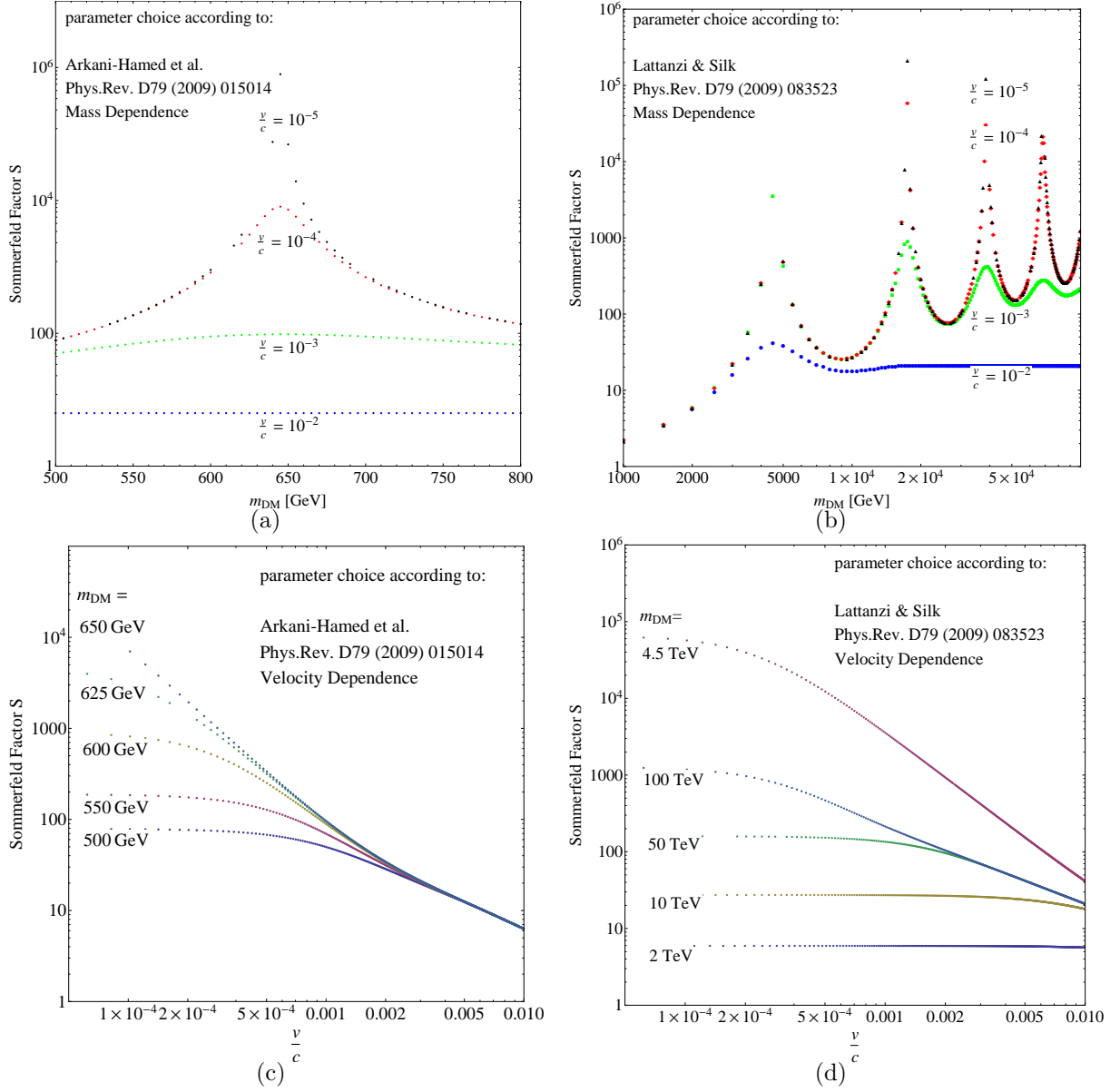


Figure 5.6.: Velocity and dark matter mass dependence of the Sommerfeld enhancement for the diagonal interaction via a Yukawa potential. We show our numerical results for the Sommerfeld factor (S) for 2 benchmark points that have been discussed in the literature. In the right panel we show our numerical results using Lattanzi and Silks [16] parameter choice - $\alpha = \frac{1}{30}, m_\phi = 90 \text{ GeV}$. In the left panel we show the results for Arkani-Hameds parameters - $\alpha = \frac{1}{100}, m_\phi = 1 \text{ GeV}$. We present the results in the same order as in [17] and agree qualitatively and quantitatively with the authors.

5.5. Sommerfeld Effect for Vector Dark Matter in $SU(2) \times SU(2) \times U(1) \times U(1)$ - Model

In the previous sections we have summarized Iengo's work [23] on fermionic dark matter to understand the important points in the derivation of the effective potential between two dark matter states. Within the non-relativistic, instantaneous Bethe-Salpeter approach, we came to realize that the pole structure in the Bethe-Salpeter equation plays a fundamental role. Baring that in mind, we feel confident to extend the work done by Iengo [23] and others to external vector particles. It seems needless to mention, that the tensor structure of the theory and the special properties of the gauge-boson propagators impede an easy transfer of QED results found in standard textbooks. The presence of gauge dependent terms and four momenta in the numerator further complicate matters. Along the derivation, we try to clearly state and justify all approximations employed. Fortunately, there are a number of articles from the QCD-community that treat glueballs as bound states of massive gluons within a Bethe-Salpeter ansatz [77, 78, 79, 80, 81]. These papers provide valuable guidance for our derivation due to the similar tensor structure of the BS-equation. For completeness, we also present the graphical representation of the Bethe-Salpeter equation for the amplitude. In the next sections we only give the graphical

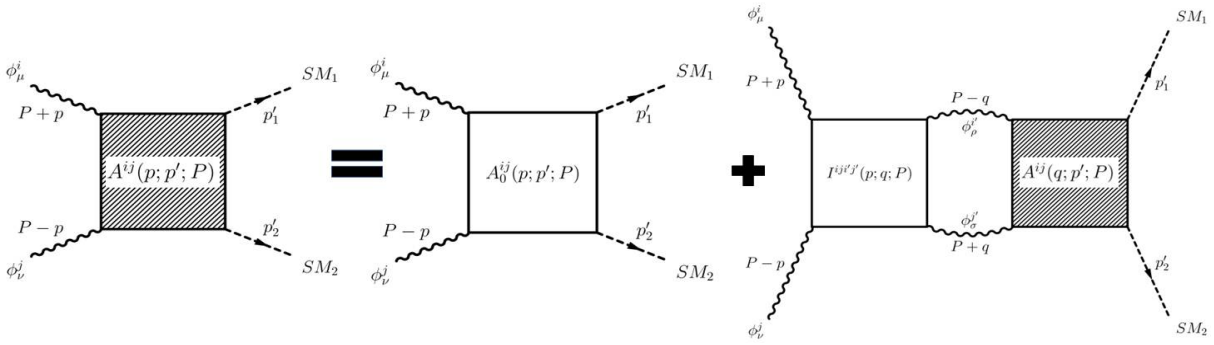


Figure 5.7.: Graphical representation of generic $2 \rightarrow 2$ scattering event from vector particles into Standard Model states. P denotes the momentum of the center of mass, p , p' and q denote relative momenta. I represents all 2 particle irreducible (2PI) graphs in the $\phi_\mu^i + \phi_\nu^j \rightarrow \phi_\rho^{i'} + \phi_\sigma^{j'}$ scattering process. A denotes the full annihilation amplitude, including nonperturbative effects, A_0 is the bare amplitude for this process.

representation of the iteration part of the Bethe-Salpeter equation, i.e. only the second term on the right hand side of fig. 5.7. In complete analogy to Refs. [23, 39], $A^{(0)ij}$ represents the bare annihilation amplitude of two dark matter particles $\phi_\mu^i + \phi_\nu^j$ into Standard Model states, neglecting nonperturbative effects between initial states. Our scattering kinematic is defined by $P = \frac{1}{2}(p_1 + p_2)$, $p = \frac{1}{2}(p_1 - p_2)$, $\omega_{\vec{p}} = \sqrt{m_\chi^2 + \vec{p}^2}$.

5.5.1. Leading Order $Z^{(1)}Z^{(1)} \rightarrow Z^{(1)}Z^{(1)}$ Bethe-Salpeter Kernel

With the $Z^{(1)}$ as our preferred dark matter candidate, it is natural to ask whether the lowest order $Z^{(1)}Z^{(1)} \rightarrow Z^{(1)}Z^{(1)}$ kernel leads to a sizable Sommerfeld enhancement. As explained in section 3.2.1, we are only interested in diagrams with light exchange particles as force carriers to start with. To leading order, we only consider diagrams with Standard Model particles in the t- and u-channel respectively²⁰. Generally, s-channel diagrams are subdominant²¹ in the nonrelativistic limit, which is why we follow [11, 23, 39] and neglect them to leading order. For beyond the Standard Model theories, however, such diagrams may develop resonances²², if there is a heavy particle Φ in the spectrum with twice the dark matter mass $m_\Phi = 2m_\chi$. In this thesis, we are going to disregard these special cases and drop all s-channel contributions.

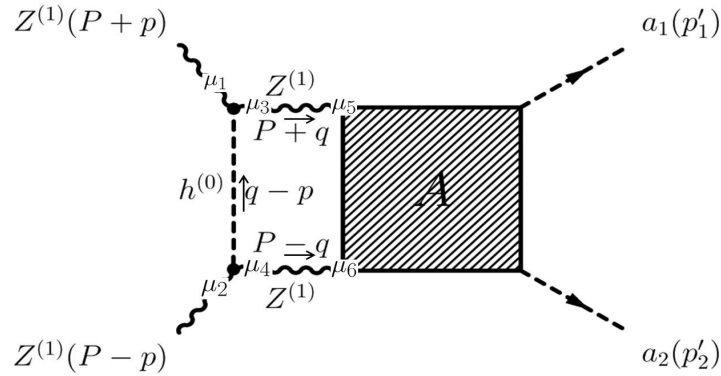


Figure 5.8.: Graphical representation of the $Z^{(1)}Z^{(1)} \rightarrow Z^{(1)}Z^{(1)}$ lowest order interaction kernel. Momentum flow is indicated by arrows and Lorentz indices are attached at all vertices for clarity. Momenta of incoming particles go into the vertices.

From the graphical representation of the amplitude depicted in figure 5.8, we can immediately read off the analytic expression using our Feynman rules in App.C.

$$A_{Z^{(1)}Z^{(1)}}^{\mu_1\mu_2} = A_{Z^{(1)}Z^{(1)}}^{(0)\mu_1\mu_2} + \int \frac{d^4q}{(2\pi)^4} \Gamma_{\mu_3}^{\mu_1} \Gamma_{\mu_4}^{\mu_2} G(q-p) D_{Z^{(1)}}^{\mu_3\mu_5}(P+q) D_{Z^{(1)}}^{\mu_4\mu_6}(P-q) A_{\mu_5\mu_6}(q, P) \quad (5.74)$$

In principle, the amplitude depends on the final state momenta (denoted by p') as well as other indices associated with the outgoing particles. This dependence however is **not**

²⁰Note that we restrict ourselves to the lowest-order 2PI graphs, so that triangle diagrams are not considered in the Bethe-Salpeter kernel. Expanding the kernel to higher order in perturbation theory would require considerable effort and should be the subject of future research.

²¹In s-channel diagrams, the denominator is proportional to $s = (p_1 + p_2)^2 \sim m_\chi^2$, so that these contributions are suppressed by the DM scale.

²²For example, s-channel diagrams can become important in full extradimensional theories due to resonances of the scattering particles with Kaluza-Klein (2)-modes (see e.g. [82]). Such scenarios are not present in our truncated version of the "deconstructed" theory.

defined by the BS-equation itself [72] and will therefore be omitted. The vertex rules for $\Gamma_{\mu_i\mu_j}$ are taken from appendix C.2.4 and the scalar and vector propagators G and $D^{\mu_k\mu_l}$ read as follows:

$$\Gamma_{\mu_j}^{\mu_i} = i g_2 m_W^{(0)} g_{\mu_j}^{\mu_i} \quad (5.75)$$

$$G(q-p) = \frac{i}{(q-p)^2 - m_{h^{(0)}}^2 + i\epsilon} \quad (5.76)$$

$$D_{Z^{(1)}}^{\mu_k\mu_l}(P \pm q) = -i \frac{\left(g^{\mu_k\mu_l} - (1-\xi) \frac{(P \pm q)^{\mu_k} (P \pm q)^{\mu_l}}{(P \pm q)^2 - \xi m_{Z^{(1)}}^2} \right)}{(P \pm q)^2 - m_{Z^{(1)}}^2 + i\epsilon} \quad (5.77)$$

Alternative Representation of the Gauge-Boson Propagator

For future discussions, it is useful to decompose the gauge boson propagator into different pole contributions. We adopt the pole prescription as found in the appendix of Ref. [40] and write:

$$\begin{aligned} D^{\mu_k\mu_l}(p) &= -i \frac{g^{\mu_k\mu_l} - p^{\mu_k} p^{\mu_l} / M^2}{p^2 - M^2 + i\epsilon} - i \frac{p^{\mu_k} p^{\mu_l} / M^2}{p^2 - \xi M^2 + i\epsilon} \\ &= -i \frac{1}{2 \omega_{\vec{p}}} [g^{\mu_k\mu_l} - p^{\mu_k} p^{\mu_l} / M^2] \left[\frac{1}{p_0 - \omega_{\vec{p}} + i\epsilon} - \frac{1}{p_0 + \omega_{\vec{p}} - i\epsilon} \right] \\ &\quad - i \frac{p^{\mu_k} p^{\mu_l}}{2 \omega_{\xi\vec{p}} M^2} \left[\frac{1}{p_0 - \omega_{\xi\vec{p}} + i\epsilon} - \frac{1}{p_0 + \omega_{\xi\vec{p}} - i\epsilon} \right] \end{aligned} \quad (5.78)$$

with the common appreviations:

$$\omega_{\vec{p}} = \sqrt{\vec{p}^2 + M^2} \quad \omega_{\xi\vec{p}} = \sqrt{\vec{p}^2 + \xi M^2}. \quad (5.79)$$

The drawback of this gauge-boson-propagator representation is the obscured good high energy behavior - UV-finiteness is not obvious from simple power counting arguments anymore. In comparison to the fermionic propagators appearing in the description of positronium and for supersymmetric dark matter considerations, we are not able to eliminate the zero-component of the loop momentum from the numerator due to the $p^{\mu_k} p^{\mu_l}$ terms. Practically, we deal with this complication by dropping the q and p dependence in the numerators of the gauge boson propagators as a first approximation and only keep $P_0 \sim m_{Z^{(1)}} \gg q_0, p_0, |\vec{q}|, |\vec{p}|$ in the leading pole region in the non-relativistic limit. An analog procedure was adopted in the calculation of leading 1-loop contributions to scalar and fermionic WIMP annihilation [76]. We are going to employ the instantaneous approximation for the $h^{(0)}$ exchange and subsequently split the scalar propagator into the instantaneous contribution and the non-instantaneous p_0 dependent part only to neglect the latter. It is easy to verify that:

$$\frac{1}{p^2 - m^2 + i\epsilon} = \frac{-1}{\vec{p}^2 + m^2} + \frac{p_0^2}{(\vec{p}^2 + m^2)(p^2 - m^2)}. \quad (5.80)$$

In the non-relativistic limit, the energy exchange is much smaller than the three momentum exchange [76]. Using the decomposed gauge boson propagators for the $Z^{(1)}$ fields in eq. (5.74) and only keeping the P dependence in the numerator²³, we find:

$$\begin{aligned}
 D_{Z^{(1)}}^{\mu_3\mu_5}(P+q)D_{Z^{(1)}}^{\mu_4\mu_6}(P-q) &\approx \left(-i \frac{1}{2\omega_{\vec{q}}} [g^{\mu_3\mu_5} - P^{\mu_3}P^{\mu_5}/m_{Z^{(1)}}^2] \times \right. \\
 &\quad \left[\frac{1}{(q_0+P_0) - \omega_{\vec{q}} + i\epsilon} - \frac{1}{(q_0+P_0) + \omega_{\vec{q}} - i\epsilon} \right] - \\
 &\quad \left. -i \frac{P^{\mu_3}P^{\mu_5}}{2\omega_{\xi\vec{q}}m_{Z^{(1)}}^2} \times \left[\frac{1}{(q_0+P_0) - \omega_{\xi\vec{q}} + i\epsilon} - \frac{1}{(q_0+P_0) + \omega_{\xi\vec{q}} - i\epsilon} \right] \right) \times \\
 &\quad (5.81) \\
 &\quad \left(-i \frac{1}{2\omega_{\vec{q}}} [g^{\mu_4\mu_6} - P^{\mu_4}P^{\mu_6}/m_{Z^{(1)}}^2] \times \right. \\
 &\quad \left[\frac{1}{(-q_0+P_0) - \omega_{\vec{q}} + i\epsilon} - \frac{1}{(-q_0+P_0) + \omega_{\vec{q}} - i\epsilon} \right] - \\
 &\quad \left. -i \frac{P^{\mu_4}P^{\mu_6}}{2\omega_{\xi\vec{q}}m_{Z^{(1)}}^2} \times \left[\frac{1}{(-q_0+P_0) - \omega_{\xi\vec{q}} + i\epsilon} - \frac{1}{(-q_0+P_0) + \omega_{\xi\vec{q}} - i\epsilon} \right] \right)
 \end{aligned}$$

In the CMS ($\vec{P} = \vec{0}$), the ω 's only depend on the three-components of the momentum vectors and therefore are independent of P . Unaffected by the numerator, we find eight poles in the product of the two $Z^{(1)}$ -propagators, four of which are non-physical, i.e. ξ dependent. We will keep them for now and only later assume, but not prove explicitly, that all ξ dependent poles cancel for a gauge invariant (on-shell) kernel. Working in unitary gauge, i.e. taking the limit $\xi \rightarrow \infty$, removes these poles altogether and no convoluted cancellation mechanism between several classes of diagrams (e.g. gauge and Goldstone boson graphs) has to take place. We work in the instantaneous approximation, therefore additional q_0 poles from the scalar exchange propagator are absent. In analogy to the argument of Iengo [23], we also neglect possible poles of the amplitude A itself. The discussion on neglecting such poles rests solely on the denominator of the diagrams, therefore differences in the numerators are irrelevant for this argument. The poles are:

- | | |
|---|--|
| (1) $q_0 = \omega_{\vec{q}} - P_0 - i\epsilon$ | (2) $q_0 = -(\omega_{\vec{q}} + P_0) + i\epsilon$ |
| (3) $q_0 = \omega_{\xi\vec{q}} - P_0 - i\epsilon$ | (4) $q_0 = -(\omega_{\xi\vec{q}} + P_0) + i\epsilon$ |
| (5) $q_0 = P_0 - \omega_{\vec{q}} + i\epsilon$ | (6) $q_0 = P_0 + \omega_{\vec{q}} - i\epsilon$ |
| (7) $q_0 = P_0 - \omega_{\xi\vec{q}} + i\epsilon$ | (8) $q_0 = P_0 + \omega_{\xi\vec{q}} - i\epsilon$ |

²³We are going to justify this approximation a posteriori by investigating the structure of the integral kernel and show that q_0 remains small at the bound state pole.

Performing the contour integral in the complex q_0 plane and arbitrarily closing the integration path in the lower half, we apply Cauchy's Residue Theorem and, in general, have to evaluate four contributions.

1. pole (1) $q_0 = \omega_{\vec{q}} - P_0 - i\epsilon$:

$$\begin{aligned}
& -i m_{W^{(0)}}^2 g_2^2 \int \frac{d^3q}{(2\pi)^3} \frac{-g_{\mu_3}^{\mu_1} g_{\mu_4}^{\mu_2}}{(\vec{q} - \vec{p})^2 + m_{h^{(0)}}^2} \frac{-2\pi i}{2\pi} \left[\frac{-i}{2\omega_{\vec{q}}} \left(g^{\mu_3\mu_5} - \frac{P^{\mu_3} P^{\mu_5}}{m_{Z^{(1)}}^2} \right) \right] \times \\
& \left[\frac{-i}{2\omega_{\vec{q}}} \left(g^{\mu_4\mu_6} - \frac{P^{\mu_4} P^{\mu_6}}{m_{Z^{(1)}}^2} \right) \left(\frac{1}{P_0 - \omega_{\vec{q}} + P_0 - \omega_{\vec{q}}} - \frac{1}{P_0 - \omega_{\vec{q}} + P_0 + \omega_{\vec{q}}} \right) + \right. \\
& \left. - \frac{i}{\omega_{\xi\vec{q}}} \left(\frac{P^{\mu_4} P^{\mu_6}}{m_{Z^{(1)}}^2} \right) \left(\frac{1}{P_0 - \omega_{\vec{q}} + P_0 - \omega_{\xi\vec{q}}} - \frac{1}{P_0 - \omega_{\vec{q}} + P_0 + \omega_{\xi\vec{q}}} \right) \right] \quad (5.82)
\end{aligned}$$

2. unphysical pole (2) $q_0 = \omega_{\xi\vec{q}} - P_0 - i\epsilon$

$$\begin{aligned}
& -i m_{W^{(0)}}^2 g_2^2 \int \frac{d^3q}{(2\pi)^3} \frac{-g_{\mu_3}^{\mu_1} g_{\mu_4}^{\mu_2}}{(\vec{q} - \vec{p})^2 + m_{h^{(0)}}^2} \frac{-2\pi i}{2\pi} \left[\frac{-i}{2\omega_{\xi\vec{q}}} \left(\frac{P^{\mu_3} P^{\mu_5}}{m_{Z^{(1)}}^2} \right) \right] \times \\
& \left[\frac{-i}{2\omega_{\vec{q}}} \left(g^{\mu_4\mu_6} - \frac{P^{\mu_4} P^{\mu_6}}{m_{Z^{(1)}}^2} \right) \left(\frac{1}{P_0 - \omega_{\xi\vec{q}} + P_0 - \omega_{\vec{q}}} - \frac{1}{P_0 - \omega_{\xi\vec{q}} + P_0 + \omega_{\vec{q}}} \right) + \right. \\
& \left. - \frac{i}{\omega_{\xi\vec{q}}} \left(\frac{P^{\mu_4} P^{\mu_6}}{m_{Z^{(1)}}^2} \right) \left(\frac{1}{P_0 - \omega_{\xi\vec{q}} + P_0 - \omega_{\xi\vec{q}}} - \frac{1}{P_0 - \omega_{\xi\vec{q}} + P_0 + \omega_{\xi\vec{q}}} \right) \right] \quad (5.83)
\end{aligned}$$

3. pole (6) $q_0 = \omega_{\vec{q}} + P_0 - i\epsilon$

$$\begin{aligned}
& -i m_{W^{(0)}}^2 g_2^2 \int \frac{d^3q}{(2\pi)^3} \frac{-g_{\mu_3}^{\mu_1} g_{\mu_4}^{\mu_2}}{(\vec{q} - \vec{p})^2 + m_{h^{(0)}}^2} \left(\frac{-2\pi i}{2\pi} \right) \times \\
& \left[\frac{-i}{2\omega_{\vec{q}}} \left(\frac{g^{\mu_3\mu_5} - P^{\mu_3} P^{\mu_5}}{m_{Z^{(1)}}^2} \right) \left(\frac{1}{P_0 + \omega_{\vec{q}} + P_0 - \omega_{\vec{q}}} - \frac{1}{P_0 + \omega_{\vec{q}} + P_0 + \omega_{\vec{q}}} \right) + \right. \\
& \left. - \frac{i}{2\omega_{\xi\vec{q}}} \left(\frac{P^{\mu_3} P^{\mu_5}}{m_{Z^{(1)}}^2} \right) \left(\frac{1}{P_0 + \omega_{\vec{q}} + P_0 - \omega_{\xi\vec{q}}} - \frac{1}{P_0 + \omega_{\vec{q}} + P_0 + \omega_{\xi\vec{q}}} \right) \right] \times \\
& \left[\frac{+i}{2\omega_{\vec{q}}} \left(g^{\mu_4\mu_6} - \frac{P^{\mu_4} P^{\mu_6}}{m_{Z^{(1)}}^2} \right) \right] \quad (5.84)
\end{aligned}$$

4. unphysical pole (8) $q_0 = \omega_{\xi\vec{q}} + P_0 - i\epsilon$

$$\begin{aligned}
& -i m_{W^{(0)}}^2 g_2^2 \int \frac{d^3q}{(2\pi)^3} \frac{-g_{\mu_3}^{\mu_1} g_{\mu_4}^{\mu_2}}{(\vec{q} - \vec{p})^2 + m_{h^{(0)}}^2} \left(\frac{-2\pi i}{2\pi} \right) \times \\
& \left[\frac{-i}{2\omega_{\vec{q}}} \left(\frac{g^{\mu_3\mu_5} - P^{\mu_3} P^{\mu_5}}{m_{Z^{(1)}}^2} \right) \left(\frac{1}{P_0 + \omega_{\xi\vec{q}} + P_0 - \omega_{\vec{q}}} - \frac{1}{P_0 + \omega_{\xi\vec{q}} + P_0 + \omega_{\vec{q}}} \right) + \right. \\
& \left. - \frac{i}{2\omega_{\xi\vec{q}}} \left(\frac{P^{\mu_3} P^{\mu_5}}{m_{Z^{(1)}}^2} \right) \left(\frac{1}{P_0 + \omega_{\xi\vec{q}} + P_0 - \omega_{\xi\vec{q}}} - \frac{1}{P_0 + \omega_{\xi\vec{q}} + P_0 + \omega_{\xi\vec{q}}} \right) \right] \times \\
& \left[\frac{+i}{2\omega_{\xi\vec{q}}} \left(\frac{P^{\mu_4} P^{\mu_6}}{m_{Z^{(1)}}^2} \right) \right] \quad (5.85)
\end{aligned}$$

Having achieved the decomposition of the kernel, we only keep terms which have small denominators. Expressions with $\frac{1}{2(P_0 - \omega_{\xi\vec{q}})}$ appear to be relevant in the Feynman gauge, but as mentioned before we suspect that non-physical ξ dependent poles eventually cancel with contributions from other diagrams for a gauge invariant kernel. Terms with $\frac{1}{2(P_0 - \omega_{\vec{q}})}$ lead to analogous expressions as found in Iengo's paper treating fermionic dark matter. We do not want to suppress the fact that for a special choice of ξ , $\frac{1}{2P_0 - \omega_{\xi\vec{q}} + \omega_{\vec{q}}}$ can develop a small denominator which depends on the gauge parameter. Nonetheless we will drop these terms since unphysical poles should not play a role in a gauge-invariant kernel. In hindsight, the leading pole approximation also justifies the negligence of q in the numerator. The leading contribution to the scattering kernel stems from poles where $q_0 \ll P_0$. Applying the approximations stated here, we find the recursion relation for the scattering amplitude:

$$\begin{aligned}
 A_{Z^{(1)}Z^{(1)}}^{\mu_1\mu_2} = & A_{Z^{(1)}Z^{(1)}}^{(0)\mu_1\mu_2} - m_{W^{(0)}}^2 g_2^2 \int \frac{d^3q}{(2\pi)^3} \frac{1}{(\vec{q} - \vec{p})^2 + m_{h^{(0)}}^2} \times \\
 & \left[\frac{1}{4\omega_{\vec{q}}^2} \left(g^{\mu_1\mu_5} - \frac{P^{\mu_1} P^{\mu_5}}{m_{Z^{(1)}}^2} \right) \left(g^{\mu_2\mu_6} - \frac{P^{\mu_2} P^{\mu_6}}{m_{Z^{(1)}}^2} \right) \left(\frac{1}{2(P_0 - \omega_{\vec{q}})} \right) + \right. \\
 & \frac{1}{4\omega_{\vec{q}}\omega_{\xi\vec{q}}} \left(g^{\mu_1\mu_5} - \frac{P^{\mu_1} P^{\mu_5}}{m_{Z^{(1)}}^2} \right) \left(\frac{P^{\mu_2} P^{\mu_6}}{m_{Z^{(1)}}^2} \right) \left(\frac{1}{2P_0 - (\omega_{\vec{q}} + \omega_{\xi\vec{q}})} \right) + \\
 & \left. \frac{1}{4\omega_{\vec{q}}\omega_{\xi\vec{q}}} \left(\frac{P^{\mu_1} P^{\mu_5}}{m_{Z^{(1)}}^2} \right) \left(g^{\mu_2\mu_6} - \frac{P^{\mu_2} P^{\mu_6}}{m_{Z^{(1)}}^2} \right) \left(\frac{1}{2P_0 - (\omega_{\vec{q}} + \omega_{\xi\vec{q}})} \right) \right] A_{\mu_5\mu_6}(\vec{q}, P_0). \tag{5.86}
 \end{aligned}$$

It is instructive to look at the Bethe-Salpeter equation for some special values of the gauge parameter ξ . Let us start with the Feynman gauge $\xi = 1$:

$$A_{\xi=1}^{\mu_1\mu_2} = A_{\xi=1}^{(0)\mu_1\mu_2} - m_{W^{(0)}}^2 g_2^2 \int \frac{d^3q}{(2\pi)^3} \frac{g^{\mu_1\mu_5} g^{\mu_2\mu_6}}{(\vec{q} - \vec{p})^2 + m_{h^{(0)}}^2} \frac{1}{4\omega_{\vec{q}}^2} \frac{A_{\mu_5\mu_6}(\vec{q}, P_0)}{2(P_0 - \omega_{\vec{q}})} \tag{5.87}$$

We would like to direct the attention to the specific tensor structure stemming from the $Z^{(1)}$ propagators. In the Feynman gauge all degrees of freedom, including the unphysical ones, propagate. This can be illustrated by looking at the completeness relation for the gauge boson polarization vectors:

$$\sum_{\lambda=0}^3 \epsilon_{\lambda}^{\mu}(k) \epsilon^{\lambda\nu}(k) = -g^{\mu\nu}, \tag{5.88}$$

which can be decomposed into a longitudinal $L^{\mu\nu}(k)$ and a transversal $T^{\mu\nu}(k)$ part [40]:

$$L^{\mu\nu}(k) = \frac{k^{\mu} k^{\nu}}{m_V^2} \tag{5.89}$$

$$T^{\mu\nu}(k) = g^{\mu\nu} - \frac{k^{\mu} k^{\nu}}{m_V^2} \tag{5.90}$$

In a general frame where k^μ is on-shell, $T^{\mu\nu}(k)$ constitutes the projection onto the three physical states of a massive vector boson [41]. For the Bethe-Salpeter equation in unitary gauge ($\xi \rightarrow \infty$), we find:

$$A_{\xi=\infty}^{\mu_1\mu_2} = A_{\xi=\infty}^{(0)\mu_1\mu_2} - \tag{5.91}$$

$$m_{W^{(0)}}^2 g_2^2 \int \frac{d^3q}{(2\pi)^3} \frac{\left(g^{\mu_1\mu_5} - \frac{P^{\mu_1}P^{\mu_5}}{m_{Z^{(1)}}^2}\right) \left(g^{\mu_2\mu_6} - \frac{P^{\mu_2}P^{\mu_6}}{m_{Z^{(1)}}^2}\right)}{(\vec{q} - \vec{p})^2 + m_{h^{(0)}}^2} \frac{1}{4\omega_{\vec{q}}^2} \frac{A_{\mu_5\mu_6}(\vec{q}, P_0)}{2(P_0 - \omega_{\vec{q}})}$$

In light of the discussion on the vector boson polarization tensor, we immediately realize that only the physical degrees of freedom of the $Z^{(1)}$ bosons propagate in unitary gauge.

Discussion of the Yukawa-Interaction Potential Strength

We proceed by adopting another approximation: in the interaction kernel we neglect the \vec{q} dependence in ω and set $\frac{1}{4\omega_{\vec{q}}^2} \approx \frac{1}{4m_{Z^{(1)}}^2}$. Following the lines of [23] and [39], the Fourier transform of the interaction kernel yields a Yukawa potential generated by the Higgs exchange:

$$V(r) \propto \frac{m_{W^{(0)}}^2 g_2^2}{4m_{Z^{(1)}}^2} \frac{1}{4\pi} \frac{e^{-m_{h^{(0)}}r}}{r}. \tag{5.92}$$

This allows us to read off the effective coupling strength of the potential:

$$\tilde{\alpha} = \frac{m_{W^{(0)}}^2 g_2^2}{16\pi m_{Z^{(1)}}^2} \tag{5.93}$$

Plugging in the Standard Model values for $m_{W^{(0)}}$, g_2 and adopting a WIMP mass of 1 TeV, we compute $\tilde{\alpha} \approx 5.4 \times 10^{-5}$.

An order of magnitude estimation of the influence of the Higgs exchange on the Sommerfeld enhancement is now achievable. As described in the section on general aspects of the Sommerfeld effect (see Sec. 3.2.1), we have to compare the binding energy $E_B \propto m_{Z^{(1)}} \tilde{\alpha}^2$ of the $Z^{(1)}Z^{(1)}$ -system with the kinetic energy of the $Z^{(1)}$ -pair; $E_{kin} \propto m_{Z^{(1)}} v_{sp}^2$. Using a single-particle velocity of $v_{sp} = 150 \frac{km}{s} \hat{=} 5 \times 10^{-4}$ (in natural units) [11], we find that the interaction strength due to the Higgs exchange is approximately one order of magnitude too small to give a sizable contribution to the Sommerfeld effect. Matters take a turn for the worse when comparing the Bohr radius of the bound state with the range of the interaction potential as an indicator for possible resonant effects:

$$\frac{1}{m_{h^{(0)}}} > \frac{1}{m_{Z^{(1)}} \tilde{\alpha}}$$

For viable $Z^{(1)}$ -masses, we realize that the Higgs interaction is too short ranged to give a sizable enhancement, which is why we neglect any Higgs contributions to the Sommerfeld effect henceforth.

5.5.2. Off-diagonal $Z^{(1)}Z^{(1)} \rightarrow W^{(1)}W^{(1)}$ Bethe-Salpeter Kernel

Computing the Higgs exchange diagram, we found that the diagonal interactions of the $Z^{(1)}$ are too weak and short ranged to contribute significantly to the Sommerfeld effect. What we mean by "diagonal interaction" is, that the particle content is not changed from the initial to the final state of the interaction kernel. This does not rule out the possibility of a Sommerfeld enhancement altogether. We make use of the special feature of the near mass degeneracy of the $W^{(1)}$ with our $Z^{(1)}$ dark matter candidate and consider off-diagonal diagrams as depicted in figure 5.9. The topology of the $Z^{(1)}Z^{(1)} \rightarrow W^{(1)}W^{(1)}$ diagram

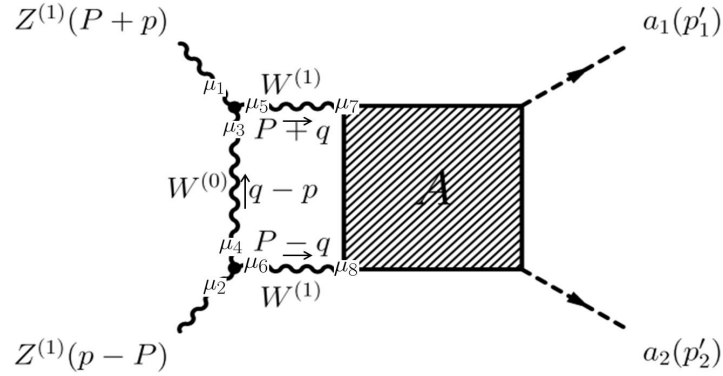


Figure 5.9.: Graphical representation of the $Z^{(1)}Z^{(1)} \rightarrow W^{(1)}W^{(1)}$ lowest order interaction kernel. Momentum flow is indicated by arrows and Lorentz indices are attached at all vertices for clarity.

is the same as the one for the $Z^{(1)}Z^{(1)} \rightarrow Z^{(1)}Z^{(1)}$ graph (5.8). Contrary to the scalar Higgs exchange particle, this time we have the $W^{(0)}$ -interaction that amounts in a more complicated kernel due to the additional Lorentz structure of the interaction vertices as well as the additional gauge propagator. To facilitate the extensive algebraic calculations we used FeynCalc [83] to perform the Lorentz tensor manipulations.

$$\begin{aligned}
 A_{Z^{(1)}W^{(1)}}^{\mu_1\mu_2} = & A_{Z^{(1)}W^{(1)}}^{(0)\mu_1\mu_2} + \int \frac{d^4q}{(2\pi)^4} \Gamma_{\mu_1\mu_3\mu_5}(P, p, q) D_{W^{(0)}}^{\mu_3\mu_4}(q-p) \Gamma_{\mu_2\mu_6\mu_4}(P, p, q) \times \\
 & D_{W^{(1)}}^{\mu_5\mu_7}(P+q) D_{W^{(1)}}^{\mu_6\mu_8}(P-q) A_{\mu_7\mu_8}(q, P_0)
 \end{aligned} \tag{5.94}$$

Applying the Feynman rules for the three gauge boson vertices C.2.2 and carefully plugging in the correct particle momenta²⁴ we obtain:

$$\begin{aligned}
 \Gamma_{\mu_1\mu_3\mu_5}(P, p, q) = & ig_2 \cos(\theta_W^{(1)}) [g_{\mu_3\mu_5}(p-P-2q)_{\mu_1} + g_{\mu_1\mu_3}(q-P-2p)_{\mu_5} + g_{\mu_1\mu_5}(p+q+2P)_{\mu_3}] \\
 \Gamma_{\mu_2\mu_6\mu_4}(P, p, q) = & ig_2 \cos(\theta_W^{(1)}) [g_{\mu_4\mu_6}(p+P-2q)_{\mu_2} + g_{\mu_2\mu_4}(q+P-2p)_{\mu_6} + g_{\mu_2\mu_6}(p+q-2P)_{\mu_4}]
 \end{aligned}$$

In the $W^{(0)}$ -propagator, we set all q and p momentum variables in the numerator to zero which eliminates the gauge parameter dependence of the exchange propagator in this

²⁴Feynman rules are given for incoming momenta

approximation. We are left with the metric tensor $g^{\mu_3\mu_4}$ in the numerator and can easily employ the instantaneous approximation to find:

$$D_{W^{(0)}}^{\mu_3\mu_4}(\vec{q} - \vec{p}) = \frac{+i g^{\mu_3\mu_4}}{(\vec{q} - \vec{p})^2 + m_{W^{(0)}}^2} \quad (5.95)$$

Omitting some Lorentz indices, setting $\theta_W^{(1)}$ to zero and contracting the vertices Γ with the $W^{(0)}$ -propagator leads to:

$$\begin{aligned} A_{Z^{(1)}W^{(1)}} = & A_{Z^{(1)}W^{(1)}}^{(0)} + ig_2^2 \int \frac{d^4q}{(2\pi)^4} \frac{1}{(\vec{q} - \vec{p})^2 + m_{W^{(0)}}^2} \times \\ & (g^{\mu_1\mu_6} P^{\mu_2} P^{\mu_5} + g^{\mu_1\mu_2} P^{\mu_5} P^{\mu_6} - 4g^{\mu_1\mu_5} P^{\mu_2} P^{\mu_6} + P^{\mu_1} (P^{\mu_2} g^{\mu_5\mu_6} - 4P^{\mu_5} g^{\mu_2\mu_6} + P^{\mu_6} g^{\mu_2\mu_5}) \\ & + 4P^2 g^{\mu_1\mu_5} g^{\mu_2\mu_6}) D_{\mu_5, W^{(1)}}^{\mu_7}(P+q) D_{\mu_6, W^{(1)}}^{\mu_8}(P-q) A_{\mu_7\mu_8}(q, P_0) \end{aligned} \quad (5.96)$$

To obtain this result, we set q and p to zero in the interaction vertices (static approximation) and only kept the leading P contributions. Since the $W^{(0)}$ -exchange does not depend on q_0 in the instantaneous approximation, we can pull the $\int \frac{dq_0}{2\pi}$ through to the $W^{(1)}$ -propagators and use an analogous pole decomposition as in section 5.5.1. Contracting the vertices, the $W^{(0)}$ -propagator and the leading terms of the two $W^{(1)}$ -propagators amounts to a rather lengthy expression in R_ξ gauge which we do not write out explicitly. Since we are interested in the contribution to the scattering amplitude from the bound state in the non-relativistic limit, we effectively put a delta-function for the loop-momentum that picks out the desired kinematic region. In the following derivations, we are going to work in unitary gauge, where only physical degrees of freedom contribute to the computed quantities. This procedure limits the number of relevant Feynman-diagrams considerably. For the off-diagonal recurrence relation in unitary gauge, we find:

$$\begin{aligned} A_{Z^{(1)}W^{(1)}}^{\xi=\infty} = & A_{Z^{(1)}W^{(1)}}^{(0), \xi=\infty} - g_2^2 \int \frac{d^3q}{(2\pi)^3} \frac{1}{((\vec{q} - \vec{p})^2 + m_{W^{(0)}}^2)} \times \\ & (g^{\mu_1\mu_6} P^{\mu_2} P^{\mu_5} + g^{\mu_1\mu_2} P^{\mu_5} P^{\mu_6} - 4g^{\mu_1\mu_5} P^{\mu_2} P^{\mu_6} + \\ & P^{\mu_1} (P^{\mu_2} g^{\mu_5\mu_6} - 4P^{\mu_5} g^{\mu_2\mu_6} + P^{\mu_6} g^{\mu_2\mu_5}) + 4P^2 g^{\mu_1\mu_5} g^{\mu_2\mu_6}) \\ & \times \frac{\left(g_{\mu_5\mu_7} - \frac{P_{\mu_5} P_{\mu_7}}{m_{W^{(1)}}^2} \right) \left(g_{\mu_6\mu_8} - \frac{P_{\mu_6} P_{\mu_8}}{m_{W^{(1)}}^2} \right)}{4\omega_{\vec{q}}^2 2(P_0 - \omega_{\vec{q}})} A^{\mu_7\mu_8}(\vec{q}, P_0). \end{aligned} \quad (5.97)$$

Let us note at this point, that the interaction coefficient is not weakened by $\frac{m_{W^{(0)}}^2}{m_{Z^{(1)}}^2}$ any more as was the case for the Higgs exchange diagram. The unsuppressed coupling strength motivates us to calculate the u-channel and the contact diagram to complete the leading order interaction kernel for the $Z^{(1)}Z^{(1)} \rightarrow W^{(1)}W^{(1)}$ system, up to a subdominant contribution with a $h^{(0)}$ in the s-channel. The tensor structure in the denominator and their respective signs imply a mixture of attractive and repulsive contributions described in the effective non-relativistic potential language.

5.5.3. Off-diagonal $Z^{(1)}Z^{(1)} \rightarrow W^{(1)}W^{(1)}$ u-channel Diagram

As we have seen in the previous section, the $Z^{(1)}Z^{(1)} \rightarrow W^{(1)}W^{(1)}$ scattering is not suppressed by small prefactors in the non-relativistic instantaneous approximation to the Bethe-Salpeter equation, hence it seems worth calculating the corresponding diagram with exchanged initial states. The calculation of the u-channel amplitude follows in complete

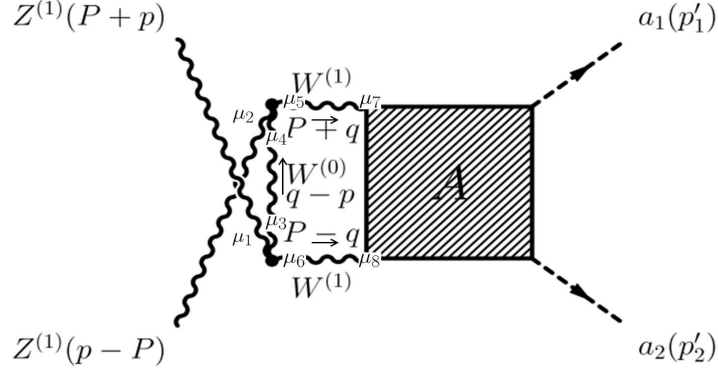


Figure 5.10.: Graphical representation of the $Z^{(1)}Z^{(1)} \rightarrow W^{(1)}W^{(1)}$ lowest order interaction kernel with exchanged initial states. Momentum flow is indicated by arrows and Lorentz indices are attached at all vertices for clarity.

analogy to the t-channel one, which is why we only give the important intermediate results.

$$A_{Z^{(1)}W^{(1)},X}^{\mu_1\mu_2} = A_{Z^{(1)}W^{(1)},X}^{(0)\mu_1\mu_2} + \int \frac{d^4q}{(2\pi)^4} \Gamma_{\mu_2\mu_4\mu_5}(P, p, q) G_{W^{(0)}}^{\mu_3\mu_4}(q+p) \Gamma_{\mu_1\mu_6\mu_3}(P, p, q) \times D_{W^{(1)}}^{\mu_5\mu_7}(P+q) D_{W^{(1)}}^{\mu_6\mu_8}(P-q) A_{\mu_7\mu_8,X}(q, P_0) \quad (5.98)$$

Using the same approximations as in section 5.5.2, we obtain the recurrence relation in unitary gauge:

$$A_{Z^{(1)}W^{(1)},X}^{\xi=\infty} \approx A_{Z^{(1)}W^{(1)},X}^{(0),\xi=\infty} - g_2^2 \int \frac{d^3q}{(2\pi)^3} \frac{1}{((\vec{q}+\vec{p})^2 + m_{W^{(0)}}^2)} \times (g^{\mu_2\mu_6} P^{\mu_1} P^{\mu_5} + g^{\mu_1\mu_2} P^{\mu_5} P^{\mu_6} - 4g^{\mu_2\mu_5} P^{\mu_1} P^{\mu_6} + P^{\mu_2} (P^{\mu_1} g^{\mu_5\mu_6} - 4P^{\mu_5} g^{\mu_1\mu_6} + P^{\mu_6} g^{\mu_1\mu_5}) + 4P^2 g^{\mu_2\mu_5} g^{\mu_1\mu_6}) \times \frac{\left(g_{\mu_5\mu_7} - \frac{P_{\mu_5} P_{\mu_7}}{m_{W^{(1)}}^2}\right) \left(g_{\mu_6\mu_8} - \frac{P_{\mu_6} P_{\mu_8}}{m_{W^{(1)}}^2}\right)}{4\omega_{\vec{q}}^2 2(P_0 - \omega_{\vec{q}})} A_X^{\mu_7\mu_8}(\vec{q}, P_0). \quad (5.99)$$

Comparing the amplitude equation with exchanged initial states to eq. (5.97), we find exactly the same tensor structure up to exchanged Lorentz indices $\mu_7 \leftrightarrow \mu_8$ or $\mu_1 \leftrightarrow \mu_2$ and different momentum flow in the $W^{(0)}$ exchange propagator.

5.5.4. Off-diagonal $Z^{(1)}Z^{(1)} \rightarrow W^{(1)}W^{(1)}$ contact Diagram

We complete the off-diagonal $Z^{(1)}Z^{(1)} \rightarrow W^{(1)}W^{(1)}$ scattering by calculating the contact diagram, which should lead to a delta-like potential in configuration space in the non-relativistic limit. The vertex factor for the $Z^{(1)}Z^{(1)}W^{(1)}W^{(1)}$ interaction is taken from

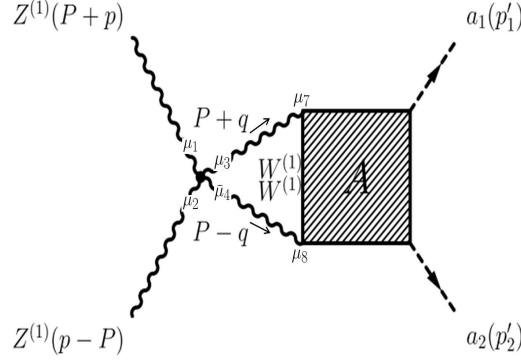


Figure 5.11.: Graphical representation of the $Z^{(1)}Z^{(1)} \rightarrow W^{(1)}W^{(1)}$ scattering amplitude for the contact kernel.

Momentum flow is indicated by arrows and Lorentz indices are attached at all vertices for clarity.

the Feynman rules in the appendix (C.2.3). We are left with the integral equation of the form:

$$A_{Z^{(1)}W^{(1)},C}^{\mu_1\mu_2} = A_{Z^{(1)}W^{(1)},C}^{(0)\mu_1\mu_2} + \int \frac{d^4q}{(2\pi)^4} \Gamma_{\mu_3\mu_4}^{\mu_1\mu_2} D_{W^{(1)}}^{\mu_3\mu_7}(P+q) D_{W^{(1)}}^{\mu_4\mu_8}(P-q) A_{\mu_7\mu_8,C}(q, P_0) \quad (5.100)$$

Without contracting the four-point vertex with the approximated gauge boson propagators we find for the Bethe-Salpeter equation in unitary gauge:

$$A_{Z^{(1)}W^{(1)},C}^{\xi=\infty} = A_{Z^{(1)}W^{(1)},C}^{(0)\xi=\infty} - g_2^2 \int \frac{d^3q}{(2\pi)^3} (g^{\mu_1\mu_4} g^{\mu_2\mu_3} + g^{\mu_1\mu_3} g^{\mu_2\mu_4} - 2g^{\mu_1\mu_2} g^{\mu_3\mu_4}) \times \quad (5.101)$$

$$\frac{\left(g_{\mu_3\mu_7} - \frac{P_{\mu_3} P_{\mu_7}}{m_{W^{(1)}}^2} \right) \left(g_{\mu_4\mu_8} - \frac{P_{\mu_4} P_{\mu_8}}{m_{W^{(1)}}^2} \right)}{4\omega_{\vec{q}}^2 2(P_0 - \omega_{\vec{q}})} A_C^{\mu_7\mu_8}(\vec{q}, P_0).$$

If we compare the different classes of diagrams by an order of magnitude estimate, we find that the ones with an $W^{(0)}$ propagator are dominant over the contact diagrams. The t- and u-channel kernels scale as:

$$I_{Z^{(1)}W^{(1)}} \sim I_{Z^{(1)}W^{(1)},X} \sim d^3q \frac{1}{\vec{q}^2 + m_{W^{(0)}}^2} \frac{1}{m_{W^{(1)}}^2} P^2 \frac{1}{P_0 - m_{W^{(1)}}} \quad (5.102)$$

$$\sim \frac{d^3q}{(\vec{q}^2 + m_{W^{(0)}}^2)(P_0 - m_{W^{(1)}})}$$

whereas the contact kernel scales as:

$$I_{Z^{(1)}W^{(1)},C} \sim \frac{d^3q}{m_{W^{(1)}}^2(P_0 - m_{W^{(1)}})}. \quad (5.103)$$

This estimate reveals a suppression of the contact term by a factor of $\sim \frac{m_{W^{(0)}}^2}{m_{W^{(1)}}^2}$.

5.5.5. Reversed off-diagonal Diagrams: $W^{(1)}W^{(1)} \rightarrow Z^{(1)}Z^{(1)}$

An exchange of in- and out- states in the four-point kernels for the gauge boson scattering does not affect the Bethe-Salpeter result except for a trivial substitution of the appropriate masses in the heavy gauge-boson propagators and in $\omega_{\vec{q}} = \sqrt{m_{Z^{(1)}}^2 + \vec{q}^2}$. Using this feature of the theory, we can directly copy the equations from the $Z^{(1)}Z^{(1)} \rightarrow W^{(1)}W^{(1)}$ computation. To see the symmetry property explicitly, it is easiest to look at the four gauge boson contact interaction vertex (C.15) which manifestly possesses the invariance of in- and out state exchange.

5.5.6. Diagonal $W^{(1)}W^{(1)} \rightarrow W^{(1)}W^{(1)}$ Scattering Diagrams

To complete the considerations on the heavy gauge boson scattering for the Bethe-Salpeter kernel we have to calculate the diagonal $W^{(1)}W^{(1)} \rightarrow W^{(1)}W^{(1)}$ contribution. Contrary to all previously calculated diagrams we have to include the massless photon exchange which we treat separately. We would like to mention that we do not consider the Higgs exchange diagrams due to a coupling suppression already explained in section 5.5.1. We

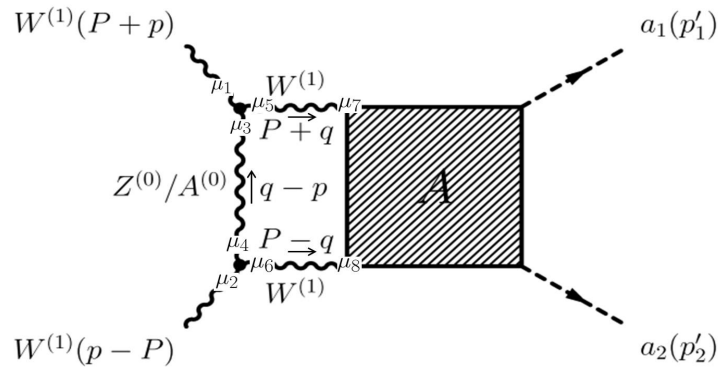


Figure 5.12.: Graphical representation of the $W^{(1)}W^{(1)} \rightarrow W^{(1)}W^{(1)}$ scattering amplitude for $Z^{(0)}$ and $A^{(0)}$ interaction kernel.

Momentum flow is indicated by arrows and Lorentz indices are attached for clarity.

write the recurrence relation for the amplitude with an $Z^{(0)}$ exchange propagator:

$$A_{W^{(1)}W^{(1)}}^{\mu_1\mu_2} = A_{W^{(1)}W^{(1)}}^{(0)\mu_1\mu_2} + \int \frac{d^3q}{(2\pi)^4} \Gamma_{\mu_3\mu_5}^{\mu_1}(q-p, -(P+q), P+p) D_{Z^{(0)}}^{\mu_3\mu_4}(q-p) \quad (5.104)$$

$$\Gamma_{\mu_4}^{\mu_2}(-q-p, P-p, -(P-q)) D_{W^{(1)}}^{\mu_5\mu_7}(P+q) D_{W^{(1)}}^{\mu_6\mu_8}(P-q) A_{\mu_7\mu_8}^{W^{(1)}W^{(1)}}(q, p', P_0)$$

Applying the usual approximations we explained in the previous sections we find the expected result in unitary gauge:

$$A_{W^{(1)}W^{(1)}}^{\xi=\infty} \approx A_{W^{(1)}W^{(1)}}^{(0),\xi=\infty} - g_2^2 \cos(\theta_W^{(0)}) \int \frac{d^3q}{(2\pi)^3} \frac{1}{(\vec{q}-\vec{p})^2 + m_{Z^{(0)}}^2} \times \quad (5.105)$$

$$(g^{\mu_1\mu_6} P^{\mu_2} P^{\mu_5} + g^{\mu_1\mu_2} P^{\mu_5} P^{\mu_6} - 4g^{\mu_1\mu_5} P^{\mu_2} P^{\mu_6} +$$

$$P^{\mu_1} (P^{\mu_2} g^{\mu_5\mu_6} - 4P^{\mu_5} g^{\mu_2\mu_6} + P^{\mu_6} g^{\mu_2\mu_5}) + 4P^2 g^{\mu_1\mu_5} g^{\mu_2\mu_6})$$

$$\times \frac{\left(g_{\mu_5\mu_7} - \frac{P_{\mu_5} P_{\mu_7}}{m_{W^{(1)}}^2}\right) \left(g_{\mu_6\mu_8} - \frac{P_{\mu_6} P_{\mu_8}}{m_{W^{(1)}}^2}\right)}{4\omega_{\vec{q}}^2 2(P_0 - \omega_{\vec{q}})} A^{\mu_7\mu_8}(\vec{q}, p', P_0)$$

which exactly coincides with the result found in the corresponding $Z^{(1)}Z^{(1)} \rightarrow W^{(1)}W^{(1)}$ calculation up to the SM Weinberg angle $\cos(\theta_W^{(0)})$ entering the vertex factor and the $Z^{(0)}$ - instead of the $W^{(0)}$ mass to account for the different exchange propagator.

5.5.7. $W^{(1)}W^{(1)} \rightarrow W^{(1)}W^{(1)}$ Photon exchange Diagram

Besides the exchange of a massive gauge boson, the $W^{(1)}W^{(1)} \rightarrow W^{(1)}W^{(1)}$ scattering kernel includes the diagram with a photon in the t-channel (see figure 5.12). This is the first time we have to deal with a massless exchange particle which could possibly lead to additional poles in the scattering amplitude (see comment in [84]). The propagator for a massless gauge boson in general R_ξ gauge is [40]:

$$D^{\mu\nu}(k) = \frac{-i}{k^2 + i\epsilon} \left(g^{\mu\nu} - (1 - \xi) \frac{k^\mu k^\nu}{k^2} \right) \quad (5.106)$$

The difference in the coupling strength discriminating the $Z^{(0)}$ - from the $A^{(0)}$ -diagram is rather simple and only involves the substitution of $g_2 \cos(\theta_W^{(0)}) \rightarrow e$ in the vertex factors. The presence of the $\frac{k^\mu k^\nu}{k^2}$ in the propagator however poses a somewhat more delicate problem, since we can not apply our usual approximation of setting the relative momenta to zero in the numerator. To circumvent this problem we choose to set the photon gauge parameter ξ_A to 1, which removes the problematic terms and leaves us with the photon propagator in a simple Lorenz gauge. If one were to calculate the on-shell kernel, the k dependence would vanish identically due to transversality. Working in unitary gauge for

the massive gauge bosons and with $\xi_A = 1$ for the photon, we find:

$$\begin{aligned}
 A_{W^{(1)}W^{(1)},A^{(0)}}^{\xi=\infty,\xi_A=1} &\approx A_{W^{(1)}W^{(1)}}^{(0),\xi=\infty,\xi_A=1} - e^2 \int \frac{d^3q}{(2\pi)^3} \frac{1}{(\vec{q} - \vec{p})^2} \times \\
 &(g^{\mu_1\mu_6} P^{\mu_2} P^{\mu_5} + g^{\mu_1\mu_2} P^{\mu_5} P^{\mu_6} - 4g^{\mu_1\mu_5} P^{\mu_2} P^{\mu_6} + \\
 &P^{\mu_1} (P^{\mu_2} g^{\mu_5\mu_6} - 4P^{\mu_5} g^{\mu_2\mu_6} + P^{\mu_6} g^{\mu_2\mu_5}) + 4P^2 g^{\mu_1\mu_5} g^{\mu_2\mu_6}) \\
 &\times \frac{g_{\mu_5\mu_7} g_{\mu_6\mu_8}}{4\omega_{\vec{q}}^2 2(P_0 - \omega_{\vec{q}})} A^{\mu_7\mu_8}(\vec{q}, p', P_0)
 \end{aligned} \tag{5.107}$$

5.5.8. $W^{(1)}W^{(1)} \rightarrow W^{(1)}W^{(1)}$ contact Diagram

The similarity of the $W^{(1)}W^{(1)} \rightarrow W^{(1)}W^{(1)}$ to the $Z^{(1)}Z^{(1)} \rightarrow W^{(1)}W^{(1)}$ scattering encountered in the previous section also holds for the contact diagram. The tensor structure remains the same and only the scalar vertex factor for the $4 \times W^{(1)}$ interaction has to be modified. According to the Feynman rules of our theory (C.15) the difference between the $Z^{(1)}Z^{(1)}W^{(1)}W^{(1)}$ and $W^{(1)}W^{(1)}W^{(1)}W^{(1)}$ factor is an overall minus sign. This is a trivial change and we do not repeat the recurrence relation but only refer to eq. (5.100) to read off the appropriate result.

In unitary gauge, this completes the lowest order scattering kernel \widehat{I} and we can write the coupled system of Bethe-Salpeter equations in matrix notation:

$$A^{ij}(\vec{p}, P) = A^{(0)ij}(\vec{p}, P) + \int \frac{d^3q}{(2\pi)^3} \widehat{I}^{ij,i'j'} A^{i'j'}(\vec{q}, P) \tag{5.108}$$

or more explicitly:

$$\begin{pmatrix} A^{ZZ} \\ A^{WW} \end{pmatrix}(\vec{p}, P) = \begin{pmatrix} A^{(0)ZZ} \\ A^{(0)WW} \end{pmatrix}(\vec{p}, P) + \int \frac{d^3q}{(2\pi)^3} \begin{pmatrix} I^{ZZZZ} & I^{ZZWW} \\ I^{WWZZ} & I^{WWWW} \end{pmatrix}(\vec{p}, \vec{q}, P) \begin{pmatrix} A^{ZZ} \\ A^{WW} \end{pmatrix}(\vec{q}, P)$$

5.6. Neglected Terms in the Ladder Approximation

In this section, we will briefly discuss classes of diagrams that are omitted in the ladder approximation to the Bethe-Salpeter equation in addition to s-channel graphs and crossed boxes. In the nonrelativistic limit, we have already demonstrated, that crossed box diagrams are suppressed in section 5.2. In unitary gauge, we will argue that all other diagrams are subdominant in comparison to the regular box in fig. 5.13(a) in the nonrelativistic, instantaneous approximation considered here. We restrict ourselves to the discussion of one-loop graphs for the $Z^{(1)}Z^{(1)} \rightarrow W^{(1)}W^{(1)}$ -kernel, but all other interaction kernels display similar topologies, so that the line of reasoning follows analogously.

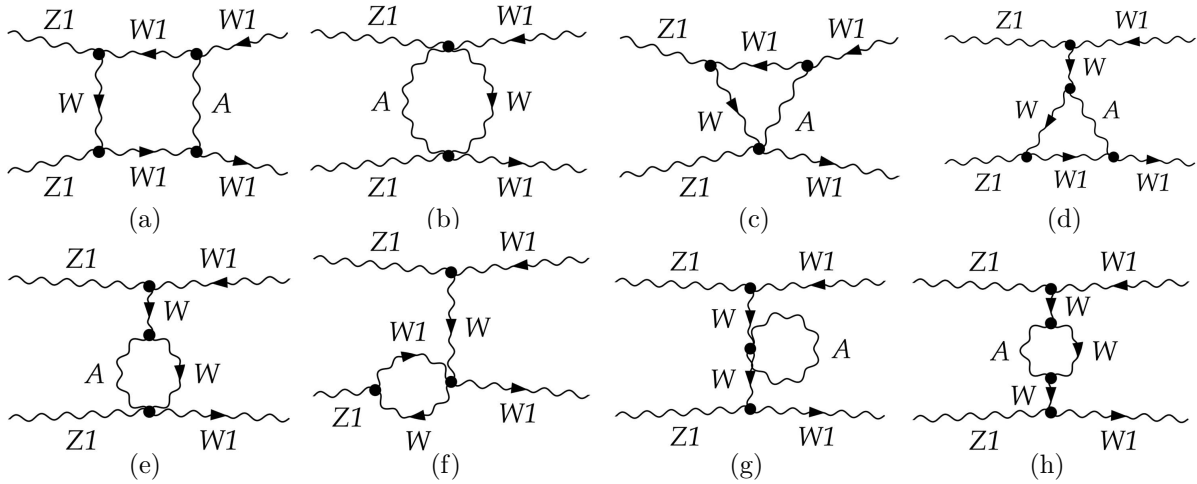


Figure 5.13.: Discussion of neglected Feynman diagrams in the ladder approximation to the Bethe-Salpeter kernel. This list is an exemplary selection of graphs that would appear in a complete one-loop calculation. We only show one-loop graphs for $Z^{(1)}Z^{(1)} \rightarrow W^{(1)}W^{(1)}$ -scattering, the other interaction kernels contain similar topologies. Note that s-channel diagrams and graphs with crossed exchange-lines are not shown here. Heavy modes are indicated by a "1".

As we have discussed in the previous sections explicitly, the box diagrams similar to 5.13(a) are enhanced in the nonrelativistic instantaneous limit, as we employ the unitary gauge. The enhancement of diagram 5.13(a) was a direct result from the integration over the zero component of the loop-momentum q , which led to the small denominator²⁵ $(P_0 - \omega_{\vec{q}}) \sim m_\chi \alpha^2$ (see e.g. eq. (5.97)) in the nonrelativistic regime. In this situation, the small denominator resulted from the interplay between the poles of the **two** heavy gauge boson propagators, which will neither occur in diagram 5.13(b) nor 5.13(c). Note, that the instantaneous limit is important for this discussion, so that the propagators of the exchange particles do not have poles in q_0 .

One might wonder, why we have not considered box diagrams with heavy modes on the ladder steps and Standard Model fields as lateral bars (Feynman graph similar to 5.13(a), but heavy and light modes interchanged in the box) in the nonrelativistic instantaneous approximation. In the instantaneous limit, the interaction range of the heavy modes in the ladder steps is very short and becomes delta-like in the limit $m_\chi \rightarrow \infty$, so that such diagrams do not influence the Schrödinger wavefunction considerably. This has been discussed in section 3.2.1.

Diagram 5.13(d) contributes to the first order correction to the triple-gauge-boson vertex and is neglected in our weakly coupled theory. The same is true for graphs 5.13(e) and 5.13(f). In principle we could include such diagrams by "dressing" the three-gauge-boson-vertices in the sense of solving the corresponding Dyson-Schwinger equations [67, 85]. A similar statement holds true for diagrams 5.13(g) and 5.13(h), which contribute to the first correction to the propagators. Such terms are in principle implemented by "dressed" two-point functions, where "dressed" is understood in the same sense as for the vertex corrections. Working with "dressed" propagators and vertices is beyond the scope of this work and we restrict ourselves to the lowest order two- and three-point functions.

5.7. Definition of the Bethe-Salpeter Wavefunction

Let us pursue the analogy to Iengo [23] and Nakanishi [68] and introduce the Bethe-Salpeter wavefunction as a generalized form factor [70] of the bound state (see also chapter 5.1 and eq. (5.41)). We follow the notation of [39] and have an annihilation cascade of the form

$$\phi_a \phi_b \rightarrow \phi_i \phi_j \rightarrow \phi'_i \phi'_j \rightarrow \cdots \rightarrow \text{SM final states} \quad (5.109)$$

in mind. Working in unitary gauge for the massive gauge bosons rotates all physical degrees of freedom into the gauge boson propagators which subsequently become transversal. The definitions given below reflect this choice of gauge, but could easily be generalized if desired. The advantage of the unitary gauge is the limited number of Feynman diagrams that have to be taken into account for the integral kernel because only the physical modes are present from the start (Goldstone bosons and ghost decouple)[40]. In the non-relativistic limit and the center of mass system we define:

$$\begin{aligned} \chi_{ij}^{\mu\nu}(\vec{q}, P_0) &= \left(g^{\mu\rho} - \frac{P^\mu P^\rho}{m_i^2} \right) \left(g^{\nu\sigma} - \frac{P^\nu P^\sigma}{m_j^2} \right) \frac{A_{\rho\sigma}^{ij}(\vec{q}, P_0)}{4\omega_{\vec{q}}^2 2(\omega_{\vec{q}} - P_0)} \\ &\approx \left(g^{\mu\rho} - \frac{P^\mu P^\rho}{m_i^2} \right) \left(g^{\nu\sigma} - \frac{P^\nu P^\sigma}{m_j^2} \right) \frac{A_{\rho\sigma}^{ij}(\vec{q}, P_0)}{4\omega_{\vec{q}}^2 \left(\frac{\vec{q}^2}{2m_r^{ij}} - \mathcal{E} + 2\delta m_{ij} \right)} \end{aligned} \quad (5.110)$$

where $\mathcal{E} = \frac{\vec{p}^2}{2m_r^{ab}}$ denotes the kinetic energy of the incoming pair, $m_r^{ij} = \frac{m_i m_j}{m_i + m_j}$ the reduced mass of the $\{ij\}$ pair and $2\delta m_{ij} = m_i + m_j - (m_a + m_b)$ parameterizes the mass splitting. Note that the order of the denominator $\frac{1}{2(\omega_{\vec{q}} - P_0)}$ in (5.110) is reversed compared to all our expressions for the recurrence relations, which gives an additional minus sign. By rewriting the recurrence relation for the scattering amplitudes in terms of Bethe-Salpeter wavefunctions, we obtain a set of coupled Schrödinger equations (see [39] for the analog MSSM result) in momentum space which can be expressed symbolically as²⁶:

$$\begin{aligned} A_{\mu_1 \mu_2}^{ij}(\vec{p}, P) &= A_{\mu_1 \mu_2}^{(0)ij} + \sum_{\{i'j'\}} \int \frac{d^3 q}{(2\pi)^3} K_{\mu_1 \mu_2 \rho \sigma}^{ij, i'j'}(\vec{p}, \vec{q}, P_0) \\ &\quad \left(g^{\rho\mu_7} - \frac{P^\rho P^{\mu_7}}{m_{i'}^2} \right) \left(g^{\sigma\mu_8} - \frac{P^\sigma P^{\mu_8}}{m_{j'}^2} \right) \frac{A_{\mu_7 \mu_8}^{i'j'}(\vec{q}, P_0)}{4\omega_{\vec{q}}^2 \left(\frac{\vec{q}^2}{2m_r^{i'j'}} - \mathcal{E} + 2\delta m_{i'j'} \right)} \end{aligned} \quad (5.111)$$

$$\begin{aligned} \Rightarrow 4\omega_{\vec{p}}^2 \left(\frac{\vec{p}^2}{2m_r^{ij}} - \mathcal{E} + 2\delta m_{ij} \right) &\left(g^{\mu_1 \rho} - \frac{P^{\mu_1} P^\rho}{m_i^2} \right)^{-1} \left(g^{\mu_2 \sigma} - \frac{P^{\mu_2} P^\sigma}{m_j^2} \right)^{-1} \chi_{\rho\sigma}^{ij}(\vec{p}, P_0) \\ &= A_{\mu_1 \mu_2}^{(0)ij}(\vec{p}, P_0) + \sum_{\{i'j'\}} \int \frac{d^3 q}{(2\pi)^3} K_{\mu_1 \mu_2}^{i, j, i', j'; \mu_7, \mu_8}(\vec{p}, \vec{q}, P_0) \chi_{\mu_7 \mu_8}^{i'j'}(\vec{q}, P_0) \end{aligned} \quad (5.112)$$

²⁶In a general R_ξ -gauge, Goldstone bosons and ghost have to be considered as well for $\{ij\}$.

$$\begin{aligned}
\Rightarrow & \left(\frac{\vec{p}^2}{2m_r^{ij}} - \mathcal{E} + 2\delta m_{ij} \right) \chi_{\mu_1 \mu_2}^{ij}(\vec{p}, P_0) \\
& = \tilde{U}_{\mu_1 \mu_2}^{(0)ij}(\vec{p}, P_0) + \sum_{\{i'j'\}} \int \frac{d^3q}{(2\pi)^3} V_{\mu_1 \mu_2}^{i,j,i',j';\mu_7,\mu_8}(\vec{p}, \vec{q}, P_0) \chi_{\mu_7 \mu_8}^{i',j'}(\vec{q}, P_0) \\
& \quad \{ij\}, \{i'j'\} \in \{ \{Z^{(1)}Z^{(1)}\}, \{W^{(1)}W^{(1)}\} \}
\end{aligned} \tag{5.113}$$

In the last step we have made use of the redefinition

$$\begin{aligned}
V_{\mu_1 \mu_2}^{i,j,i',j';\mu_7,\mu_8}(\vec{p}, \vec{q}, P_0) &= \frac{1}{4\omega_{\vec{p}}^2} \left(g_{\mu_1}^\rho - \frac{P_{\mu_1} P^\rho}{m_i^2} \right) \left(g_{\mu_2}^\sigma - \frac{P_{\mu_2} P^\sigma}{m_j^2} \right) K_{\rho\sigma}^{i,j,i',j';\mu_7,\mu_8}(\vec{p}, \vec{q}, P_0) \\
\tilde{U}_{\mu_1 \mu_2}^{(0)ij}(\vec{p}, P_0) &= \frac{1}{4\omega_{\vec{p}}^2} \left(g_{\mu_1}^\rho - \frac{P_{\mu_1} P^\rho}{m_i^2} \right) \left(g_{\mu_2}^\sigma - \frac{P_{\mu_2} P^\sigma}{m_j^2} \right) A_{\rho\sigma}^{(0)ij}(\vec{p}, P_0)
\end{aligned}$$

to express the Bethe-Salpeter equation as an effective Schrödinger equation in the non-relativistic, instantaneous limit with relative momenta p , q neglected in the numerators. The integral kernels $K_{\mu_1 \mu_2}^{i,j,i',j';\mu_7,\mu_8}(\vec{p}, \vec{q}, P_0)$ and correspondingly $V_{\mu_1 \mu_2}^{i,j,i',j';\mu_7,\mu_8}(\vec{p}, \vec{q}, P_0)$ are a sum of different contributions, associated to the appropriate field theory diagrams for each combination $\{ij, i'j'\}$. In the approximation applied above, we immediately realize that $\chi_{\mu\nu}$ is transversal on the mass shell:

$$P^\mu \chi_{\mu\nu} = P^\nu \chi_{\mu\nu} = 0 \tag{5.114}$$

due to the vanishing right hand side of eq. (5.113).

5.8. Summary of Integral Kernels

We have just recast the recurrence relation for the amplitudes $A^{\mu\nu}$ into a set of equations for the Bethe-Salpeter amplitudes $\chi_{\mu\nu}^{ij}$. We were able to extract the lowest order interaction kernels from field theory diagrams by applying our Feynman rules. After all transformations applied so far, let us briefly summarize the integral kernels to have them compactly on one page. The results are obtained within the instantaneous ladder approximation with all small momenta q, p disregarded in the numerators and in unitary gauge:

$$\begin{aligned}
V_{\mu_1\mu_2}^{ZZWW, \mu_7\mu_8}(\vec{p}, \vec{q}, P) &= \frac{1}{4\omega_{\vec{p}}^2} \left[g_{\mu_1}^\rho - \frac{P_{\mu_1} P^\rho}{m_{Z(1)}^2} \right] \left[g_{\mu_2}^\sigma - \frac{P_{\mu_2} P^\sigma}{m_{Z(1)}^2} \right] \times \\
&\left\{ \frac{g_2^2}{(\vec{q} - \vec{p})^2 + m_{W(0)}^2} [g_\rho^{\mu_8} P_\sigma P^{\mu_7} + g_{\rho\sigma} P^{\mu_7} P^{\mu_8} - 4g_\rho^{\mu_7} P_\sigma P^{\mu_8} \right. \\
&\quad \left. + P_\rho (P_\sigma g^{\mu_7\mu_8} - 4P^{\mu_7} g_\sigma^{\mu_8} + P^{\mu_8} g_\sigma^{\mu_7}) + 4P^2 g_\rho^{\mu_7} g_\sigma^{\mu_8}] \right. \\
&\quad \left. + \frac{g_2^2}{(\vec{q} + \vec{p})^2 + m_{W(0)}^2} [\rho \leftrightarrow \sigma] \right. \\
&\quad \left. + g_2^2 [g_\rho^{\mu_8} g_\sigma^{\mu_7} + g_\rho^{\mu_7} g_\sigma^{\mu_8} - 2g_{\rho\sigma} g^{\mu_7\mu_8}] \right\}
\end{aligned} \tag{5.115}$$

$$\begin{aligned}
V_{\mu_1\mu_2}^{WWWW, \mu_7\mu_8}(\vec{p}, \vec{q}, P) &= \frac{1}{4\omega_{\vec{p}}^2} \left[g_{\mu_1}^\rho - \frac{P_{\mu_1} P^\rho}{m_{W(1)}^2} \right] \left[g_{\mu_2}^\sigma - \frac{P_{\mu_2} P^\sigma}{m_{W(1)}^2} \right] \times \\
&\left\{ \left[\frac{g_2^2 \text{Cos}[\theta_W^0]}{(\vec{q} - \vec{p})^2 + m_{Z(0)}^2} + \frac{e^2}{(\vec{q} - \vec{p})^2} \right] [g_\rho^{\mu_8} P_\sigma P^{\mu_7} + g_{\rho\sigma} P^{\mu_7} P^{\mu_8} - 4g_\rho^{\mu_7} P_\sigma P^{\mu_8} \right. \\
&\quad \left. + P_\rho (P_\sigma g^{\mu_7\mu_8} - 4P^{\mu_7} g_\sigma^{\mu_8} + P^{\mu_8} g_\sigma^{\mu_7}) + 4P^2 g_\rho^{\mu_7} g_\sigma^{\mu_8}] \right. \\
&\quad \left. - g_2^2 [g_\rho^{\mu_8} g_\sigma^{\mu_7} + g_\rho^{\mu_7} g_\sigma^{\mu_8} - 2g_{\rho\sigma} g^{\mu_7\mu_8}] \right\}
\end{aligned} \tag{5.116}$$

The $V_{\mu_1\mu_2}^{WWZZ, \mu_7\mu_8}(\vec{p}, \vec{q}, P)$ integral kernel is identical to eq. (5.115) up to a trivial substitution of $m_{Z(1)}^2 \leftrightarrow m_{W(1)}^2$. Note that the $\omega_{\vec{p}}$'s have to be adjusted to the incoming particles, i.e. $\omega_{\vec{p}} = \sqrt{m_{Z(1)}^2 + \vec{p}^2}$ for the $V_{\mu_1\mu_2}^{ZZWW, \mu_7\mu_8}(\vec{p}, \vec{q}, P)$ kernel and $\omega_{\vec{p}} = \sqrt{m_{W(1)}^2 + \vec{p}^2}$ for the $V_{\mu_1\mu_2}^{WWZZ, \mu_7\mu_8}(\vec{p}, \vec{q}, P)$ and $V_{\mu_1\mu_2}^{WWWW, \mu_7\mu_8}(\vec{p}, \vec{q}, P)$ case.

5.9. Spin Decomposition of Tensor Fields

Even though we have already introduced a number of approximations to the Bethe-Salpeter equation, it remains rather hard to determine the overall sign of the effective potential. The non-relativistic Schrödinger equation 5.113 still contains different bound state spin contributions. By introducing a set of projection operators we hope to disentangle different spin configurations and thereby simplifying the calculations.

A general second-rank tensor $T^{\mu\nu}$ can be decomposed into a 10 component symmetric and a 6 component anti-symmetric part [86, 87]. These tensors can subsequently be decomposed into their spin representations. We take the projection operators given by Barnes [86] to treat our bound state amplitude formed by two vector particles. The general $T^{\mu\nu}$ decomposes into representations $\mathbf{D}(2) \oplus 3 \cdot \mathbf{D}(1) \oplus 2 \cdot \mathbf{D}(0)$ which give just the right number of degrees of freedom, i.e. 16. The corresponding projection operators in momentum space are:

$$\begin{aligned}
P_2^{\mu\nu\mu'\nu'} &= \frac{1}{2} \left[\theta^{\mu\mu'} \theta^{\nu\nu'} + \theta^{\mu\nu'} \theta^{\nu\mu'} \right] - \frac{1}{3} \theta^{\mu\nu} \theta^{\mu'\nu'} \\
P_1^{\mu\nu\mu'\nu'} &= \frac{1}{2k^2} \left[\theta^{\mu\mu'} k^\nu k^{\nu'} + \theta^{\nu\nu'} k^\mu k^{\mu'} + \theta^{\mu\nu'} k^\nu k^{\mu'} + \theta^{\nu\mu'} k^\mu k^{\nu'} \right] \\
P_0^{\mu\nu\mu'\nu'} &= \frac{1}{12} \psi^{\mu\nu} \psi^{\mu'\nu'} \\
A_1^{(1),\mu\nu\mu'\nu'} &= \frac{1}{2k^2} \left[g^{\mu\mu'} k^\nu k^{\nu'} - g^{\nu\nu'} k^\mu k^{\mu'} - g^{\mu\nu'} k^\nu k^{\mu'} + g^{\nu\mu'} k^\mu k^{\nu'} \right] \\
A_1^{(2),\mu\nu\mu'\nu'} &= \frac{1}{2} \left[g^{\mu\mu'} g^{\nu\nu'} - g^{\mu\nu'} g^{\nu\mu'} \right] - \frac{1}{2k^2} \left[g^{\mu\mu'} k^\nu k^{\nu'} - g^{\nu\nu'} k^\mu k^{\mu'} - g^{\mu\nu'} k^\nu k^{\mu'} + g^{\nu\mu'} k^\mu k^{\nu'} \right]
\end{aligned} \tag{5.117}$$

with the shorthand notation:

$$\theta^{\mu\nu} = g^{\mu\nu} - \frac{k^\mu k^\nu}{k^2} \qquad \psi^{\mu\nu} = g^{\mu\nu} - 4 \frac{k^\mu k^\nu}{k^2}$$

The derivation of these projection operators and their particular four-momentum dependence are neatly explained in [87] and shall not be repeated here. We will however give the explicit expressions for the projection operators $P_{(S)}$ for the spin-2, spin-1 and spin-0 subspaces²⁷[87]:

$$\begin{aligned}
\widehat{P}_{(2),\sigma\rho}^{\mu\nu} &= -\frac{1}{3} g^{\mu\nu} g_{\sigma\rho} + \frac{1}{2} (g_\sigma^\mu g_\rho^\nu + g_\rho^\mu g_\sigma^\nu) \\
&+ \frac{1}{3k^2} (g^{\mu\nu} k_\sigma k_\rho + k^\mu k^\nu g_{\sigma\rho}) + \frac{2}{3k^4} k^\mu k^\nu k_\sigma k_\rho \\
&- \frac{1}{2k^2} (g_\rho^\nu k^\mu k_\sigma + g_\sigma^\mu k^\nu k_\rho + g_\rho^\mu k^\nu k_\sigma + g_\sigma^\nu k^\mu k_\rho)
\end{aligned} \tag{5.118}$$

²⁷We have corrected a few typos in the expressions given by [87], so that the projection operator identities hold in our case.

$$\begin{aligned}
\widehat{P}_{(1),\sigma\rho}^{\mu\nu} &= \frac{1}{2}(g_\sigma^\mu g_\rho^\nu - g_\rho^\mu g_\sigma^\nu) \\
&+ \frac{1}{2k^2}(g_\rho^\nu k^\mu k_\sigma + g_\sigma^\mu k^\nu k_\rho + g_\rho^\mu k^\nu k_\sigma + g_\sigma^\nu k^\mu k_\rho) \\
&- \frac{2}{k^4}k^\mu k^\nu k_\sigma k_\rho
\end{aligned} \tag{5.119}$$

$$\begin{aligned}
\widehat{P}_{(0),\sigma\rho}^{\mu\nu} &= \frac{1}{3}g^{\mu\nu}g_{\sigma\rho} - \frac{1}{3k^2}(g^{\mu\nu}k_\sigma k_\rho + k^\mu k^\nu g_{\sigma\rho}) \\
&+ \frac{4}{3k^4}k^\mu k^\nu k_\sigma k_\rho
\end{aligned} \tag{5.120}$$

It is important to note that [86, 87] discuss spin projectors for fundamental tensor fields. We on the other hand have to deal with a composite state, potentially involving relative momenta p and q to describe the compound object. We define the projectors using four-momentum P^μ and plug them into eq. (5.113) to decouple the BS-equation into different subspaces (which are not necessarily the spin subspaces for the compound object), utilizing the special property of projection operators, i.e. $\mathbb{1} = \sum_i \widehat{P}_{(i)}(P)$ and $\widehat{P}_{(i)}^2(P) = \widehat{P}_{(i)}(P)$. On the bound state pole, the inhomogeneous contribution $\widetilde{U}_{\mu_1\mu_2}^{(0)}(\vec{p})$ is subdominant [39] and will be neglected in the following. We eventually drop some Lorentz indices and momentum dependences for brevity and write:

$$\begin{aligned}
\left(\frac{\vec{p}^2}{2m_r^{ij}} - \mathcal{E} + 2\delta m_{ij}\right)\chi_{\mu_1\mu_2}^{ij} &\propto \sum_{\{i',j'\}} \int \frac{d^3q}{(2\pi)^3} V_{\mu_1\mu_2}^{i,j,i',j';\mu_7,\mu_8}(\vec{p}, \vec{q}, P_0) \mathbb{1} \chi_{\mu_7\mu_8}^{i',j'}(\vec{q}, P_0) \\
&= \sum_{l=0}^2 \sum_{\{i',j'\}} \int \frac{d^3q}{(2\pi)^3} V^{i,j,i',j'}(\vec{p}, \vec{q}, P_0) \widehat{P}_{(l)}^2 \chi^{i',j'}(\vec{q}, P_0) \\
\Rightarrow \left(\frac{\vec{p}^2}{2m_r^{ij}} - \mathcal{E} + 2\delta m_{ij}\right)\widehat{P}_{(l)} \chi^{ij} &\propto \sum_{l=0}^2 \sum_{\{i',j'\}} \int \frac{d^3q}{(2\pi)^3} \widehat{P}_{(l)} V^{i,j,i',j'}(\vec{p}, \vec{q}, P_0) \widehat{P}_{(l)} \widehat{P}_{(l)} \chi^{i',j'}(\vec{q}, P_0)
\end{aligned}$$

In our approximation, neglecting all q, p in the numerator of the interaction term, it can be shown that $\widehat{P}_{(l')}(P) V^{i,j,i',j'}(\vec{p}, \vec{q}, P_0) \widehat{P}_{(l)}(P) = \widetilde{V}_{i,j,i',j'}^{(l' \rightarrow l)} \delta_{l'l} \equiv \widetilde{V}_{i,j,i',j'}^{(l)}$, i.e. the interaction kernel is blockdiagonal with subspaces defined by the projection operators. Having achieved this decomposition we can look at each subspace separately.

$$\Rightarrow \left(\frac{\vec{p}^2}{2m_r^{ij}} - \mathcal{E} + 2\delta m_{ij}\right)\chi_{l'}^{ij} = \sum_{\{i',j'\}} \int \frac{d^3q}{(2\pi)^3} \widetilde{V}_{i,j,i',j'}^{(l')} \chi_{l'}^{i',j'} \tag{5.121}$$

We have introduced the notation:

$$\chi_l^{i',j'}(\vec{q}, P) = \widehat{P}_{(l)}(P) \chi^{i',j'}(\vec{q}, P_0) \tag{5.122}$$

5.9.1. Tensor Decomposition of the Bethe-Salpeter Amplitude

We write the Bethe-Salpeter amplitude in terms of Lorentz tensors. The most general structure we can write down in momentum space is:

$$\chi_{ij}^{\mu\nu}(q, P) = f_0^{ij} g^{\mu\nu} - f_1^{ij} \frac{P^\mu P^\nu}{P^2} + f_4^{ij} \frac{q^\mu q^\nu}{q^2} + f_2^{ij} P^\mu q^\nu + f_3^{ij} P^\nu q^\mu + f_5^{ij} \epsilon^{\mu\nu\rho\sigma} P_\rho q_\sigma. \quad (5.123)$$

The coefficients f_k^{ij} ; $\{ij\} \in \{ZZ, WW\}$ in principle depend on Lorentz scalars involving contractions of q and P . From the transversality condition (5.114) we immediately realize that $f_0 = f_1$ and $f_2 = f_3 = 0$.

$\widehat{P}_{(0)}(\mathbf{P})$ -subspace

Applying the projection operator $\widehat{P}_{(0)}(P)$ to eq. (5.123) we find²⁸:

$$\widehat{P}_{(0)}^{\mu\nu\rho\sigma}(P) \chi_{\rho\sigma}^{ij}(\vec{q}, P) \equiv \chi_{(0),ij}^{\mu\nu}(\vec{q}, P) = \left(g^{\mu\nu} - \frac{P^\mu P^\nu}{P^2} \right) \left(\frac{3f_0^{ij}(\vec{q}, P) + f_4^{ij}(\vec{q}, P)}{3} \right) \quad (5.124)$$

Going back to the homogeneous Bethe-Salpeter equation (5.121), setting the diagonal $Z^{(1)} Z^{(1)} \rightarrow Z^{(1)} Z^{(1)}$ kernel to zero²⁹ and contracting $\widetilde{V}_{ZZWW}^{(0)}$ with $\chi_{(0)}^{WW}$ leads to:

$$\begin{aligned} & \left(\frac{\vec{p}^2}{2m_r^2} - \mathcal{E} + 2\delta m_{ZZ} \right) \left(g^{\mu\nu} - \frac{P^\mu P^\nu}{P^2} \right) \phi_{(0)}^{ZZ}(\vec{p}, P) \\ &= g_2^2 \frac{P^2}{\omega_{\vec{p}}^2} \int \frac{d^3 q}{(2\pi)^3} \left(\frac{1}{m_{W(0)}^2 + (\vec{q} - \vec{p})^2} + \frac{1}{m_{W(0)}^2 + (\vec{q} + \vec{p})^2} - \frac{1}{P^2} \right) \left(g^{\mu\nu} - \frac{P^\mu P^\nu}{P^2} \right) \phi_{(0)}^{WW}(\vec{q}, P) \end{aligned} \quad (5.125)$$

where we have defined:

$$\phi_{(0)}^{ij}(\vec{q}, P) = \left(\frac{3f_0^{ij}(\vec{q}, P) + f_4^{ij}(\vec{q}, P)}{3} \right) \quad (5.126)$$

$$\chi_{(0), ZZ/WW}^{\mu\nu}(\vec{q}, P) = \left(g^{\mu\nu} - \frac{P^\mu P^\nu}{P^2} \right) \phi_{(0)}^{ZZ/WW}(\vec{q}, P) \quad (5.127)$$

The tensor structure of the Bethe-Salpeter wavefunction can be factored out and (5.121) reduces to a coupled system of scalar equations in the $\widehat{P}_{(0)}(P)$ subspace:

$$\begin{pmatrix} \left(\frac{\vec{p}^2}{2m_r^2} - \mathcal{E} + 2\delta m_{ZZ} \right) \phi_{(0)}^{ZZ}(\vec{p}, P) \\ \left(\frac{\vec{p}^2}{2m_r^2} - \mathcal{E} + 2\delta m_{WW} \right) \phi_{(0)}^{WW}(\vec{p}, P) \end{pmatrix} = \int \frac{d^3 q}{(2\pi)^3} \begin{pmatrix} \widetilde{V}_{ZZZZ}^{(0)}(\vec{p}, \vec{q}, P) & \widetilde{V}_{ZZWW}^{(0)}(\vec{p}, \vec{q}, P) \\ \widetilde{V}_{WWZZ}^{(0)}(\vec{p}, \vec{q}, P) & \widetilde{V}_{WWWW}^{(0)}(\vec{p}, \vec{q}, P) \end{pmatrix} \cdot \begin{pmatrix} \phi_{(0)}^{ZZ}(\vec{q}, P) \\ \phi_{(0)}^{WW}(\vec{q}, P) \end{pmatrix} \quad (5.128)$$

²⁸Note that $P \cdot q = 0$, since P only possesses a nonvanishing P_0 in the CMS and the zero-component of q has already been integrated out.

²⁹The lowest order interaction kernel is suppressed, see discussion in section 5.5.1.

with the matrix elements:

$$\tilde{V}_{ZZZZ}^{(0)}(\vec{p}, \vec{q}, P) \approx 0 \quad (5.129)$$

$$\tilde{V}_{ZZWW}^{(0)}(\vec{p}, \vec{q}, P) = \frac{g_2^2 P^2}{\omega_p^2(m_{W^{(0)}}^2 + (\vec{q} - \vec{p})^2)} + \frac{g_2^2 P^2}{\omega_p^2(m_{W^{(0)}}^2 + (\vec{q} + \vec{p})^2)} - \frac{g_2^2}{\omega_p^2} \quad (5.130)$$

$$\tilde{V}_{WWZZ}^{(0)}(\vec{p}, \vec{q}, P) = \frac{g_2^2 P^2}{\omega_p^2(m_{W^{(0)}}^2 + (\vec{q} - \vec{p})^2)} + \frac{g_2^2 P^2}{\omega_p^2(m_{W^{(0)}}^2 + (\vec{q} + \vec{p})^2)} - \frac{g_2^2}{\omega_p^2} \quad (5.131)$$

$$\tilde{V}_{WWWW}^{(0)}(\vec{p}, \vec{q}, P) = \frac{g_2^2 \text{Cos}^2(\theta_W^{(0)}) P^2}{\omega_p^2(m_{Z^{(0)}}^2 + (\vec{q} - \vec{p})^2)} + \frac{e^2 P^2}{\omega_p^2(\vec{q} - \vec{p})^2} + \frac{g_2^2}{\omega_p^2} \quad (5.132)$$

In the $\hat{P}_{(0)}$ subspace, the scalar amplitudes $\phi_{(0)}^{ij}$ can be functions of q^2 and P^2 , therefore a redefinition of momentum $q \rightarrow -q$ in the second term of the kernel does not change the physics. We combine the contributions from the t- and u-channel diagrams and get a factor of two in front of the gauge boson exchange terms. As we already realized, the contact term is suppressed by $\frac{m_{W^{(0)}}^2}{m_{W^{(1)}}^2}$ and henceforth we are going to neglect it as an approximation. This reduces the number of terms in the BS-equation even further³⁰:

$$\tilde{V}_{ZZZZ}^{(0)}(\vec{p}, \vec{q}, P) \approx 0 \quad (5.133)$$

$$\tilde{V}_{ZZWW}^{(0)}(\vec{p}, \vec{q}, P) \approx \frac{2 g_2^2 P^2}{\omega_p^2(m_{W^{(0)}}^2 + (\vec{q} - \vec{p})^2)} \approx \frac{2 g_2^2}{(m_{W^{(0)}}^2 + (\vec{q} - \vec{p})^2)} \quad (5.134)$$

$$\tilde{V}_{WWZZ}^{(0)}(\vec{p}, \vec{q}, P) \approx \frac{2 g_2^2 P^2}{\omega_p^2(m_{W^{(0)}}^2 + (\vec{q} - \vec{p})^2)} \approx \frac{2 g_2^2}{(m_{W^{(0)}}^2 + (\vec{q} - \vec{p})^2)} \quad (5.135)$$

$$\begin{aligned} \tilde{V}_{WWWW}^{(0)}(\vec{p}, \vec{q}, P) &\approx \frac{g_2^2 \text{Cos}^2(\theta_W^{(0)}) P^2}{\omega_p^2(m_{Z^{(0)}}^2 + (\vec{q} - \vec{p})^2)} + \frac{e^2 P^2}{\omega_p^2(\vec{q} - \vec{p})^2} \\ &\approx \frac{g_2^2 \text{Cos}^2(\theta_W^{(0)})}{(m_{Z^{(0)}}^2 + (\vec{q} - \vec{p})^2)} + \frac{e^2}{(\vec{q} - \vec{p})^2} \end{aligned} \quad (5.136)$$

We have to solve a coupled system of Schrödinger equations (eq. (5.128)) which can in principle be accomplished by diagonalizing the matrix valued potential. Unfortunately, due to the difference in the denominators of $\tilde{V}_{ZZWW}^{(0)}(\vec{p}, \vec{q}, P)$ and $\tilde{V}_{WWWW}^{(0)}(\vec{p}, \vec{q}, P)$, one loses the simple Yukawa-like interaction structure by the diagonalization. The approximated interaction potential has the form:

$$\begin{pmatrix} 0 & a \\ a & b \end{pmatrix} \quad (5.137)$$

with eigenvalues:

$$\lambda_{1,2} = \frac{1}{2}(b \pm \sqrt{4a^2 + b^2}) \quad (5.138)$$

³⁰To leading order, we set $\frac{P^2}{\omega_q^2} = 1$.

We realize however, that we obtain one attractive (λ_1) and one repulsive (λ_2) contribution to the potential in the diagonalization process. Therefore, before even solving the decoupled system of equations explicitly, we are able to make an important statement which was the primary goal of the entire project. In the scattering process of two vector particles, there is at least one irreducible component that leads to an **attractive** force and the formation of a loosely bound two-particle state in the non-relativistic instantaneous limit. In our case this two-particle state is a mixture of $Z^{(1)}Z^{(1)}$ and $W^{(1)}W^{(1)}$ which can lead to a Sommerfeld enhanced annihilation amplitude. Instead of diagonalizing the potential matrix directly, one can follow the treatment of Hryczuk [39] and solve the equations by a partial wave decomposition ansatz to deal with the system of Schrödinger equations numerically. It is common to Fourier-transform the Schrödinger equation into configuration space:

$$\begin{aligned} \left(\frac{\vec{p}^2}{2m_r^{ZZ}} - \mathcal{E} + 2\delta m_{ZZ}\right) \phi_{(0)}^{ZZ}(\vec{p}, P) &= \int \frac{d^3q}{(2\pi)^3} \frac{2g_2^2}{(m_{W^{(0)}}^2 + (\vec{q} - \vec{p})^2)} \phi_{(0)}^{WW}(\vec{q}, P) \\ \int \frac{d^3p}{(2\pi)^3} e^{-i\vec{p}\cdot\vec{x}} \left(\frac{\vec{p}^2}{2m_r^{ZZ}} - \mathcal{E} + 2\delta m_{ZZ}\right) \phi_{(0)}^{ZZ}(\vec{p}, P) \\ &= 2g_2^2 \int \frac{d^3p}{(2\pi)^3} \int \frac{d^3q}{(2\pi)^3} e^{-i\vec{p}\cdot\vec{x}} \frac{1}{(m_{W^{(0)}}^2 + (\vec{q} - \vec{p})^2)} \phi_{(0)}^{WW}(\vec{q}, P) \end{aligned}$$

after a momentum shift $\vec{p} \rightarrow \vec{p}' + \vec{q}$ on the r.h.s.

$$\begin{aligned} &= 2g_2^2 \int \frac{d^3p'}{(2\pi)^3} \int \frac{d^3q}{(2\pi)^3} e^{-i(\vec{p}'+\vec{q})\cdot\vec{x}} \frac{1}{(m_{W^{(0)}}^2 + \vec{p}'^2)} \phi_{(0)}^{WW}(\vec{q}, P) \\ &= 2g_2^2 \int \frac{d^3p'}{(2\pi)^3} \frac{1}{(m_{W^{(0)}}^2 + \vec{p}'^2)} e^{-i\vec{p}'\cdot\vec{x}} \int \frac{d^3q}{(2\pi)^3} e^{-i\vec{q}\cdot\vec{x}} \phi_{(0)}^{WW}(\vec{q}, P) \\ \Rightarrow \left(-\frac{\partial_x^2}{2m_r^{ZZ}} - \mathcal{E} + 2\delta m_{ZZ}\right) \phi_{(0)}^{ZZ}(\vec{x}, P) &= \frac{2g_2^2}{4\pi} \frac{e^{-m_{W^{(0)}}|\vec{x}|}}{|\vec{x}|} \phi_{(0)}^{WW}(\vec{x}, P) \end{aligned} \quad (5.139)$$

Analogously, we can transform the second part of the matrix equation (5.128):

$$\begin{aligned} \left(-\frac{\partial_x^2}{2m_r^{WW}} - \mathcal{E} + 2\delta m_{WW}\right) \phi_{(0)}^{WW}(\vec{x}, P) &= \frac{2g_2^2}{4\pi} \frac{e^{-m_{W^{(0)}}|\vec{x}|}}{|\vec{x}|} \phi_{(0)}^{ZZ}(\vec{x}, P) \\ &+ \left(\frac{g_2^2 \text{Cos}^2(\theta_W^{(0)})}{4\pi} \frac{e^{-m_{Z^{(0)}}|\vec{x}|}}{|\vec{x}|} + \frac{e^2}{4\pi} \frac{1}{|\vec{x}|} \right) \phi_{(0)}^{WW}(\vec{x}, P) \end{aligned} \quad (5.140)$$

The vector boson exchange leads to a considerably larger Yukawa-potential coupling strength in comparison to the Higgs case. We define three coupling parameters using SM-values for g_2 and $\theta_W^{(0)}$ (see app. A):

$$\alpha_1 = \frac{e^2}{4\pi} \approx \frac{1}{128} \quad \tilde{\alpha}_2 = \frac{2g_2^2}{4\pi} \approx 0.0662 \quad \alpha_3 = \frac{g_2^2 \text{Cos}^2(\theta_W^{(0)})}{4\pi} \approx 0.0253 \quad (5.141)$$

$\widehat{\mathbf{P}}_{(1)}(\mathbf{P})$ -subspace

For the $\widehat{P}_{(1)}(P)$ subspace we proceed in complete analogy to the $\widehat{P}_{(0)}(P)$ case and apply the projection operator $\widehat{P}_{(1)}(P)$ to eq. (5.123) and use the transversality condition (5.114) to find:

$$\widehat{P}_{(1)}^{\mu\nu\rho\sigma}(P)\chi_{\rho\sigma}^{ij}(\vec{q}, P) \equiv \chi_{(1),ij}^{\mu\nu}(\vec{q}, P) = f_5^{ij} \epsilon^{\mu\nu\rho\sigma} P_\rho q_\sigma \quad (5.142)$$

$\epsilon^{\mu\nu\rho\sigma}$ denotes the completely antisymmetric Levi-Civita symbol. Note, in the center of mass system $\chi_{(1),ij}^{\mu\nu}$ is only non-zero for $\rho = 0$, therefore $\chi_{(1),ij}^{\mu\nu}$ can be reduced to $f_5^{ij} P_0 \epsilon^{mnk} q_k$; $m, n, k \in \{1, 2, 3\}$; $ij \in \{ZZ, WW\}$. Going back to the homogeneous Bethe-Salpeter equation (5.121) we have to calculate the contractions between $\widetilde{V}_{ij'j'}^{(1)}$ and $\chi_{(1)}^{i'j'}$. As for the $\widehat{P}_{(0)}(P)$ subspace $\widetilde{V}_{ZZWW}^{(1)}$ and $\widetilde{V}_{WWZZ}^{(1)}$ contain three contributions in our truncation scheme, the t- and u-channel $W^{(0)}$ exchange as well as the four gauge boson contact term (see eq. (5.115)). To leading order, we neglect the Higgs-exchange and set $\widetilde{V}_{ZZZZ}^{(1)}$ to zero. The diagonal $\widetilde{V}_{WWWW}^{(1)}$ involves the $Z^{(0)}$, $A^{(0)}$ t-channel exchange and the contact term. We give the results of the contraction explicitly:

$$\widehat{P}_{(1)}(P)V^{ZZZZ}(\vec{p}, \vec{q}, P)\widehat{P}_{(1)}(P)\chi_{(1)}^{ZZ}(\vec{q}, P) \approx 0 \quad (5.143)$$

$$\widehat{P}_{(1)}(P)V_{t\text{-channel}}^{ZZWW}(\vec{p}, \vec{q}, P)\widehat{P}_{(1)}(P)\chi_{(1)}^{WW}(\vec{q}, P) = f_5^{WW} \frac{P^2}{\omega_p^2 m_{W^{(0)}}^2 + (\vec{q} - \vec{p})^2} g_2^2 \epsilon^{\mu\nu\rho\sigma} P_\rho q_\sigma \quad (5.144)$$

$$\widehat{P}_{(1)}(P)V_{u\text{-channel}}^{ZZWW}(\vec{p}, \vec{q}, P)\widehat{P}_{(1)}(P)\chi_{(1)}^{WW}(\vec{q}, P) = -f_5^{WW} \frac{P^2}{\omega_p^2 m_{W^{(0)}}^2 + (\vec{q} + \vec{p})^2} g_2^2 \epsilon^{\mu\nu\rho\sigma} P_\rho q_\sigma \quad (5.145)$$

$$\widehat{P}_{(1)}(P)V_{\text{contact}}^{ZZWW}(\vec{p}, \vec{q}, P)\widehat{P}_{(1)}(P)\chi_{(1)}^{WW}(\vec{q}, P) = 0 \quad (5.146)$$

The difference between the t- and u-channel contribution stems from the topology of the diagrams. The potential terms differ by an exchange of the final state Lorentz indices which directly leads to the minus sign upon contraction with the antisymmetric Levi-Civita symbol. The difference in the $W_{(0)}$ -boson propagator is a result from the different momentum flow. Changing q to $-q$ in the integration for the u-channel term, we realize that the t- and u-channel contributions are in fact equal as argued in the glueball literature (see e.g. [78]). The contraction of the reversed off-diagonal kernel $\widehat{P}_{(1)}(P)V_i^{WWZZ}(\vec{p}, \vec{q}, P)\widehat{P}_{(1)}(P)$ with $\chi_{(1)}^{ZZ}(\vec{q}, P)$ leads to similar expressions:

$$\widehat{P}_{(1)}(P)V_{t\text{-channel}}^{WWZZ}(\vec{p}, \vec{q}, P)\widehat{P}_{(1)}(P)\chi_{(1)}^{ZZ}(\vec{q}, P) = f_5^{ZZ} \frac{P^2}{\omega_p^2 m_{W^{(0)}}^2 + (\vec{q} - \vec{p})^2} g_2^2 \epsilon^{\mu\nu\rho\sigma} P_\rho q_\sigma \quad (5.147)$$

$$\widehat{P}_{(1)}(P)V_{u\text{-channel}}^{WWZZ}(\vec{p}, \vec{q}, P)\widehat{P}_{(1)}(P)\chi_{(1)}^{ZZ}(\vec{q}, P) = -f_5^{ZZ} \frac{P^2}{\omega_p^2 m_{W^{(0)}}^2 + (\vec{q} + \vec{p})^2} g_2^2 \epsilon^{\mu\nu\rho\sigma} P_\rho q_\sigma \quad (5.148)$$

$$\widehat{P}_{(1)}(P)V_{\text{contact}}^{WWZZ}(\vec{p}, \vec{q}, P)\widehat{P}_{(1)}(P)\chi_{(1)}^{ZZ}(\vec{q}, P) = 0 \quad (5.149)$$

Last but not least, we have to perform the contraction between the diagonal $\widehat{P}_{(1)}(P)V_i^{WWWW}(\vec{p}, \vec{q}, P)\widehat{P}_{(1)}(P)$ and $\chi_{(1)}^{WW}(\vec{q}, P)$ to obtain:

$$\widehat{P}_{(1)}(P)V_{Z^{(0)}-exchange}^{WWWW}(\vec{p}, \vec{q}, P)\widehat{P}_{(1)}(P)\chi_{(1)}^{WW}(\vec{q}, P) = f_5^{WW} \frac{P^2}{\omega_{\vec{p}}^2} \frac{g_2^2 \text{Cos}^2(\theta_W^{(0)})}{m_{Z^{(0)}}^2 + (\vec{q} - \vec{p})^2} \epsilon^{\mu\nu\rho\sigma} P_\rho q_\sigma \quad (5.150)$$

$$\widehat{P}_{(1)}(P)V_{A^{(0)}-exchange}^{WWWW}(\vec{p}, \vec{q}, P)\widehat{P}_{(1)}(P)\chi_{(1)}^{WW}(\vec{q}, P) = f_5^{WW} e^2 \frac{P^2}{\omega_{\vec{p}}^2} \frac{1}{(\vec{q} - \vec{p})^2} \epsilon^{\mu\nu\rho\sigma} P_\rho q_\sigma \quad (5.151)$$

$$\widehat{P}_{(1)}(P)V_{contact}^{WWWW}(\vec{p}, \vec{q}, P)\widehat{P}_{(1)}(P)\chi_{(1)}^{WW}(\vec{q}, P) = 0 \quad (5.152)$$

Now we are in the position to write down the coupled system of Bethe-Salpeter equations for the $\widehat{P}_{(1)}(P)$ subspace. In comparison to the $\widehat{P}_{(0)}(P)$ calculation, the Lorentz structure does not factor out and we have to keep it for the moment.

$$\begin{aligned} & \begin{pmatrix} \left(\frac{\vec{p}^2}{2m_r^2} - \mathcal{E} + 2\delta m_{ZZ} \right) \chi_{(1),ZZ}^{\mu\nu}(\vec{p}, P) \\ \left(\frac{\vec{p}^2}{2m_r^2} - \mathcal{E} + 2\delta m_{WW} \right) \chi_{(1),WW}^{\mu\nu}(\vec{p}, P) \end{pmatrix} \\ &= \int \frac{d^3q}{(2\pi)^3} \begin{pmatrix} \widetilde{V}_{ZZZZ}^{(1)}(\vec{p}, \vec{q}, P) & \widetilde{V}_{ZZWW}^{(1)}(\vec{p}, \vec{q}, P) \\ \widetilde{V}_{WWZZ}^{(1)}(\vec{p}, \vec{q}, P) & \widetilde{V}_{WWWW}^{(1)}(\vec{p}, \vec{q}, P) \end{pmatrix} \cdot \begin{pmatrix} \chi_{(1),ZZ}^{\mu\nu}(\vec{q}, P) \\ \chi_{(1),WW}^{\mu\nu}(\vec{q}, P) \end{pmatrix} \end{aligned} \quad (5.153)$$

Where we have reshuffled some terms to define the scalar potential matrix elements:

$$\widetilde{V}_{ZZZZ}^{(1)}(\vec{p}, \vec{q}, P) \approx 0 \quad (5.154)$$

$$\widetilde{V}_{ZZWW}^{(1)}(\vec{p}, \vec{q}, P) \approx \frac{2g_2^2}{m_{W^{(0)}}^2 + (\vec{q} - \vec{p})^2} \quad (5.155)$$

$$\widetilde{V}_{WWZZ}^{(1)}(\vec{p}, \vec{q}, P) \approx \frac{2g_2^2}{m_{W^{(0)}}^2 + (\vec{q} - \vec{p})^2} \quad (5.156)$$

$$\widetilde{V}_{WWWW}^{(1)}(\vec{p}, \vec{q}, P) \approx \frac{g_2^2 \text{Cos}^2(\theta_W^{(0)})}{m_{Z^{(0)}}^2 + (\vec{q} - \vec{p})^2} + \frac{e^2}{(\vec{q} - \vec{p})^2} \quad (5.157)$$

$\widehat{P}_{(2)}(\mathbf{P})$ -subspace

Finally, we apply the projection operator $\widehat{P}_{(2)}(P)$ to eq. (5.123) to find the BS-amplitude in this subspace:

$$\widehat{P}_{(2)}^{\mu\nu\rho\sigma}(P)\chi_{\rho\sigma}^{ij}(\vec{q}, P) \equiv \chi_{(2),ij}^{\mu\nu}(\vec{q}, P) = \frac{f_4^{ij}}{3} \left(-g^{\mu\nu} + \frac{P^\mu P^\nu}{P^2} + 3 \frac{q^\mu q^\nu}{q^2} \right) \quad (5.158)$$

To find the interaction potential, we repeat the analysis of the $\widehat{P}_{(1)}(P)$ subspace and also find the coupled system of Schrödinger equations:

$$\begin{aligned} & \begin{pmatrix} \left(\frac{\vec{p}^2}{2m_{ZZ}^2} - \mathcal{E} + 2\delta m_{ZZ} \right) \chi_{(2),ZZ}^{\mu\nu}(\vec{p}, P) \\ \left(\frac{\vec{p}^2}{2m_{WW}^2} - \mathcal{E} + 2\delta m_{WW} \right) \chi_{(2),WW}^{\mu\nu}(\vec{p}, P) \end{pmatrix} \\ &= \int \frac{d^3q}{(2\pi)^3} \begin{pmatrix} \widetilde{V}_{ZZZZ}^{(2)}(\vec{p}, \vec{q}, P) & \widetilde{V}_{ZZWW}^{(2)}(\vec{p}, \vec{q}, P) \\ \widetilde{V}_{WWZZ}^{(2)}(\vec{p}, \vec{q}, P) & \widetilde{V}_{WWWW}^{(2)}(\vec{p}, \vec{q}, P) \end{pmatrix} \cdot \begin{pmatrix} \chi_{(2),ZZ}^{\mu\nu}(\vec{q}, P) \\ \chi_{(2),WW}^{\mu\nu}(\vec{q}, P) \end{pmatrix}, \end{aligned} \quad (5.159)$$

with the $\widetilde{V}_{ij'j'}^{(2)}(\vec{p}, \vec{q}, P)$ matrix elements:

$$\widetilde{V}_{ZZZZ}^{(2)}(\vec{p}, \vec{q}, P) \approx 0 \quad (5.160)$$

$$\widetilde{V}_{ZZWW}^{(2)}(\vec{p}, \vec{q}, P) \approx \frac{2g_2^2}{m_{W(0)}^2 + (\vec{q} - \vec{p})^2} + \frac{g_2^2}{2\omega_p^2} \quad (5.161)$$

$$\widetilde{V}_{WWZZ}^{(2)}(\vec{p}, \vec{q}, P) \approx \frac{2g_2^2}{m_{W(0)}^2 + (\vec{q} - \vec{p})^2} + \frac{g_2^2}{2\omega_p^2} \quad (5.162)$$

$$\widetilde{V}_{WWWW}^{(2)}(\vec{p}, \vec{q}, P) \approx \frac{g_2^2 \text{Cos}^2(\theta_W^{(0)})}{m_{Z(0)}^2 + (\vec{q} - \vec{p})^2} + \frac{e^2}{(\vec{q} - \vec{p})^2} - \frac{g_2^2}{2\omega_p^2}. \quad (5.163)$$

The last terms in the potential are the result from the contact diagrams which are suppressed by $\mathcal{O}\left(\frac{m_{W(0)}^2}{m_{W(1)}^2}\right)$ and can approximately be neglected. The fact that the scalar interaction potentials are the same for all $\widehat{P}_{(i)}(P)$ subspaces indicates that the approximations applied so far, especially neglecting all relative momenta p , q in the numerator of the kernel, only retain "spin"-independent interactions. If one opts for spin-spin and spin-orbit terms one should keep the relative momentum dependence of the interaction kernel. In the absence of spin-orbit terms, the total spin of the two-body system is conserved [62]. Due to the similarity between the tensor structures of our matrix elements and the QCD-ones, considered for the Bethe-Salpeter treatment of glueballs, one expects to transfer a number of their results up to factors of δm and modifications owed to the mass of our SM-exchange particles instead of massive gluons. In fact, [77] give the potential of the one gluon exchange in configuration space.

5.10. Solution of the Coupled Schrödinger Equations

We introduced Iengo's solution to the Schrödinger equation for diagonal interactions in section 5.4 and have realized, that the enhancement factor S is tightly related to the wavefunction of the homogeneous equation. According to [18, 34, 39] this also holds, if off-diagonal potential contributions are involved. In analogy to the single-channel Sommerfeld enhancement (5.55), we define the enhanced s-wave annihilation cross section as:

$$\sigma = \begin{pmatrix} \phi^{ZZ}(0) \\ \phi^{WW}(0) \end{pmatrix}^\dagger \sigma_0 \begin{pmatrix} \phi^{ZZ}(0) \\ \phi^{WW}(0) \end{pmatrix}, \quad (5.164)$$

with the annihilation matrix:

$$\sigma_0 \propto \begin{pmatrix} |A_{Z^{(1)}Z^{(1)} \rightarrow SM}^0|^2 & (A_{Z^{(1)}Z^{(1)} \rightarrow SM}^0)^* A_{W^{(1)}W^{(1)} \rightarrow SM}^0 \\ (A_{W^{(1)}W^{(1)} \rightarrow SM}^0)^* A_{Z^{(1)}Z^{(1)} \rightarrow SM}^0 & |A_{W^{(1)}W^{(1)} \rightarrow SM}^0|^2 \end{pmatrix} \quad (5.165)$$

In the $\widehat{P}_{(0)}(P)$ subspace we have to analyze the scalar equations³¹:

$$\left[-\frac{\vec{\nabla}^2}{2m_r^{ij}} - \mathcal{E} + 2\delta m^{ij} \right] \phi_{(0)}^{ij}(\vec{r}) + \sum_{\{i'j'\}} V^{ij i'j'}(|\vec{r}|) \phi_{(0)}^{i'j'}(\vec{r}) = 0 \quad (5.166)$$

In the following we will drop the subscript (0) from the wavefunctions and introduce the shorthand notation $|\vec{r}| \equiv r$ and $|\vec{p}| \equiv p$, not to be confused with 4-momentum p^μ . To lowest order within the non-relativistic instantaneous approximation, the interaction potential displays spherical symmetry. From standard quantum mechanics textbooks [42, 43] we know that the Laplace operator Δ in spherical coordinates reads:

$$\Delta = \frac{1}{r^2} \frac{\partial}{\partial r} \left[r^2 \frac{\partial}{\partial r} \right] + \frac{1}{r^2 \sin \theta} \frac{\partial}{\partial \theta} \left[\sin \theta \frac{\partial}{\partial \theta} \right] + \frac{1}{r^2 \sin^2 \theta} \left[\frac{\partial^2}{\partial \phi^2} \right]. \quad (5.167)$$

We also introduce the angular momentum operator

$$-\hat{l}^2 = \frac{1}{\sin \theta} \frac{\partial}{\partial \theta} \left[\sin \theta \frac{\partial}{\partial \theta} \right] + \frac{1}{\sin^2 \theta} \left[\frac{\partial^2}{\partial \phi^2} \right], \quad (5.168)$$

whose eigenfunctions are the spherical harmonics $Y_{lm}(\theta, \phi)$:

$$\hat{l}^2 Y_{lm}(\theta, \phi) = l(l+1) Y_{lm}(\theta, \phi). \quad (5.169)$$

If we normalize $Y_{l,m}(\theta, \phi)$ according to:

$$\int_0^\pi d\theta \int_0^{2\pi} d\phi Y_{l,m}^*(\theta, \phi) Y_{l',m'}(\theta, \phi) = \delta_{l,l'} \delta_{m,m'}, \quad (5.170)$$

³¹See equations (5.139) and (5.140), to read off the correct potentials in configuration space. In the following we focus our analysis on the $\widehat{P}_{(0)}(P)$ subspace, the results for the other two projections would follow analogously.

the spherical harmonics may be expressed in terms of associated Legendre polynomials $P_l^m(\cos \theta)$:

$$Y_{l,m}(\theta, \phi) = \sqrt{\frac{(2l+1)(l-m)!}{4\pi(l+m)!}} P_l^m(\cos \theta) \times e^{im\phi}. \quad (5.171)$$

In section 5.4, we have demonstrated, that the Sommerfeld enhancement is determined by the solution of the scattering problem for a given initial state. Here we generalize this derivation to a coupled multi-state system. Owing to the axis defined by the incident particles, the scattering geometry displays cylindrical symmetry. In comparison to rotationally invariant problems, m is not a good quantum number any more and we have to expand the angular part of $\phi_p^{ij}(\vec{r})$ in terms of Legendre polynomials [43]:

$$\phi_p^{ij}(\vec{r}) = \sum_{l=0}^{\infty} B_l^{ij} P_l(\cos \theta) R_{p,l}^{ij}(r). \quad (5.172)$$

Plugging (5.172) into (5.166), we obtain the radial Schrödinger equation for each partial wave separately³²:

$$\left\{ \frac{1}{2m_r^{ij}} \left[\frac{1}{r^2} \frac{\partial}{\partial r} \left[r^2 \frac{\partial}{\partial r} \right] - \frac{l(l+1)}{r^2} \right] + \mathcal{E} \left(1 - \frac{2\delta m^{ij}}{\mathcal{E}} \right) \right\} B_l^{ij} R_{p,l}^{ij}(r) - \sum_{\{i'j'\}} V_{i'j'}^{ij}(r) B_l^{i'j'} R_{p,l}^{i'j'}(r) = 0. \quad (5.173)$$

Asymptotically, the potential is negligible, the system decouples and the radial wavefunctions behave as [39]:

$$\begin{cases} R_{p,l}^{ab}(r) \xrightarrow{r \rightarrow \infty} n_l^{ab} \frac{1}{r} \sin(p^{ab}r - \frac{1}{2}l\pi + \delta_l^{ab}) & , \text{ for the incoming dark matter pair} \\ R_{p,l}^{ij}(r) \xrightarrow{r \rightarrow \infty} n_l^{ij} \frac{e^{ip^{ij}r}}{r} & , \text{ for scattered states} \end{cases} \quad (5.174)$$

where $p^{ij} = \sqrt{2m_r^{ij}\mathcal{E} - 4m_r^{ij}\delta m^{ij}}$. Alternatively, the scattering solution might be cast in a more familiar way:

$$\phi^{ij}(\vec{r}) = c^{ij} e^{ip^{ij}z} + f^{ij}(r, \theta) \frac{e^{ip^{ij}r}}{r}, \quad (5.175)$$

The coefficients c^{ij} depend on the normalization of the incoming $\{ij\}$ probability current density and $f^{ij}(\theta)$ denotes the scattering amplitude. Using the asymptotic form of $e^{ip^{ij}z}$ [43]:

$$e^{ip^{ij}z} \xrightarrow{z \rightarrow \infty} \frac{1}{2ip^{ij}r} \sum_l (2l+1) P_l(\cos(\theta)) (e^{ip^{ij}r} - (-1)^l e^{-ip^{ij}r}), \quad (5.176)$$

³²In our sign convention, the potential is defined e.g. as $V^{ZZWW}(r) = -\frac{2g_2^2}{4\pi} \frac{e^{-m_W(0)r}}{r}$.

we evaluate (5.172) and (5.175) in the asymptotic limit $r \rightarrow \infty$:

$$\begin{aligned} \phi_l^{ij}(\vec{r}) &\xrightarrow{r \rightarrow \infty} c^{ij} \frac{1}{2ip^{ij}r} (2l+1) P_l(\cos(\theta)) \left(e^{ip^{ij}r} - (-1)^l e^{-ip^{ij}r} \right) + f^{ij} \frac{e^{ip^{ij}r}}{r} \\ &= B_l^{ij} P_l(\cos(\theta)) \frac{n_l^{ij}}{r} \frac{1}{2i} \left(e^{i(p^{ij}r - \frac{1}{2}\pi l + \delta_l^{ij})} - e^{-i(p^{ij}r - \frac{1}{2}\pi l + \delta_l^{ij})} \right) \end{aligned} \quad (5.177)$$

Comparing the coefficients for the incoming wave $e^{-ip^{ij}r}$, we are able to determine the expansion coefficients B_l^{ij} and find:

$$B_l^{ij} = i^l (2l+1) \frac{c^{ij}}{p^{ij} n_l^{ij}} e^{i\delta_l^{ij}}. \quad (5.178)$$

Physically, imposing (5.175) implies the boundary condition, that the scattered waves are purely outgoing and the incoming wave amplitude is normalized to c^{ij} [34].

To simplify the radial Schrödinger equation it is advantageous to introduce the reduced wavefunction $\chi_{p,l}^{ij}(r)$, so that $R_{p,l}^{ij}(r) = \frac{n_l^{ij} e^{-i\delta_l^{ij}}}{c^{ij}} \frac{\chi_{p,l}^{ij}(r)}{r}$, where we pull out the asymptotic normalization for convenience. In this parameterization, the radial kinetic term becomes:

$$\frac{1}{r^2} \frac{\partial}{\partial r} \left[r^2 \frac{\partial}{\partial r} \frac{\chi_{p,l}(r)}{r} \right] = \frac{\chi_{p,l}''(r)}{r}; \quad (5.179)$$

and we obtain the following wave equation for $\chi(r)$:

$$\frac{\partial^2}{\partial r^2} \chi_{p,l}^{ij}(r) + 2m_r^{ij} \mathcal{E} \left(\left[\left(1 - \frac{2\delta m^{ij}}{\mathcal{E}} \right) - \frac{l(l+1)}{2m_r^{ij} \mathcal{E} r^2} \right] \chi_{p,l}^{ij}(r) - \frac{1}{\mathcal{E}} \sum_{\{i'j'\}} V_{i'j'}^{ij}(r) \chi_{p,l}^{i'j'}(r) \right) = 0 \quad (5.180)$$

For numerical calculations it is favorable to introduce the dimensionless quantity $x \equiv p \cdot r$ [39]. Due to this substitution, we have to transform the derivative terms, according to:

$$\frac{\partial}{\partial r} \chi(r) \rightarrow \frac{\partial x}{\partial r} \frac{\partial}{\partial x} \chi(x) \quad \Rightarrow \quad \frac{\partial^2}{\partial r^2} \chi(r) \rightarrow p^2 \frac{\partial^2}{\partial x^2} \chi(x) \quad (5.181)$$

Making further use of the definition of $\mathcal{E} = \frac{p^2}{2m_r^{ab}} = \frac{1}{2} m_r^{ab} v^2$ in the non-relativistic limit, we transform (5.180):

$$\frac{\partial^2}{\partial x^2} \chi_{p,l}^{ij}(x) + \frac{m_r^{ij}}{m_r^{ab}} \left[\left[\left(1 - \frac{2\delta m^{ij}}{\mathcal{E}} \right) - \frac{m_r^{ab} l(l+1)}{m_r^{ij} x^2} \right] \chi_{p,l}^{ij}(x) - \frac{1}{\mathcal{E}} \sum_{\{i'j'\}} V_{i'j'}^{ij}(x) \chi_{p,l}^{i'j'}(x) \right] = 0, \quad (5.182)$$

which agrees with eq. (3.9) in [39] up to the orbital momentum term and a different sign definition for V .

Explicitly, the coupled system of Schrödinger equations reads:

$$\frac{\partial^2}{\partial x^2} \chi_{p,l}^{ZZ}(x) + \left[1 - \frac{l(l+1)}{x^2} \right] \chi_{p,l}^{ZZ}(x) + \frac{2}{v} \frac{2g_2^2}{4\pi} \frac{1}{x} \text{Exp} \left[-\frac{m_{W^{(0)}} x}{\frac{1}{2} m_{Z^{(1)}} v} \right] \chi_{p,l}^{WW}(x) = 0 \quad (5.183)$$

$$\begin{aligned} \frac{\partial^2}{\partial x^2} \chi_{p,l}^{WW}(x) + \frac{m_{Z^{(1)}} + \delta m}{m_{Z^{(1)}}} \left\{ \left[\left(1 - \frac{2\delta m}{\frac{1}{4} m_{Z^{(1)}} v^2} \right) - \frac{m_{Z^{(1)}}}{m_{Z^{(1)}} + \delta m} \frac{l(l+1)}{x^2} + \right. \right. \\ \left. \left. + \frac{2}{v} \left(\frac{g_2^2 c_W^2}{4\pi} \frac{1}{x} \text{Exp} \left[-\frac{m_{Z^{(0)}} x}{\frac{1}{2} m_{Z^{(1)}} v} \right] + \frac{e^2}{4\pi} \frac{1}{x} \right) \right] \chi_{p,l}^{WW}(x) \right. \\ \left. + \frac{2}{v} \frac{2g_2^2}{4\pi} \frac{1}{x} \text{Exp} \left[-\frac{m_{W^{(0)}} x}{\frac{1}{2} m_{Z^{(1)}} v} \right] \chi_{p,l}^{ZZ}(x) \right\} = 0. \end{aligned} \quad (5.184)$$

We have introduced the abbreviation $c_w \equiv \cos \theta_W^{(0)}$ and continue to use the relative velocity $v = \frac{p}{m_r} = \frac{p}{\frac{1}{2} m_{Z^{(1)}}}$, which is connected to the single particle velocity via $v = 2 v_{sp}$.

From (5.164), we remember the connection between the wavefunction $\phi_{p,l}^{ij}(0)$ and the enhanced cross section σ . It is convenient and straight forward to express σ in terms of the reduced dimensionless wavefunction. For s-wave annihilation we write:

$$\phi_{p,l=0}(\vec{r}) = \frac{\chi_{p,l=0}(r)}{pr} \underset{r \rightarrow 0}{\approx} \overbrace{\chi_{p,l=0}(0)}{=0} + \frac{(\partial_r \chi_{p,l=0}(r)|_{r \rightarrow 0})}{p r} = \frac{\partial_r \chi_{p,l=0}(r)|_{r \rightarrow 0}}{p} \quad (5.185)$$

After substituting $x = p r$, the Sommerfeld-enhanced cross section is conveniently expressed as:

$$\sigma = \left(\begin{array}{c} \partial_x \chi_{p,l=0}^{ZZ}(x)|_{x \rightarrow 0} \\ \partial_x \chi_{p,l=0}^{WW}(x)|_{x \rightarrow 0} \end{array} \right)^\dagger \sigma_0 \left(\begin{array}{c} \partial_x \chi_{p,l=0}^{ZZ}(x)|_{x \rightarrow 0} \\ \partial_x \chi_{p,l=0}^{WW}(x)|_{x \rightarrow 0} \end{array} \right), \quad (5.186)$$

During the preparation of this thesis, another article by Iengo and Hryczuk [62] appeared where they discuss electroweak corrections and the Sommerfeld effect for Majorana dark matter nearly degenerate with charginos transforming in the adjoint representation of $SU(2)_W$. For s-wave annihilation, our dimensionless reduced Schrödinger equations (5.183, 5.184) coincide³³ with their equations (1.10) and (1.11) up to factors of $\sqrt{2}$ in $V^{WWZZ}(x)$ and $V^{ZZWW}(x)$.³⁴ We also find agreement between (5.186) and eq. (1.14) of [62] for the Sommerfeld enhanced cross section.

³³Notice that [62] work with the single particle velocity $v_{single-particle}$ which is related to our convention as described in the body of our text.

³⁴In our case, due to the bosonic nature of $Z^{(1)}$, we have included t- and u-channel annihilation diagrams. The presence of both diagrams, together with the Feynman rules, led to the particular coefficients in $V^{WWZZ}(x)$ and $V^{ZZWW}(x)$.

In order to compare our results to the existing literature on excited dark matter [34] that deal with a coupled system of states as well, it is useful to cast the Schrödinger equation in a different form:

$$\frac{\partial^2}{\partial x^2} \vec{\chi}(x) = \widehat{M}(x) \vec{\chi}(x). \quad (5.187)$$

In 5.187 we introduce the vector of reduced radial wavefunctions $\vec{\chi}(x) = \begin{pmatrix} \chi^{ZZ}(x) \\ \chi^{WW}(x) \end{pmatrix}$.

Our matrix operator $\widehat{M}(x)$ reads:

$$\widehat{M}(x) = \begin{pmatrix} \frac{l(l+1)}{x^2} - 1 & -\frac{4\alpha_2}{v} e^{-\frac{m_{W(0)}x}{p}} \frac{1}{x} \\ -\frac{4\alpha_2}{v} e^{-\frac{m_{W(0)}x}{p}} \frac{1}{x} & \frac{2\delta m}{\epsilon} - 1 + \frac{l(l+1)}{x^2} - \frac{2\alpha_2 c_W^2}{v} e^{-\frac{m_{Z(0)}x}{p}} \frac{1}{x} - \frac{2}{v} \frac{e^2}{4\pi} \frac{1}{x} \end{pmatrix}, \quad (5.188)$$

and is consistent in signs with [34]³⁵. Note that we have an interaction potential on the diagonal entry of \widehat{M} in comparison to [34], who consider a $U(1)$ vector interaction coupling the two-particle states and obtain purely off-diagonal interaction entries. We introduce the shorthand notation³⁶:

$$V_{od}(x) \equiv V_{off-diag}(x) = \frac{4\alpha_2}{v} e^{-\frac{m_{W(0)}x}{p}} \frac{1}{x} \quad (5.189)$$

$$V_d(x) \equiv V_{diag}(x) = \frac{2\alpha_2 c_W^2}{v} e^{-\frac{m_{Z(0)}x}{p}} \frac{1}{x} + \frac{2}{v} \frac{e^2}{4\pi} \frac{1}{x}, \quad (5.190)$$

for brevity. In order to check consistency with [34], it is most appropriate to introduce:

$$\begin{aligned} \epsilon_v^2 &= 1 \\ \epsilon_\phi &= \frac{m_{W(0)}}{p} = \frac{m_{W(0)}}{\frac{1}{2}m_{Z(1)}v} \\ \tilde{\epsilon}_\phi &= \frac{m_{Z(0)}}{p} = \frac{m_{Z(0)}}{\frac{1}{2}m_{Z(1)}v} \\ \epsilon_\delta^2(x) &= \frac{2\delta m}{\epsilon} - V_d(x). \end{aligned}$$

That way $\widehat{M}(x)$ transforms to:

$$\widehat{M}(x) = \begin{pmatrix} \frac{l(l+1)}{x^2} - \epsilon_v^2 & -V_{od}(x) \\ -V_{od}(x) & \frac{l(l+1)}{x^2} - \epsilon_v^2 + \epsilon_\delta^2(x) \end{pmatrix}, \quad (5.191)$$

which formally agrees with eq. (3.2) in [34]. However, due to the diagonal potential $V_{diag}(x)$, ϵ_δ^2 is not a constant anymore and care should be taken in adapting the results of

³⁵N.B., that the notation differs by a rescaling of x . In order to agree with [34] we would have to set $x \rightarrow \frac{\alpha_2}{v} x$. Physically, this corresponds to a change of measure. We refer everything to the de Broglie wavelength $1/p$ of the DM pair, whereas [34] measure in Bohr radii of the bound state.

³⁶Note, that $V_{off-diag}$ and V_{diag} are dimensionless in our notation.

the above mentioned paper. It is straight forward to find the eigenvalues and eigenvectors of $\widehat{M}(x)$. For $\epsilon_\delta \neq 0$ we obtain:

$$\lambda_\pm = \frac{l(l+1)}{x^2} - \epsilon_v^2 + \frac{\epsilon_\delta^2(x)}{2} \pm \sqrt{V_{od}(x)^2 + \left(\frac{\epsilon_\delta^2(x)}{2}\right)^2} \quad (5.192)$$

$$\chi_\pm = \frac{1}{\sqrt{2}} \begin{pmatrix} \mp \sqrt{1 \mp \frac{1}{\sqrt{1+(V_{od}(x)/(\epsilon_\delta^2(x)/2))^2}}} \\ \sqrt{1 \pm \frac{1}{\sqrt{1+(V_{od}(x)/(\epsilon_\delta^2(x)/2))^2}}} \end{pmatrix}. \quad (5.193)$$

Notably, the eigenvectors only depend on the ratio of mass splitting and off-diagonal potential. Parametrically, neglecting all numerical factors $\mathcal{O}(1)$, this ratio scales as:

$$\begin{aligned} \frac{V_{od}}{\epsilon_\delta^2} &\sim \frac{\frac{\alpha_2}{v} \frac{e^{-\epsilon_\phi x}}{x}}{\frac{\delta m}{\epsilon} - \frac{\alpha_2}{v} \frac{e^{-\tilde{\epsilon}_\phi x}}{x} - \frac{\alpha_2}{vx}} \\ &\sim \frac{\frac{\alpha_2}{r} e^{-m_{W(0)} r}}{\delta m - \frac{\alpha_2}{r} [e^{-m_{Z(0)} r} + 1]}. \end{aligned}$$

We immediately realize two limiting cases, one where the potential terms ($\sim \alpha_2/r$) dominate over the mass splitting ($\sim \delta m$) and vice versa.

1. Potential $\gg \delta m$

In this case we neglect the mass splitting term in ϵ_δ^2 , the rest remains unchanged. In our specific example, the potentials become strong at short distances $1/r < m_{Z(0)}$. For the eigenvalues and eigenvectors of \widehat{M} , we find the analogon to (5.192):

$$\begin{aligned} \lambda_\pm &\approx \frac{l(l+1)}{x^2} - \epsilon_v^2 + \frac{V_d(x)}{2} \pm \sqrt{V_{od}(x)^2 + \left(\frac{V_d(x)}{2}\right)^2} \\ \chi_\pm &\approx \frac{1}{\sqrt{2}} \begin{pmatrix} \mp \sqrt{1 \mp \frac{|V_d(x)/2|}{\sqrt{(V_d(x)/2)^2 + V_{od}(x)^2}}} \\ \sqrt{1 \pm \frac{|V_d(x)/2|}{\sqrt{(V_d(x)/2)^2 + V_{od}(x)^2}}} \end{pmatrix}. \end{aligned}$$

The presence $V_d(x)$ makes the diagonalization of \widehat{M} nontrivial. This is the major difference to the Schrödinger equation studied in [34], where the diagonal potential was absent and the eigenvectors $\chi_\pm \rightarrow 1/\sqrt{2}(\mp 1, 1)^T$ follow from an x -independent 45° rotation.

2. Potential $\ll \delta m$

We can directly implement this limit in (5.191) where \widehat{M} is diagonal and the Schrödinger equation decouples:

$$\begin{aligned} \lambda_\pm &\approx \frac{l(l+1)}{x^2} - \epsilon_v^2 + \frac{\epsilon_\delta^2}{2} \pm \frac{\epsilon_\delta^2}{2} + \mathcal{O}(V(x)^2) \\ \chi_+ &\approx \begin{pmatrix} 0 \\ 1 \end{pmatrix} & \chi_- &\approx \begin{pmatrix} 1 \\ 0 \end{pmatrix} \end{aligned}$$

In the limiting cases where the diagonalization of \widehat{M} is independent of x , we can introduce an approximate decoupled Schrödinger equation of the form:

$$\chi_{\pm}(x) = \lambda_{\pm}(x)\chi_{\pm}(x). \quad (5.194)$$

In the intermediate regime $V_{od}(x) \sim \frac{\epsilon_d^2}{2}$, however, the interplay of the different energy scales leads to nontrivial diagonalization matrices that depend on x explicitly. This gives rise to non-diagonal derivative terms of the diagonalization matrix itself [34] and we are not able to decouple the system.

Numerical Solution of the Coupled Schrödinger Equations - Technical Details

Having discussed the limiting cases of the reduced radial Schrödinger equation (5.187), we turn our attention to the numerical solution of (5.183) and (5.184). In the asymptotic limit $x \rightarrow \infty$, equations (5.183) and (5.184) decouple and we retrieve the boundary conditions (5.174) at infinity. Together with the requirement, that the solutions to the radial wave-equations have to be regular at the origin ($\chi^{ij}(x=0) \stackrel{!}{=} 0$), we are left to solve the ordinary differential equations (ODEs) as a boundary value problem (BVP), i.e. the solutions have to satisfy boundary conditions at two distinct points, x_1 and x_2 , of the independent variable, x . Such scenarios have been addressed in the literature and we are going to adopt the numerical treatment of BVPs as outlined in [88]. In comparison to initial value problems (IVP), the setup we are dealing with is a little more involved, since one is not able to begin the numerical iteration from a single point, let's say x_1 , where the specific solution of the ODE is uniquely determined. A method called "shooting" solves this problem by introducing a number of arbitrary initial conditions at x_1 that is equal to the number of boundary conditions that would have to be fulfilled at x_2 in the original BVP. One cleverly varies the free initial parameters at x_1 via a Newton-Raphson method [88] until the boundary conditions at x_2 are met.

We have implemented the whole algorithm in *Mathematica* and used a Runge-Kutta 4 (RK4) [89] update procedure to integrate the ODE between the two endpoints³⁷. Instead of starting at the origin $x = 0 \equiv x_0$ and integrating χ^{ZZ} and χ^{WW} to infinity, we have chosen to set the boundary conditions at numerical infinity (x_{∞}) and iterate backwards. In our case, we found more reliable solutions and were able to automatically pick out the asymptotically damped modes of χ^{WW} , when the WW-pair can not go on-shell ($\mathcal{E} < 2\delta m$).

³⁷The continuous ODE is discretized and the iteration relates points that are separated by small but finite differences. The number of steps is denoted by N_{It} in the following. For a detailed description of the method, c.f. e.g. [89]. For completeness, we give our *Mathematica* routine for the coupled system in App. E. For the implementation, we used the lecture notes [90] as guidance.

In particular, we use:

$$\chi^{ZZ}(x) \xrightarrow{x \rightarrow \infty} \sin(x + \delta) \quad (5.195)$$

$$\chi^{WW}(x) \xrightarrow{x \rightarrow \infty} n^{WW} \exp(-k'x) \quad (5.196)$$

$$k' = \sqrt{-\frac{m_{Z(1)} + \delta m}{m_{Z(1)}} \left(1 - \frac{2\delta m}{\mathcal{E}}\right)} \approx i \sqrt{\left(1 - \frac{2\delta m}{\mathcal{E}}\right)}$$

and set up the shooting method such that we vary the scattering phase δ and the amplitude n^{WW} at numerically infinity until we obtain regular solutions for χ^{ZZ} and χ^{WW} at the origin. For specific integrations, we have defined $x_\infty \equiv 25$ and chosen the Runge-Kutta step size $h = \frac{x_\infty - x_0}{N_{It}}$ so that the wavefunctions close to the origin are sampled sufficiently well. N_{It} denotes the number of steps between the two endpoints of the integration interval. Numerically, we demand³⁸:

$$|\chi^{ZZ}(0)| < \epsilon \quad |\chi^{WW}(0)| < \epsilon,$$

where we introduce the desired accuracy ϵ of the shooting procedure.

Validation of our Numerical Routines

In order to validate our method, we revisited the simple ODE for the single-channel Sommerfeld enhancement (5.64) and this time solve the boundary value problem with the procedure described above.

We find excellent agreement between the two methods, however, we had minor issues with our shooting routine in the low velocity region and were not able to sample parameter points with $v/c < 10^{-4}$ efficiently. Probing the low velocity parameter range numerically would have required a drastic increase in Runge-Kutta iteration steps N_{It} , leading to a significant slowdown of the integration process. In order to obtain the $v/c = 10^{-5}$ mass dependence plot in fig. 5.14 for example, we had to set $N_{It} = 500000$ for stable results.

We have already sketched the line of reasoning behind the particular form of fig. 5.14 in Sec. 5.4 and shall not repeat it here. For comprehensive discussion, we refer to the existing literature on the single-channel Sommerfeld effect [11, 23, 38, 16].

³⁸In fact, we do not iterate all the way to $x = 0$, but stop at a small parameter $x_0 = \tilde{\epsilon}$ so that we do not run into troubles with the divergent potentials $V^{ij'j'}(x)$ at the origin.

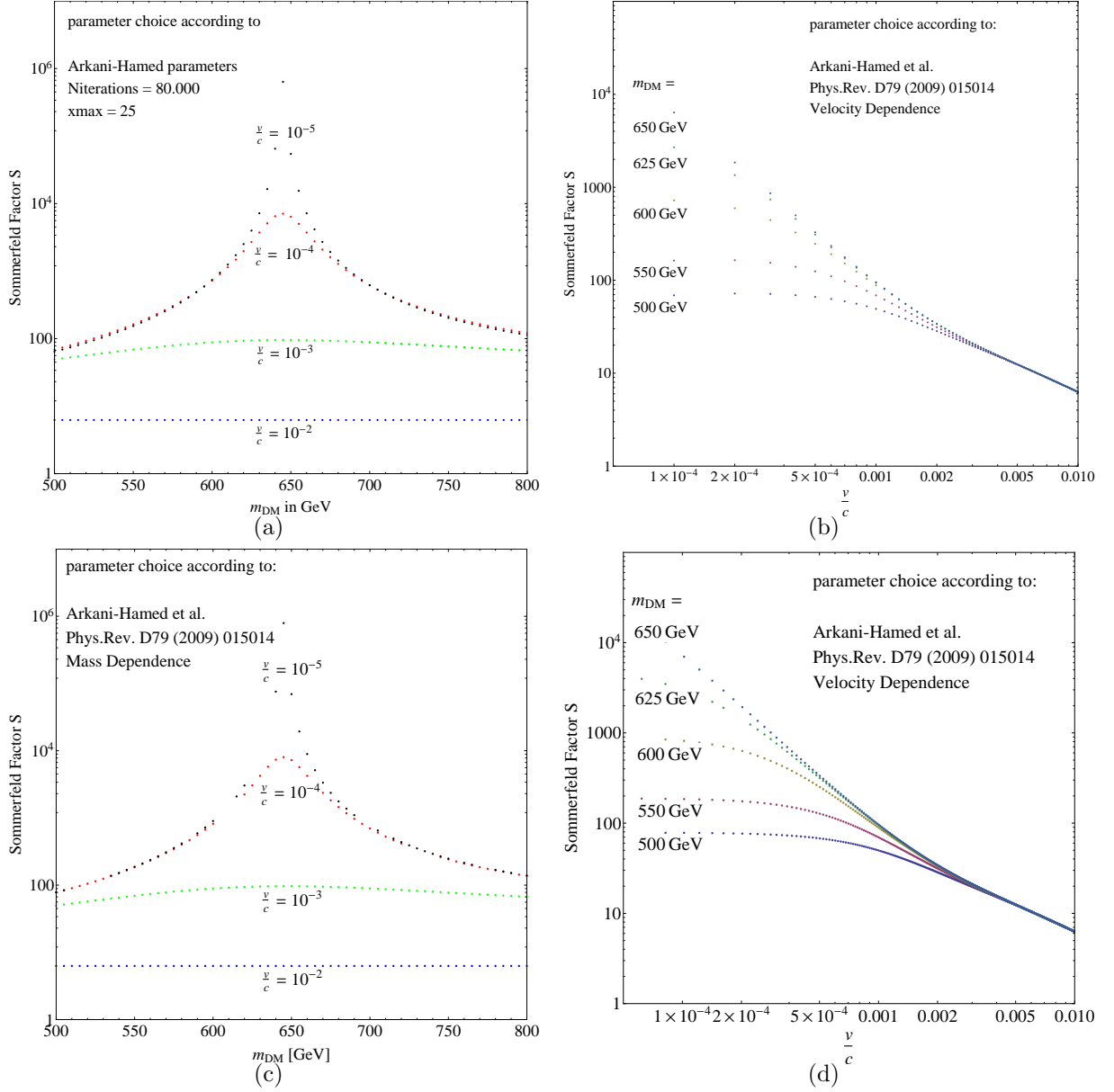


Figure 5.14: Validation of the numerical shooting method via velocity and dark matter mass dependence of the Sommerfeld enhancement for single-channel Yukawa interaction. We show our numerical results for the Sommerfeld factor (S) for the Arkani-Hamed parameter point discussed in Sec. 5.4 for our *shooting routine* (top panel) and *Iengos routine* (lower panel). Explicitly, we use $\alpha = \frac{1}{100}$, $m_\phi = 1\text{GeV}$.

Numerical Solution of the Coupled Schrödinger Equations - Numerical Results

In comparison to other authors working on the Sommerfeld effect of coupled systems who obtain similar effective Schrödinger equations as (5.183) and (5.184)[18, 62, 34], our model has a preferred mass splitting $\delta m \approx 0.01$ GeV, which was the result from electroweak symmetry breaking in the gauge boson multiplet (c.f. Sec. 4.6.3 and Sec. 4.6.4). This is approximately one order of magnitude smaller than the mass splittings considered in supersymmetric scenarios [18, 62]. On the other hand, our generic mass splitting is at least an order of magnitude larger than the one required for excited dark matter³⁹[34, 91, 92], so that our model covers the intermediate range of parameter space. As we have seen in Sec. 3.2.1, the mass splitting plays a vital role and controls the influence of the gauge multiplet partners on the Sommerfeld phenomenology of the DM candidate via eq. (3.6).

If we assume a generic mass splitting of $\mathcal{O}(10^{-2})$ GeV in accordance with Sec. 4.6.4 and vary the relative velocity of the DM pair⁴⁰ $v \in \{3 \times 10^{-4}, \dots, 10^{-2}\}$ as well as the dark matter mass $m_\chi \in \{300 \text{ GeV}, \dots, 5 \text{ TeV}\}$, we cover the range where the $W_{(1)}^\pm$ -pair can go on-shell, i.e. $2\delta m \lesssim \frac{1}{4}m_\chi v^2$. Due to the intricate interplay between the three different energy scales,

- $\epsilon_{kin} \approx \frac{1}{4}m_\chi v^2$ (kinetic energy of the DM pair),
- $\epsilon_{Bind} \approx m_\chi \alpha^2$ (binding energy due to long range potential) and
- $\epsilon_{split} = 2\delta m$ (mass splitting in the dark sector),

we expect interesting parameter dependences of the Schrödinger wavefunctions $\chi^{ZZ}(x)$ and $\chi^{WW}(x)$. These are directly related to the Sommerfeld factor⁴¹ via eq. (5.186). In order to get an overview of the parametric behavior of the Sommerfeld enhancement we exemplarily plot $|\partial_x \chi^{WW}(x)|_{x=0}$ in the $v - m_{DM}$ plane (see fig. 5.15 and 5.16), before we continue to investigate special parameter settings in greater detail. Doing so, we try to clarify the physics of the coupled Schrödinger equations (5.183) and (5.184). Making contact to dark matter phenomenology, $|\partial_x \chi^{WW}(x)|_{x=0}$ is important in our brief discussion on enhanced dark matter annihilation into two photons.

³⁹N.B.: In Refs. [34, 91, 92], purely off-diagonal interaction potentials are considered which is different to our problem, where diagonal and off-diagonal entries occur.

⁴⁰We chose the velocity range around the present day rms value $v \approx 10^{-3}$ [11].

⁴¹In this section we will use "Sommerfeld factor" for the derivatives of the reduced two-particle wavefunctions $\partial_x \chi^{ij}(x)|_{x=0}$ and the proper Sommerfeld enhancement, defined in eq. (5.186) simultaneously. Whenever we give plots of $\partial_x \chi^{ij}(x)|_{x=0}$, one has to multiply these results with the bare annihilation matrix σ_0 .

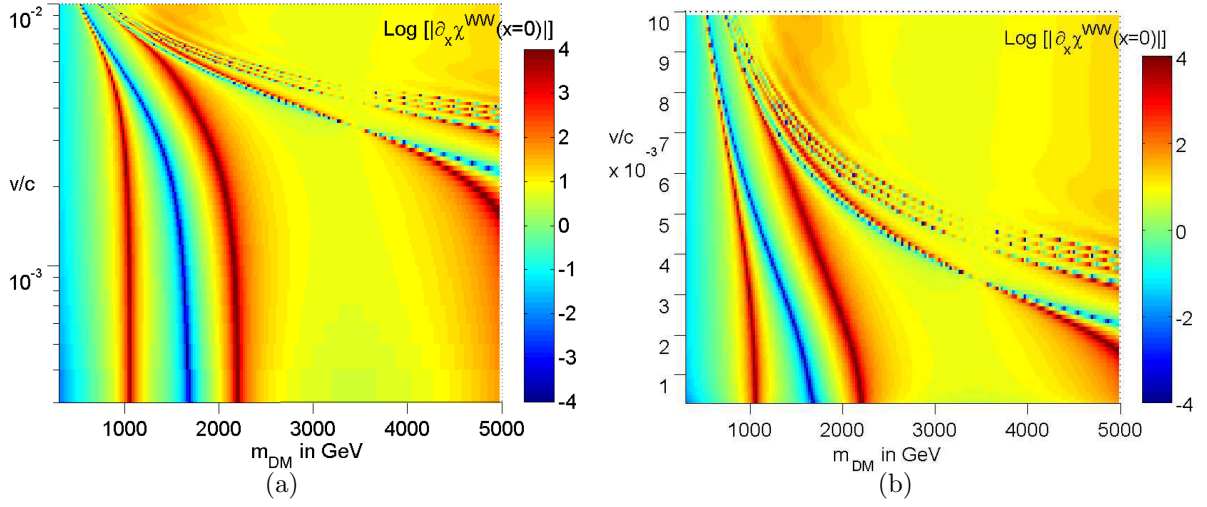


Figure 5.15.: Numerical solution of the coupled system of Schrödinger equations (5.183) and (5.184) for fixed DM mass splitting $\delta m = 0.01$ GeV. We exemplarily depict $\text{Log}[\partial_x \chi^{WW}(x)|_{x=0}]$ with logarithmic (a) and linear (b) velocity axis. The threshold region, where the $W_{(1)}^\pm$ -pair can go on-shell is accompanied by multiple resonance lines, best visible in (b).

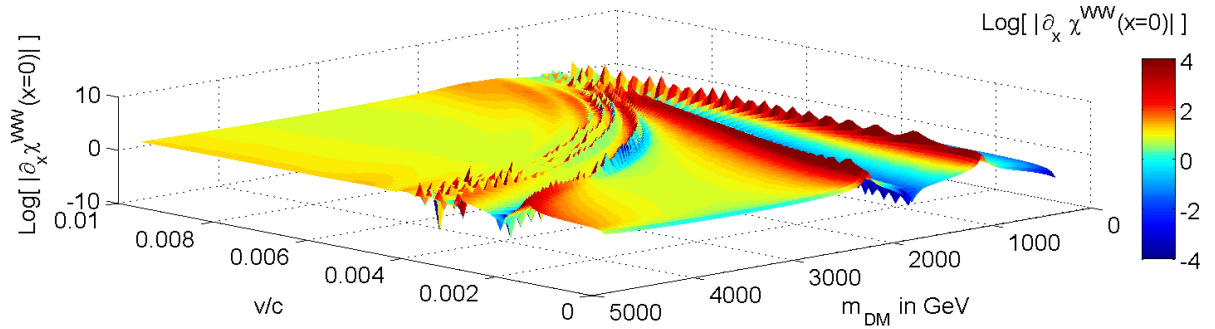


Figure 5.16.: 3D plot of the numerical solution of equations (5.183) and (5.184) for fixed DM mass splitting $\delta m = 0.01$ GeV. We exemplarily depict $|\partial_x \chi^{WW}(x)|_{x=0}$ from a somewhat different perspective as in fig. 5.15 to highlight the trenches in the Sommerfeld enhancement which have not been discussed before.

In fig. 5.15 and fig. 5.16, clear resonances are visible that have also been reported in the works of [18, 62], who obtained similar Schrödinger equations. Besides the resonance peaks, we observe additional "trenches", where $|\partial_x \chi^{ij}(x)|_{x=0} \ll 1$. To our knowledge, this feature has not been discussed in the literature so far. Despite the trenches, we are able to follow the analysis of Hisano et al. [18] in order to explain the resonance features by a simplified model⁴² of the electroweak potential (5.189). In this approximation scheme, one neglects the mass splitting δm and the electromagnetic interaction by setting $c_w = 1$.

⁴²In Ref. [16], there is a similar approximation for the single channel Sommerfeld enhancement.

The Yukawa potentials are approximated by finite square wells [18]:

$$V(r) = \begin{pmatrix} 0 & -b_1\alpha_2\sqrt{2}m_{W^{(0)}} \\ -b_1\alpha_2\sqrt{2}m_{W^{(0)}} & -b_1\alpha_2m_{W^{(0)}} \end{pmatrix} \theta((b_2 m_{W^{(0)}})^{-1} - r), \quad (5.197)$$

with numerical constants b_1 and b_2 and the SU(2) coupling $\alpha_2 \equiv \frac{g_2^2}{4\pi}$. In this notation, the approximate results derived by [18] are readily transferred. Since the full approximation formulae are rather lengthy and given in eq. (56) of [18]⁴³, we only write down the approximate version in the limit of small $v \ll \sqrt{\frac{\alpha_2 m_{W^{(0)}}}{m_\chi}} \stackrel{m_\chi=1TeV}{\approx} 0.05$. For the neutral channel, one finds:

$$\partial_x \chi^{ZZ}(x)|_{x=0} \propto \left(\cos \sqrt{4\alpha_2 m_\chi / m_{W^{(0)}}} \right)^{-1} + 2 \left(\cosh \sqrt{2\alpha_2 m_\chi / m_{W^{(0)}}} \right)^{-1} \quad (5.198)$$

From eq. (5.198), it is applicable that $\partial_x \chi^{ZZ}(x)|_{x=0}$ is enhanced considerably, when $\sqrt{4\alpha_2 m_\chi / m_{W^{(0)}}} = (2n + 1)\pi/2$, $n \in \mathbb{N}_0$, which reflects the occurrence of bound state resonances [18], the same resonance structure occurs for the charged channel.

The particular coefficients in (5.198) are a direct result of the parameter choice in (5.197) for the potential depth b_1 and the interaction range b_2 . Since (5.197) is only a crude approximation of the electroweak potential, we expect the general result to be more complicated than (5.198). If we do not restrict ourselves to the parameter choice of [18], but leave the relative coefficients in (5.198) as free parameters, one gains higher flexibility to model the full two-state system. We come back to this point in a moment.

Before we proceed discussing the potential well approximation any further, we show specific cuts through the parameter space depicted in fig. 5.15 and extend the parameter region to different mass splittings δm in fig. 5.19. In order to clarify what happens near the "trench" regions, we plot a sequence of wavefunctions around one specific parameter point in fig. 5.18.

⁴³Note, that Hisano's [18] d_{22} is directly proportional to $\partial_x \chi^{ZZ}(x)|_{x=0}$ in our case. It should be noted, that the final annihilation step is handled differently by Hisano et al. [18] and Iengo et al. [62]. In this thesis we follow Ref. [62], which is why we only relate Hisano's diagonal components d_{22} to our notation. Later on, we generalize the potential well approximation for both $Z^{(1)}Z^{(1)}$ and $W_{(1)}^+W_{(1)}^-$ annihilation channels in eq. 5.200.

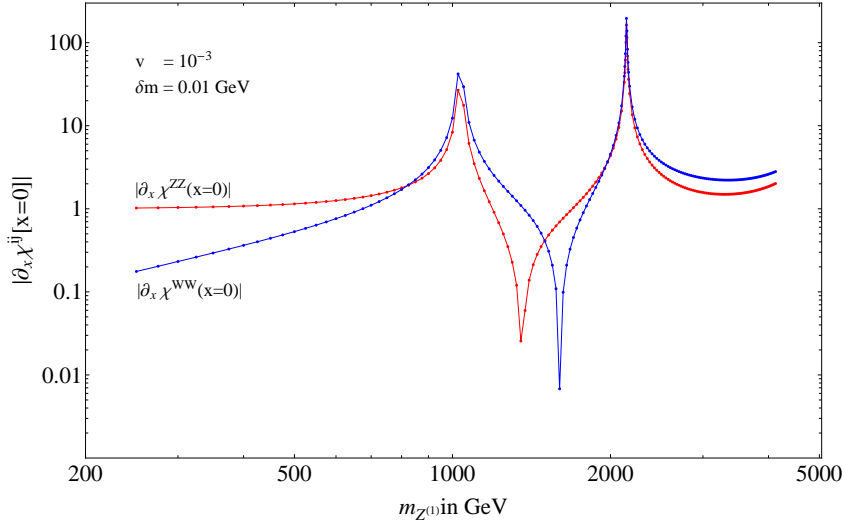


Figure 5.17.: Numerical solution of equations (5.183) and (5.184) for fixed DM mass splitting $\delta m = 0.01$ GeV and velocity $v = 10^{-3}$. For $|\partial_x \chi^{WW}(x=0)|$, this is a particular slice through the contour of fig. 5.15.

In comparison to the usual mass dependence plots of the Sommerfeld enhancement (e.g. fig. 5 in [18]) the striking feature of our mass splitting region is the existence of parameter regions where $\partial_x \chi^{ij}(x)|_{x=0} \ll 1$. In order to find out what happens to the wavefunction at these special points, we have exemplarily looked at $\chi^{WW}(x)$ for different DM masses around the dip.

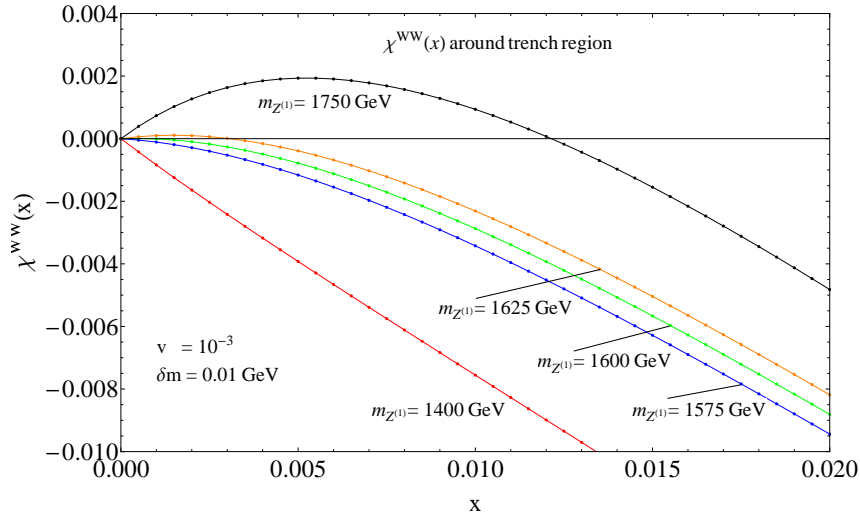


Figure 5.18.: Numerical solution for $\chi^{WW}(x)$ for fixed DM mass splitting $\delta m = 0.01$ GeV and velocity $v = 10^{-3}$ for dark matter mass points around the dip in fig. 5.17.

As applicable from figs. 5.17 and 5.18, the dip region in fig. 5.17 corresponds to a point in parameter space, where the two-particle wavefunction develops an additional node. Physically, this might be interpreted as follows: the scattering length is determined by the range of the potential $\propto \frac{1}{m_\phi}$. When we increase the dark matter mass, we simultaneously decrease the corresponding de Broglie wavelength $\lambda_{dB} \propto \frac{1}{m_\chi v}$ so that more wave-nodes fit into the scattering region. This is exactly the phenomenon we see in the sequence illustrated in fig. 5.18.

As we have mentioned, to our knowledge, the "trenches" have not been addressed in the literature up to this point. In light of the similarities between our and Hisanos [18] Schrödinger equations, one might wonder, why this is the case. Plainly, it is a matter of δm . The supersymmetry inspired Sommerfeld calculations (e.g. [18, 75]) work with mass splittings of $\mathcal{O}(0.1)$ GeV, i.e. one order of magnitude larger than our generic value of $\mathcal{O}(0.01)$ GeV. A larger mass splitting naturally implies a higher on-shell threshold for the $W_{(1)}^\pm$ -pair via $2\delta m = \frac{1}{4}m_\chi v^2$. For the direct comparison, this means, that the supersymmetry models, for equal velocities, have threshold masses m_χ^{thr} that are an order of magnitude higher than ours, so that interference effects between the WW and the ZZ -channel are less prominent. This point is highlighted, once we investigate the influence of the mass splitting δm in the dark sector on the Sommerfeld factor.

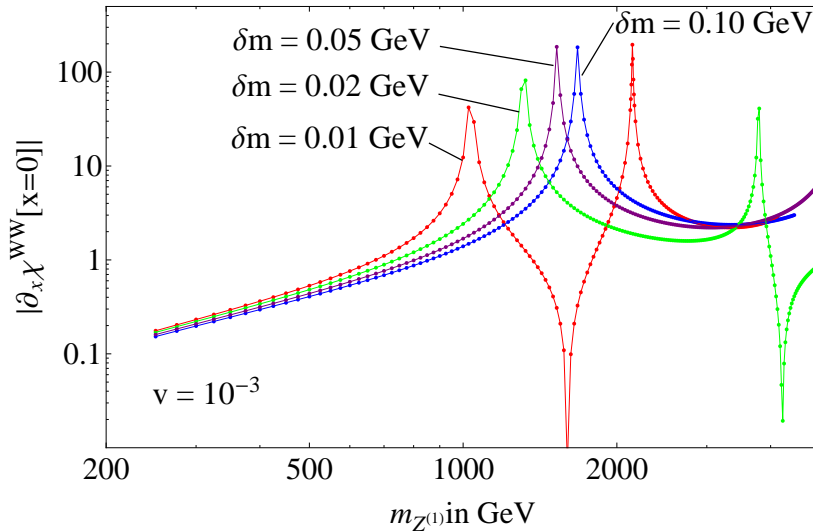


Figure 5.19.: Parametric δm dependence of the numerical solution for $\chi^{WW}(x)$ for fixed velocity $v = 10^{-3}$. For detailed explanation, see main text.

Particularly, the $\delta m = 0.02$ GeV sweep (green line in fig. 5.19) shows a normal first resonance without any dips. For higher m_χ , however, the second resonance structure is more complicated and contains a "dip" which we attribute to negative interference between

the annihilation channels. The mass sweeps with $\delta m > 0.02$ GeV have on-shell regions far from the investigated range $m_\chi \in \{300, \dots, 5000\}$ GeV, so that deconstructive interference effects do not show up and the graphs look similar to the once obtained by e.g. [18].

Fig. 5.19 allows another observation. In accordance with the remarks in Ref. [18], the resonances move to heavier m_χ for larger δm . This can be seen, once one introduces the mass splitting δm into the approximate electroweak potential (5.197). Starting from the parameter choice of [18], (5.197) can be diagonalized analytically, yielding the potential energy of the attractive state in the limit $\delta m \lesssim \alpha_2 m_{W(0)}$:

$$|\lambda_-| \approx 16\alpha_2 m_{W(0)}/9 - 4\delta m/3, \quad (5.199)$$

so that the potential energy is reduced for increasing δm .

Upon discussing the parametric dependence of the Sommerfeld enhancement on the mass splitting as well as showing a single cut through the $m_\chi - v$ parameter space, let us come back to the approximate solution of the coupled Schrödinger equations with a finite well interaction potential. Instead of (5.198), we now use the more general approximation:

$$d^{ij} := a_1^{ij} \left(\cos \sqrt{s_1^{ij} \alpha_2 m_\chi / m_{W(0)}} \right)^{-1} + a_2^{ij} \left(\cosh \sqrt{s_2^{ij} \alpha_2 m_\chi / m_{W(0)}} \right)^{-1}, \quad (5.200)$$

and try to find coefficients $a_{1,2}^{ij}$ and $s_{1,2}^{ij}$ to fit the lowest resonance. As proof of principle, we show that we are able to model trenches with the more general approximation (5.200). In fig. 5.20, we realize that the first peak and "trench" position is approximated relatively well by (5.200), the exact line-shape however varies from the numerical result especially in the higher m_χ region. For an improved analytical approximation of the electroweak potential, Ref. [34] looks very promising. The detailed analysis of such revised approximation schemes, however, is beyond the scope of this work.

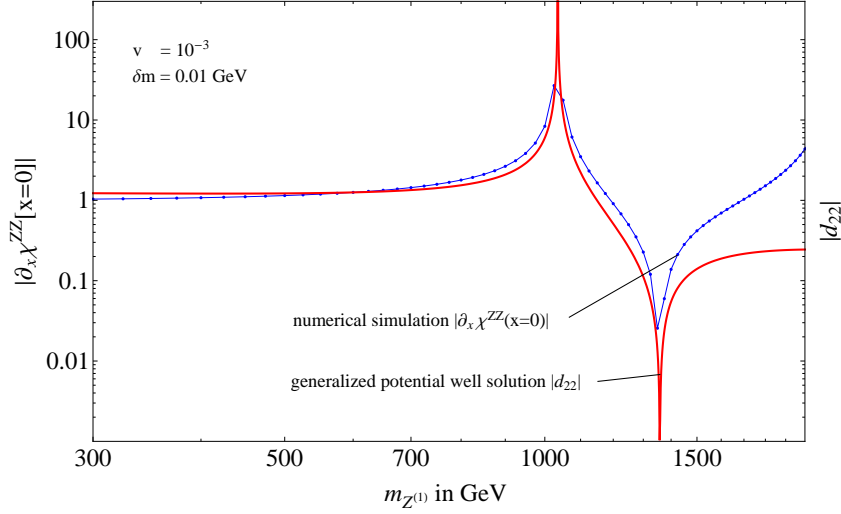


Figure 5.20.: Proof of principle, that we are able to model "trench" resonances with a generalized version of Hisanos [18] finite well potential approximation. Exemplarily, we fit the first resonance in the $|\partial_x \chi^{ZZ}(x=0)|$ mass sweep for $\delta m = 0.01$ GeV, $v = 10^{-3}$. Fit parameters in (5.200): $s_1^{ZZ} = 4.76$, $s_2^{ZZ} = 2.38$, $a_1^{ZZ} = \frac{\sqrt{2}}{10}$ and $a_2^{ZZ} = \frac{12}{10}$

Dark Matter Annihilation into Standard Model Photons

After this somewhat academic discussion on the behaviour of the reduced two-particle wavefunctions $\chi^{ij}(x)$, we would like to make contact to a physical situation, where the Sommerfeld enhancement can play a significant role. We follow the notation of Hryczuk et al. [75] and remind the reader, that the Sommerfeld enhanced amplitude $A_{Z^{(1)}Z^{(1)} \rightarrow SM}$ for $Z^{(1)}$ -dark matter annihilation into any compatible SM-final state is related to the reduced two-particle wavefunctions χ^{ij} via [75]:

$$A_{Z^{(1)}Z^{(1)} \rightarrow SM} = [\partial_x \chi^{ZZ}(x=0)] A_{Z^{(1)}Z^{(1)} \rightarrow SM}^0 + [\partial_x \chi^{WW}(x=0)] A_{W_{(1)}^+ W_{(1)}^- \rightarrow SM}^0. \quad (5.201)$$

In eq. (5.201), $A_{ij \rightarrow SM}^0$, denotes the leading order annihilation amplitude of the $\{ij\}$ -pair. In this section, we briefly comment on the Sommerfeld enhanced dark matter annihilation into two photons. This process leads to monoenergetic gamma-rays with energy $E_\gamma \sim m_\chi$, which is considered to be a smoking-gun signature for DM [93, 94]. For the $\gamma\gamma$ -final state, the lowest order annihilation amplitude $A_{Z^{(1)}Z^{(1)} \rightarrow \gamma^{(0)}\gamma^{(0)}}^0$ occurs only at one-loop level⁴⁴, whereas the annihilation in the $W_{(1)}^+ W_{(1)}^-$ -channel proceeds via tree-level processes. To a very crude estimate, we therefore neglect $A_{Z^{(1)}Z^{(1)} \rightarrow \gamma^{(0)}\gamma^{(0)}}^0$ in eq. (5.201),⁴⁵

⁴⁴Ohlsson et al. calculate the one-loop annihilation for neutral SU(2) vector bosons in non-minimal UED [93]. This model contains fermions, which are not present in our theory, so that a straight forward transfer of their results is not possible without further investigation.

⁴⁵Note, that we expect the Sommerfeld-type box diagram with W -bosons in the loop to be sizable in the nonrelativistic limit, so that the exact values for S should not be overemphasized.

so that the Sommerfeld enhancement S is given by:

$$S \approx \frac{|A_{Z^{(1)}Z^{(1)} \rightarrow \gamma^{(0)}\gamma^{(0)}}|^2}{|A_{W_{(1)}^+W_{(1)}^- \rightarrow \gamma^{(0)}\gamma^{(0)}}|^2} \approx |\partial_x \chi^{WW}(x=0)|^2 \quad (5.202)$$

This estimate has to be taken with some care. As we have seen in fig. 5.17, $\partial_x \chi^{ZZ}(x=0)$ can be considerably larger than $\partial_x \chi^{WW}(x=0)$, especially in the low dark matter mass regime. Since it is the product of $\partial_x \chi^{ij}(x=0)$ and $A_{ij \rightarrow SM}^0$, that is relevant, the derivative term could overcompensate the one-loop suppression of the amplitude $Z^{(1)}Z^{(1)} \rightarrow \gamma^{(0)}\gamma^{(0)}$ so that a complete analysis, similar to the fermionic case considered in Ref. [62], becomes necessary. This is beyond the scope of our current work and would have to be the subject of future research. In order to get a rough estimate of the enhancement factors that are achievable around the bound state resonances, we plot $S_{\gamma\gamma}$ as given in eq. (5.202) for current day dark matter velocity $v \approx 10^{-3}$ [11].

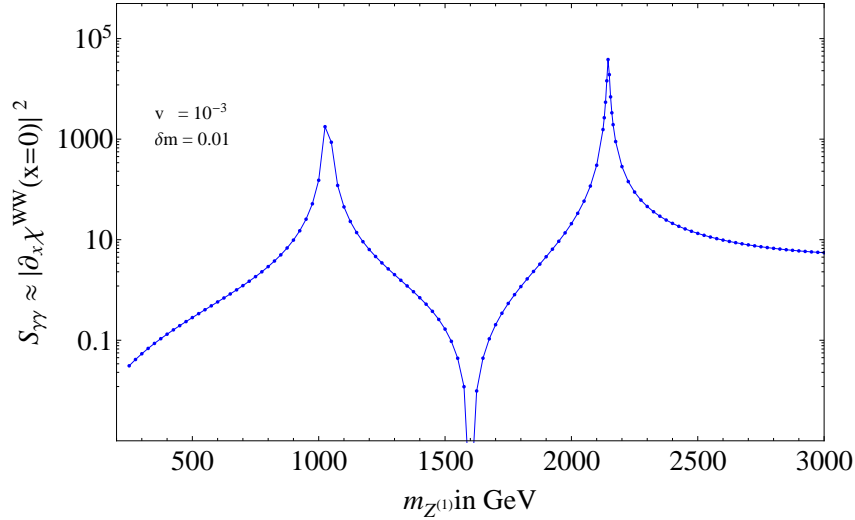


Figure 5.21.: Dark matter mass dependence of estimated Sommerfeld enhancement factor $S_{\gamma\gamma}$ (5.202) for $Z^{(1)}$ -pair annihilation into two Standard Model photons. The plot is shown for a generic mass splitting $\delta m = 0.01$ GeV and present day DM-velocity $v = 10^{-3}$.

In fig. 5.21, we find Sommerfeld enhancements up to $\mathcal{O}(10^4 - 10^5)$, which is comparable to the single-channel Sommerfeld factor discussed in section 5.4. As we have mentioned before, this scenario has to be investigated in greater detail and only illustrates, that the Sommerfeld effect has to be taken into account for generic dark matter annihilation models.

Sommerfeld Effect of Coupled System - Conclusion

As we have seen in the contour plot (fig. 5.15) of the Sommerfeld enhancement in the $m_\chi - v$ -plane, we are able to find specific parameter settings where the annihilation of the $Z^{(1)}$ dark matter candidate is significantly enhanced. In particular, a strong Sommerfeld enhancement is obtained for $Z^{(1)}$ -masses $m_{Z^{(1)}} \approx 1$ TeV and $m_{Z^{(1)}} \approx 2.15$ TeV at a present day velocity $v = 10^{-3}$ [11]. These parameter regions lead to a significantly lower cross section at the time of decoupling ($v \approx 0.3$ [39]) of the dark matter particle from the thermal bath. Thus our vector dark matter model is able to account for the tension between annihilation cross sections required for the correct relic abundance of WIMPs and the one needed in order to explain potential indirect WIMP signals in cosmic ray observations (see Sec. 5 for references and discussion) from a particle physics perspective. In fig. 5.15(a) we realized, that the enhanced Sommerfeld peaks are nearly velocity independent for $v \lesssim 2 \times 10^{-3}$, thus not only dark matter particles with velocities of present day values $v = 10^{-3}$ are enhanced but also particles in the lower tail of the velocity distribution are subject to the resonant Sommerfeld effect.

Following this discussion, we have briefly mentioned the possibility of a Sommerfeld enhanced annihilation cross section into two Standard Model photons. Such a process gives rise to monoenergetic gamma-rays, which is one of the most promising indirect dark matter search channels [94]. We found approximate enhancement factors of $\mathcal{O}(10^4)$ for special dark matter masses, where bound state resonances occur. The detailed investigation of this process involves the calculation of the one-loop $Z^{(1)}Z^{(1)} \rightarrow \gamma^{(0)}\gamma^{(0)}$ amplitude and should be subject of future research.

6. Summary and Outlook

In this thesis we have investigated the Sommerfeld effect for vector dark matter. Following an introduction to general aspects of the Sommerfeld effect in Sec. 3.2.1, we have motivated the study of vector dark matter (paragraph 3.3), which arises for example in Little Higgs models as well as extradimensional theories. The Sommerfeld effect [19] is a non-perturbative effect, that leads to a velocity dependent two-particle annihilation cross-section in the presence of a long-range force in the nonrelativistic limit. It turns out that this approach corresponds to the solution of a quantum mechanical scattering problem, where the long range interactions are encoded into an effective nonrelativistic potential. For attractive forces, this modifies the wavefunction of the dark matter pair which leads to an increase in the annihilation cross section. As we have reviewed in Sec. 3.2, this allows for reconciling anomalies in cosmic ray observations with annihilation cross sections that yield the correct thermal relic abundance.

The focus of this work was twofold. In chapter 4, we have introduced a minimal vector dark matter toy model in the form of a $SU(2) \times SU(2) \times U(1) \times U(1)$ gauge theory, which was inspired by dimensional deconstruction [22]. In our model, we have implemented a discrete \mathcal{Z}_2 -symmetry to guarantee the stability of the dark matter candidate. Starting from the Lagrangian (4.1), we have calculated the complete mass spectrum of this theory in sections 4.5 and 4.6 and found that either the neutral $U(1)_Y$ or $SU(2)_L$ vector boson is a viable dark matter candidate. In the $SU(2)$ case, the dark matter candidate $Z^{(1)}$, is nearly mass degenerate with the $W_{(1)}^\pm$ with a generic splitting of $\mathcal{O}(10^{-2})$ GeV (see fig. 4.6), which led to interesting effects for the Sommerfeld phenomenology in the second part of this thesis.

Upon deriving the mass spectrum and interactions of our theory, which are expressed in terms of Feynman rules in Appendix C, we turned our attention to the Sommerfeld effect itself. We followed the outlines of Iengo [23], developed for fermionic dark matter, and pursued a Bethe-Salpeter approach (reviewed in Sec. 5.1) in order to account for nonperturbative effects in field theory language by a resummation of Feynman diagrams. We have encountered the ladder approximation in the nonrelativistic limit in section 5.2 and motivated that box diagrams are enhanced in this kinematic regime. In section 5.3,

we analyzed the calculation of Iengo [23] for fermionic dark matter in greater detail in order to understand the subtle points of the formalism along the lines of a known example. In chapter 5.5, we focused on the derivation of the interaction kernel for our vector dark matter model. From the lowest order field theory diagrams we obtained the interaction potential for the nonrelativistic Schrödinger equation (5.128). Due to the presence of nearly mass degenerate states in the dark sector, the potential is matrix valued in the space of two-particle states. Our results coincide with the ones of Refs. [18, 23] for fermionic dark matter, which indicates that the spin structure of the theory is subdominant in the non-relativistic instantaneous limit. The solution of this scattering problem is directly related to the enhanced annihilation cross section via eq. (5.164). In the following, we focused on the numerical solution of the coupled system of Schrödinger equations and have presented our results in section 5.10. In fig. 5.15, we found that a considerable enhancement of the dark matter annihilation cross section is possible for special regions in parameter space.

Improvements and Outlook

We would like to add a few points how to extend some of the calculations and discussions considered in this thesis. The following list is not intended to be exhaustive, but only states major points that would require some effort and are beyond the scope of this work.

- An obvious point would be the extension of our two-site lattice model (see Sec. 4) to a larger number of gauge groups. The natural extension of our minimal vector dark matter toy model could contain three SU(2) and U(1) groups respectively. This extension would require considerable more effort to calculate the complete mass spectrum and interaction vertices after symmetry breaking due to the larger field content. The three-site model, on the other hand has the advantage that it is able to model KK-(2) modes that are not contained in our theory that potentially have significant influence on e.g. relic density calculations [95]. Additionally, the three-site model allows to include a KK-parity conserving fermionic sector [96].
- We have studied the non-perturbative effects with an Bethe-Salpeter ansatz (Sec. 5.1) and introduced the ladder approximation, where we only considered the lowest order field theory diagrams in the interaction kernel. In order to treat relativistic effects correctly, one would have to go beyond this approximation scheme and regard higher loop-diagrams in the interaction kernel [70], which naturally leads to the evaluation of a great number of field theory diagrams. In this thesis we restricted ourselves to leading order calculations and followed existing work on the Sommerfeld effect for dark matter scenarios [11, 23, 39].
- In the course of deriving the Bethe-Salpeter kernel and subsequently the interaction potential in the effective Schrödinger equation in Sec. 5.5 we restricted ourselves to

leading terms, neglecting relative momentum dependences that give subdominant contributions to the interaction. Neglecting these terms corresponded to dropping spin-spin and spin-orbit interactions which should be considered in a more complete analysis. As starting point, articles on the Bethe-Salpeter approach for glueballs in QCD [77, 78, 79] might give valuable insights to spin-dependent terms, since the tensor structure of diagrams with gluon-gluon external states interacting via another gluon is similar to our case of $SU(2)$ gauge-bosons interacting via vector-boson exchange.

- In the Bethe-Salpeter approach 5.3 we came across the instantaneous approximation, where the energy dependence of the interaction mediator is neglected to first order. A natural extension would be the inclusion of such effects that describe non-instantaneous effects that lead to a relative time variable in the Fourier transformed Bethe-Salpeter equation [71].
- For a consistent treatment of higher order effects with the Bethe-Salpeter approach, one should replace the free propagators and vertices in the ladder-approximation with dressed ones, that can in principle be obtained by solving Dyson-Schwinger equations [67].
- As is known in the literature, the treatment of bound-state problems requires some non-perturbative approximation scheme [70, 72]. In such scenarios it is a nontrivial issue how to maintain external gauge invariance [97]. A systematic investigation of the gauge invariance of the Bethe-Salpeter equation for external vector particles, is beyond the scope of this work and should be addressed in future research in analogy to e.g. [97, 98].
- In the final part of this thesis we have derived the Sommerfeld enhancement to vector dark matter in our toy model 5.5 but did not consider any astrophysical and cosmological implications of our model. In principle we could follow the steps of [11, 34, 18, 14, 62] to perform detailed relic density calculations or possible reheating effects from enhanced interaction cross sections.

A. Parameters and Relations in the Standard Model

Numerical values for Standard Model parameters¹ are taken from [50] at the electroweak scale in the \overline{MS} scheme.

$$\begin{aligned}\frac{g'}{\sqrt{2}} &= g_1 = 0.357 \\ \frac{g}{\sqrt{2}} &= g_2 = 0.652 \\ v_0 &= 246 \text{ GeV} \quad \Rightarrow m_H = \sqrt{\frac{\lambda}{2}} v_0 \\ m_W &= 80.398 \pm 0.025 \text{ GeV} \quad m_Z = 91.1876 \pm 0.0021 \text{ GeV} \\ \sin^2(\theta_W^{(0)}) &= 0.23116,\end{aligned}$$

where g_1 and g_2 denote the $U(1)_Y$ and $SU(2)_W$ gauge couplings, respectively. $\theta_W^{(0)}$ is the Weinberg angle in the Standard Model.

Relations between m_Z , m_W , α , $\theta_W^{(0)}$ and g_1 , g_2 , v_0 at tree level:

$$m_W^2 = \frac{g_2^2 v_0^2}{4}, \quad m_Z^2 = \frac{g_2^2 + g_1^2}{4} v_0^2 \quad (\text{A.1})$$

$$\tan \theta_W^{(0)} = \frac{g'}{g} = \frac{g_1}{g_2} \quad (\text{A.2})$$

$$\sin^2 \theta_W^{(0)} = 1 - \frac{m_W^2}{m_Z^2} = 1 - \frac{\frac{v_0^2}{4} g_2^2}{\frac{v_0^2}{4} (g_2^2 + g_1^2)} = \frac{g_1^2}{g_2^2 + g_1^2} \quad (\text{A.3})$$

$$e = g_1 \cos \theta_W^{(0)} = \frac{g_2 g_1}{\sqrt{g_2^2 + g_1^2}} = g_2 \sin \theta_W^{(0)} \quad (\text{A.4})$$

$$\alpha = \frac{e^2}{4\pi} = \frac{g_2^2 \sin^2 \theta_W^{(0)}}{4\pi} \sim \frac{1}{128} \quad (\text{at } m_W^2) \quad (\text{A.5})$$

e ... electron charge, α ... finestructure constant

¹The factor $\sqrt{2}$ in the definition of g and g' reflects the presence of the normalization factor $\frac{1}{\sqrt{N+1}}$, commonly invoked in deconstructed models. In this notation, g_1 and g_2 are the Standard Model gauge couplings.

B. Gauge Fixing

In gauge theories, gauge fixing denotes a mathematical procedure for coping with redundant degrees of freedom of the dynamical field variables [40]. In general, a gauge theory represents **physically** distinct field configurations as different equivalence classes, where any two configurations within the same class are related by a gauge transformation. This feature leads to redundancies in the description of the theory. In order to obtain physical predictions, one has to come up with a consistent method to suppress or constrain these unphysical degrees of freedom¹.

In principle there exist a number of methods to implement the above mentioned constraints on the dynamical variables in the Lagrangian. Historically, well known gauge fixing prescriptions invented for QED, include the Lorentz gauge $\partial_\mu A^\mu = 0$ or the non-covariant Coulomb-gauge $\vec{\partial}\vec{A} = 0$ [58].

For our work, we chose to start with a generalized covariant, renormalizable R_ξ gauge. In such a gauge, the Goldstone bosons are not eliminated explicitly [56]. The advantage of this class of gauges is the transparently good high energy behavior of the gauge field propagators [58]. It contains a number of popular gauges as limiting cases, such as the Landau gauge ($\xi = 0$), the t'Hooft-Feynman gauge ($\xi = 1$) and the unitary gauge ($\xi \rightarrow \infty$).

Using textbook path integral quantization à la Faddeev and Popov [41], we are free to choose gauge fixing functions $f_i(A)$ for each gauge field and add a gauge fixing term to the Lagrangian. A priori these are functions of the gauge fields and their derivatives.

$$\mathcal{L}_{gauge-fixing} = \sum_{i=\text{gauge functions}} -\frac{1}{2\xi_i} [f_i]^2 \quad (\text{B.1})$$

For practical purposes, one opts for gauge functions that are convenient for computations. In this line of reasoning we choose our gauge functions to cancel all mixing terms between gauge bosons and Goldstone modes arising from the kinetic terms of the scalar fields explicitly so that an interpretation of the extended Lagrangian in terms of particle excitations becomes possible, i.e. the propagators are diagonal. This extended Lagrangian is to

¹For an introduction to gauge fixing, cf. e.g.[40, 41, 58]

be used to derive the Feynman rules of the theory. However, all physical quantities have to be independent of the special choice of gauge [41], so keeping the ξ parameter until the end of all calculations constitutes a practical cross check, at the same time increasing the calculational workload. Eventually, we are going to employ the unitary gauge in our Sommerfeld calculations for vector dark matter in the nonrelativistic limit.

First, we are going to demonstrate how the mixing terms arise explicitly from the Lagrangian when gauge fixing terms are omitted, before we proceed to construct convenient gauge fixing functions that cancel the afore mentioned mixings. Having determined a suitable gauge fixing Lagrangian we calculate the ξ dependent masses of the (would-be) Goldstone bosons that remained massless in the previous analysis. We find that the (would-be) Goldstone boson masses exactly equal the gauge boson ones up to an overall factor of ξ . This result exactly coincides with standard textbook examples (see e.g.[40, 58]).

B.0.1. Mixing Terms between Gauge Fields and Goldstone Bosons

We perform the analysis for the H_{W^5} field in greater detail, the mixing terms for the remaining scalars follow analogously.

1. H_{W^5} mixing terms

For later convenience we split H_{W^5} into the VEV and the dynamic part:

$$\begin{aligned}
 H_{W^5} &= \langle H_{W^5} \rangle_0 + \phi_W \\
 \langle H_{W^5} \rangle_0 &= \frac{1}{\sqrt{2}} \begin{pmatrix} v_2 & 0 \\ 0 & v_2 \end{pmatrix} \\
 \phi_W &= \begin{pmatrix} \frac{1}{\sqrt{2}}(\psi_{w^5,1}[x] - i\chi_{w^5,1}^{(3)}[x]) & i\chi_{w^5,1}^{(+)}[x] \\ i\chi_{w^5,2}^{(-)}[x] & \frac{1}{\sqrt{2}}(\psi_{w^5,2}[x] - i\chi_{w^5,2}^{(3)}[x]) \end{pmatrix} \quad (\text{B.2})
 \end{aligned}$$

To find the mixing terms between the gauge- and the Goldstone bosons one has to expand the kinetic term of the Higgs fields, in the case of H_{W^5} this is:

$$\begin{aligned}
 \text{tr} \left[(D_\mu H_{W^5})^\dagger (D^\mu H_{W^5}) \right] &= \text{tr} \left[\left\{ \partial_\mu (\langle H_{W^5}^\dagger \rangle_0 + \phi_W^\dagger) - ig (\tilde{W}_{I,\mu}^{\tilde{\tau}})^\dagger (\langle H_{W^5}^\dagger \rangle_0 + \phi_W^\dagger) + ig (\langle H_{W^5}^\dagger \rangle_0 + \phi_W^\dagger) (\tilde{W}_{II,\mu}^{\tilde{\tau}})^\dagger \right\}^* \right. \\
 &\quad \left. * \left\{ \partial^\mu (\langle H_{W^5} \rangle_0 + \phi_W) + ig \tilde{W}_I^\mu (\langle H_{W^5} \rangle_0 + \phi_W) \frac{\tilde{\tau}}{2} - ig \tilde{W}_{II}^\mu (\langle H_{W^5} \rangle_0 + \phi_W) \frac{\tilde{\tau}}{2} \right\} \right] \quad (\text{B.3})
 \end{aligned}$$

which contains:

$$\begin{aligned}
tr \left[(D_\mu H_{W^5})^\dagger (D^\mu H_{W^5}) \right] \Big|_{\text{mixing}} &= tr \left[ig\vec{W}_I^\mu \left\{ \left(\partial_\mu \phi_W^\dagger \right) \overbrace{\langle H_{W^5} \rangle_0}^{\frac{v_2}{\sqrt{2}} \mathbb{1}_{2 \times 2}} \frac{\vec{\tau}}{2} - \frac{\vec{\tau}}{2} \overbrace{\langle H_{W^5}^\dagger \rangle_0}^{\frac{v_2}{\sqrt{2}} \mathbb{1}_{2 \times 2}} (\partial_\mu \phi_W) \right\} \right] \\
&+ tr \left[ig\vec{W}_{II}^\mu \left\{ \overbrace{\langle H_{W^5}^\dagger \rangle_0}^{\frac{v_2}{\sqrt{2}} \mathbb{1}_{2 \times 2}} \frac{\vec{\tau}}{2} (\partial_\mu \phi_W) - \left(\partial_\mu \phi_W^\dagger \right) \frac{\vec{\tau}}{2} \overbrace{\langle H_{W^5} \rangle_0}^{\frac{v_2}{\sqrt{2}} \mathbb{1}_{2 \times 2}} \right\} \right]
\end{aligned} \tag{B.4}$$

2. H_B mixing terms

Treating H_B the same way as H_W and resorting to a similar notation for the VEV and dynamic part of the field we find:

$$(D_\mu H_{B^5})^\dagger (D^\mu H_{B^5}) \Big|_{\text{mixing}} = ig'Y (-B_{I,\mu} + B_{II,\mu}) \left[\overbrace{\langle H_{B^5}^\dagger \rangle_0}^{\frac{1}{\sqrt{2}}v_1} (\partial^\mu \phi_B) - (\partial^\mu \phi_B^\dagger) \overbrace{\langle H_{B^5} \rangle_0}^{\frac{1}{\sqrt{2}}v_1} \right] \tag{B.5}$$

3. H_I mixing terms

$$\begin{aligned}
(D_\mu H_I)^\dagger (D^\mu H_I) \Big|_{\text{mixing}} &= ig\vec{W}_I^\mu \left[\overbrace{\langle H_I^\dagger \rangle_0}^{\frac{1}{\sqrt{2}}(0,v)} \frac{\vec{\tau}}{2} (\partial_\mu \phi_I) - \left(\partial_\mu \phi_I^\dagger \right) \frac{\vec{\tau}}{2} \overbrace{\langle H_I \rangle_0}^{\frac{1}{\sqrt{2}}(0,v)^T} \right] \\
&+ ig'Y B_I^\mu \left[\overbrace{\langle H_I^\dagger \rangle_0}^{\frac{1}{\sqrt{2}}(0,v)} \frac{\vec{\tau}}{2} (\partial_\mu \phi_I) - \left(\partial_\mu \phi_I^\dagger \right) \frac{\vec{\tau}}{2} \overbrace{\langle H_I \rangle_0}^{\frac{1}{\sqrt{2}}(0,v)^T} \right]
\end{aligned} \tag{B.6}$$

4. H_{II} mixing terms

$$\begin{aligned}
(D_\mu H_{II})^\dagger (D^\mu H_{II}) \Big|_{\text{mixing}} &= ig\vec{W}_{II}^\mu \left[\overbrace{\langle H_{II}^\dagger \rangle_0}^{\frac{1}{\sqrt{2}}(0,v)} \frac{\vec{\tau}}{2} (\partial_\mu \phi_{II}) - \left(\partial_\mu \phi_{II}^\dagger \right) \frac{\vec{\tau}}{2} \overbrace{\langle H_{II} \rangle_0}^{\frac{1}{\sqrt{2}}(0,v)^T} \right] \\
&+ ig'Y B_{II}^\mu \left[\overbrace{\langle H_{II}^\dagger \rangle_0}^{\frac{1}{\sqrt{2}}(0,v)} \frac{\vec{\tau}}{2} (\partial_\mu \phi_{II}) - \left(\partial_\mu \phi_{II}^\dagger \right) \frac{\vec{\tau}}{2} \overbrace{\langle H_{II} \rangle_0}^{\frac{1}{\sqrt{2}}(0,v)^T} \right]
\end{aligned} \tag{B.7}$$

Rearranging all mixing terms as coefficients of the four gauge fields and taking into account that the gauge group generators $\frac{\vec{\tau}}{2}$ commute with the VEV of H_{W^5} leads to:

1. Mixing Terms for \vec{W}_I^μ :

$$ig\vec{W}_I^\mu \left[tr \left[-\langle H_{W^5}^\dagger \rangle_0 \frac{\vec{\tau}}{2} (\partial_\mu \phi_W) + \left(\partial_\mu \phi_W^\dagger \right) \frac{\vec{\tau}}{2} \langle H_{W^5} \rangle_0 \right] + \langle H_I^\dagger \rangle_0 \frac{\vec{\tau}}{2} (\partial_\mu \phi_I) - \left(\partial_\mu \phi_I^\dagger \right) \frac{\vec{\tau}}{2} \langle H_I \rangle_0 \right] \tag{B.8}$$

2. Mixing Terms for \vec{W}_{II}^μ :

$$ig\vec{W}_{II}^\mu \left[tr \left[+\langle H_{W^5}^\dagger \rangle_0 \frac{\vec{\tau}}{2} (\partial_\mu \phi_W) - (\partial_\mu \phi_W^\dagger) \frac{\vec{\tau}}{2} \langle H_{W^5} \rangle_0 \right] + \langle H_{II}^\dagger \rangle_0 \frac{\vec{\tau}}{2} (\partial_\mu \phi_{II}) - (\partial_\mu \phi_{II}^\dagger) \frac{\vec{\tau}}{2} \langle H_{II} \rangle_0 \right] \quad (\text{B.9})$$

N.B.: the sign change in the terms connected with H_{W^5} is a direct result of the different transformation property of the H_{W^5} field under $SU(2)_I$ and $SU(2)_{II}$

3. Mixing Terms for B_I^μ

$$ig'YB_I^\mu \left[+ (\partial_\mu \phi_B^\dagger) \langle H_{B^5} \rangle_0 - \langle H_{B^5}^\dagger \rangle_0 (\partial_\mu \phi_B) + \langle H_I^\dagger \rangle_0 (\partial_\mu \phi_I) - (\partial_\mu \phi_I^\dagger) \langle H_I \rangle_0 \right] \quad (\text{B.10})$$

4. Mixing Terms for B_{II}^μ

$$ig'YB_{II}^\mu \left[- (\partial_\mu \phi_B^\dagger) \langle H_{B^5} \rangle_0 + \langle H_{B^5}^\dagger \rangle_0 (\partial_\mu \phi_B) + \langle H_{II}^\dagger \rangle_0 (\partial_\mu \phi_{II}) - (\partial_\mu \phi_{II}^\dagger) \langle H_{II} \rangle_0 \right] \quad (\text{B.11})$$

As for the W gauge fields there is a sign change in the terms connected with H_{B^5} due to the different transformation properties of H_{B^5} under $U(1)_I$ and $U(1)_{II}$

B.0.2. Construction of Gauge Functions

Following the lines of [58], we make an ansatz for the four gauge fixing functions \vec{f}_I , \vec{f}_{II} , f_{III} and f_{IV} and show that this choice cancels all mixing terms between gauge- and Goldstone-bosons and simultaneously yields the correct mass spectrum for the Goldstone modes.

1. Gauge Function for $SU(2)_I$

$$\vec{f}_I = \partial_\mu \vec{W}_I^\mu + ig\xi \left[tr \left[+\langle H_{W^5}^\dagger \rangle_0 \frac{\vec{\tau}}{2} \phi_W - \phi_W^\dagger \frac{\vec{\tau}}{2} \langle H_{W^5} \rangle_0 \right] - \langle H_I^\dagger \rangle_0 \frac{\vec{\tau}}{2} \phi_I + \phi_I^\dagger \frac{\vec{\tau}}{2} \langle H_I \rangle_0 \right] \quad (\text{B.12})$$

One immediately realizes the special structure of this gauge fixing function. Compared to the mixing terms we wrote down for the W_I field, the partial derivative that used to act on the ϕ_I got shifted to the W_I field itself. Simultaneously, all signs of the Higgs terms changed relative to eq. (B.8). Incorporated in $\frac{1}{2\xi} [f_i]^2$, the particular structure of the gauge fixing function enables us to cancel the gauge field Goldstone boson mixing terms arising in the gauge part of the Lagrangian after a partial integration.

2. Gauge Function for $SU(2)_{II}$

$$\vec{f}_{II} = \partial_\mu \vec{W}_{II}^\mu + ig\xi \left[tr \left[-\langle H_{W^5}^\dagger \rangle_0 \frac{\vec{\tau}}{2} \phi_W + \phi_W^\dagger \frac{\vec{\tau}}{2} \langle H_{W^5} \rangle_0 \right] - \langle H_{II}^\dagger \rangle_0 \frac{\vec{\tau}}{2} \phi_{II} + \phi_{II}^\dagger \frac{\vec{\tau}}{2} \langle H_{II} \rangle_0 \right] \quad (\text{B.13})$$

In comparison to \vec{f}_I there are relative minus signs due to different transformation property of H_{W^5} under $SU(2)_I$ and $SU(2)_{II}$

3. Gauge Function for $U(1)_I$

$$f_{III} = \partial_\mu B_I^\mu + ig'Y\xi \left[\langle H_{B^5}^\dagger \rangle_0 \phi_B - \phi_B^\dagger \langle H_{B^5} \rangle_0 - \langle H_I^\dagger \rangle_0 \phi_I + \phi_I^\dagger \langle H_I \rangle_0 \right] \quad (\text{B.14})$$

4. Gauge Function for $U(1)_{II}$

$$f_{IV} = \partial_\mu B_{II}^\mu + ig'Y\xi \left[-\langle H_{B^5}^\dagger \rangle_0 \phi_B + \phi_B^\dagger \langle H_{B^5} \rangle_0 - \langle H_{II}^\dagger \rangle_0 \phi_{II} + \phi_{II}^\dagger \langle H_{II} \rangle_0 \right] \quad (\text{B.15})$$

B.0.3. Gauge Fixing Lagrangian $\mathcal{L}_{\text{gauge-fixing}}$

Having all gauge fixing functions at hand, we cast $\mathcal{L}_{\text{gauge-fixing}}$ into standard textbook form [58] and write:

$$\begin{aligned} \mathcal{L}_{\text{gauge-fixing}} &= \sum_i -\frac{1}{2\xi} [f_i]^2 \\ &= -\frac{1}{2\xi} [\vec{f}_I]^2 - \frac{1}{2\xi} [\vec{f}_{II}]^2 - \frac{1}{2\xi} [f_{III}]^2 - \frac{1}{2\xi} [f_{IV}]^2 \end{aligned} \quad (\text{B.16})$$

In principle we could have chosen different gauge parameters ξ for each gauge group individually².

Expanding the gauge fixing Lagrangian, we obtain a polynomial in Higgs VEVs, dynamic Higgs terms and derivatives of gauge fields. We find expressions of the form:

$$-\frac{1}{2\xi} \left[\overbrace{(\partial_\mu A^\mu)^2}^{\text{term 1}} + \overbrace{2ig\xi (\partial_\mu A^\mu) (\text{Higgs-part})}^{\text{term 2}} + \overbrace{(ig\xi (\text{Higgs-part}))^2}^{\text{term 3}} \right] \quad (\text{B.17})$$

"A" in this case generically represents gauge fields and the "Higgs-part" corresponds to terms including dynamical scalar degrees of freedom as well as vacuum expectation values.

Cancellation of Gauge- and Goldstone Boson Mixing

We will explicitly demonstrate the cancellation of the mixing terms between Goldstone- and gauge-bosons arising from the Higgs kinetic Lagrangian through the expressions in "term 2" for the special case of \vec{W}_I . Analog considerations equally apply to all other gauge fields.

For the gauge fixing function (B.12) we adopt the general formula (B.17) from above to find:

$$-ig \left(\partial_\mu \vec{W}_I^\mu \right) \cdot \left[tr \left[+\langle H_{W^5}^\dagger \rangle_0 \frac{\vec{\tau}}{2} \phi_W - \phi_W^\dagger \frac{\vec{\tau}}{2} \langle H_{W^5} \rangle_0 \right] - \langle H_I^\dagger \rangle_0 \frac{\vec{\tau}}{2} \phi_I + \phi_I^\dagger \frac{\vec{\tau}}{2} \langle H_I \rangle_0 \right] \quad (\text{B.18})$$

²During the calculation of the Sommerfeld enhancement to vector dark matter, we are going to make use of this freedom to treat the photon propagator separate from the massive gauge bosons.

and compare this to the mixing terms in the gauge Lagrangian from the covariant derivatives (see eq. (B.8))

$$-ig\vec{W}_I^\mu \left[tr \left[+\langle H_{W^5}^\dagger \rangle_0 \frac{\vec{\tau}}{2} (\partial_\mu \phi_W) - \left(\partial_\mu \phi_W^\dagger \right) \frac{\vec{\tau}}{2} \langle H_{W^5} \rangle_0 \right] - \langle H_I^\dagger \rangle_0 \frac{\vec{\tau}}{2} (\partial_\mu \phi_I) + \left(\partial_\mu \phi_I^\dagger \right) \frac{\vec{\tau}}{2} \langle H_I \rangle_0 \right] \quad (\text{B.19})$$

After a partial integration in the gauge fixing Lagrangian we can shift the partial derivative from the \vec{W}_I to the Higgs fields and get an additional minus sign which leads to the exact cancellation of all mixing terms. As mentioned in the introduction to gauge fixing, the absence of such mixing terms enables us to interpret the remaining expressions in the Lagrangian in terms of physical particle excitations.

Goldstone Boson Mass

Other than expressions responsible for the cancellation of gauge- and Goldstone- boson mixings, the gauge fixing Lagrangian also includes contributions giving rise to ξ dependent Goldstone-boson masses.

”Term 3” in equation (B.17) contains expressions quadratic in scalar fields, thus contributing to the mass matrices in the scalar sector. In the case of the gauge fixing function \vec{f}_I for $SU(2)_I$ we obtain:

$$\frac{g^2 \xi}{2} \left[tr \left[+\langle H_{W^5}^\dagger \rangle_0 \frac{\vec{\tau}}{2} \phi_W - \phi_W^\dagger \frac{\vec{\tau}}{2} \langle H_{W^5} \rangle_0 \right] - \langle H_I^\dagger \rangle_0 \frac{\vec{\tau}}{2} \phi_I + \phi_I^\dagger \frac{\vec{\tau}}{2} \langle H_I \rangle_0 \right]^2 \quad (\text{B.20})$$

Evaluating these terms for all other gauge fixing functions is rather cumbersome and not very enlightening. We implemented these terms in *Mathematica* to evaluate the scalar mass spectrum and the eigenvectors for the complete gauge-fixed Lagrangian automatically.

The Neutral Higgs Sector with Gauge Fixing Terms

In accordance with our preceding analysis without the gauge fixing terms (section 4.5), we split the neutral 10×10 Higgs mass matrix into three distinct blocks. The gauge fixing terms do not give rise to inter-block mixing, but cause mixings within the three sub-blocks separately. For completeness we show the mass matrices explicitly:

In the basis $(\chi_0^{(3)} \psi_0 \psi_1) \left(\widetilde{M}_{diag}^n \right)^2 (\chi_0^{(3)} \psi_0 \psi_1)^T$

$$\left(\widetilde{M}_{diag}^n \right)^2 = \begin{pmatrix} \frac{1}{8} v_0^2 (g^2 + 4g'^2 Y^2) \xi & 0 & 0 \\ 0 & v_0^2 \lambda & 0 \\ 0 & 0 & 2M_0^2 + v_0^2 \lambda \end{pmatrix} \quad (\text{B.21})$$

In the basis $(\psi_{W^5,1} \psi_{W^5,2} h_{B^5}^{(1)}) \left(\widetilde{M}_{scalar}^n \right)^2 (\psi_{W^5,1} \psi_{W^5,2} h_{B^5}^{(1)})^T$

$$\left(\widetilde{M}_{scalar}^n \right)^2 = \begin{pmatrix} M' + 2v_2^2(\lambda_1 + \lambda_2) & -M' + 2v_2^2 \lambda_2 & 0 \\ -M' + 2v_2^2 \lambda_2 & M' + \frac{M_0^2 v_0^2 + 4v_2^4 (\lambda_1 + \lambda_2)}{2v_2^2} & -\frac{M_0^2 v_0^2}{2v_1 v_2} \\ 0 & -\frac{M_0^2 v_0^2}{2v_1 v_2} & \frac{M_0^2 v_0^2}{2v_1^2} + 2v_1^2 \lambda_B \end{pmatrix} \quad (\text{B.22})$$

In the basis $(h_{B^5}^{(2)} \chi_1^{(3)} \chi_{W^5,2}^{(3)} \chi_{W^5,1}^{(3)}) \left(\widetilde{M}_{ps}^n \right)^2 (h_{B^5}^{(2)} \chi_1^{(3)} \chi_{W^5,2}^{(3)} \chi_{W^5,1}^{(3)})^T$

$$\left(\widetilde{M}_{ps}^n \right)^2 = \begin{pmatrix} \frac{M_0^2 v_0^2}{2v_1^2} + 2g'^2 v_1^2 Y^2 \xi & \frac{M_0^2 v_0}{v_1} - g'^2 v_0 v_1 Y^2 \xi & -\frac{M_0^2 v_0^2}{2v_1 v_2} & 0 \\ \frac{M_0^2 v_0}{v_1} - g'^2 v_0 v_1 Y^2 \xi & 2M_0^2 + \frac{1}{8} v_0^2 (g^2 + 4g'^2 Y^2) \xi & -\frac{M_0^2 v_0}{v_2} + \frac{1}{4} g^2 v_0 v_2 \xi & -\frac{1}{4} g^2 v_0 v_2 \xi \\ -\frac{M_0^2 v_0^2}{2v_1 v_2} & -\frac{M_0^2 v_0}{v_2} + \frac{1}{4} g^2 v_0 v_2 \xi & M' + \frac{1}{2} \left(\frac{M_0^2 v_0^2}{v_2^2} - M_0^2 \frac{v_0^2}{v_2^2} + g^2 v_2^2 \xi \right) & M' - \frac{1}{2} g^2 v_2^2 \xi \\ 0 & -\frac{1}{4} g^2 v_0 v_2 \xi & M' - \frac{1}{2} g^2 v_2^2 \xi & M' + \frac{1}{2} g^2 v_2^2 \xi \end{pmatrix} \quad (\text{B.23})$$

Only $\left(\widetilde{M}_{diag}^n \right)^2$ and $\left(\widetilde{M}_{ps}^n \right)^2$ contain ξ dependent contributions which coincides with our earlier observation of massless Goldstone modes in these particular sectors (see 1a and 1c). For now we are only interested in the gauge dependent mass eigenvalues therefore we only reevaluate the mass spectrum for $\left(\widetilde{M}_{diag}^n \right)^2$ and $\left(\widetilde{M}_{ps}^n \right)^2$. The mass of the Goldstone mode from the diagonal block is directly accessible. Before continuing to diagonalize the pseudoscalar sector it is beneficial to apply an orthogonal transformation and change the field basis: $\chi_{W^5,e/o}^{(3)} = \frac{1}{\sqrt{2}} (\chi_{W^5,1}^{(3)} \pm \chi_{W^5,2}^{(3)})$ to find

$(h_{B^5}^{(2)} \chi_1^{(3)} \chi_{W^5,e}^{(3)} \chi_{W^5,o}^{(3)}) \left(\widetilde{M}_{ps}^n \right)^2 (h_{B^5}^{(2)} \chi_1^{(3)} \chi_{W^5,e}^{(3)} \chi_{W^5,o}^{(3)})^T \dots$

$$\begin{pmatrix} \frac{M_0^2 v_0^2}{2v_1^2} + 2g'^2 Y^2 \xi v_1^2 & \frac{v_0 (M_0^2 - g'^2 Y^2 \xi v_1^2)}{v_1} & -\frac{M_0^2 v_0^2}{2\sqrt{2}v_1 v_2} & \frac{M_0^2 v_0^2}{2\sqrt{2}v_1 v_2} \\ v_0 (M_0^2 - g'^2 Y^2 \xi v_1^2) & 2M_0^2 + \frac{1}{8} (g^2 + 4g'^2 Y^2) \xi v_0^2 & -\frac{M_0^2 v_0}{\sqrt{2}v_2} & -\frac{v_0 (-2M_0^2 + g^2 \xi v_2^2)}{\sqrt{2}v_2} \\ -\frac{M_0^2 v_0^2}{2\sqrt{2}v_1 v_2} & -\frac{M_0^2 v_0}{\sqrt{2}v_2} & 2M' + \frac{M_0^2 v_0^2}{4v_2^2} & -\frac{M_0^2 v_0^2}{4v_2^2} \\ \frac{M_0^2 v_0^2}{2\sqrt{2}v_1 v_2} & -\frac{v_0 (-2M_0^2 + g^2 \xi v_2^2)}{2\sqrt{2}v_2} & -\frac{M_0^2 v_0^2}{4v_2^2} & \frac{M_0^2 v_0^2}{4v_2^2} + g^2 \xi v_2^2 \end{pmatrix}$$

The diagonalization proceeds in a straight forward way, the formerly massless Goldstone modes acquire ξ dependent masses whereas the formerly massive modes remain unchanged.

A summary of all neutral Goldstone bosons masses is given by³:

$$\left\{ m_{GB_{Z(0)}}^2, m_{GB_{\gamma(1)/Z(1)}}^2 \right\} = \left\{ \frac{1}{8} v_0^2 (g^2 + 4g'^2 Y^2) \xi, \right. \\ \left. \frac{1}{16} \left(g^2 (v_0^2 + 8v_2^2) + 4g'^2 (v_0^2 + 4v_1^2) Y^2 \pm \sqrt{g^4 (v_0^2 + 8v_2^2)^2 + 8g^2 g'^2 (v_0^4 - 4v_0^2 v_1^2 - 8(v_0^2 + 4v_1^2) v_2^2) Y^2 + 16g'^4 (v_0^2 + 4v_1^2)^2 Y^4} \right) \xi \right\} \quad (\text{B.24})$$

We realize that the gauge eigenstate $\chi_0^{(3)}$ is equivalent to the Goldstone boson for the Standard Model Z ($GB_{Z(0)}$) and no mixing with other scalar modes occurs. For the Goldstone boson associated with dark photon ($GB_{\gamma(1)}$) we obtain a mixing between different gauge eigenstates according to the eigenvector:

$$\begin{pmatrix} v_1 \left(4g'^2 Y^2 (v_0^2 + 4v_1^2) - g^2 (v_0^2 + 8v_2^2) + \sqrt{16g'^4 Y^4 (v_0^2 + 4v_1^2)^2 + g^4 (v_0^2 + 8v_2^2)^2 + 8g^2 g'^2 Y^2 (v_0^4 - 4v_0^2 v_1^2 - 8(v_0^2 + 4v_1^2) v_2^2)} \right) \\ \frac{2\sqrt{2}g^2 v_0^2 v_2}{4\sqrt{2}g^2 v_0 v_2} \\ - \frac{4g'^2 Y^2 (v_0^2 + 4v_1^2) + g^2 (v_0^2 - 8v_2^2) + \sqrt{16g'^4 Y^4 (v_0^2 + 4v_1^2)^2 + g^4 (v_0^2 + 8v_2^2)^2 + 8g^2 g'^2 Y^2 (v_0^4 - 4v_0^2 v_1^2 - 8(v_0^2 + 4v_1^2) v_2^2)}}{4\sqrt{2}g^2 v_0 v_2} \\ 0 \\ 1 \end{pmatrix}$$

The Goldstone boson associated with $Z_{(1)}$ ($GB_{Z(1)}$) is realized through a mixing between the gauge eigenstates according to:

$$\begin{pmatrix} v_1 \left(4g'^2 Y^2 (v_0^2 + 4v_1^2) - g^2 (v_0^2 + 8v_2^2) - \sqrt{16g'^4 Y^4 (v_0^2 + 4v_1^2)^2 + g^4 (v_0^2 + 8v_2^2)^2 + 8g^2 g'^2 Y^2 (v_0^4 - 4v_0^2 v_1^2 - 8(v_0^2 + 4v_1^2) v_2^2)} \right) \\ \frac{2\sqrt{2}g^2 v_0^2 v_2}{4\sqrt{2}g^2 v_0 v_2} \\ - \frac{4g'^2 Y^2 (v_0^2 + 4v_1^2) + g^2 (v_0^2 - 8v_2^2) - \sqrt{16g'^4 Y^4 (v_0^2 + 4v_1^2)^2 + g^4 (v_0^2 + 8v_2^2)^2 + 8g^2 g'^2 Y^2 (v_0^4 - 4v_0^2 v_1^2 - 8(v_0^2 + 4v_1^2) v_2^2)}}{4\sqrt{2}g^2 v_0 v_2} \\ 0 \\ 1 \end{pmatrix}$$

We are able to parameterize these eigenvectors in terms of the gauge boson masses:

$$GB_{\gamma(1)} : \begin{pmatrix} \frac{v_1}{v_2} \frac{1}{\sqrt{2}m_{W^\pm(0)}^2} \left(m_{A(1)}^2 - m_{W^\pm(1)}^2 \right) \\ - \frac{v_0}{v_2} \frac{1}{2\sqrt{2}m_{W^\pm(0)}^2} \left(m_{A(1)}^2 - m_{W^\pm(1)}^2 + m_{W^\pm(0)}^2 \right) \\ 0 \\ 1 \end{pmatrix} \quad (\text{B.25})$$

$$GB_{Z(1)} : \begin{pmatrix} \frac{v_1}{v_2} \frac{1}{\sqrt{2}m_{W^\pm(0)}^2} \left(m_{Z(1)}^2 - m_{W^\pm(1)}^2 \right) \\ - \frac{v_0}{v_2} \frac{1}{2\sqrt{2}m_{W^\pm(0)}^2} \left(m_{Z(1)}^2 - m_{W^\pm(1)}^2 + m_{W^\pm(0)}^2 \right) \\ 0 \\ 1 \end{pmatrix} \quad (\text{B.26})$$

³Note that we only give the results in terms of the original gauge couplings g and g' . The transition to the SM couplings includes only a rescaling by a factor $\frac{1}{\sqrt{2}}$ as explained in the footnote of sec. (4.5.4)

The Charged Higgs Sector with Gauge Fixing Terms

The points mentioned in the discussion of the neutral Higgs sector equally apply to the charged case. For simplicity we split the charged scalar mass matrix into two separate blocks that do not mix amongst each other. We decouple the contribution for $\chi_0^{(+)} (M_{diag}^{ch})^2 \chi_0^{(-)}$:

$$\left(M_{diag}^{ch}\right)^2 = \frac{1}{8}g^2v_0^2\xi \quad (\text{B.27})$$

The remaining 3×3 block is written in the basis $(\chi_1^{(+)} \chi_{W^{5,2}}^{(+)} \chi_{W^{5,1}}^{(+)}) (M_{ps}^{ch})^2 (\chi_1^{(-)} \chi_{W^{5,2}}^{(-)} \chi_{W^{5,1}}^{(-)})$

$$\left(M_{ps}^{ch}\right)^2 = \begin{pmatrix} 2M_0^2 + \frac{1}{8}g^2\xi v_0^2 & -\frac{M_0^2v_0}{2v_2} + \frac{1}{4}g^2\xi v_0v_2 & -\frac{M_0^2v_0}{2v_2} + \frac{1}{4}g^2\xi v_0v_2 \\ -\frac{M_0^2v_0}{2v_2} + \frac{1}{4}g^2\xi v_0v_2 & M' + \frac{M_0^2v_0^2}{4v_2^2} + \frac{1}{2}g^2\xi v_2^2 + v_2^2\lambda_1 & -M' + \frac{1}{2}g^2\xi v_2^2 - v_2^2\lambda_1 \\ -\frac{M_0^2v_0}{2v_2} + \frac{1}{4}g^2\xi v_0v_2 & -M' + \frac{1}{2}g^2\xi v_2^2 - v_2^2\lambda_1 & M' + \frac{M_0^2v_0^2}{4v_2^2} + \frac{1}{2}g^2\xi v_2^2 + v_2^2\lambda_1 \end{pmatrix} \quad (\text{B.28})$$

We perform a basis change from the $\chi_{W^{5,1/2}}^{(\pm)}$ to a new symmetric and antisymmetric basis

$\chi_{W^{5,e/o}}^{(\pm)} = \frac{1}{\sqrt{2}} (\chi_{W^{5,1}}^{(\pm)} \pm \chi_{W^{5,2}}^{(\pm)})$ and define $(\chi_1^{(+)} \chi_{W^{5,e}}^{(+)} \chi_{W^{5,o}}^{(+)}) (\widehat{M}_{ps}^{ch})^2 (\chi_1^{(-)} \chi_{W^{5,e}}^{(-)} \chi_{W^{5,o}}^{(-)})^T$:

$$\left(\widehat{M}_{ps}^{ch}\right)^2 = \begin{pmatrix} 2M_0^2 + \frac{1}{8}g^2\xi v_0^2 & \sqrt{2} \left(-\frac{M_0^2v_0}{2v_2} + \frac{1}{4}g^2\xi v_0v_2\right) & 0 \\ \sqrt{2} \left(-\frac{M_0^2v_0}{2v_2} + \frac{1}{4}g^2\xi v_0v_2\right) & \frac{M_0^2v_0^2}{4v_2^2} + g^2\xi v_2^2 & 0 \\ 0 & 0 & 2M' + \frac{M_0^2v_0^2}{4v_2^2} + 2v_2^2\lambda_1 \end{pmatrix} \quad (\text{B.29})$$

Diagonalization of the $(\widehat{M}_{ps}^{ch})^2$ yields four Goldstone modes with ξ dependent masses.

$$\left\{ m_{GB_{W(0)}^\pm}^2, m_{GB_{W(1)}^\pm}^2 \right\} = \left\{ \frac{1}{8}g^2v_0^2\xi, \frac{1}{8}g^2(v_0^2 + 8v_2^2)\xi \right\} \quad (\text{B.30})$$

The gauge eigenstates $\chi_0^{(\pm)}$ are directly identified with the Goldstone bosons $GB_{W(0)}^\pm$ associated to the Standard Model W and no additional diagonalization is required. Compared to the neutral sector, the mixing between the charged pseudo-scalars that form the Goldstone bosons $GB_{W(1)}^\pm$ is far simpler, the corresponding eigenvector is: $\left(\frac{v_0}{2\sqrt{2}v_2}, 1, 0\right)^T$

B.0.4. Discussion

We have chosen a special set of gauge fixing functions $f_i(A)$ that cancel the mixing terms between gauge- and Goldstone bosons on the Lagrangian level. The analysis of the particle mass spectrum yields an equal number of massive vector- and massless Goldstone modes before the incorporation of gauge fixing terms. Properly taking into account the gauge fixing Lagrangian renders the Goldstone bosons massive with a gauge parameter dependent mass. It is important to note that the Goldstone masses are exactly equal to the gauge boson masses up to a factor of $\sqrt{\xi}$. This is a clear indication that they can not be physical degrees of freedom of the theory but are rather mathematical devices to cancel the redundant degrees of freedom of the gauge fields and implement the constraints on the dynamical variables in the Lagrangian. Notably, we are able to take the limit $\xi \rightarrow \infty$ to make the Goldstone bosons infinitely heavy and decouple them (together with the ghosts) from our theory. This is commonly referred to as choosing a unitary gauge. Doing so, one is left with the physical degrees of freedom at the price of a seemingly ill defined high energy behavior of the gauge boson propagators. In the following, we would like to summarize the scalar sector by giving the transformation properties and masses of all scalar and pseudo-scalar particles.

Goldstone-Bosons

We are going to start from the exact mass eigenstates and continue to perform several approximations in order to reduce the interaction vertices to the leading terms. We will elaborate on this point in the following sections in greater detail and explain our intentions.

$$\begin{aligned}
GB_{Z(0)}[x] &= \chi_0^{(3)}[x] \\
m_{GB_{Z(0)}}^2 &= \frac{1}{8} v_0^2 (g^2 + 4g'^2 Y^2) \xi \\
\\
GB_{Z(1)}[x] &= \frac{1}{norm} \left(c_1 h_{B5}^{(2)}[x] + c_2 \chi_1^{(3)}[x] + \chi_{W5,o}^{(3)}[x] \right) \\
c_1 &= \frac{v_1}{v_2} \frac{1}{\sqrt{2} m_{W\pm(0)}^2} (m_{Z(1)}^2 - m_{W\pm(1)}^2) \\
c_2 &= -\frac{v_0}{v_2} \frac{1}{2\sqrt{2} m_{W\pm(0)}^2} (m_{Z(1)}^2 - m_{W\pm(1)}^2 + m_{W\pm(0)}^2) \\
norm &= \frac{1}{2\sqrt{2} v_2 m_{W\pm(0)}^2} \sqrt{8m_{W\pm(0)}^4 v_2^2 + (m_{Z(1)}^2 - m_{W\pm(1)}^2 + m_{W\pm(0)}^2)^2 v_0^2 + 4(m_{Z(1)}^2 - m_{W\pm(1)}^2)^2 v_1^2} \\
m_{GB_{Z(1)}}^2 &= \frac{1}{16} \left(g^2 (v_0^2 + 8v_2^2) + 4g'^2 (v_0^2 + 4v_1^2) Y^2 - \sqrt{(g^4 (v_0^2 + 8v_2^2)^2 + 8g^2 g'^2 (v_0^4 - 4v_0^2 v_1^2 - 8(v_0^2 + 4v_1^2) v_2^2) Y^2 + 16g'^4 (v_0^2 + 4v_1^2)^2 Y^4)} \right) \xi \\
\\
GB_{A(1)}[x] &= \frac{1}{norm} \left(\tilde{c}_1 h_{B5}^{(2)}[x] + \tilde{c}_2 \chi_1^{(3)}[x] + \chi_{W5,o}^{(3)}[x] \right) \\
\tilde{c}_1 &= \frac{v_1}{v_2} \frac{1}{\sqrt{2} m_{W\pm(0)}^2} (m_{A(1)}^2 - m_{W\pm(1)}^2) \\
\tilde{c}_2 &= -\frac{v_0}{v_2} \frac{1}{2\sqrt{2} m_{W\pm(0)}^2} (m_{A(1)}^2 - m_{W\pm(1)}^2 + m_{W\pm(0)}^2) \\
norm &= \frac{1}{2\sqrt{2} v_2 m_{W\pm(0)}^2} \sqrt{8m_{W\pm(0)}^4 v_2^2 + (m_{A(1)}^2 - m_{W\pm(1)}^2 + m_{W\pm(0)}^2)^2 v_0^2 + 4(m_{A(1)}^2 - m_{W\pm(1)}^2)^2 v_1^2} \\
m_{GB_{A(1)}}^2 &= \frac{1}{16} \left(g^2 (v_0^2 + 8v_2^2) + 4g'^2 (v_0^2 + 4v_1^2) Y^2 + \sqrt{(g^4 (v_0^2 + 8v_2^2)^2 + 8g^2 g'^2 (v_0^4 - 4v_0^2 v_1^2 - 8(v_0^2 + 4v_1^2) v_2^2) Y^2 + 16g'^4 (v_0^2 + 4v_1^2)^2 Y^4)} \right) \xi \\
\\
GB_{W\pm(0)}[x] &= \chi_0^{(\pm)}[x] \\
m_{GB_{W\pm(0)}}^2 &= \frac{1}{8} g^2 v_0^2 \xi \\
\\
GB_{W\pm(1)}[x] &= \frac{1}{norm} \left(v_0 \chi_1^{(\pm)}[x] + 2\sqrt{2} v_2 \chi_{W5,e}^{(\pm)}[x] \right) \\
norm &= \sqrt{v_0^2 + 8v_2^2} \\
m_{GB_{W\pm(1)}}^2 &= \frac{1}{8} g^2 (v_0^2 + 8v_2^2) \xi
\end{aligned} \tag{B.31}$$

Neutral Physical Higgs Fields

$$h^{(0)}[x] = \psi_0[x]$$

$$m_{h^{(0)}}^2 = v_0^2 \lambda$$

$$h^{(1)}[x] = \psi_1[x]$$

$$m_{h^{(1)}}^2 = 2M_0^2 + v_0^2 \lambda$$

the following fields are part of the scalar Higgs sector and we take the approximate diagonalizations:

$$\phi_1[x] = \frac{1}{\sqrt{2}} \left(-\psi_{W^5,1}[x] + \psi_{W^5,2}[x] \right)$$

$$m_{\phi_1}^2 = 2 \left(M' + v_2^2 \lambda_1 \right)$$

$$\phi_2[x] = \frac{1}{\sqrt{2}} \left(\psi_{W^5,1}[x] + \psi_{W^5,2}[x] \right)$$

$$m_{\phi_2}^2 = 2v_2^2 (\lambda_1 + 2\lambda_2)$$

$$\phi_3[x] = h_{B^5}^{(1)}[x]$$

$$m_{\phi_3}^2 = 2v_1^2 \lambda_B$$

$$\begin{aligned} \phi_{4/5}[x] &= \frac{1}{norm_{4/5}} \left(\frac{\sqrt{2}v_2}{v_1} h_{B^5}^{(2)}[x] + \frac{2\sqrt{2}v_2}{v_0} \chi_1^{(3)}[x] + \tilde{c}_{4/5} \chi_{W^5,e}^{(3)}[x] + \chi_{W^5,o}^{(3)}[x] \right) \\ \tilde{c}_{4/5} &= \frac{\left(-4M'v_1^2 + M_0^2(v_0^2 + 4v_1^2) \right) v_2^2 \pm \sqrt{16M'^2 v_1^4 v_2^4 - 8M'M_0^2 v_1^2 (v_0^2 + 4v_1^2) v_2^4 + M_0^4 (4v_1^2 v_2^2 + v_0^2 (v_1^2 + v_2^2))^2}}{M_0^2 v_0^2 v_1^2} \\ &= \frac{4v_2^2}{M_0^2 v_0^2} \left(m_{\phi_{5/4}}^2 - 2M' \right) - 1 = \frac{m_{\phi_{5/4}}^2 - 2M'}{m_{\phi_{5/4}}^2 - m_{\phi_1}^2} - 1 \\ norm_{4/5} &= \sqrt{1 + 2v_2^2 \left(\frac{4}{v_0^2} + \frac{1}{v_1^2} \right) + \left(\frac{4v_2^2}{M_0^2 v_0^2} \left(m_{\phi_{5/4}}^2 - 2M' \right) - 1 \right)^2} \\ m_{\phi_{4/5}}^2 &= \frac{M_0^2 v_0^2 v_1^2 + \left(M_0^2 v_0^2 + 4(M' + M_0^2) v_1^2 \right) v_2^2 \mp \sqrt{16M'^2 v_1^4 v_2^4 - 8M'M_0^2 v_1^2 (v_0^2 + 4v_1^2) v_2^4 + M_0^4 (4v_1^2 v_2^2 + v_0^2 (v_1^2 + v_2^2))^2}}{4v_1^2 v_2^2} \end{aligned}$$

(B.32)

Charged Physical Higgs Fields

$$\phi_1^{(\pm)}[x] = \frac{1}{norm} \left(-2\sqrt{2}v_2 \chi_1^{(\pm)}[x] + v_0 \chi_{W^5,e}^{(\pm)}[x] \right)$$

$$norm = \sqrt{v_0^2 + 8v_2^2}$$

$$m_{\phi_1^{(\pm)}}^2 = \frac{1}{4} M_0^2 \left(8 + \frac{v_0^2}{v_2^2} \right)$$

$$\phi_2^{(\pm)}[x] = \chi_{W^5,o}^{(\pm)}[x]$$

$$m_{\phi_2^{(\pm)}}^2 = 2M' + M_0^2 \frac{v_0^2}{4v_2^2} + 2v_2^2 \lambda_1$$

(B.33)

B.1. Approximations to the Basistransformation between Gauge- and Mass Eigenstates

For certain processes it is phenomenologically legitimate to neglect subdominant mixings induced by diagonalizing mass matrices, despite using the exact solution for the mass eigenvalues themselves. If one is primarily interested in leading contributions to the scattering amplitude, we might think of each vertex factor expanded as $\Gamma(1 + \epsilon + \mathcal{O}(\epsilon^2))$, where subdominant contributions from mixings are parameterized by a small parameter $|\epsilon| \ll 1$. As long as there is no cancellation of leading order terms, we consistently neglect $\mathcal{O}(\epsilon)$ terms to reduce the calculational workload. In the scalar sector of our theory we exploit the specific feature of the particle mass spectrum and the hierarchy of vacuum expectation values to find a natural expansion parameter $\tilde{\epsilon} = \frac{v_0}{v_{1,2}}$.

For the Sommerfeld effect, we are particularly concerned with a few specific classes of vertices and diagrams. Only interactions between two nearly mass degenerate non-Standard Model states with one lighter state (which is supposed to act as the long range force carrier) are of principal importance [11, 23]. In case of four particle interactions, which can be relevant for higher loop order corrected integral kernels in vector dark matter models, we are exclusively interested in four-point functions with two nearly mass degenerate (1)-mode particles and two (0)-modes. For $Z^{(1)}$ dark matter, the relevant vertices either contain two $Z^{(1)}$ or $W_{(1)}^\pm$ (or a combination thereof) together with one or two (0)-modes. In a generalized R_ξ gauge, we allow for the corresponding vertices with Goldstone bosons and ghosts, since these contributions have to cancel non-physical degrees of freedom in the gauge boson diagrams.

In the general model without restrictions on any of the parameters it is virtually impossible to find a physically reasonable approximation to the basis transformation. For the Sommerfeld effect, however, we are interested in a region of parameter space where the lightest non-Standard-Model particle is the $SU(2)$ -like neutral gauge boson which already fixes the range of v_1 and v_2 to the white region in figure (4.3). The mixing coefficients for the Goldstone bosons only depend on v_1 and v_2 , if one assumes the gauge couplings g and g' and the Standard Model VEV v_0 as fixed. We depict the magnitudes of the expansion coefficients in the $v_1 - v_2$ plane to illustrate the validity of neglecting terms of $\mathcal{O}(\tilde{\epsilon})$. In order to get a numerical estimate of the approximation error, we explicitly state all results for the representative reference point $v_1 = 4000 \text{ GeV}$ and $v_2 = 1100 \text{ GeV}$ (see Sec. 4.5.4).

For convenience we introduce the following parameters:

$$\Delta m \equiv \sqrt{m_{W^{(1)}}^2 - m_{Z^{(1)}}^2} \quad (\text{B.34})$$

$$\delta m \equiv m_{W^{(1)}} - m_{Z^{(1)}} \quad (\text{B.35})$$

which are related through:

$$\delta m \approx \frac{\Delta m^2}{2m_{Z^{(1)}}} \quad (\text{B.36})$$

In the relevant parameter region the relation $\Delta m^2 < m_{W^{(0)}}^2$ (far away from the gauge boson mass level crossing, even $\Delta m^2 \ll m_{W^{(0)}}^2$) holds. At our reference point 4.5.4 we find:

$$\begin{aligned} \Delta m &\approx 3.5 \text{ GeV} \\ m_{W^{(0)}} &\approx 80 \text{ GeV} \end{aligned}$$

B.1.1. Approximation of the $\text{GB}_{Z^{(1)}}$ Eigenvector

The exact eigenvector for the transformation between gauge- and mass eigenstate for the $Z^{(1)}$ Goldstone boson is given in eq. (B.31) and we proceed utilizing the special properties of the mass spectrum to approximate the eigenvector⁴:

$$\begin{aligned} \text{GB}_{Z^{(1)}}[x] &\propto \left(c_1 h_{B^5}^{(2)}[x] + c_2 \chi_1^{(3)}[x] + \chi_{W^{5,o}}^{(3)}[x] \right) \\ c_1 &= - \frac{v_1}{\sqrt{2}v_2} \underbrace{\left(\frac{\Delta m}{m_{W^{(0)}}} \right)^2}_{\epsilon} \approx -\mathcal{O}(1) \cdot \left(\frac{\Delta m}{m_{W^{(0)}}} \right)^2, \end{aligned} \quad (\text{B.37})$$

with the small expansion parameter $\epsilon(v_1, v_2)$ and the coefficient

$$c_2 = - \frac{v_0}{2\sqrt{2}v_2} \frac{-\Delta m^2 + m_{W^{(0)}}^2}{m_{W^{(0)}}^2} = - \frac{v_0}{2\sqrt{2}v_2} (1 - \epsilon), \quad (\text{B.38})$$

which is suppressed by the hierarchy between the electroweak scale ($\propto v_0$) and the new physics scale ($\propto v_2$). These expansion coefficients have to be compared to the 1 in front of $\chi_{W^{5,o}}^{(3)}[x]$. For our reference point 4.5.4 we find:

$$c_1 \approx -0.005 \quad c_2 \approx -0.079.$$

To illustrate the size of our approximation, we plot ϵ as well as the c_1 and c_2 individually in the $v_1 - v_2$ plane.

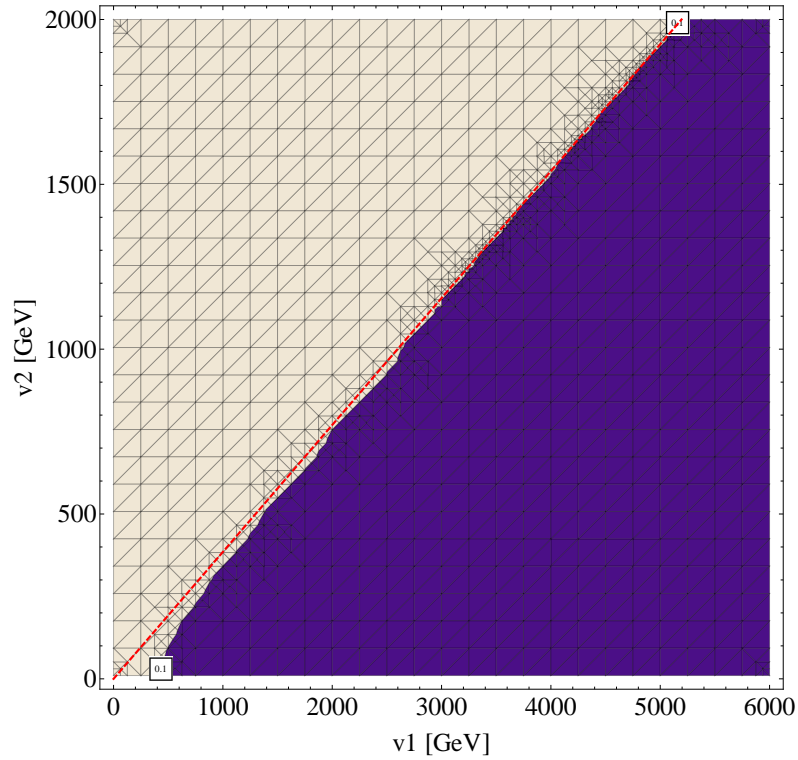


Figure B.1.: v_1 and v_2 dependence of $\epsilon = \left(\frac{\Delta m}{m_{W(0)}}\right)^2$. The red dashed line indicates the crossover from a $U(1)$ -like to a $SU(2)$ -like dark matter candidate as obtained from $\cos \theta_{W(1)}$. The blue region corresponds to $\epsilon < 0.10$ and covers almost all of the relevant parameter region.

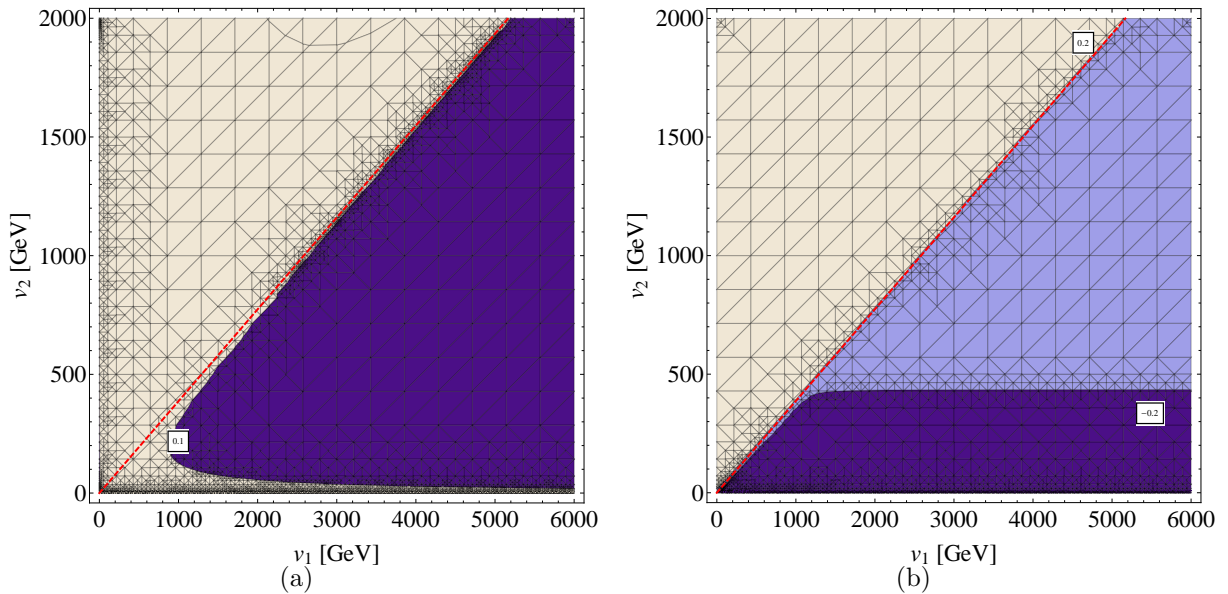


Figure B.2.: Expansion parameters c_1 and c_2 for the $Z^{(1)}$ Goldstone boson in the $v_1 - v_2$ plane. a) dark blue: $|c_1| < 0.1$. b) light blue: $|c_2| < 0.2$, dark blue: $c_2 < -0.2$.

If we neglect terms of order ϵ , we obtain an approximate eigenstate for $GB_{Z^{(1)}}$ with the correct normalization:

$$GB_{Z^{(1)}}[x] \approx \frac{1}{\sqrt{v_0^2 + (2\sqrt{2}v_2)^2}} \left(2\sqrt{2}v_2\chi_{W^5,o}^{(3)}[x] - v_0\chi_1^{(3)}[x] \right), \quad (\text{B.39})$$

which simplifies even further under the assumption of a hierarchy $v_0 < v_{1,2}$. In this approximation, the mixing with the modes from \tilde{H}_1 are neglected and the $Z^{(1)}$ Goldstone boson is solely $\chi_{W^5,o}^{(3)}[x]^5$:

$$GB_{Z^{(1)}}[x] \approx \chi_{W^5,o}^{(3)}[x] \quad (\text{B.40})$$

B.1.2. Approximation of the $GB_{\gamma^{(1)}}$ Eigenvector

Analogously to $GB_{Z^{(1)}}$, we try to find a reasonable approximation for $GB_{\gamma^{(1)}}$. In this case we do not have a small expansion parameter ϵ but a large mass splitting between $m_{\gamma^{(1)}}^2$ and $m_{W^{(1)}}^2$ which we can use to our advantage.

$$\begin{aligned} GB_{\gamma^{(1)}}[x] &\propto \left(\tilde{c}_1 h_{B^5}^{(2)}[x] + \tilde{c}_2 \chi_1^{(3)}[x] + \chi_{W^5,o}^{(3)}[x] \right) \\ \tilde{c}_1 &= \frac{v_1}{\sqrt{2}v_2} \frac{m_{\gamma^{(1)}}^2 - m_{W^{(1)}}^2}{m_{W^{(0)}}^2} \\ \tilde{c}_2 &= -\frac{v_0}{2\sqrt{2}v_2} \frac{m_{\gamma^{(1)}}^2 - m_{W^{(1)}}^2 + m_{W^{(0)}}^2}{m_{W^{(0)}}^2} \approx -\frac{v_0}{2\sqrt{2}v_2} \frac{m_{\gamma^{(1)}}^2 - m_{W^{(1)}}^2}{m_{W^{(0)}}^2} \end{aligned} \quad (\text{B.41})$$

where \tilde{c}_2 is suppressed by the hierarchy between the weak scale ($\propto v_0$) and the compactification scale ($\propto v_2$). We have to compare the expansion coefficients to 1 in front of $\chi_{W^5,o}^{(3)}[x]$. For our reference point we find:

$$\begin{aligned} \tilde{c}_1 &\approx 400 \\ \tilde{c}_2 &\approx -12 \end{aligned}$$

As applicable from figure (B.3), we can neglect $\chi_{W^5,o}^{(3)}$ to a very good approximation to obtain the eigenvector for $GB_{\gamma^{(1)}}$:

$$GB_{\gamma^{(1)}}[x] \approx \frac{1}{\sqrt{v_0^2 + (2v_1)^2}} \left(2v_1 h_{B^5}^{(2)}[x] - v_0 \chi_1^{(3)}[x] \right) \quad (\text{B.42})$$

⁴Coefficients are **not** normalized, this however is irrelevant for the comparison of their relative orders of magnitude.

⁵If one were to make contact to extra dimensional theories, this is consistent with UED (see remark in chapter 4.2.2), where the 5-components of the gauge fields furnish the Goldstone bosons in the limit $R^{-1} \gg m_{W^{(0)}}$.

for a reasonably large hierarchy $v_0 < v_1$ the mixing simplifies further and the mixing with the modes from \tilde{H}_1 are neglected altogether. The $\gamma^{(1)}$ Goldstone boson is equivalent to $h_{B^5}^{(2)}[x]$:

$$GB_{\gamma^{(1)}}[x] \approx h_{B^5}^{(2)}[x] \quad (\text{B.43})$$

To validate the assumption of a mostly $h_{B^5}^{(2)}[x]$ like $GB_{\gamma^{(1)}}$ we plot the expansion parameters \tilde{c}_1 and \tilde{c}_2 in the $v_1 - v_2$ plane:

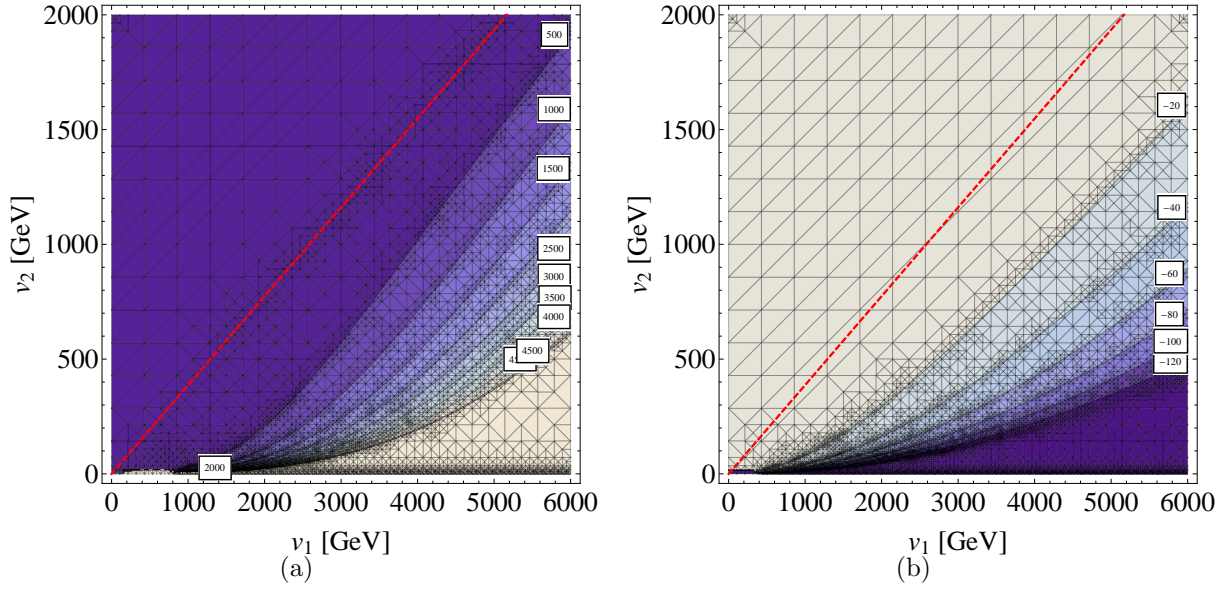


Figure B.3.: Expansion parameters \tilde{c}_1 and \tilde{c}_2 for the $\gamma^{(1)}$ Goldstone boson in the $v_1 - v_2$ plane
a) \tilde{c}_1 : is an order of magnitude larger than \tilde{c}_2 b) \tilde{c}_2 is v_0/v_2 hierarchy suppressed.

Approximation to the $\phi_{4/5}$ Eigenvectors

Contrary to the eigenvectors of $GB_{Z^{(1)}}$ and $GB_{\gamma^{(1)}}$ the eigenvectors for the physical fields $\phi_{4/5}$ not only depend on the VEVs v_1 and v_2 but also on the parameters M_0 and M' from the scalar potential. This fact renders the approximation an intricate business. Depending on the relative magnitude of M_0 and M' the size of the coefficients will change.

$$\begin{aligned} \phi_{4/5}[x] &\propto \left(\frac{\sqrt{2}v_2}{v_1} h_{B^5}^{(2)}[x] + \frac{2\sqrt{2}v_2}{v_0} \chi_1^{(3)}[x] + \tilde{c}_{4/5} \chi_{W^{5,e}}^{(3)}[x] + \chi_{W^{5,o}}^{(3)}[x] \right) \\ \tilde{c}_{4/5} &= \frac{(-4M'v_1^2 + M_0^2(v_0^2 + 4v_1^2))v_2^2 \pm \sqrt{16M'^2v_1^4v_2^4 - 8M'M_0^2v_1^2(v_0^2 + 4v_1^2)v_2^4 + M_0^4(4v_1^2v_2^2 + v_0^2(v_1^2 + v_2^2))^2}}{M_0^2v_0^2v_1^2} \\ &= \frac{4v_2^2}{M_0^2v_0^2} (m_{\phi_{5/4}}^2 - 2M') - 1 \end{aligned} \quad (\text{B.44})$$

For a parameter region around our reference point 4.5.4 we find that $\phi_{4/5}[x]$ can be approximated by a mixture between $\chi_1^{(3)}[x]$ and $\chi_{W^{5,e}}^{(3)}[x]$. For the reference point 4.5.4

itself we find the coefficients:

$$\phi_4[x] : \begin{pmatrix} 0.39 \\ 12.65 \\ 3.90 \\ 1. \end{pmatrix} \quad \phi_5[x] : \begin{pmatrix} 0.39 \\ 12.65 \\ -41.27 \\ 1. \end{pmatrix}$$

As a first approximation we neglect all terms suppressed by either the gauge boson mass hierarchy or the hierarchy between the compactification scale (represented by the Higgs VEVs v_1 and v_2) and the electroweak scale (v_0) and therefore effectively block-diagonalize the transformation between gauge- and mass-eigenstates. If we were not to neglect v_0 we always end up with a mixing between the Goldstone sector and the sector of $\phi_{4/5}$ which complicates the basis transformation considerably. In the preferred region of parameter space this approximation produces an error of $\mathcal{O}(10\%)$ in the mixing of states.

For now we will use⁶:

$$\begin{pmatrix} GB_{\gamma^{(1)}} \\ GB_{Z^{(1)}} \\ \phi_4 \\ \phi_5 \end{pmatrix} = \begin{pmatrix} 1 & 0 & 0 & 0 \\ 0 & 1 & 0 & 0 \\ 0 & 0 & \alpha_1 & \beta_1 \\ 0 & 0 & \alpha_2 & \beta_2 \end{pmatrix} \begin{pmatrix} h_{B^5}^{(2)} \\ \chi_{W^5,o}^{(3)} \\ \chi_1^{(3)} \\ \chi_{W^5,e}^{(3)} \end{pmatrix} \quad (\text{B.45})$$

and do not express the transformation for the Higgs degrees of freedom $\phi_{4/5}$ explicitly, since they are neglectable for the Sommerfeld effect due to their large mass which disqualifies them as long range force carriers. They are not mass degenerate with the dark matter candidate in the relevant region of parameter space either, hence their contribution to Sommerfeld relevant diagrams is not required as a first approximation (see discussion in Sec. 3.2.1).

B.2. Faddeev-Popov-Ghosts

Having constructed the gauge fixing functions to cancel the mixing terms between vector bosons and scalar fields in section B.0.2 we are able to derive the Lagrangian for the anti-commuting scalar Faddeev-Popov ghosts [99] by applying infinitesimal gauge transformations to the gauge fixing functions. The gauge transformations for the H_{W^5} and H_{B^5} have to be taken into account carefully and special attention should be attributed to the subtle difference between the fundamental and anti-fundamental transformation properties of the aforementioned fields under $SU(2)_I / SU(2)_{II}$ and $U(1)_I / U(1)_{II}$ respectively.

⁶Note that the Goldstone-bosons for the $Z^{(1)}$ and $\gamma^{(1)}$ are formed by pseudo-scalar modes from the bifundamental $SU(2)$ and $U(1)$ doublets respectively in this approximation.

Following the calculations in Appendix B of Cheng/Li [58] for the Standard Model closely we finally obtain the ghost Lagrangian:

$$\mathcal{L}_{Ghost} = \int d^4x \begin{pmatrix} w_I^i(x) \\ w_{II}^k(x) \\ \chi_I(x) \\ \chi_{II}(x) \end{pmatrix}^\dagger \begin{pmatrix} M_{11}^{ij} & M_{12}^{il} & M_{13}^i & M_{14}^i \\ M_{21}^{kj} & M_{22}^{kl} & M_{23}^k & M_{24}^k \\ M_{31}^j & M_{32}^l & M_{33} & M_{34} \\ M_{41}^j & M_{42}^l & M_{43} & M_{44} \end{pmatrix} \begin{pmatrix} w_I^j(x) \\ w_{II}^l(x) \\ \chi_I(x) \\ \chi_{II}(x) \end{pmatrix} \quad (\text{B.46})$$

with matrix elements:

$$\begin{aligned} M_{11}^{ij} &= \left(-\partial_\mu \left(\partial^\mu \delta^{ij} - g\epsilon^{ijk} W_I^{\mu,k} \right) - g^2 \xi \left\{ \text{tr} \left(\langle H_W^\dagger \rangle_0 \frac{\mathbb{1}}{2} \langle H_W \rangle_0 \delta^{ij} + \langle H_W^\dagger \rangle_0 \frac{\tau^i}{2} \phi_W \frac{\tau^j}{2} + \frac{\tau^j}{2} \phi_W^\dagger \frac{\tau^i}{2} \langle H_W \rangle_0 \right) \right. \\ &\quad \left. + \langle H_I^\dagger \rangle_0 \frac{\mathbb{1}}{2} \langle H_I \rangle_0 \delta^{ij} + \langle H_I^\dagger \rangle_0 \frac{\tau^i \tau^j}{4} \phi_I + \phi_I^\dagger \frac{\tau^j \tau^i}{4} \langle H_I \rangle_0 \right\} \Big) \\ M_{12}^{il} &= g^2 \xi \text{tr} \left(\langle H_W^\dagger \rangle_0 \frac{\mathbb{1}}{2} \langle H_W \rangle_0 \delta^{il} + \langle H_W^\dagger \rangle_0 \frac{\tau^i \tau^l}{4} \phi_W + \phi_W^\dagger \frac{\tau^l \tau^i}{4} \langle H_W \rangle_0 \right) \\ M_{13}^i &= -\frac{Y g g' \xi}{2} \left(2 \langle H_I^\dagger \rangle_0 \tau^i \langle H_I \rangle_0 + \phi_I^\dagger \tau^i \langle H_I \rangle_0 + \langle H_I^\dagger \rangle_0 \tau^i \phi_I \right) \\ M_{14}^i &= 0 \\ M_{21}^{kj} &= g^2 \xi \text{tr} \left(\langle H_W^\dagger \rangle_0 \frac{\mathbb{1}}{2} \langle H_W \rangle_0 \delta^{kj} + \langle H_W^\dagger \rangle_0 \frac{\tau^k}{2} \phi_W \frac{\tau^j}{2} + \frac{\tau^j}{2} \phi_W^\dagger \frac{\tau^k}{2} \langle H_W \rangle_0 \right) \\ M_{22}^{kl} &= \left(-\partial_\mu \left(\partial^\mu \delta^{kl} - g\epsilon^{klm} W_{II}^{\mu,m} \right) - g^2 \xi \left\{ \text{tr} \left(\langle H_W^\dagger \rangle_0 \frac{\mathbb{1}}{2} \langle H_W \rangle_0 \delta^{kl} + \langle H_W^\dagger \rangle_0 \frac{\tau^k \tau^l}{4} \phi_W + \phi_W^\dagger \frac{\tau^l \tau^k}{4} \langle H_W \rangle_0 \right) \right. \right. \\ &\quad \left. \left. + \langle H_{II}^\dagger \rangle_0 \frac{\mathbb{1}}{2} \langle H_{II} \rangle_0 \delta^{kl} + \langle H_{II}^\dagger \rangle_0 \frac{\tau^k \tau^l}{4} \phi_{II} + \phi_{II}^\dagger \frac{\tau^l \tau^k}{4} \langle H_{II} \rangle_0 \right\} \right) \\ M_{23}^k &= 0 \\ M_{24}^k &= -\frac{Y g g' \xi}{2} \left(2 \langle H_{II}^\dagger \rangle_0 \tau^k \langle H_{II} \rangle_0 + \langle H_{II}^\dagger \rangle_0 \tau^k \phi_{II} + \phi_{II}^\dagger \tau^k \langle H_{II} \rangle_0 \right) \\ M_{31}^j &= -\frac{Y g g' \xi}{2} \left(2 \langle H_I^\dagger \rangle_0 \tau^j \langle H_I \rangle_0 + \langle H_I^\dagger \rangle_0 \tau^j \phi_I + \phi_I^\dagger \tau^j \langle H_I \rangle_0 \right) \\ M_{32}^l &= 0 \\ M_{33} &= - \left(\partial_\mu \partial^\mu + g'^2 Y^2 \xi \left(2 |\langle H_B \rangle_0|^2 + \langle H_B^\dagger \rangle_0 \phi_B + \phi_B^\dagger \langle H_B \rangle_0 + 2 |\langle H_I \rangle_0|^2 + \langle H_I^\dagger \rangle_0 \phi_I + \phi_I^\dagger \langle H_I \rangle_0 \right) \right) \\ M_{34} &= g'^2 Y^2 \xi \left(2 |\langle H_B \rangle_0|^2 + \langle H_B^\dagger \rangle_0 \phi_B + \phi_B^\dagger \langle H_B \rangle_0 \right) \\ M_{41}^j &= 0 \\ M_{42}^l &= -\frac{Y g g' \xi}{2} \left(2 \langle H_{II}^\dagger \rangle_0 \tau^l \langle H_{II} \rangle_0 + \langle H_{II}^\dagger \rangle_0 \tau^l \phi_{II} + \phi_{II}^\dagger \tau^l \langle H_{II} \rangle_0 \right) \\ M_{43} &= g'^2 Y^2 \xi \left(2 |\langle H_B \rangle_0|^2 + \langle H_B^\dagger \rangle_0 \phi_B + \phi_B^\dagger \langle H_B \rangle_0 \right) \\ M_{44} &= - \left(\partial_\mu \partial^\mu + g'^2 Y^2 \xi \left(2 |\langle H_B \rangle_0|^2 + \langle H_B^\dagger \rangle_0 \phi_B + \phi_B^\dagger \langle H_B \rangle_0 + 2 |\langle H_{II} \rangle_0|^2 + \langle H_{II}^\dagger \rangle_0 \phi_{II} + \phi_{II}^\dagger \langle H_{II} \rangle_0 \right) \right). \end{aligned} \quad (\text{B.47})$$

We immediately realize, that the ghost Lagrangian gives rise to gauge field - ghost as well as to scalar-ghost interaction vertices that have to be taken into account when working in a non-unitary gauge.

The appropriate bilinear terms in (B.46) yields the mass matrix for the Faddeev-Popov

ghosts. The resulting 8×8 matrix is identical to the gauge boson mass matrix up to an overall factor of ξ . Hence, the corresponding eigenspectrum coincides with the one already derived for the gauge bosons and the transformation between gauge- and mass eigenstates can readily be copied from 4.6. It is important to note that the ghost fields are not self-adjoint, hence no factor of $\frac{1}{2}$ is necessary in the definition of the neutral ghost masses. Similar to the linear combinations constituting the mass eigenstates of the gauge boson, we are able to define an intermediate ghost field basis:

$$w_{e/o}^i = \frac{1}{\sqrt{2}} (w_I^i \pm w_{II}^i), \quad i \in \{1, 2, 3\}$$

$$\chi_{e/o} = \frac{1}{\sqrt{2}} (\chi_I \pm \chi_{II})$$

and in a subsequent diagonalization step we obtain:

$$w_{(0)}^\pm = \frac{1}{\sqrt{2}} (w_e^1 \mp iw_e^2)$$

$$w_{(1)}^\pm = \frac{1}{\sqrt{2}} (w_o^1 \mp iw_o^2)$$

$$w_Z^{(0)} = w_e^3 \cos \theta_W^{(0)} - \chi_e \sin \theta_W^{(0)} \tag{B.48}$$

$$w_Z^{(1)} = w_o^3 \cos \theta_W^{(1)} - \chi_o \sin \theta_W^{(1)}$$

$$w_\gamma^{(0)} = -w_e^3 \sin \theta_W^{(0)} + \chi_e \cos \theta_W^{(0)}$$

$$w_\gamma^{(1)} = -w_o^3 \sin \theta_W^{(1)} + \chi_o \cos \theta_W^{(1)}$$

C. Feynman Rules for the $SU(2) \times SU(2) \times U(1) \times U(1)$ Gauge Theory

This chapter gives a comprehensive list of Feynman rules for our theory used in the calculations of the Sommerfeld effect for $Z^{(1)}$ vector dark matter. We have written the Lagrangian in section 4.1 in the gauge eigenbasis and successively calculated the transformation to the mass eigenstates. The mass eigenstates and their interactions reflect the conservation of a discrete \mathcal{Z}_2 symmetry of the Lagrangian, leading to the fact, that only vertices with an even number of non-Standard-Model fields show up. As mentioned in section B.1 we neglect subleading contributions to interaction vertices resulting from the field transformation in the scalar sector to the mass eigenbasis. Therefore, we expect our Feynman rules to differ from the ones given by Gustafsson [100] by terms of order $\frac{v_0}{v_2}$.

C.1. Field Content and Propagators

We want to emphasize, that we have derived the mass eigenstates in a covariant R_ξ gauge, so that Ghosts (denoted by ω or c) and pseudo-Goldstone bosons (denoted by GB) are present for finite values of the gauge parameter ξ . The notation used in the body of this thesis should clearly indicate the correspondence of the Ghosts and pseudo-Goldstone bosons to their associated gauge boson. For the sake of brevity, we only give the expressions of interactions either present in the Standard Model or relevant to our Sommerfeld calculation. We cross-check our Standard Model Feynman rules with Cheng/Li [58] and Böhm/Denner/Joos [40] whenever their vertex rules are applicable.

As mentioned in section 3.4, our theory can be thought of as a truncated version of a lattice-ized 5 dimensional theory [51], where we have cut the Kaluza-Klein tower after the first excitation. It should be stressed however, that we have constructed a completely renormalizable 4 dimensional gauge invariant theory so that the truncation does not affect gauge invariance and unitarity (for detailed discussion see Sec. 3.4 as well as e.g. [51, 22, 52]). After the spontaneous symmetry breaking $SU(2)_I \times SU(2)_{II} \times U(1)_I \times U(1)_{II} \rightarrow U(1)_{em}$ we employ the following gauge field notation:

- $A^{(0)}/\gamma^{(0)}$... Standard Model Photon
 $Z^{(0)}$... Standard Model Z-boson
 $W_{(0)}^\pm$... Standard Model W-bosons
 $A^{(1)}/\gamma^{(1)}$... heavy $U(1)$ -like gauge boson
 $Z^{(1)}$... heavy $SU(2)$ -like neutral gauge boson
 $W_{(1)}^\pm$... heavy charged $SU(2)$ - gauge bosons

We follow the conventions of Cheng/Li [58] for the propagators, the field definitions may however differ by a global phase:

$$\begin{array}{c} \mu \bullet \text{---} \overset{V}{\text{wavy}} \text{---} \bullet \nu \end{array} \quad \frac{-i}{k^2 - m_V^2 + i\epsilon} [g_{\mu\nu} - (1 - \xi) \frac{k_\mu k_\nu}{k^2 - \xi m_V^2}] \quad (\text{C.1})$$

$$\begin{array}{c} \bullet \text{---} \overset{\phi}{\text{dashed}} \text{---} \bullet \end{array} \quad \text{Scalars:} \quad \frac{i}{k^2 - m_\phi^2 + i\epsilon} \quad (\text{C.2})$$

$$\begin{array}{c} \bullet \text{---} \overset{GB}{\text{dashed}} \text{---} \bullet \end{array} \quad \text{Goldstone-Bosons:} \quad \frac{i}{k^2 - \xi m_V^2 + i\epsilon} \quad (\text{C.3})$$

$$\begin{array}{c} \bullet \cdots \blacktriangleright \cdots \bullet \end{array} \quad \text{Ghosts:} \quad \frac{-i}{k^2 - \xi m_V^2 + i\epsilon} \quad (\text{C.4})$$

where $\xi = 1$ is the Feynman gauge, $\xi = 0$ the Landau gauge and $\xi = \infty$ the unitary gauge. The standard Feynman $+i\epsilon$ pole-prescription is adopted throughout our work. The Goldstone boson masses (see section B.0.3) are equal to the gauge boson masses (m_V) up to a factor $\sqrt{\xi}$.

C.2. Vertex Rules

If possible we express the vertex rules in terms of the gauge couplings and masses of the gauge bosons. In our conventions we have the following relations amongst the parameters of our theory:

$$g_2 = \frac{g}{\sqrt{2}} \qquad g_1 = \frac{g'}{\sqrt{2}} \qquad (\text{C.5})$$

the gauge boson mass for the $W^{(0)}$ can be written as:

$$m_{W^{(0)}} = \frac{g v_0}{2\sqrt{2}} = \frac{g_2 v_0}{2} \qquad (\text{C.6})$$

We can further use the fact, that the Weinberg angle of the heavy modes $\theta_{W^{(1)}}$ tends to zero away from the level crossing (see fig. 4.3), which we use to set $\sin\theta_{W^{(1)}}^{(1)} = 0$ and $\cos\theta_{W^{(1)}}^{(1)} = 1$ as an approximation. When we diagonalized the mass matrices in order to derive approximated field transformations between the gauge- and the mass-eigenstates we used several features of the mass spectrum (see section B.1), which are reflected in the Feynman rules as well (e.g. the correct analysis of the particle mass spectrum yielded $m_{W^{(1)}}^2 = \frac{1}{8}g^2(v_0^2 + 8v_2^2)$ which reduces to $m_{W^{(1)}}^2 = g^2v_2^2$ in the $v_0^2 \ll v_2^2$ -limit).

To simplify the vertex rules further, we use the following relations¹:

$$\tan\theta_W^{(0)} = \frac{g'}{g} = \frac{g_1}{g_2} \qquad (\text{C.7})$$

$$m_Z = \frac{m_W}{\cos\theta_W^{(0)}} \qquad (\text{C.8})$$

$$g_1 = \frac{e}{\cos\theta_W^{(0)}} \qquad (\text{C.9})$$

$$g_2 = \frac{e}{\sin(\theta_W^{(0)})} \qquad (\text{C.10})$$

C.2.1. Notation

In this section, we are going to comment on our phase convention for the fields and make contact to the Standard Model literature [40, 58]. Whenever one picks up a different book, it is almost certain, that the conventions are going to vary in one way or another, therefore cross-referencing results becomes somewhat tedious. In order to simplify the reader's ability to check our results, we give a dictionary to translate our Standard Model vertex rules to the ones found in the textbooks [40, 58] used by us as a reference. Our Feynman rules differ by global phases for some fields, which are physically irrelevant (if used consistently).

¹we choose to work in conventions of $e = +|e|$ so that $e = g_2 \cdot \sin\theta_W^{(0)} = g_1 \cdot \sin\theta_W^{(0)}$ is positive

Connection to Böhm/Denner/Joos

Most checks were performed along [40], we therefore give a short list of rules how to convert our vertex results² into the ones obtained by Böhm/Denner/Joos.

- multiply our vertex-factor with (+i) for each $GB_{(0)}^{(+)}$
- multiply our vertex-factor with (-i) for each $GB_{(0)}^{(-)}$
- multiply our vertex-factor with (-1) for each $GB_Z^{(0)}$
- multiply our vertex-factor with (+1) for each $GB_A^{(0)}$
- multiply our vertex-factor with (-1) for each $\bar{c}_Z^{(0)}$ or $c_Z^{(0)}$
- multiply our vertex-factor with (-1) for each $Z^{(0)}$

Connection to Cheng/Li

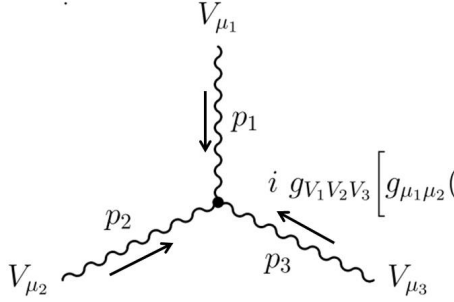
For completeness, we also make contact to [58], since we used this book as reference for several discussions on the spontaneous symmetry breaking, e.g. in Appendix B.0.4.

- multiply our vertex-factor with (-i) for each $GB_{(0)}^{(+)}$
- multiply our vertex-factor with (+i) for each $GB_{(0)}^{(-)}$
- multiply our vertex-factor with (-1) for each $GB_Z^{(0)}$
- multiply our vertex-factor with (+1) for each $GB_A^{(0)}$

²We found these rules by comparing different vertices one by one and match the results consistently.

C.2.2. Triple Vector Boson Vertices

The interaction terms between three gauge fields originate from the kinetic part of the gauge Lagrangian (4.2) and is a direct result of the non-abelian structure of our theory. We give an exhaustive list of Feynman rules for our model in terms of mass eigenstates, momentum flow is indicated by arrows if relevant:



$$i g_{V_1 V_2 V_3} \left[g_{\mu_1 \mu_2} (p_2 - p_1)_{\mu_3} + g_{\mu_1 \mu_3} (p_1 - p_3)_{\mu_2} + g_{\mu_2 \mu_3} (p_3 - p_2)_{\mu_1} \right]$$

with the couplings:

$$g_{A^{(0)} W_{(1,0)}^+ W_{(1,0)}^-} = g_2 \sin \theta_W^{(0)} = e \quad (\text{C.11})$$

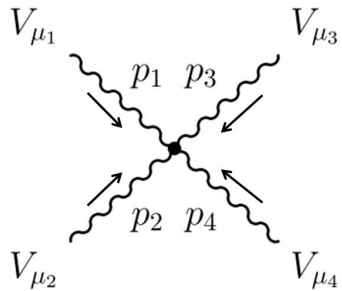
$$g_{Z^{(1)} W_{(0,1)}^+ W_{(1,0)}^-} = g_2 \cos \theta_W^{(1)} \stackrel{\theta_W^{(1)} \approx 0}{\approx} g_2 \quad (\text{C.12})$$

$$g_{Z^{(0)} W_{(0,1)}^+ W_{(0,1)}^-} = g_2 \cos \theta_W^{(0)} \quad (\text{C.13})$$

$$g_{A^{(1)} W_{(0,1)}^+ W_{(1,0)}^-} = g_2 \sin \theta_W^{(1)} \stackrel{\theta_W^{(1)} \approx 0}{\approx} 0 \quad (\text{C.14})$$

C.2.3. Quartic Vector Boson Vertices

As the vector-vector-vector vertices, the interaction terms between four gauge fields also arise from the field strength tensors in the Lagrangian. We find the following Feynman rules: with the couplings:



$$i g_{V_1 V_2 V_3 V_4} \left[2g_{\mu_1 \mu_2} g_{\mu_3 \mu_4} - g_{\mu_1 \mu_3} g_{\mu_2 \mu_4} - g_{\mu_1 \mu_4} g_{\mu_2 \mu_3} \right]$$

$$g_{A^{(0)}A^{(0)}W_{(1,0)}^+W_{(1,0)}^-} = -g_2^2 \sin^2 \theta_W^{(0)} = -e^2 \quad (\text{C.15})$$

$$g_{Z^{(0)}A^{(0)}W_{(1,0)}^+W_{(1,0)}^-} = -g_2^2 \sin \theta_W^{(0)} \cos \theta_W^{(0)} = -e g_2 \cos \theta_W^{(0)} \quad (\text{C.16})$$

$$g_{W_{(0,1)}^+W_{(0,1)}^+W_{(0,1)}^-W_{(0,1)}^-} = g_2^2 \quad (\text{C.17})$$

Note, other authors [100] find a geometrical factor of $\frac{3}{2}$ for the vertex factors with four KK-1-modes as a result of an integration over the extra dimension, which is not the case in the 4D-theory.

$$g_{W_{(1,0)}^+W_{(1,0)}^+W_{(0,1)}^-W_{(0,1)}^-} = g_2^2 \quad (\text{C.18})$$

$$g_{W_{(1,0)}^+W_{(0,1)}^+W_{(1,0)}^-W_{(0,1)}^-} = g_2^2 \quad (\text{C.19})$$

$$g_{Z^{(0)}Z^{(0)}W_{(1,0)}^+W_{(1,0)}^-} = -g_2^2 \cos \theta_W^{(0)} \quad (\text{C.20})$$

$$g_{Z^{(1)}Z^{(1)}W_{(1,0)}^+W_{(1,0)}^-} = -g_2^2 \cos \theta_W^{(1)} \approx -g_2^2 \quad (\text{C.21})$$

$$g_{Z^{(1)}Z^{(0)}W_{(1,0)}^+W_{(0,1)}^-} = -g_2^2 \cos \theta_W^{(0)} \cos \theta_W^{(1)} \approx -g_2^2 \cos \theta_W^{(0)} \quad (\text{C.22})$$

$$g_{A^{(0)}Z^{(1)}W_{(1,0)}^+W_{(0,1)}^-} = -g_2^2 \cos \theta_W^{(1)} \sin \theta_W^{(0)} \quad (\text{C.23})$$

Besides the vertices shown above, we get additional interactions proportional to $\sin \theta_W^{(1)}$, which tend to zero in the limit $\theta_W^{(1)} \rightarrow 0$

$$g_{A^{(0)}A^{(1)}W_{(1,0)}^+W_{(0,1)}^-} = -g_2^2 \sin \theta_W^{(0)} \sin \theta_W^{(1)} \approx 0 \quad (\text{C.24})$$

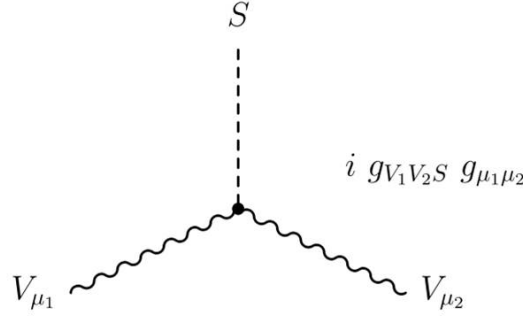
$$g_{A^{(1)}A^{(1)}W_{(1,0)}^+W_{(1,0)}^-} = -g_2^2 \sin^2 \theta_W^{(1)} \approx 0 \quad (\text{C.25})$$

$$g_{A^{(1)}Z^{(0)}W_{(1,0)}^+W_{(0,1)}^-} = -g_2^2 \cos \theta_W^{(0)} \sin \theta_W^{(1)} \approx 0 \quad (\text{C.26})$$

$$g_{A^{(1)}Z^{(1)}W_{(1,0)}^+W_{(1,0)}^-} = -g_2^2 \cos \theta_W^{(1)} \sin \theta_W^{(1)} \approx 0 \quad (\text{C.27})$$

C.2.4. Vector-Vector-Scalar-Vertices

The Vector-Vector-Scalar vertices arise from the Higgs-kinetic terms in (4.2), the gauge fixing functions in (B.1) only contribute to the mass of the unphysical scalar pseudo-Goldstone bosons and cancel scalar-gauge-mixing terms. In order to derive the Feynman rules, we used the approximate basis transformations in the scalar sector (see Sec. B.1). As consistency check, we compared our results to the Feynman rules given in the PhD-thesis of Gustafsson [100] and for the Standard Model interactions we cross checked our Feynman rules with the ones in [58] and [40]. Note: to arrive at the vertex-factor one has to multiply the appropriate coefficient in the interaction Lagrangian by $ig_{\mu\nu}$ and possible symmetry factors.



The Vertices for the Standard Model (derived from our interaction Lagrangian):

$$g_{Z^{(0)}Z^{(0)}h^{(0)}} = \frac{g_2 m_Z^{(0)}}{\cos \theta_W^{(0)}} \quad (\text{C.28})$$

$$g_{W_{(0)}^+ W_{(0)}^- h^{(0)}} = g_2 m_W^{(0)} \quad (\text{C.29})$$

$$g_{W_{(0)}^\mp A^{(0)} GB_{(0)}^\pm} = \pm i e m_W^{(0)} \quad (\text{C.30})$$

$$g_{W_{(0)}^\mp Z^{(0)} GB_{(0)}^\pm} = \mp i e m_W^{(0)} \frac{\sin \theta_W^{(0)}}{\cos \theta_W^{(0)}} \quad (\text{C.31})$$

Interactions involving non-Standard-Model states:

$$g_{A^{(0)}W_{(1)}^\mp GB_{(1)}^\pm} = \mp i e m_W^{(1)} \quad (\text{C.32})$$

$$g_{Z^{(0)}W_{(1)}^\mp GB_{(1)}^\pm} = \mp \frac{ig_2^2 \left(-v_0^2 \sec \theta_W^{(0)} + \cos \theta_W^{(0)} (v_0^2 + 8v_2^2) \right)}{2\sqrt{v_0^2 + 8v_2^2}} \approx \mp i g_2 \cos \theta_W^{(0)} m_W^{(1)} \quad (\text{C.33})$$

$$g_{Z^{(1)}W_{(0)}^\mp GB_{(1)}^\pm} = \pm \frac{ig_2^2 \left(8v_2^2 \cos \theta_W^{(1)} + v_0^2 \sin \theta_W^{(1)} \tan \theta_W^{(0)} \right)}{2\sqrt{v_0^2 + 8v_2^2}} \approx \pm i g_2 \cos \theta_W^{(1)} m_W^{(1)} \quad (\text{C.34})$$

$$g_{Z^{(1)}W_{(1)}^\mp GB_{(0)}^\pm} = \mp i e m_W^{(0)} \frac{\sin \theta_W^{(1)}}{\cos \theta_W^{(0)}} \approx 0 \quad (\text{C.35})$$

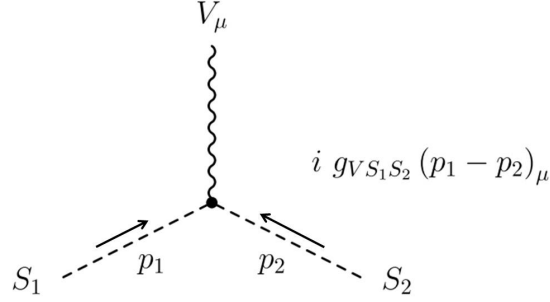
$$g_{W_{(1)}^\mp W_{(0)}^\pm GB_Z^{(1)}} = \mp i g_2 m_W^{(1)} \quad (\text{C.36})$$

$$g_{Z^{(1)}Z^{(1)}h^{(0)}} = \frac{1}{2} g_2^2 v_0 \cos^2 \theta_W^{(1)} + g_1 g_2 v_0 \sin \theta_W^{(1)} \cos \theta_W^{(1)} + \frac{1}{2} g_1^2 v_0 \sin^2 \theta_W^{(1)} \approx g_2 m_W^{(0)} \quad (\text{C.37})$$

$$g_{W_{(1)}^- W_{(1)}^+ h^{(0)}} = g_2 m_W^{(0)} \quad (\text{C.38})$$

C.2.5. Scalar-Scalar-Gauge-Vertices

These interactions arise from the Higgs kinetic terms in (4.2), which lead to derivative couplings and one has to be careful how to treat the momentum-flow of the particles. We work in conventions, where all momenta are ingoing. Following [40], for a Lagrangian of the form $\mathcal{L}_I = g\phi_1 V^\mu (\partial_\mu \phi_2)$ the vertex rule is: $g (p_2)_\mu$



For the Standard Model we find:

$$g_{A^{(0)}GB_{(0)}^-GB_{(0)}^+} = -e \quad (\text{C.39})$$

$$g_{Z^{(0)}GB_{(0)}^-GB_{(0)}^+} = -g_2 \left(\frac{\cos^2 \theta_W^{(0)} - \sin^2 \theta_W^{(0)}}{2 \cos \theta_W^{(0)}} \right) \quad (\text{C.40})$$

$$g_{Z^{(0)}h^{(0)}GB_Z^{(0)}} = -i \frac{g_2}{2 \cos \theta_W^{(0)}} \quad (\text{C.41})$$

$$g_{W_{(0)}^\mp h^{(0)}GB_{(0)}^\pm} = -i \frac{g_2}{2} \quad (\text{C.42})$$

$$g_{W_{(0)}^\mp GB_Z^{(0)}GB_{(0)}^\pm} = \pm \frac{g_2}{2} \quad (\text{C.43})$$

and for interaction vertices involving non-Standard-Model fields³:

$$g_{A^{(0)}GB_{(1)}^-GB_{(1)}^+} = -e \quad (\text{C.44})$$

$$g_{W_{(0)}^\mp GB_Z^{(1)}GB_{(1)}^\pm} = \mp g_2 \quad (\text{C.45})$$

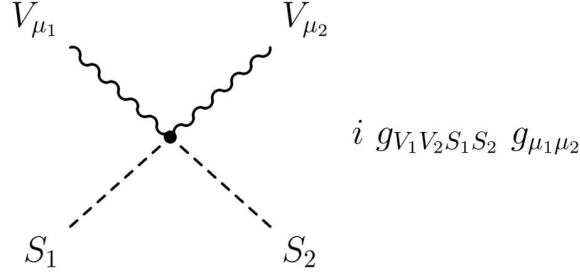
$$g_{Z^{(0)}GB_{(1)}^-GB_{(1)}^+} = -\frac{1}{2}g_2 \left(2 \cos \theta_W^{(0)} - \frac{v_0^2}{v_0^2 + 8v_2^2} \sec \theta_W^{(0)} \right) \approx -g_2 \cos \theta_W^{(0)} \quad (\text{C.46})$$

$$g_{W_{(1)}^\mp GB_{(1)}^\pm h^{(0)}} = -i \frac{g_2}{2} \frac{m_W^{(0)}}{m_W^{(1)}} = \mathcal{O}\left(\frac{v_0}{v_2}\right) \approx 0 \quad (\text{C.47})$$

³A vertex we have neglected due to the approximations in the field rotation, but present in Gustafsson's thesis: $g_{Z^{(1)}GB_Z^{(1)}h^{(0)}} = i \frac{g_2}{2} \frac{m_Z^{(0)}}{m_Z^{(1)}} = \mathcal{O}\left(\frac{v_0}{v_2}\right)$

C.2.6. Scalar-Scalar-Gauge-Gauge-Vertices

This class of vertices stems from the kinetic terms of the scalar fields (4.2). In order to arrive at the vertex rules, it is sufficient to multiply the appropriate coefficient of the interaction Lagrangian with $i g_{\mu\nu}$ and symmetry factors if necessary.



We begin with the Standard Model vertices to compare our notation to Refs. [40, 58]:

$$g_{A^{(0)}A^{(0)}GB_{(0)}^+GB_{(0)}^-} = 2 e^2 \quad (\text{C.48})$$

$$g_{Z^{(0)}Z^{(0)}GB_{(0)}^+GB_{(0)}^-} = g_2^2 \frac{(\cos^2 \theta_W^{(0)} - \sin^2 \theta_W^{(0)})^2}{2 \cos \theta_W^{(0)}} \quad (\text{C.49})$$

$$g_{Z^{(0)}Z^{(0)}h^{(0)}h^{(0)}} = g_2^2 \frac{(\cos^2 \theta_W^{(0)} + \sin^2 \theta_W^{(0)})^2}{2 \cos \theta_W^{(0)}} = \frac{g_2^2}{2 \cos \theta_W^{(0)}} \quad (\text{C.50})$$

$$g_{Z^{(0)}Z^{(0)}GB_Z^{(0)+}GB_Z^{(0)-}} = g_2^2 \frac{(\cos^2 \theta_W^{(0)} + \sin^2 \theta_W^{(0)})^2}{2 \cos \theta_W^{(0)}} = \frac{g_2^2}{2 \cos \theta_W^{(0)}} \quad (\text{C.51})$$

$$g_{A^{(0)}W_{(0)}^\mp GB_{(0)}^\pm h^{(0)}} = \pm i \frac{g_2 e}{2} \quad (\text{C.52})$$

$$g_{A^{(0)}W_{(0)}^\mp GB_{(0)}^\pm GB_Z^{(0)}} = - \frac{g_2 e}{2} \quad (\text{C.53})$$

$$g_{Z^{(0)}W_{(0)}^\mp GB_{(0)}^\pm h^{(0)}} = \mp i \frac{g_2 e}{2} \tan \theta_W^{(0)} \quad (\text{C.54})$$

$$g_{Z^{(0)}W_{(0)}^\mp GB_{(0)}^\pm GB_Z^{(0)}} = + i \frac{g_2 e}{2} \tan \theta_W^{(0)} \quad (\text{C.55})$$

$$g_{W_{(0)}^+W_{(0)}^-GB_{(0)}^+GB_{(0)}^-} = \frac{g_2^2}{2} \quad (\text{C.56})$$

$$g_{W_{(0)}^+W_{(0)}^-h^{(0)}h^{(0)}} = \frac{g_2^2}{2} \quad (\text{C.57})$$

$$g_{W_{(0)}^+W_{(0)}^-GB_Z^{(0)+}GB_Z^{(0)-}} = \frac{g_2^2}{2} \quad (\text{C.58})$$

Vertices containing non-Standard-Model fields:

$$g_{A^{(0)}A^{(0)}GB_{(1)}^+GB_{(1)}^-} = 2 e^2 \quad (\text{C.59})$$

$$g_{A^{(0)}W_{(0)}^\mp GB_{(1)}^\pm GB_Z^{(1)}} = \frac{2\sqrt{2}g_2^2 v_2 \sin \theta_W^{(0)}}{\sqrt{v_0^2 + 8v_2^2}} \approx g_2 e \quad (\text{C.60})$$

$$g_{W_{(0)}^{(\mp)}W_{(0)}^{(\mp)}GB_{(1)}^{(\pm)}GB_{(1)}^{(\pm)}} = -\frac{4g_2^2 v_2^2}{v_0^2 + 8v_2^2} \approx -2g_2^2 \quad (\text{C.61})$$

$$g_{W_{(0)}^{(+)}W_{(0)}^{(-)}GB_{(1)}^{(+)}GB_{(1)}^{(-)}} = \frac{1}{2}g_2^2 \left(2 - \frac{v_0^2}{v_0^2 + 8v_2^2} \right) \approx g_2^2 \quad (\text{C.62})$$

$$g_{W_{(0)}^{(+)}W_{(0)}^{(-)}GB_Z^{(1)}GB_Z^{(1)}} = 2 g_2^2 \quad (\text{C.63})$$

$$g_{W_{(1)}^{(+)}W_{(1)}^{(-)}GB_{(0)}^{(+)}GB_{(0)}^{(-)}} = \frac{g_2^2}{2} \quad (\text{C.64})$$

$$g_{W_{(1)}^{(+)}W_{(1)}^{(-)}GB_Z^{(0)}GB_Z^{(0)}} = \frac{g_2^2}{2} \quad (\text{C.65})$$

$$g_{W_{(1)}^{(+)}W_{(1)}^{(-)}h^{(0)}h^{(0)}} = \frac{g_2^2}{2} \quad (\text{C.66})$$

$$g_{A^{(0)}Z^{(0)}GB_{(1)}^{(+)}GB_{(1)}^{(-)}} = g_2^2 \left(\sin 2\theta_W^{(0)} - \frac{v_0^2 \tan \theta_W^{(0)}}{v_0^2 + 8v_2^2} \right) \approx g_2^2 \sin 2\theta_W^{(0)} \quad (\text{C.67})$$

$$g_{W_{(0)}^{(\mp)}Z^{(0)}GB_{(1)}^{(\pm)}GB_Z^{(1)}} = \frac{2\sqrt{2} \cos \theta_W^{(0)} g_2^2 v_2}{\sqrt{v_0^2 + 8v_2^2}} \approx g_2^2 \cos \theta_W^{(0)} \quad (\text{C.68})$$

$$g_{Z^{(0)}Z^{(0)}GB_{(1)}^{(+)}GB_{(1)}^{(-)}} = \frac{g_2^2 \left(v_0^2 \cos^2 2\theta_W^{(0)} \sec^2 \theta_W^{(0)} + 32v_2^2 \cos^2 \theta_W^{(0)} \right)}{2(v_0^2 + 8v_2^2)} \approx 2g_2^2 \cos^2 \theta_W^{(0)} \quad (\text{C.69})$$

$$g_{W_{(1)}^{(\mp)}Z^{(1)}GB_{(0)}^{(\pm)}GB_Z^{(0)}} = g_2 e \frac{\sin \theta_W^{(1)}}{2 \cos \theta_W^{(0)}} \approx 0 \quad (\text{C.70})$$

$$g_{W_{(1)}^{(\mp)}Z^{(1)}GB_{(0)}^{(\pm)}h^{(0)}} = \mp i g_2 e \frac{\sin \theta_W^{(1)}}{2 \cos \theta_W^{(0)}} \approx 0 \quad (\text{C.71})$$

$$g_{Z^{(1)}Z^{(1)}GB_{(0)}^{(+)}GB_{(0)}^{(-)}} = \frac{1}{2}g_2^2 \cos^2 \theta_W^{(1)} - g_1 g_2 \sin \theta_W^{(1)} \cos \theta_W^{(1)} + \frac{1}{2}g_1^2 \sin^2 \theta_W^{(1)} \approx \frac{g_2^2}{2} \quad (\text{C.72})$$

$$g_{Z^{(1)}Z^{(1)}GB_Z^{(0)}GB_Z^{(0)}} = \frac{1}{2}g_2^2 \cos^2 \theta_W^{(1)} + g_1 g_2 \sin \theta_W^{(1)} \cos \theta_W^{(1)} + \frac{1}{2}g_1^2 \sin^2 \theta_W^{(1)} \approx \frac{g_2^2}{2} \quad (\text{C.73})$$

$$g_{Z^{(1)}Z^{(1)}h^{(0)}h^{(0)}} = \frac{1}{2}g_2^2 \cos^2 \theta_W^{(1)} + g_1 g_2 \sin \theta_W^{(1)} \cos \theta_W^{(1)} + \frac{1}{2}g_1^2 \sin^2 \theta_W^{(1)} \approx \frac{g_2^2}{2} \quad (\text{C.74})$$

$$g_{W_{(1)}^{(\pm)}A^{(0)}GB_{(1)}^{(\mp)}h^{(0)}} = \pm i \frac{e g_2 m_W^{(0)}}{2 m_W^{(1)}} \approx 0 \quad (\text{C.75})$$

$$g_{Z^{(1)}Z^{(1)}GB_{(1)}^+GB_{(1)}^-} = \frac{g_2^2 v_0^2 \cos^2 [\theta_W^{(0)} + \theta_W^{(1)}] \sec^2 \theta_W^{(0)}}{2(v_0^2 + 8v_2^2)} \approx 0 \quad (\text{C.76})$$

$$g_{Z^{(1)}Z^{(1)}GB_Z^{(1)}GB_Z^{(1)}} = 2 \cos^2 \theta_W^{(1)} g_2^2 \approx 2g_2^2 \quad (\text{C.77})$$

$$g_{W_{(1)}^\mp W_{(1)}^\mp GB_{(1)}^\pm GB_{(1)}^\pm} = \frac{16g_2^2 v_2^2}{v_0^2 + 8v_2^2} \approx 2g_2^2 \quad (\text{C.78})$$

$$g_{W_{(1)}^+ W_{(1)}^- GB_{(1)}^+ GB_{(1)}^-} = \frac{g_2^2 (v_0^2 + 16v_2^2)}{2(v_0^2 + 8v_2^2)} \approx g_2^2 \quad (\text{C.79})$$

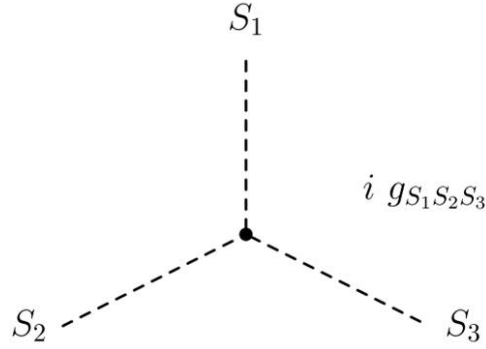
$$g_{W_{(1)}^+ W_{(1)}^- GB_Z^{(1)} GB_Z^{(1)}} \approx 0 \quad (\text{C.80})$$

$$g_{Z^{(1)}W_{(1)}^\pm GB_Z^{(1)} GB_{(1)}^\mp} = -\frac{2\sqrt{2}g_2^2 v_2 \cos \theta_W^{(1)}}{\sqrt{v_0^2 + 8v_2^2}} \approx -g_2^2 \quad (\text{C.81})$$

Note: We do not have a vertex for the $Z^{(0)}Z^{(0)}GB_Z^{(1)}GB_Z^{(1)}$ interaction, due to the approximated field rotation in the scalar sector.

C.2.7. Triple Scalar Vertices

For the charged Goldstone bosons we have used the exact transformation between gauge- and mass- eigenstates and only truncate terms of order $\frac{v_0}{v_2}$ according to our approximations described in section B.1. This enables us to compare some of the non-Standard Model results to Gustafsson [100]. The origin of these vertices is the scalar potential (4.19). We also compare our Standard Model results to [40]:



The Standard-Model interactions:

$$g_{h^{(0)}h^{(0)}h^{(0)}} = -\frac{3}{2}g_2 \frac{m_{h^{(0)}}^2}{m_W^{(0)}} \quad (\text{C.82})$$

$$g_{h^{(0)}GB_Z^{(0)}GB_Z^{(0)}} = -\frac{1}{2}g_2 \frac{m_{h^{(0)}}^2}{m_W^{(0)}} \quad (\text{C.83})$$

$$g_{h^{(0)}GB_{(0)}^+GB_{(0)}^-} = -\frac{1}{2}g_2 \frac{m_{h^{(0)}}^2}{m_W^{(0)}} \quad (\text{C.84})$$

$$g_{GB_Z^{(0)}GB_{(0)}^+GB_{(0)}^-} = 0 \quad (\text{C.85})$$

and a number of interactions involving non-Standard-Model fields⁴:

$$g_{h^{(0)}GB_{(1)}^+GB_{(1)}^-} = -\frac{g_2}{2}m_W^{(0)} \left(\frac{m_{h^{(0)}}}{m_W^{(1)}} \right)^2 = \mathcal{O}\left(\frac{v_0^2}{v_2^2}\right) \approx 0 \quad (\text{C.86})$$

$$g_{h^{(0)}GB_Z^{(1)}GB_Z^{(1)}} = -M_0^2 \frac{v_0}{2v_2^2} = \mathcal{O}(1)v_0 \quad (\text{C.87})$$

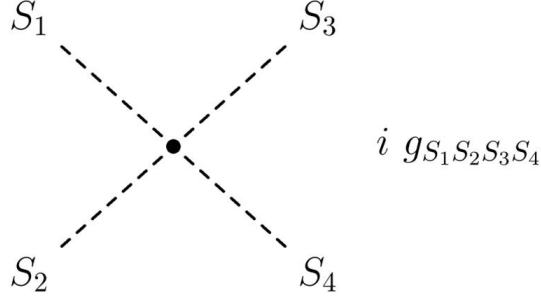
$$g_{GB_Z^{(1)}GB_{(1)}^\pm GB_{(0)}^\mp} = \frac{\pm i M_0^2 v_0}{\sqrt{2}v_2 \sqrt{v_0^2 + 8v_2^2}} = \mathcal{O}(1)v_0 \approx \pm i \frac{M_0^2}{v_2^2} \frac{v_0}{4} \quad (\text{C.88})$$

$$g_{GB_Z^{(0)}GB_{(1)}^+GB_{(1)}^-} = 0 \quad (\text{C.89})$$

⁴Note that the combination $\frac{M_0^2}{v_2^2}$ is the coupling constant of a ϕ^4 term in the scalar potential V_{WW} of section 4.5, to stay in the perturbative regime it is of $\mathcal{O}(1)$ at most.

C.2.8. Quartic Scalar Vertices

The origin of these vertices is also the Higgs potential (4.19). As consistency check, we compare our Standard Model results to [40]:



$$g_{h^{(0)}h^{(0)}h^{(0)}h^{(0)}} = -\frac{3}{4}g_2^2 \frac{m_{h^{(0)}}^2}{m_{W^{(0)}}^2} \quad (\text{C.90})$$

$$g_{GB_Z^{(0)}GB_Z^{(0)}GB_Z^{(0)}GB_Z^{(0)}} = -\frac{3}{4}g_2^2 \frac{m_{h^{(0)}}^2}{m_{W^{(0)}}^2} \quad (\text{C.91})$$

$$g_{h^{(0)}h^{(0)}GB_Z^{(0)}GB_Z^{(0)}} = -\frac{g_2^2}{4} \frac{m_{h^{(0)}}^2}{m_{W^{(0)}}^2} \quad (\text{C.92})$$

And the interactions involving non-Standard-Model fields:

$$g_{GB_{(1)}^+GB_{(1)}^-GB_{(0)}^+GB_{(0)}^-} = -\frac{2(2M_0^2 + \lambda v_0^2)}{v_0^2 + 8v_2^2} \approx -\frac{M_0^2}{2v_2^2} \quad (\text{C.93})$$

$$g_{GB_{(1)}^\pm GB_{(1)}^\pm GB_{(0)}^\mp GB_{(0)}^\mp} = -\frac{2\lambda v_0^2}{v_0^2 + 8v_2^2} \approx 0 \quad (\text{C.94})$$

$$g_{GB_{(1)}^+GB_{(1)}^-GB_Z^{(0)}GB_Z^{(0)}} = -\frac{4M_0^2 + \lambda v_0^2}{(v_0^2 + 8v_2^2)} \approx -\frac{M_0^2}{2v_2^2} \quad (\text{C.95})$$

$$g_{GB_{(0)}^+GB_{(0)}^-GB_Z^{(1)}GB_Z^{(1)}} = -\frac{M_0^2}{2v_2^2} \quad (\text{C.96})$$

$$g_{GB_Z^{(1)}GB_Z^{(1)}GB_Z^{(0)}GB_Z^{(0)}} = -\frac{M_0^2}{2v_2^2} \quad (\text{C.97})$$

$$g_{GB_{(1)}^+GB_{(1)}^-h^{(0)}h^{(0)}} = -\frac{4M_0^2 + \lambda v_0^2}{(v_0^2 + 8v_2^2)} \approx -\frac{M_0^2}{2v_2^2} \quad (\text{C.98})$$

$$g_{GB_Z^{(1)}GB_Z^{(1)}h^{(0)}h^{(0)}} = -\frac{M_0^2}{2v_2^2} \quad (\text{C.99})$$

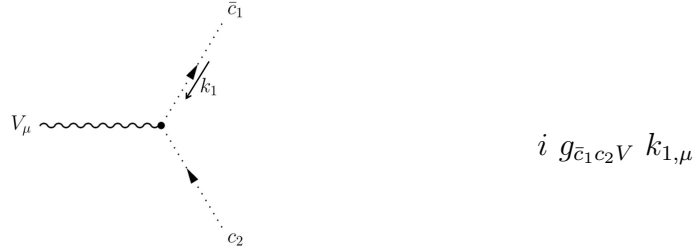
$$g_{GB_Z^{(1)}GB_Z^{(1)}GB_{(1)}^+GB_{(1)}^-} = \frac{-M_0^2 v_0^2 + 16(\lambda_1 + 2\lambda_2)v_2^4}{2v_2^2(v_0^2 + 8v_2^2)} \approx (\lambda_1 + 2\lambda_2) \quad (\text{C.100})$$

$$g_{GB_Z^{(1)}GB_Z^{(1)}GB_Z^{(1)}GB_Z^{(1)}} = 3(\lambda_1 + 2\lambda_2) \quad (\text{C.101})$$

$$g_{GB_{(1)}^+GB_{(1)}^+GB_{(1)}^-GB_{(1)}^-} = -\frac{2(8M_0^2 v_0^2 + \lambda v_0^4 - 64v_2^4(\lambda_1 + 2\lambda_2))}{(v_0^2 + 8v_2^2)^2} \approx 2(\lambda_1 + 2\lambda_2) \quad (\text{C.102})$$

C.2.9. Ghost - Anti-Ghost - Gauge Vertices

The ghost-gauge boson interactions arise from the ghost Lagrangian described in section B.2. One can choose a physical gauge, where no ghosts are present in the theory. Since we began to work in a generalized R_ξ gauge, we give the Feynman rules for their interactions.



$$g_{\bar{c}_{(0)}^\pm c_{(0)}^\pm A^{(0)}} = \pm e \quad (\text{C.103})$$

$$g_{\bar{c}_A^{(0)} c_{(0)}^\mp W_{(0)}^\pm} = \pm e \quad (\text{C.104})$$

$$g_{\bar{c}_{(0)}^\pm c_A^{(0)} W_{(0)}^\pm} = \mp e \quad (\text{C.105})$$

$$g_{\bar{c}_{(0)}^\pm c_{(0)}^\pm Z^{(0)}} = \pm g_2 \cos \theta_W^{(0)} \quad (\text{C.106})$$

$$g_{\bar{c}_Z^{(0)} c_{(0)}^\mp W_{(0)}^\pm} = \pm g_2 \cos \theta_W^{(0)} \quad (\text{C.107})$$

$$g_{\bar{c}_{(0)}^\pm c_Z^{(0)} W_{(0)}^\pm} = \mp g_2 \cos \theta_W^{(0)} \quad (\text{C.108})$$

$$g_{\bar{c}_{(0)}^\pm c_{(1)}^\pm Z_{(1)}} = \pm g_2 \cos \theta_W^{(1)} \quad (\text{C.109})$$

$$g_{\bar{c}_{(1)}^\pm c_{(0)}^\pm Z_{(1)}} = \pm g_2 \cos \theta_W^{(1)} \quad (\text{C.110})$$

$$g_{\bar{c}_{(1)}^\pm c_Z^{(0)} W_{(1)}^\pm} = \mp g_2 \cos \theta_W^{(0)} \quad (\text{C.111})$$

$$g_{\bar{c}_Z^{(0)} c_{(1)}^\mp W_{(1)}^\pm} = \pm g_2 \cos \theta_W^{(0)} \quad (\text{C.112})$$

$$g_{\bar{c}_{(0)}^\pm c_Z^{(1)} W_{(1)}^\pm} = \mp g_2 \cos \theta_W^{(1)} \quad (\text{C.113})$$

$$g_{\bar{c}_Z^{(1)} c_{(0)}^\mp W_{(1)}^\pm} = \pm g_2 \cos \theta_W^{(1)} \quad (\text{C.114})$$

$$g_{\bar{c}_{(1)}^\pm c_A^{(0)} W_{(1)}^\pm} = \mp e \quad (\text{C.115})$$

$$g_{\bar{c}_A^{(0)} c_{(1)}^\mp W_{(1)}^\pm} = \pm e \quad (\text{C.116})$$

$$g_{\bar{c}_Z^{(1)} c_{(1)}^\mp W_{(0)}^\pm} = \pm g_2 \cos \theta_W^{(1)} \quad (\text{C.117})$$

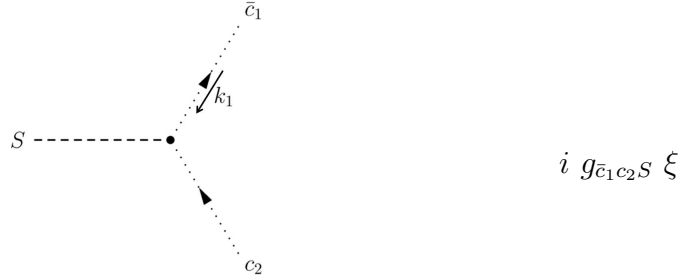
$$g_{\bar{c}_{(1)}^\pm c_Z^{(1)} W_{(0)}^\pm} = \mp g_2 \cos \theta_W^{(1)} \quad (\text{C.118})$$

$$g_{\bar{c}_{(1)}^\pm c_{(1)}^\pm A^{(0)}} = \pm e \quad (\text{C.119})$$

$$g_{\bar{c}_{(1)}^\pm c_{(1)}^\pm Z^{(0)}} = \pm g_2 \cos \theta_W^{(0)} \quad (\text{C.120})$$

C.2.10. Ghost - Anti-Ghost - Scalar Vertices

The special structure of our gauge fixing functions induce couplings between scalars and ghosts. Origin of those interactions is once more the Faddeev-Popov-Lagrangian (B.46).



$$g_{\bar{c}_A^{(0)} c_{(0)}^\mp GB_{(0)}^\pm} = 0 \quad (\text{C.121})$$

$$g_{\bar{c}_{(0)}^\pm c_A^{(0)} GB_{(0)}^\pm} = \mp i e m_W^{(0)} \quad (\text{C.122})$$

$$g_{\bar{c}_{(0)}^\pm c_{(0)}^\pm GB_Z^{(0)}} = \pm i \frac{g_2 m_Z^{(0)} \cos \theta_W^{(0)}}{2} \quad (\text{C.123})$$

$$g_{\bar{c}_Z^{(0)} c_{(0)}^\mp GB_{(0)}^\pm} = \pm i \frac{g_2 m_W^{(0)}}{2 \cos \theta_W^{(0)}} \quad (\text{C.124})$$

$$g_{\bar{c}_{(0)}^\pm c_Z^{(0)} GB_{(0)}^\pm} = \mp i \frac{g_2 m_W^{(0)}}{2 \cos \theta_W^{(0)}} \left(\cos^2 \theta_W^{(0)} - \sin^2 \theta_W^{(0)} \right) \quad (\text{C.125})$$

$$g_{\bar{c}_Z^{(0)} c_Z^{(0)} h^{(0)}} = - \frac{g_2 m_W^{(0)}}{2 \cos^2 \theta_W^{(0)}} \quad (\text{C.126})$$

$$g_{\bar{c}_{(0)}^\pm c_{(0)}^\pm h^{(0)}} = - \frac{g_2 m_W^{(0)}}{2} \quad (\text{C.127})$$

D. Gauge Transformations

In order to fix our sign convention for the gauge transformations, which also influences the notation in the covariant derivatives, we introduce two explicit examples relevant for this thesis.

SU(2) Gauge Transformations in the Fundamental Representation

Take a complex doublet $H(x) = (h_1[x] \ h_2[x])^T$; $h_{1,2}[x] \in \mathbb{C}$, which transforms under the fundamental representation of $SU(2)$ according to:

$$H(x) \rightarrow H'(x) = \exp\left[\frac{-i\tau^a \alpha^a(x)}{2}\right] H(x) \quad (\text{D.1})$$

τ^a ... Pauli matrices $a = 1, 2, 3$ $\alpha^a(x)$... $SU(2)$ transformation parameters
The Pauli spin matrices τ^i are taken as:

$$\tau^1 = \begin{pmatrix} 0 & 1 \\ 1 & 0 \end{pmatrix} \quad \tau^2 = \begin{pmatrix} 0 & -i \\ i & 0 \end{pmatrix} \quad \tau^3 = \begin{pmatrix} 1 & 0 \\ 0 & -1 \end{pmatrix} \quad (\text{D.2})$$

and the corresponding $SU(2)$ Lie algebra is given by:

$$\left[\frac{\tau^i}{2}, \frac{\tau^j}{2}\right] = i\epsilon^{ijk} \frac{\tau^k}{2}. \quad (\text{D.3})$$

Our convention for the gauge transformation of a $SU(2)$ doublet in the fundamental representation implies a covariant derivative of the form¹:

$$D_\mu = \partial_\mu - ig \frac{\tau^a}{2} W_\mu^a(x) \quad (\text{D.4})$$

where g is the $SU(2)$ gauge coupling and $\frac{\tau^a}{2}$ are the $SU(2)$ generators in the fundamental representation.

¹Note: other authors use the opposite sign in the exponential map to define their gauge transformation. We adopt the notation presented in the chapter on non-abelian gauge theories by Cheng/Li [58].

SU(2) Gauge Transformations in the Anti-Fundamental Representation

In the special case of $SU(2)$ the fundamental $\mathbf{2}$ and anti-fundamental $\bar{\mathbf{2}}$ representations are equivalent. Nonetheless, the gauge transformations and correspondingly the covariant derivatives have a change in sign. For completeness we state the transformation properties explicitly.

For a $SU(2)$ doublet $H(x) = (h_1[x] \ h_2[x])^T$ in the **anti**-fundamental representation, the gauge transformation is defined via:

$$H(x) \rightarrow H'(x) = H(x) \exp \left[\frac{+i\tau^a \alpha^a(x)}{2} \right] \quad (\text{D.5})$$

which implies a covariant derivative of the form:

$$D_\mu = \partial_\mu + igW_\mu^a(x) \frac{\tau^a}{2} \quad (\text{D.6})$$

E. Numerical Shooting Routine

For completeness, we document our *Mathematica*-code to solve the coupled system of Schrödinger equations of section 5.10. The boundary value problem is solved via a "shooting" process. All numerical recipes were adopted from Refs. [88, 89, 90].

```
(*****
***** potential definition *****
*****
p =  $\frac{1}{2}mz1 v$ 
Vzzww[x_]:= -  $\frac{2}{v} \frac{2g^2}{4\pi} \frac{\text{Exp}[-\frac{mw0x}{p}]}{x}$ ;
Vwwzz[x_]:= -  $\frac{2}{v} \frac{2g^2}{4\pi} \frac{\text{Exp}[-\frac{mw0x}{p}]}{x}$ ;
Vwww[x_]:= -  $\frac{2}{v} \left( \frac{g^2 c \theta^2}{4\pi} \frac{\text{Exp}[-\frac{mz0x}{p}]}{x} + \frac{g^2 s \theta^2}{4\pi} \frac{1}{x} \right)$ ;

(* definition of the ODE in  $\vec{f}$  *)
(*  $\frac{d}{dx} \begin{pmatrix} f[[1]] \\ f[[2]] \\ f[[3]] \\ f[[4]] \end{pmatrix} == \frac{d}{dx} \begin{pmatrix} \chi_{zz}(x) \\ \chi_{zz}'(x) \\ \chi_{ww}(x) \\ \chi_{ww}'(x) \end{pmatrix} = \begin{pmatrix} \chi_{zz}'(x) \\ \chi_{zz}''(x) \\ \chi_{ww}'(x) \\ \chi_{ww}''(x) \end{pmatrix}$  *)

(* use ODE to express  $\frac{d^2}{dx^2} \chi^{ij}(x)$  in terms of  $\chi^{ij}(x)$  and  $\frac{d}{dx} \chi^{ij}(x)$  *)

G[x_, f_]:=  $\begin{pmatrix} f[[2]] \\ -f[[1]] + V_{zzww}[x]f[[3]] \\ f[[4]] \\ -\left(\frac{mz1+\delta m}{mz1}\right) * \left(\left(1 - \frac{2\delta m}{\epsilon}\right) - V_{www}[x]\right) f[[3]] - V_{wwzz}[x]f[[1]] \end{pmatrix}$ 

*****
*** parameters for integration of ODE ***
*****
xmax = 25;      (*upper boundary -> numerically infinity *)
NIt = 50000;    (* number of RK4-steps *)
```

```
(*****
***** shooting variable *****)
***** initialization *****)
*****
```

```
(***** textbook asymptotic *****)
***  $\phi_{zz}[x \rightarrow \infty] \sim \sin[x + \delta \text{Streu}]$  ***
***  $\phi_{ww}[x \rightarrow \infty] \sim \text{Amp Exp}[-\sqrt{q_{ww}x}]$  ***
***  $q_{ww} = -\frac{mz1+\delta m}{mz1} \left(1 - \frac{2\delta m}{\epsilon}\right)$  ***
***  $k_{\text{prime}} = \sqrt{-\frac{mz1+\delta m}{mz1} \left(1 - \frac{2\delta m}{\epsilon}\right)}$  ***
```

```
(*****
**** execution of all routines, so that new parameters are correctly initialized ****)
*****
```

```
ODERK4Update[G-, fn-, xn-, dx-]:=Module[{k1, k2, k3, k4}, (*RK4 update – step*)
```

```
k1 = dxG[xn, fn];
```

```
(* G denotes a multi-component vector, depending on the order of the ODE and
the number of coupled equations. Consequently  $k_i$  is a vector too!!! *)
```

```
k2 = dxG[xn + (1/2)dx, fn + (1/2)k1];
```

```
k3 = dxG[xn + 1/2dx, fn + 1/2k2];
```

```
k4 = dxG[xn + dx, fn + k3];
```

```
Return[fn + 1/6k1 + 1/3k2 + 1/3k3 + 1/6k4];
```

```
ODE[G-, f0-, x0-, dx-, Ns-]:=Module[{fvals, index, xn},
```

```
(*initialize a table fvals with zeros, so that one can address the entries of fvals later on.*)
```

```
fvals = Table[{0, Table[0, {jj, 1, Length[f0]}]}, {ii, 1, Ns}];
```

```
(* treat initial values separately, all other entries of fvals are written via a For-loop. *)
```

```
fvals[[1, 1]] = x0; fvals[[1, 2]] = f0;
```

```
For[index = 2, index ≤ Ns, index = index + 1,
```

```
xn = x0 + (index - 1)dx;
```

```
fvals[[index, 1]] = xn; (* write the x-values in fvals-array *)
```

```
fvals[[index, 2]] = ODERK4Update[G, fvals[[index - 1, 2]], fvals[[index - 1, 1]], dx];
```

```
(* take  $x_{n-1}, \psi_{n-1}, \psi'_{n-1}$  and calculate  $x_n, \psi_n$  and  $\psi'_n$  *)
```

```
Return[fvals];
```

(* u returns the reduced wavefunction on the left boundary $x = 0$
for arbitrary input parameters Ampl and δ_{Streu} *)

```

u[Ampl,  $\delta_{scatter}$ ]:=Module [
{fval, retval,  $\phi_{zz}$ Asymp,  $\phi_{zzp}$ Asymp,  $\phi_{ww}$ Asymp,  $\phi_{wwp}$ Asymp, startx, kprime},
kprime =  $\sqrt{-\frac{mz1+\delta m}{mz1} \left(1 - \frac{2\delta m}{\epsilon}\right)}$ ;
 $\phi_{zz}$ Asymp = Sin[xmax +  $\delta_{scatter}$ ];
 $\phi_{zzp}$ Asymp = Cos[xmax +  $\delta_{scatter}$ ];
 $\phi_{ww}$ Asymp = AmplExp[-kprimemax];
 $\phi_{wwp}$ Asymp = -kprimeAmplExp[-kprimemax];
fval = ODE[G, { $\phi_{zz}$ Asymp,  $\phi_{zzp}$ Asymp,  $\phi_{ww}$ Asymp,  $\phi_{wwp}$ Asymp},
xmax,  $\frac{-1}{(NIt-0.999999)}xmax$ , NIt];
(*** As above, I do not go directly to zero to determine the wavefunction
and the derivative, but to the second last point of the RK-integration for stability ***)
(*****)

```

```

retval = { {
fval[[Length[fval], 2, 1]] (* returns  $\phi_{zz}[0]^*$ ),
{fval[[Length[fval], 2, 3]] (* returns  $\phi_{ww}[0]^*$ ),
{fval[[Length[fval] - 1, 2, 2]] (* returns  $\phi_{zz}' [\Delta x = \frac{xmax}{NIt}]^*$ ),
{fval[[Length[fval] - 1, 2, 4]] (* returns  $\phi_{ww}' [\Delta x = \frac{xmax}{NIt}]^*$ )};
Return[retval]; };

```

(*cur : current value for $u[rpsi0, ipsi0]^*$)

(*ngrad : numerical GRADIENT *)

```

Gradu[Ampl,  $\delta_{scatter}$ , dAmpl, dStreu]:=Module [ {ngrad, cur1, cur2, current},
current = u[Ampl,  $\delta_{scatter}$ ];
cur1 = current[[1, 1]];
cur2 = current[[2, 1]];
ngrad = {  $\frac{u[Ampl+dAmpl, \delta_{scatter}][[1, 1]] - cur1}{dAmpl}$ ,  $\frac{u[Ampl, \delta_{scatter}+dStreu][[1, 1]] - cur1}{dStreu}$ ,
 $\frac{u[Ampl+dAmpl, \delta_{scatter}][[2, 1]] - cur2}{dAmpl}$ ,  $\frac{u[Ampl, \delta_{scatter}+dStreu][[2, 1]] - cur2}{dStreu}$  };
Return[ngrad]; };

```

```

Shoot[initialAmp_, initialδStreu_, dAmpL_, dStreu_, epsi_] := Module [
{ir, ii, res1, res2, counter, gradient, residue, sol, delamp, delphase,
delampi, delphasi, restable, countermax, φzzpof0, φwwpof0},

delamp = dAmpL;
delphase = dStreu;
counter = 1;
countermax = 40;
(* quit routine, if more than "countermax" shooting trials are necessary. *)
ir = initialAmp;
ii = initialδStreu;
residue = u[ir, ii];
res1 = residue[[1, 1]];
(* returns φzz(0) for specified values of Amp and δStreu at infinity *)
res2 = residue[[2, 1]];
(* returns φww(0) for specified values of Amp and δStreu at infinity *)
restable = Table[{i, {0, 0}}, {i, 1, countermax}];
(* restable is going to contain the differences between φzz[0], φww[0] and zero. *)

While [(((Abs[res1] > epsi) || (Abs[res2] > epsi)) && (counter < countermax)),
(* vary the initial conditions at xmax until the BC at zero are satisfied with precision
eps or the number of shooting-iterations exceeds the maximum value countermax. *)
(*****
(***) Implementation of Newton – Raphsen method      (***)
(***) I used Numerical Recipes as reference           (***)
(***) p.380 and following                             (***)
(*****

gradient = Gradu[ir, ii, delamp, delphase];
(* solve linear system:  $\hat{J} * \delta \underline{\text{cond}} == -\phi(\underline{\text{cond}})$  *)
sol = Solve[{gradient[[1]] * delampi + gradient[[2]] * delphasei == -res1, gradient[[3]] *
delampi + gradient[[4]] * delphasei == -res2}, {delampi, delphasei}];
delamp = sol[[1, 1, 2]];
delphase = sol[[1, 2, 2]];
Clear[sol, residue, delampi, delphasi];

```

```
(* calculate new input values for Amp and  $\delta$ Streu *)
{ir, ii} = {ir, ii} + {delamp, delphase};
(* evaluate  $\phi_{zz}[0]$  und  $\phi_{ww}[0]$  with the new initial conditions
for new input values Amp and  $\delta$ Streu *)
residue = u[ir, ii];
res1 = residue[[1, 1]]; (* difference res1 =  $\phi_{zz}[0] - 0$  *)
res2 = residue[[2, 1]]; (* difference res2 =  $\phi_{ww}[0] - 0$  *)
restable[[counter, 2, 1]] = res1;
restable[[counter, 2, 2]] = res2;
counter = counter + 1;
 $\phi_{zzpof0}$  = residue[[3, 1]];
 $\phi_{wwpof0}$  = residue[[4, 1]];
If[(counter > (countermax - 1)),
Return[{Root-Finding failed to converge to desired precision, restable}],
Return[{ir, ii, res1, res2, counter, restable,  $\phi_{zzpof0}$ ,  $\phi_{wwpof0}$ }]];
(* If the shoot-routine converges, it returns the result in the following order: *)
(*
(1) best initial value for Amp at xmax;
(2) best initial value for  $\delta$ Streu at xmax;
(3)  $\phi_{zz}[0]$ ;
(4)  $\phi_{ww}[0]$ ;
(5) # of steps to achieve desired precision eps, so that
|  $\phi_{zz}[0]$  | < eps and |  $\phi_{ww}[0]$  | < eps;
(6) deviation of |  $\phi_{zz}[0]$  | and |  $\phi_{ww}[0]$  | from zero
*)];
```

Bibliography

In the pdf-version of this thesis, we have included links to all references that are available online. To access papers from the pre-arXiv era, the DOI-numbers link to the journal servers directly. All links as of June 22, 2012. We have also included back references for all citations within the pdf for ease of navigation.

- [1] Gianfranco Bertone, Dan Hooper, and Joseph Silk. “Particle dark matter: Evidence, candidates and constraints”. In: *Phys.Rept.* 405 (2005), pp. 279–390. DOI: [10.1016/j.physrep.2004.08.031](https://doi.org/10.1016/j.physrep.2004.08.031). arXiv:[hep-ph/0404175](https://arxiv.org/abs/hep-ph/0404175) [[hep-ph](#)] (cit. on pp. 1, 3, 5).
- [2] F. Zwicky. “On the Masses of Nebulae and of Clusters of Nebulae”. In: *Astrophys.J.* 86 (1937), pp. 217–246 (cit. on pp. 1, 3, 5).
- [3] John Ellis. “Searching for Particle Physics Beyond the Standard Model at the LHC and Elsewhere”. In: (2011). arXiv:[1102.5009](https://arxiv.org/abs/1102.5009) [[hep-ph](#)] (cit. on pp. 1, 3, 5, 39).
- [4] Gerard Jungman, Marc Kamionkowski, and Kim Griest. “Supersymmetric dark matter”. In: *Phys.Rept.* 267 (1996), pp. 195–373. DOI: [10.1016/0370-1573\(95\)00058-5](https://doi.org/10.1016/0370-1573(95)00058-5). arXiv:[hep-ph/9506380](https://arxiv.org/abs/hep-ph/9506380) [[hep-ph](#)] (cit. on pp. 1, 3, 5, 6).
- [5] Lars Bergstrom. “Dark Matter Evidence, Particle Physics Candidates and Detection Methods”. In: (2012). arXiv:[1205.4882](https://arxiv.org/abs/1205.4882) [[astro-ph.HE](#)] (cit. on pp. 1, 3, 5).
- [6] David Griffiths. *Introduction to elementary particles*. Wiley-VCH, 2008 (cit. on pp. 1, 3, 5).
- [7] Oscar Adriani et al. “An anomalous positron abundance in cosmic rays with energies 1.5-100 GeV”. In: *Nature* 458 (2009), pp. 607–609. DOI: [10.1038/nature07942](https://doi.org/10.1038/nature07942). arXiv:[0810.4995](https://arxiv.org/abs/0810.4995) [[astro-ph](#)] (cit. on pp. 1, 3, 7, 44).
- [8] J. Chang et al. “An excess of cosmic ray electrons at energies of 300-800 GeV”. In: *Nature* 456 (2008), pp. 362–365. DOI: [10.1038/nature07477](https://doi.org/10.1038/nature07477) (cit. on pp. 1, 3, 7, 44).
- [9] Aharonian, F. et al. “Spectrum and variability of the Galactic center VHE γ -ray source HESS J1745-290”. In: *A&A* 503.3 (2009), pp. 817–825. DOI: [10.1051/0004-6361/200811569](https://doi.org/10.1051/0004-6361/200811569) (cit. on pp. 1, 3, 7, 44).

- [10] A. A. Abdo et al. “Measurement of the Cosmic Ray $e^+ + e^-$ Spectrum from 20 GeV to 1 TeV with the Fermi Large Area Telescope”. In: *Phys. Rev. Lett.* 102 (18 May 2009), p. 181101. DOI: [10.1103/PhysRevLett.102.181101](https://doi.org/10.1103/PhysRevLett.102.181101) (cit. on pp. 1, 3, 7, 44).
- [11] Nima Arkani-Hamed et al. “A Theory of Dark Matter”. In: *Phys.Rev.* D79 (2009), p. 015014. DOI: [10.1103/PhysRevD.79.015014](https://doi.org/10.1103/PhysRevD.79.015014). arXiv:0810.0713 [hep-ph] (cit. on pp. 1, 3, 6–9, 44, 52, 60, 63, 67, 72, 100, 102, 109, 110, 112, 113, 127).
- [12] John David March-Russell and Stephen Mathew West. “WIMPonium and Boost Factors for Indirect Dark Matter Detection”. In: *Phys.Lett.* B676 (2009), pp. 133–139. DOI: [10.1016/j.physletb.2009.04.010](https://doi.org/10.1016/j.physletb.2009.04.010). arXiv:0812.0559 [astro-ph] (cit. on pp. 1, 3, 44).
- [13] Qing-Hong Cao, Ian Low, and Gabe Shaughnessy. “From Pamela to CDMS and Back”. In: *Phys.Lett.* B691 (2010), pp. 73–76. DOI: [10.1016/j.physletb.2010.06.023](https://doi.org/10.1016/j.physletb.2010.06.023). arXiv:0912.4510 [hep-ph] (cit. on pp. 1, 3, 44).
- [14] Douglas P. Finkbeiner et al. “Consistent Scenarios for Cosmic-Ray Excesses from Sommerfeld-Enhanced Dark Matter Annihilation”. In: *JCAP* 1105 (2011), p. 002. DOI: [10.1088/1475-7516/2011/05/002](https://doi.org/10.1088/1475-7516/2011/05/002). arXiv:1011.3082 [hep-ph] (cit. on pp. 1, 3, 7, 44, 52, 113).
- [15] Mathias Garny, Alejandro Ibarra, and Stefan Vogl. “Dark matter annihilations into two light fermions and one gauge boson: General analysis and antiproton constraints”. In: *JCAP* 1204 (2012), p. 033. arXiv:1112.5155 [hep-ph] (cit. on pp. 1, 3).
- [16] Massimiliano Lattanzi and Joseph I. Silk. “Can the WIMP annihilation boost factor be boosted by the Sommerfeld enhancement?” In: *Phys.Rev.* D79 (2009). * Brief entry *, p. 083523. DOI: [10.1103/PhysRevD.79.083523](https://doi.org/10.1103/PhysRevD.79.083523). arXiv:0812.0360 [astro-ph] (cit. on pp. 1, 3, 63, 65, 100, 103).
- [17] Brant Robertson and Andrew Zentner. “Dark Matter Annihilation Rates with Velocity-Dependent Annihilation Cross Sections”. In: *Phys.Rev.* D79 (2009), p. 083525. DOI: [10.1103/PhysRevD.79.083525](https://doi.org/10.1103/PhysRevD.79.083525). arXiv:0902.0362 [astro-ph.CO] (cit. on pp. 1, 3, 63, 65).
- [18] Junji Hisano et al. “Non-perturbative effect on dark matter annihilation and gamma ray signature from galactic center”. In: *Phys.Rev.* D71 (2005), p. 063528. DOI: [10.1103/PhysRevD.71.063528](https://doi.org/10.1103/PhysRevD.71.063528). arXiv:hep-ph/0412403 [hep-ph] (cit. on pp. 1, 3, 7–9, 14, 39, 44, 52, 93, 102–108, 112, 113).

-
- [19] A. Sommerfeld. “Über die Beugung und Bremsung der Elektronen”. In: *Annalen der Physik* 403.3 (1931), pp. 257–330. DOI: [10.1002/andp.19314030302](https://doi.org/10.1002/andp.19314030302) (cit. on pp. 1, 3, 7, 111).
- [20] Thomas Appelquist, Hsin-Chia Cheng, and Bogdan A. Dobrescu. “Bounds on universal extra dimensions”. In: *Phys. Rev. D* 64 (2001), p. 035002. DOI: [10.1103/PhysRevD.64.035002](https://doi.org/10.1103/PhysRevD.64.035002). arXiv:[hep-ph/0012100](https://arxiv.org/abs/hep-ph/0012100) (cit. on pp. 1, 5, 10).
- [21] Hsin-Chia Cheng and Ian Low. “TeV symmetry and the little hierarchy problem”. In: *JHEP* 0309 (2003), p. 051. arXiv:[hep-ph/0308199](https://arxiv.org/abs/hep-ph/0308199) [[hep-ph](#)] (cit. on pp. 1, 10).
- [22] Nima Arkani-Hamed, Andrew G. Cohen, and Howard Georgi. “(De)constructing dimensions”. In: *Phys.Rev.Lett.* 86 (2001), pp. 4757–4761. DOI: [10.1103/PhysRevLett.86.4757](https://doi.org/10.1103/PhysRevLett.86.4757). arXiv:[hep-th/0104005](https://arxiv.org/abs/hep-th/0104005) [[hep-th](#)] (cit. on pp. 1, 3, 13, 14, 34, 111, 135).
- [23] Roberto Iengo. “Sommerfeld enhancement: General results from field theory diagrams”. In: *JHEP* 0905 (2009), p. 024. DOI: [10.1088/1126-6708/2009/05/024](https://doi.org/10.1088/1126-6708/2009/05/024). arXiv:[0902.0688](https://arxiv.org/abs/0902.0688) [[hep-ph](#)] (cit. on pp. 2, 4, 7, 8, 48, 52–54, 56, 60, 62, 63, 66, 67, 69, 72, 82, 100, 111, 112, 127).
- [24] K.G. Begeman, A.H. Broeils, and R.H. Sanders. “Extended rotation curves of spiral galaxies: Dark haloes and modified dynamics”. In: *Mon.Not.Roy.Astron.Soc.* 249 (1991), p. 523 (cit. on p. 5).
- [25] W.J.G. de Blok and A. Bosma. “High-resolution rotation curves of low surface brightness galaxies”. In: *Astron.Astrophys.* 385 (2002), p. 816. DOI: [10.1051/0004-6361:20020080](https://doi.org/10.1051/0004-6361:20020080). arXiv:[astro-ph/0201276](https://arxiv.org/abs/astro-ph/0201276) [[astro-ph](#)] (cit. on p. 5).
- [26] Nick Kaiser and Gordon Squires. “Mapping the dark matter with weak gravitational lensing”. In: *Astrophys.J.* 404 (1993), pp. 441–450. DOI: [10.1086/172297](https://doi.org/10.1086/172297) (cit. on p. 5).
- [27] Douglas Clowe et al. “A direct empirical proof of the existence of dark matter”. In: *Astrophys.J.* 648 (2006), pp. L109–L113. DOI: [10.1086/508162](https://doi.org/10.1086/508162). arXiv:[astro-ph/0608407](https://arxiv.org/abs/astro-ph/0608407) [[astro-ph](#)] (cit. on p. 5).
- [28] E. Komatsu et al. “Seven-Year Wilkinson Microwave Anisotropy Probe (WMAP) Observations: Cosmological Interpretation”. In: *Astrophys.J.Suppl.* 192 (2011), p. 18. DOI: [10.1088/0067-0049/192/2/18](https://doi.org/10.1088/0067-0049/192/2/18) (cit. on p. 5).
- [29] D. Larson et al. “Seven-Year Wilkinson Microwave Anisotropy Probe (WMAP) Observations: Power Spectra and WMAP-Derived Parameters”. In: *Astrophys.J.Suppl.* 192 (2011), p. 16. DOI: [10.1088/0067-0049/192/2/16](https://doi.org/10.1088/0067-0049/192/2/16). arXiv:[1001.4635](https://arxiv.org/abs/1001.4635) [[astro-ph.C0](#)] (cit. on pp. 5, 6).

- [30] Stephen P. Martin. “A Supersymmetry primer”. In: (1997). arXiv:[hep-ph/9709356](#) [[hep-ph](#)] (cit. on pp. 5, 14).
- [31] Kim Griest and David Seckel. “Three exceptions in the calculation of relic abundances”. In: *Phys. Rev. D* 43 (10 1991), pp. 3191–3203. DOI: [10.1103/PhysRevD.43.3191](#) (cit. on p. 6).
- [32] John R. Ellis et al. “Calculations of neutralino-stau coannihilation channels and the cosmologically relevant region of MSSM parameter space”. In: *Astropart.Phys.* 13 (2000), pp. 181–213. DOI: [10.1016/S0927-6505\(99\)00104-8](#), [10.1016/S0927-6505\(99\)00104-8](#). arXiv:[hep-ph/9905481](#) [[hep-ph](#)] (cit. on p. 6).
- [33] Fiona Burnell and Graham D. Kribs. “The Abundance of Kaluza-Klein dark matter with coannihilation”. In: *Phys.Rev.* D73 (2006), p. 015001. DOI: [10.1103/PhysRevD.73.015001](#). arXiv:[hep-ph/0509118](#) [[hep-ph](#)] (cit. on p. 6).
- [34] Tracy R. Slatyer. “The Sommerfeld enhancement for dark matter with an excited state”. In: *JCAP* 1002 (2010), p. 028. DOI: [10.1088/1475-7516/2010/02/028](#). arXiv:[0910.5713](#) [[hep-ph](#)] (cit. on pp. 6, 8, 9, 44, 93, 95, 97–99, 102, 107, 113).
- [35] Dan Hooper, Pasquale Blasi, and Pasquale Dario Serpico. “Pulsars as the Sources of High Energy Cosmic Ray Positrons”. In: *JCAP* 0901 (2009), p. 025. DOI: [10.1088/1475-7516/2009/01/025](#). arXiv:[0810.1527](#) [[astro-ph](#)] (cit. on pp. 7, 44).
- [36] Hasan Yuksel, Matthew D. Kistler, and Todor Stanev. “TeV Gamma Rays from Geminga and the Origin of the GeV Positron Excess”. In: *Phys.Rev.Lett.* 103 (2009), p. 051101. DOI: [10.1103/PhysRevLett.103.051101](#). arXiv:[0810.2784](#) [[astro-ph](#)] (cit. on pp. 7, 44).
- [37] Stefano Profumo. “Dissecting cosmic-ray electron-positron data with Occam’s Razor: the role of known Pulsars”. In: *Central Eur.J.Phys.* 10 (2011), pp. 1–31. DOI: [10.2478/s11534-011-0099-z](#). arXiv:[0812.4457](#) [[astro-ph](#)] (cit. on pp. 7, 44).
- [38] S. Cassel. “Sommerfeld factor for arbitrary partial wave processes”. In: *J.Phys.G* G37 (2010), p. 105009. DOI: [10.1088/0954-3899/37/10/105009](#). arXiv:[0903.5307](#) [[hep-ph](#)] (cit. on pp. 7, 8, 52, 54, 63, 100).
- [39] Andrzej Hryczuk, Roberto Iengo, and Piero Ullio. “Relic densities including Sommerfeld enhancements in the MSSM”. In: *JHEP* 1103 (2011), p. 069. DOI: [10.1007/JHEP03\(2011\)069](#). arXiv:[1010.2172](#) [[hep-ph](#)] (cit. on pp. 7–9, 66, 67, 72, 82, 86, 89, 93–95, 110, 112).
- [40] M. Böhm, A. Denner, and H. Joos. *Gauge theories of the strong and electroweak interaction*. B.G. Teubner Verlag, 2001 (cit. on pp. 7, 14, 16, 19, 21, 33, 42, 68, 71, 78, 82, 115, 116, 135, 137, 138, 140, 142, 143, 146, 147).

-
- [41] Michael E. Peskin and Dan V. Schroeder. *An Introduction To Quantum Field Theory (Frontiers in Physics)*. Westview Press, 1995 (cit. on pp. 7, 20, 21, 42, 72, 115, 116).
- [42] J. J. Sakurai. *Modern Quantum Mechanics (Revised Edition)*. 1st ed. Addison Wesley, Sept. 1993 (cit. on pp. 8, 61, 93).
- [43] L.D. Landau and E.M. Lifshitz. *Quantum Mechanics - Non-Relativistic Theory*. 3rd ed. Pergamon Press, 1977 (cit. on pp. 8, 61, 93, 94).
- [44] Straumann Norbert. *Quantenmechanik - Nichtrelativistische Quantentheorie*. 1st ed. Springer, Berlin, Heidelberg, 19772002 (cit. on pp. 8, 61, 64).
- [45] Martin Schmaltz and David Tucker-Smith. “Little Higgs review”. In: *Ann.Rev.Nucl.Part.Sci.* 55 (2005), pp. 229–270. DOI: [10.1146/annurev.nucl.55.090704.151502](https://doi.org/10.1146/annurev.nucl.55.090704.151502). arXiv:[hep-ph/0502182](https://arxiv.org/abs/hep-ph/0502182) [[hep-ph](#)] (cit. on p. 10).
- [46] Dan Hooper and Stefano Profumo. “Dark matter and collider phenomenology of universal extra dimensions”. In: *Phys.Rept.* 453 (2007), pp. 29–115. DOI: [10.1016/j.physrep.2007.09.003](https://doi.org/10.1016/j.physrep.2007.09.003). arXiv:[hep-ph/0701197](https://arxiv.org/abs/hep-ph/0701197) [[hep-ph](#)] (cit. on pp. 10, 44, 52).
- [47] Hsin-Chia Cheng, Konstantin T. Matchev, and Martin Schmaltz. “Radiative corrections to Kaluza-Klein masses”. In: *Phys.Rev.* D66 (2002), p. 036005. DOI: [10.1103/PhysRevD.66.036005](https://doi.org/10.1103/PhysRevD.66.036005). arXiv:[hep-ph/0204342](https://arxiv.org/abs/hep-ph/0204342) [[hep-ph](#)] (cit. on pp. 11, 17, 33, 34).
- [48] Thomas Flacke, A. Menon, and Daniel J. Phalen. “Non-minimal universal extra dimensions”. In: *Phys.Rev.* D79 (2009), p. 056009. DOI: [10.1103/PhysRevD.79.056009](https://doi.org/10.1103/PhysRevD.79.056009). arXiv:[0811.1598](https://arxiv.org/abs/0811.1598) [[hep-ph](#)] (cit. on p. 11).
- [49] Raman Sundrum. “Tasi 2004 lectures: To the fifth dimension and back”. In: (2005), pp. 585–630. arXiv:[hep-th/0508134](https://arxiv.org/abs/hep-th/0508134) [[hep-th](#)] (cit. on pp. 11, 34).
- [50] K. Nakamura et al. “Review of particle physics”. In: *J.Phys.G* G37 (2010), p. 075021. DOI: [10.1088/0954-3899/37/7A/075021](https://doi.org/10.1088/0954-3899/37/7A/075021) (cit. on pp. 11, 114).
- [51] Hsin-Chia Cheng et al. “The Standard model in the latticized bulk”. In: *Phys.Rev.* D64 (2001), p. 065007. DOI: [10.1103/PhysRevD.64.065007](https://doi.org/10.1103/PhysRevD.64.065007). arXiv:[hep-th/0104179](https://arxiv.org/abs/hep-th/0104179) [[hep-th](#)] (cit. on pp. 13–15, 18–20, 22, 23, 31, 33, 135).
- [52] Christopher T. Hill, Stefan Pokorski, and Jing Wang. “Gauge invariant effective Lagrangian for Kaluza-Klein modes”. In: *Phys.Rev.* D64 (2001). 21 pages, 4 figures Report-no: FERMILAB-Pub-01/043-T, p. 105005. DOI: [10.1103/PhysRevD.64.105005](https://doi.org/10.1103/PhysRevD.64.105005). arXiv:[hep-th/0104035](https://arxiv.org/abs/hep-th/0104035) [[hep-th](#)] (cit. on pp. 13–15, 135).

- [53] J.F. Oliver, J. Papavassiliou, and A. Santamaria. “Bounds on models with one latticized extra dimension”. In: *Phys.Rev.* D68 (2003), p. 096003. DOI: [10.1103/PhysRevD.68.096003](https://doi.org/10.1103/PhysRevD.68.096003). arXiv:[hep-ph/0306296](https://arxiv.org/abs/hep-ph/0306296) [[hep-ph](#)] (cit. on pp. 13–15, 22).
- [54] Tomas Hallgren and Tommy Ohlsson. “Indirect detection of Kaluza-Klein dark matter from latticized universal dimensions”. In: *JCAP* 0606 (2006), p. 014. DOI: [10.1088/1475-7516/2006/06/014](https://doi.org/10.1088/1475-7516/2006/06/014). arXiv:[hep-ph/0510174](https://arxiv.org/abs/hep-ph/0510174) [[hep-ph](#)] (cit. on pp. 13–15, 18, 22).
- [55] Tomas Hallgren. *Phenomenological Studies of Dimensional Deconstruction*. online. 2005. eprint: <http://kth.diva-portal.org/smash/get/diva2:14451/FULLTEXT01> (cit. on pp. 13–15, 33).
- [56] Alexander Mück, Apostolos Pilaftsis, and Reinhold Ruckl. “Minimal higher dimensional extensions of the standard model and electroweak observables”. In: *Phys.Rev.* D65 (2002), p. 085037. DOI: [10.1103/PhysRevD.65.085037](https://doi.org/10.1103/PhysRevD.65.085037). arXiv:[hep-ph/0110391](https://arxiv.org/abs/hep-ph/0110391) [[hep-ph](#)] (cit. on pp. 17, 115).
- [57] Andrzej J. Buras, Michael Spranger, and Andreas Weiler. “The Impact of universal extra dimensions on the unitarity triangle and rare K and B decays”. In: *Nucl.Phys.* B660 (2003), pp. 225–268. DOI: [10.1016/S0550-3213\(03\)00250-5](https://doi.org/10.1016/S0550-3213(03)00250-5). arXiv:[hep-ph/0212143](https://arxiv.org/abs/hep-ph/0212143) [[hep-ph](#)] (cit. on p. 17).
- [58] Ta-Pei Cheng and Ling-Fong Li. *Gauge Theory of Elementary Particle Physics*. Clarendon Press, 1984 (cit. on pp. 21, 35, 38, 42, 115, 116, 118, 119, 133, 135–138, 140, 143, 150).
- [59] Peter W. Higgs. “Broken symmetries, massless particles and gauge fields”. In: *Phys.Lett.* 12 (1964), pp. 132–133. DOI: [10.1016/0031-9163\(64\)91136-9](https://doi.org/10.1016/0031-9163(64)91136-9) (cit. on p. 25).
- [60] Georges Aad et al. “Combined search for the Standard Model Higgs boson using up to 4.9 fb⁻¹ of pp collision data at sqrt(s) = 7 TeV with the ATLAS detector at the LHC”. In: *Phys.Lett.* B710 (2012), pp. 49–66. arXiv:[1202.1408](https://arxiv.org/abs/1202.1408) [[hep-ex](#)] (cit. on p. 31).
- [61] Serguei Chatrchyan et al. “Search for the standard model Higgs boson decaying into two photons in pp collisions at sqrt(s)=7 TeV”. In: *Phys.Lett.* B710 (2012), pp. 403–425. arXiv:[1202.1487](https://arxiv.org/abs/1202.1487) [[hep-ex](#)] (cit. on p. 31).
- [62] Andrzej Hryczuk and Roberto Iengo. “The one-loop and Sommerfeld electroweak corrections to the Wino dark matter annihilation”. In: *JHEP* 1201 (2012), p. 163. DOI: [10.1007/JHEP01\(2012\)163](https://doi.org/10.1007/JHEP01(2012)163). arXiv:[1111.2916](https://arxiv.org/abs/1111.2916) [[hep-ph](#)] (cit. on pp. 39, 92, 96, 102–104, 109, 113).

-
- [63] J.A.R. Cembranos, V. Gammaldi, and A.L. Maroto. “Dark matter origin of the gamma ray emission from the galactic center observed by HESS”. In: (2012). arXiv:[1204.0655 \[hep-ph\]](#) (cit. on p. 44).
- [64] T. Kobayashi et al. “The most likely sources of high energy cosmic-ray electrons in supernova remnants”. In: *Astrophys.J.* 601 (2004), pp. 340–351. DOI: [10.1086/380431](#). arXiv:[astro-ph/0308470 \[astro-ph\]](#) (cit. on p. 44).
- [65] Steen Hannestad and Thomas Tram. “Sommerfeld Enhancement of DM Annihilation: Resonance Structure, Freeze-Out and CMB Spectral Bound”. In: *JCAP* 1101 (2011), p. 016. DOI: [10.1088/1475-7516/2011/01/016](#). arXiv:[1008.1511 \[astro-ph.CO\]](#) (cit. on pp. 44, 60–62).
- [66] Ilias Cholis et al. “High Energy Positrons From Annihilating Dark Matter”. In: *Phys.Rev.* D80 (2009), p. 123511. DOI: [10.1103/PhysRevD.80.123511](#). arXiv:[0809.1683 \[hep-ph\]](#) (cit. on p. 44).
- [67] E.E. Salpeter and H.A. Bethe. “A Relativistic equation for bound state problems”. In: *Phys.Rev.* 84 (1951), pp. 1232–1242. DOI: [10.1103/PhysRev.84.1232](#) (cit. on pp. 45, 51, 58, 81, 113).
- [68] Noboru Nakanishi. “A General survey of the theory of the Bethe-Salpeter equation”. In: *Prog.Theor.Phys.Suppl.* 43 (1969), pp. 1–81 (cit. on pp. 45, 47, 53, 82).
- [69] Z.K. Silagadze. “Wick-Cutkosky model: An Introduction”. In: (1998). arXiv:[hep-ph/9803307 \[hep-ph\]](#) (cit. on p. 45).
- [70] Claude Itzykson and Jean-Bernard Zuber. *Quantum Field Theory*. McGraw Hill, 1980 (cit. on pp. 45, 47, 50, 52–54, 57, 82, 112, 113).
- [71] W. Greiner and J. Reinhardt. *Quantum Electrodynamics*. Springer, 1992 (cit. on pp. 45, 113).
- [72] V. B. Berestetskii, E. M. Lifshitz, and L. P. Pitaevskii. *Quantum Electrodynamics: Landau and Lifshitz Course of Theoretical Physics*. Pergamon Press, 1982 (cit. on pp. 47–49, 51, 56, 68, 113).
- [73] William Celmaster and Frank S. Henyey. “ON THE INSTANTANEOUS APPROXIMATION FOR A GAUGE THEORY WITH DRESSED VERTICES”. In: *Phys.Rev.* D17 (1978), p. 3268. DOI: [10.1103/PhysRevD.17.3268](#) (cit. on p. 53).
- [74] R.S. Bhalerao and S.A. Gurvitz. “NONINSTANTANEOUS APPROXIMATION TO THE BETHE-SALPETER EQUATION”. In: *Phys.Rev.* C28 (1983), p. 383. DOI: [10.1103/PhysRevC.28.383](#) (cit. on p. 53).

- [75] Andrzej Hryczuk. “The Sommerfeld enhancement for scalar particles and application to sfermion co-annihilation regions”. In: *Phys.Lett.* B699 (2011), pp. 271–275. DOI: [10.1016/j.physletb.2011.04.016](https://doi.org/10.1016/j.physletb.2011.04.016). arXiv:[1102.4295](https://arxiv.org/abs/1102.4295) [hep-ph] (cit. on pp. 54, 106, 108).
- [76] M. Drees, J.M. Kim, and K.I. Nagao. “Potentially Large One-loop Corrections to WIMP Annihilation”. In: *Phys.Rev.* D81 (2010), p. 105004. DOI: [10.1103/PhysRevD.81.105004](https://doi.org/10.1103/PhysRevD.81.105004). arXiv:[0911.3795](https://arxiv.org/abs/0911.3795) [hep-ph] (cit. on pp. 56, 68, 69).
- [77] J.M. Cornwall and A. Soni. “Glueballs as Bound States of Massive Gluons”. In: *Phys.Lett.* B120 (1983), p. 431. DOI: [10.1016/0370-2693\(83\)90481-1](https://doi.org/10.1016/0370-2693(83)90481-1) (cit. on pp. 66, 92, 113).
- [78] S. Rai Choudhury and Asoke N. Mitra. “GLUEBALLS UNDER HARMONIC CONFINEMENT”. In: *Phys.Rev.* D28 (1983), pp. 2201–2204. DOI: [10.1103/PhysRevD.28.2201](https://doi.org/10.1103/PhysRevD.28.2201) (cit. on pp. 66, 90, 113).
- [79] M.H. Thomas, M. Lust, and H.J. Mang. “Glueballs as bound states of massive transverse gluons”. In: *J.Phys.G* G18 (1992), pp. 1125–1131. DOI: [10.1088/0954-3889/18/7/004](https://doi.org/10.1088/0954-3889/18/7/004) (cit. on pp. 66, 113).
- [80] J.Y. Cui, J.M. Wu, and H.Y. Jin. “Glueball spectrum from the B.S. equation”. In: *Phys.Lett.* B424 (1998), pp. 381–389. DOI: [10.1016/S0370-2693\(98\)00121-X](https://doi.org/10.1016/S0370-2693(98)00121-X). arXiv:[hep-ph/9711379](https://arxiv.org/abs/hep-ph/9711379) [hep-ph] (cit. on p. 66).
- [81] E.E. Boos and A.I. Davydychev. *Infrared problems of describing the glueball and an estimation of its mass.* 1988. eprint: <http://wino.physik.uni-mainz.de/~davyd/preprints/glueball.pdf> (cit. on p. 66).
- [82] Mitsuru Kakizaki et al. “Significant effects of second KK particles on LKP dark matter physics”. In: *Phys.Rev.* D71 (2005), p. 123522. DOI: [10.1103/PhysRevD.71.123522](https://doi.org/10.1103/PhysRevD.71.123522). arXiv:[hep-ph/0502059](https://arxiv.org/abs/hep-ph/0502059) [hep-ph] (cit. on p. 67).
- [83] R. Mertig, M. Bohm, and Ansgar Denner. “FEYN CALC: Computer algebraic calculation of Feynman amplitudes”. In: *Comput.Phys.Commun.* 64 (1991), pp. 345–359. DOI: [10.1016/0010-4655\(91\)90130-D](https://doi.org/10.1016/0010-4655(91)90130-D) (cit. on p. 73).
- [84] Csaba Csaki et al. “Gauge theories on an interval: Unitarity without a Higgs”. In: *Phys.Rev.* D69 (2004), p. 055006. DOI: [10.1103/PhysRevD.69.055006](https://doi.org/10.1103/PhysRevD.69.055006). arXiv:[hep-ph/0305237](https://arxiv.org/abs/hep-ph/0305237) [hep-ph] (cit. on p. 78).
- [85] F.J. Dyson. “The S matrix in quantum electrodynamics”. In: *Phys.Rev.* 75 (1949), pp. 1736–1755. DOI: [10.1103/PhysRev.75.1736](https://doi.org/10.1103/PhysRev.75.1736) (cit. on p. 81).
- [86] K.J. Barnes. “Lagrangian Theory for the Second-Rank Tensor Field”. In: *J. Math. Phys.* 6 (5 May 1965), pp. 788–794. DOI: [10.1063/1.1704335](https://doi.org/10.1063/1.1704335) (cit. on pp. 85, 86).

-
- [87] A. J. Macfarlane and W. Tait. “Tensor formulation of spin-1 and spin-2 fields”. In: *Communications in Mathematical Physics* 24 (3 1972), pp. 211–224. DOI: [10.1007/BF01877713](https://doi.org/10.1007/BF01877713) (cit. on pp. 85, 86).
- [88] William Press et al. *Numerical Recipes in C*. 2nd. Cambridge, UK: Cambridge University Press, 1992 (cit. on pp. 99, 152).
- [89] Wolfgang Kinzel and Georg Reents. *Physics by Computer*. 1st. Secaucus, NJ, USA: Springer-Verlag New York, Inc., 1997 (cit. on pp. 99, 152).
- [90] Joel Franklin. *Scientific Computation*. online. Reed College, 2011. eprint: <http://academic.reed.edu/physics/courses/P367.S11/Physics367/Lecture/files/Week.2.pdf> (cit. on pp. 99, 152).
- [91] Fang Chen, James M. Cline, and Andrew R. Frey. “A New twist on excited dark matter: Implications for INTEGRAL, PAMELA/ATIC/PPB-BETS, DAMA”. In: *Phys.Rev.* D79 (2009), p. 063530. DOI: [10.1103/PhysRevD.79.063530](https://doi.org/10.1103/PhysRevD.79.063530). arXiv:0901.4327 [hep-ph] (cit. on p. 102).
- [92] Fang Chen et al. “Exciting dark matter in the galactic center”. In: *Phys.Rev.* D81 (2010), p. 043523. DOI: [10.1103/PhysRevD.81.043523](https://doi.org/10.1103/PhysRevD.81.043523). arXiv:0911.2222 [hep-ph] (cit. on p. 102).
- [93] Johan Bonnevier et al. “Monoenergetic Gamma-Rays from Non-Minimal Kaluza-Klein Dark Matter Annihilations”. In: *Phys.Rev.* D85 (2012), p. 043524. arXiv:1104.1430 [hep-ph] (cit. on p. 108).
- [94] W.B. Atwood et al. “The Large Area Telescope on the Fermi Gamma-ray Space Telescope Mission”. In: *Astrophys.J.* 697 (2009), pp. 1071–1102. DOI: [10.1088/0004-637X/697/2/1071](https://doi.org/10.1088/0004-637X/697/2/1071). arXiv:0902.1089 [astro-ph.IM] (cit. on pp. 108, 110).
- [95] G. Belanger, M. Kakizaki, and A. Pukhov. “Dark matter in UED: The Role of the second KK level”. In: *JCAP* 1102 (2011). 18 pages, 6 figures, p. 009. arXiv:1012.2577 [hep-ph] (cit. on p. 112).
- [96] Yang Bai, Gustavo Burdman, and Christopher T. Hill. “Topological Interactions in Warped Extra Dimensions”. In: *JHEP* 1002 (2010), p. 049. DOI: [10.1007/JHEP02\(2010\)049](https://doi.org/10.1007/JHEP02(2010)049). arXiv:0911.1358 [hep-ph] (cit. on p. 112).
- [97] Masako Bando, Masayasu Harada, and Taichiro Kugo. “External gauge invariance and anomaly in BS vertices and bound states”. In: *Prog.Theor.Phys.* 91 (1994), pp. 927–948. DOI: [10.1143/PTP.91.927](https://doi.org/10.1143/PTP.91.927). arXiv:hep-ph/9312343 [hep-ph] (cit. on p. 113).

- [98] Joannis Papavassiliou and Apostolos Pilaftsis. “Gauge invariant resummation formalism for two point correlation functions”. In: *Phys.Rev.* D54 (1996), pp. 5315–5335. DOI: [10.1103/PhysRevD.54.5315](https://doi.org/10.1103/PhysRevD.54.5315). arXiv:[hep-ph/9605385](https://arxiv.org/abs/hep-ph/9605385) [[hep-ph](#)] (cit. on p. 113).
- [99] L.D. Faddeev and V.N. Popov. “Feynman diagrams for the Yang-Mills field”. In: *Physics Letters B* 25.1 (1967), pp. 29 –30. DOI: [10.1016/0370-2693\(67\)90067-6](https://doi.org/10.1016/0370-2693(67)90067-6) (cit. on p. 132).
- [100] Michael Gustafsson. “Light from Dark Matter: Hidden Dimensions, Supersymmetry, and Inert Higgs”. In: (2008). Ph.D. Thesis (Advisor: Lars Bergstrom). eprint: www.diva-portal.org/smash/get/diva2:198091/FULLTEXT01 (cit. on pp. 135, 140, 146).

List of Figures

3.1. Exemplary KK-number-violating vertex	12
3.2. Generic moose diagram for $N + 1$ gauge groups G	13
4.1. Moose diagram representing Higgs fields, vacuum expectation values and gauge couplings	15
4.2. v_1 and v_2 dependence of the neutral \mathcal{Z}_2 -odd gauge boson masses	36
4.3. v_1 and v_2 dependence of $\cos \theta_W^{(1)}$	37
4.4. VEV dependence of the Gauge Boson Mass Spectrum	40
4.5. Gauge boson mass spectrum - closeup of the level crossing	40
4.6. Generic mass splitting in the heavy gauge boson sector	41
4.7. Weinberg Mixing Angle of the Dark Sector	41
5.1. Graphical representation of $2 \rightarrow 2$ scattering event for scalar particles	45
5.2. Box diagrams in the description of positronium in QED	49
5.3. Graphical representation of $2 \rightarrow 2$ scattering iteration for lowest order interaction kernel in the Ladder approximation	54
5.4. Poles in the q_0 plane for fermionic dark matter candidates	55
5.5. Example of Numerical Results for Iengos model	63
5.6. Sommerfeld enhancement for diagonal interaction via a Yukawa potential	65
5.7. Graphical representation of $2 \rightarrow 2$ scattering event from vector particles into Standard Model states	66
5.8. Graphical representation of the $Z^{(1)} Z^{(1)} \rightarrow Z^{(1)} Z^{(1)}$ lowest order interaction kernel	67
5.9. Graphical representation of the $Z^{(1)} Z^{(1)} \rightarrow W^{(1)} W^{(1)}$ lowest order interaction kernel	73
5.10. Graphical representation of the $Z^{(1)} Z^{(1)} \rightarrow W^{(1)} W^{(1)}$ lowest order interaction kernel with exchanged initial states	75
5.11. Graphical representation of the $Z^{(1)} Z^{(1)} \rightarrow W^{(1)} W^{(1)}$ scattering amplitude for the contact kernel	76
5.12. Graphical representation of the $W^{(1)} W^{(1)} \rightarrow W^{(1)} W^{(1)}$ scattering amplitude for $Z^{(0)}$ and $A^{(0)}$ interaction kernel	77

5.13. Neglected diagrams in the ladder approximation to the Bethe-Salpeter kernel	80
5.14. Validation of the numerical shooting method via Sommerfeld enhancement for Yukawa interaction potential	101
5.15. Contour-plot for the Sommerfeld enhancement of our vector dark matter model.	103
5.16. 3D-plot for the Sommerfeld enhancement of our vector dark matter model.	103
5.17. Mass dependence of Sommerfeld enhancement in the vector dark matter model for $v = 10^{-3}$	105
5.18. Wavefunction around the trench region.	105
5.19. Influence of mass splitting δm on the Sommerfeld enhancement.	106
5.20. General model of zero-energy resonances in finite well potential approxi- mation - data fit.	108
5.21. Approximate Sommerfeld Factor for DM-Annihilation into Two Photons .	109
B.1. v_1 and v_2 dependence of $\epsilon = \left(\frac{\Delta m}{m_{W(0)}}\right)^2$	129
B.2. Expansion parameters c_1 and c_2 for the $Z^{(1)}$ Goldstone boson in the $v_1 - v_2$ plane	129
B.3. Expansion parameters \tilde{c}_1 and \tilde{c}_2 for the $\gamma^{(1)}$ Goldstone boson in the $v_1 - v_2$ plane	131

Acknowledgment

First and foremost, I would like to thank Dr. Thomas Flacke for his inexhaustible patience, explaining a great number of issues concerning BSM-phenomenology. Without our regular discussion sessions, this work would not have been possible. I would also like to acknowledge Thomas for suggesting the interesting subject of my thesis in the first place as well as his valuable comments in the final stage of this work.

Sincere thanks are given to Prof. Rückl for the opportunity to join his research group as a Diploma student and for valuable input and discussion towards the progress of this work.

I am grateful for the support from the "Studienstiftung des deutschen Volkes" during my studies.

I would like to thank Julian Treu and Eva-Maria Fürst for careful proofreading of this manuscript.

Last but not least, I am in debt to my parents for their endless support of all decisions I have made in life so far.

Selbständigkeitserklärung

Gemäß der allgemeinen Studien- und Prüfungsordnung für den Diplomstudiengang Physik an der Julius-Maximilians-Universität Würzburg erkläre ich hiermit, dass ich diese Arbeit selbstständig verfasst, keine anderen als die angegebenen Quellen und Hilfsmittel verwendet habe und die Arbeit bisher keiner anderen Prüfungsbehörde unter Erlangung eines akademischen Grades vorgelegt wurde.

Würzburg, den 26. Juni 2012

Enrico Herrmann